PACIFIC EARTHQUAKE ENGINEERING RESEARCH CENTER

Guidelines for Performing Hazard-Consistent One-Dimensional Ground Response Analysis for Ground Motion Prediction

Jonathan P. Stewart
Kioumars Afshari

Department of Civil and Environmental Engineering
University of California, Los Angeles

Youssef M.A. Hashash

Department of Civil and Environmental Engineering
University of Illinois, Urbana-Champaign

Project Review Panel:

Thomas Shantz
Brian S.-J. Chiou

California Department of Transportation
Sacramento, California

Yousef Bozorgnia
Christine A. Goulet

Pacific Earthquake Engineering Research Center
Berkeley, California

PEER 2014/16
OCTOBER 2014

Disclaimer

The opinions, findings, and conclusions or recommendations expressed in this publication are those of the author(s) and do not necessarily reflect the views of the study sponsor(s) or the Pacific Earthquake Engineering Research Center.

Guidelines for Performing Hazard-Consistent One-Dimensional Ground Response Analysis for Ground Motion Prediction

Jonathan P. Stewart, PhD, PE
Kioumars Afshari
Department of Civil and Environmental Engineering
University of California, Los Angeles

Youssef M.A. Hashash, PhD
Department of Civil and Environmental Engineering
University of Illinois, Urbana-Champaign

Project Review Panel:

Thomas Shantz, PE
Brian S.-J. Chiou, PhD
California Department of Transportation
Sacramento, California

Yousef Bozorgnia, PhD, PE
Christine A. Goulet, PhD
Pacific Earthquake Engineering Research Center
Berkeley, California

PEER Report 2014/16
Pacific Earthquake Engineering Research Center
Headquarters, University of California at Berkeley

October 2014

ABSTRACT

Along with source and path effects, site response analysis is a vital component of earthquake ground motion prediction. Semi-empirical ground motion prediction equations (GMPEs) include terms for modeling site response that are based on simple metrics of site condition, such as the time-average shear-wave velocity in the upper 30 m of the site (V_{S30}). Because site terms in GMPEs are derived from global ground motion databases and are based on incomplete information on the site condition, their predictions represent average levels of site response observed at sites conditional on V_{S30}. Such predictions are referred to as ergodic.

Actual site response at a given site is likely to be different from this global average. Viewed in this context, the actual site response for a particular site and intensity measure can be understood as being the sum of the ergodic estimate from a global model and a (generally unknown) site term (denoted η_S). If the level of site-specific error (η_S) can be identified and used to adjust the ergodic model, the ground motion analysis becomes more accurate (i.e., bias is removed), and the dispersion of the predicted ground motions is reduced. Therefore, site-specific evaluations of site response are always useful. The question is how that evaluation should be undertaken.

In this report, we consider the use of one-dimensional (1D) ground response analysis (GRA) to estimate site-specific site response. We show that previous studies investigating the usefulness of GRA to estimate observed site response (as evaluated from recordings) have achieved mixed success. This occurs because actual site response involves a variety of physical processes, some of which are not captured by 1D analysis. Resolution of questions related to the effectiveness of GRA, given the mixed results from the literature, is beyond the scope of this project. Instead, we summarize the relevant literature and describe future work that may resolve these questions.

Most of the work presented in this report concerns recommendations for performing GRA and using the results of those analyses to develop hazard-consistent estimates of site-specific ground motions. We describe in some detail recommendations for performing the GRA, assuming the analyst has a good working knowledge of the fundamentals of site response. Some important aspects of these recommendations include the following:

1. Shear-wave velocity profiles should be based on measurements, not estimates;
2. Nonlinear modulus reduction and damping versus strain curves can be derived from material-specific tests or generic relationships derived from test databases, but these relationships are generally not reliable at strains beyond about 0.3-0.5%;
3. The shear strength of soil should be considered in developing modulus reduction (MR) relationships at large strains;
4. Equivalent-linear methods of GRA should be used for small- to moderate-strain problems, and diagnostics are presented for identifying when such methods become unreliable;

5. Nonlinear methods of GRA should be used for large strain problems, and procedures are presented for identifying a priori when such analyses are likely to be required; and
6. Input ground motion selection for GRA should follow, with some modification, accepted norms for structural engineering applications, and we provide detailed recommendations for developing target spectra, selecting motions, and scaling or modifying the selected motions for compatibility with the target spectra.

Once GRA have been completed, it is necessary to interpret the results in the form of ground motion amplification functions that are conditioned on the amplitude of the input shaking. We suggest a three-parameter function for this relationship and provide detailed recommendations for how to estimate the parameters given suites of GRA results.

The standard deviation of the site amplification (denoted $\phi_{\ln Y}$) computed directly from GRA results is considered unreliable—it is generally too high below the fundamental site period and too low above. For this reason, we recommend the use of standard deviations inferred from ground motion data analysis. We find these values of $\phi_{\ln Y}$ to be consistent (between-periods and

between-studies) at $\phi_{\ln Y} \approx 0.3$. This level of consistency is not found with the standard deviation term representing site-to-site variability (i.e., the variability that can, in principal, be removed with a site-specific analysis). That standard deviation, denoted ϕ_{2S}, exhibits regional variations and variations across periods. We present expressions for computing site-specific within-event standard deviation terms based in part on $\phi_{\ln Y}$ and ϕ_{2S}. A significant consideration in this regard is whether the site response computed from GRA is non-ergodic. This is currently unknown and falls within the realm of engineering judgment.

Armed with a mean amplification function and the applicable standard deviation terms, the most robust merging of GRA with PSHA requires replacement of the site term in a GMPE with the mean amplification function, and use of that modified GMPE in the hazard integral. We developed a local version (i.e., not housed on a public server) of the open-source seismic hazard software platform OpenSHA that performs these calculations. This implementation properly handles modified standard deviation terms, which produces the most accurate hazard analysis results (i.e., hazard curves, uniform hazard spectra). This implementation also accounts for site effects in the disaggregation.

When implementation of GRA within the hazard integral is not considered practical, then the reference site (usually rock) hazard curves are modified using the mean site amplification function and (in some cases) $\phi_{\ln Y}$. We present various options for this modification, but the method having the least bias relative to the probabilistic approach is the modified hybrid approach. This method involves modifying the reference site ground motion for a point on the hazard curve using the mean site amplification derived from mean expected ground motion levels for the reference site. Spreadsheet solutions for this, and other approximate methods, are provided in an electronic supplement:

http://apps.peer.berkeley.edu/publications/peer_reports/reports_2014/electronic-supplement-2014-16.zip.

ACKNOWLEDGMENTS

This study was sponsored by the Pacific Earthquake Engineering Research Center (PEER) Lifelines program, with funding from the California Department of Transportation. This support is gratefully acknowledged.

Any opinions, findings, and conclusions or recommendations expressed in this material are those of the authors and do not necessarily reflect those of the funding agencies.

This study benefited from the input and expert opinion of the advisory committee consisting of Tom Shantz, Youssef M.A. Hashash, Brian S.-J. Chiou, Yousef Bozorgnia, and Christine A. Goulet. Their helpful suggestions and comments are acknowledged.

CONTENTS

ABSTRACT ..... **iii**

ACKNOWLEDGMENTS ..... **v**

TABLE OF CONTENTS ..... **vii**

LIST OF TABLES ..... **xi**

LIST OF FIGURES ..... **xiii**

1 INTRODUCTION AND LITERATURE REVIEW **1**

1.1 Accuracy of 1D Ground Response Analysis **1**

1.1.1 California Surface Records: Baturay and Stewart [2003] 2

1.1.2 Japan Vertical Array Data: Thompson et al. [2012] 4

1.2 Merging Results of GRA with PSHA **6**

1.2.1 Site-Specific Nonlinear Ground Motion Amplification Function 6

1.2.2 Hybrid Method 9

1.2.3 Modified Hybrid Approach 11

1.2.4 Modifying the Hazard Integral 12

1.2.5 Convolution Method 12

2 PROTOCOLS FOR PERFORMING GROUND RESPONSE ANALYSES AND INTERPRETATION OF RESULTS **15**

2.1 Introduction **15**

2.2 Dynamic Soil Properties: Backbone Curve **15**

2.2.1 Shear-Wave Velocity Profile and its Uncertainty 16

2.2.2 Modulus Reduction and its Uncertainty 19

2.2.3 Constraining Backbone Curve at Large Strains using Shear Strength 26

2.2.4 Software Implementation of Backbone Curves 34

2.3 Dynamic Soil Properties: Damping **34**

2.3.1 Evaluation of Strain-Dependent Damping 35

2.3.2 Damping Implementation in GRA 39

2.3.3 Application of Laboratory-Based Soil Damping for Field Conditions 41

2.4 Equivalent-Linear Versus Nonlinear Methods of Analysis 42

2.4.1 Judging Differences between Equivalent-Linear and Nonlinear Analysis Results.....43

2.4.2 *A Priori* Evaluation of Conditions Leading to Different Equivalent Linear and Nonlinear Analysis Results.....45

2.5 Input Motion Selection 47

2.5.1 Target Spectra 48

2.5.2 Ground Motion Time Series Selection 52

2.5.3 Ground Motion Time Series Scaling 59

2.6 Fitting Ground Response Analysis Results to Site Amplification Function *y*|*x*.....60

2.6.1 Input Motions Derived for Single Hazard Level 61

2.6.2 Input Motions Derived for Multiple Hazard Levels 62

2.6.3 Variations across Periods.....63

3 DISPERSION OF SITE AMPLIFICATION AND ITS IMPLEMENTATION IN PROBABILISTIC SEISMIC HAZARD ANALYSIS.....67

3.1 Introduction.....67

3.2 Components of Ground Motion Variability.....68

3.2.1 Ground Motion Components Expressed in GMPE Framework 68

3.2.2 Ground Motion Components Relative to Predictions from GMPE with Location-Specific Site Factors.....68

3.3 Estimating Uncertainty in Site Amplification from Simulations 70

3.3.1 Li and Assimaki [2011] 70

3.3.2 Rathje et al. [2010].....72

3.3.3 Kwok et al. [2008] 74

3.3.4 Bazzurro and Cornell [2004b] 76

3.4 Estimating Uncertainty Terms from Recorded Ground Motion Data 78

3.4.1 Kaklamanos et al. [2013] 79

3.4.2 Lin et al. [2011].....80

3.4.3 Rodriguez-Marek et al. [2011].....81

3.4.4 Rodriguez-Marek et al. [2013].....82

3.4.5 Atkinson [2006] 84

3.5 Synthesis of Findings 85

3.5.1 Standard Deviation of Site Amplification ($\sigma_{\ln Y}$) 85

3.5.2 Standard Deviation of Site-to-Site Variability (σ_{S2S}).....87

4 IMPLEMENTATION AND TESTING OF METHODS FOR MERGING GROUND RESPONSE ANALYSIS RESULTS IN PSHA 89

4.1 Introduction 89

4.2 Spreadsheet Routines 89

4.2.1 Fitting the Mean Amplification Function 89

4.2.2 Interpolation of Site Parameters over a Range of Periods 93

4.2.3 Simplified Methods for Merging GRA with PSHA 94

4.3 OpenSHA Implementation 95

4.4 Comparative Analyses of GRA Implementation Methods 97

5 SUMMARY AND CONCLUSIONS 103

5.1 Scope of Work 103

5.2 Summary of Recommendations 104

5.2.1 Value of Site-Specific Site Response 104

5.2.2 Merging GRA with Hazard Analysis Results for Reference Site Condition 105

5.2.3 Guidelines for Performing GRA 106

5.3 Future Work 108

REFERENCES 111

APPENDIX A SOIL PROFILE AND GRA RESULTS FOR THE EXAMPLE SITE 119

LIST OF TABLES

Table 2.1 Model parameters for velocity profile uncertainty for generic site classes [Toro 1995]. NEHRP site classes defined in Dobry et al. [2000]; Geomatrix site categories defined in Chiou et al. [2008]. 19

Table 2.2 Summary of attributes of hyperbolic MR curve models from literature. 22

Table 2.3 Parameters for Darendeli [2001] model for modulus reduction. 22

Table 2.4 Parameters for Menq [2003] model for modulus reduction.....23

Table 2.5 GeoIndex soil classes [Roblee and Chiou 2004]. 23

Table 2.6 GeoIndex model parameters for modulus reduction [Roblee and Chiou 2004]. 23

Table 2.7 COV valued of inherent variability of soil shear strength parameters (from Jones et al. [2002]). 32

Table 2.8 Summary of attributes of hyperbolic soil damping models from literature. 36

Table 2.9 Parameters for Darendeli [2001] model for soil damping. 37

Table 2.10 Parameters for Menq [2003] model for soil damping.....37

Table 2.11 GeoIndex model parameters for damping [Roblee and Chiou 2004]. 37

Table 2.12 List of records from PEER website using Step I criteria for example site based on following criteria: 6.0 < M < 7.5, 5 km < R_{JB} < 40 km, and V_{S30} > 600 m/sec. 55

Table 2.13 Parameters for mean amplification equation for PGA obtained from different approaches.....63

Table 3.1 Sources of variability considered in simulation-based studies of ϕ_{nY}. 70

Table 3.2 Datasets and GMPEs utilized for the regions considered by Rodriguez-Marek et al. [2013].....83

Table 4.1 Sites investigated for comparative study of GRA implementation methods. 97

LIST OF FIGURES

Figure 1.1 Comparison of recorded spectra to two sets of predictions: rock GMPE with empirical amplification factors and rock GMPE with GRA [Baturay and Stewart 2003]; rock GMPE spectrum is also shown. 3

Figure 1.2 Prediction residuals and their standard deviations for NEHRP C, D, and Hlm sites (Holocene lacustrine or marine geology); modified from Baturay and Stewart [2003]. 4

Figure 1.3 Surface-to-downhole transfer functions indicating site amplification effects from data (marked as ETF) and GRA (marked as SH1D). Part (a) provides an example of poor fit. Part (b) shows good fit. The right side of the figure shows dispersion curves from four SASW tests conducted in the vicinity of the sites [Thompson et al. 2012]. 6

Figure 1.4 Intensity measure amplification levels from individual GRAs (symbols) and fit curves. A downward slope in the fit curves illustrates the effects of nonlinearity. 7

Figure 1.5 Hazard curves for PGA as derived using fully probabilistic approach (labeled PSHA) and hybrid approach for sites with V_{S30} = 250 and 180 m/sec. The results indicate underestimation of hazard at long return periods with the hybrid method [Goulet and Stewart 2009]. 11

Figure 2.1 Schematic illustration of backbone curve and small strain and large strain hysteresis loops. $G_{\max}$ is the maximum (small strain) shear modulus, G is the secant shear modulus for a given strain level, and τ_{ff} is the shear stress at failure. 16

Figure 2.2 Variation of standard deviation and correlation coefficient of V_S with depth for generic and site-specific conditions (adapted from Toro [1995]). 17

Figure 2.3 (a) Modulus reduction and (b) damping curves for soils with different plasticity indexes [Vucetic and Dobry 1991]. 20

Figure 2.4 Illustration of pseudo reference strain γ_r and effect of α on the shape of modulus reduction curves. 21

Figure 2.5 Effect of depth on reference shear strain (γ_r) for different categories of soils [Roblee and Chiou 2004]. 23

Figure 2.6 Variation of reference shear strain (γ_r) versus confining stress (σ'_0/p_a) for different models. 24

Figure 2.7 The data for normalized modulus from the resonant column and torsional shear tests (from Darendeli [2001]). 25

Figure 2.8 An example of the mean and standard deviation of modulus reduction curves [Darendeli 2001]....26

Figure 2.9 Standard deviation of G/G_{max} for a Quaternary soil (OCR = 1.0, PI = 20 and σ'_0 = 100 kPa from Darendeli [2001] and Zhang et al. [2008] models. Values below G/G_{max} of 0.1 are not shown due to lack of data for those large strain levels. 26

Figure 2.10 Backbone curve and strength ratio derived from Darendeli [2001] model for an example soil with PI = 20, OCR = 2, and V_S = 180 m/sec. 27

Figure 2.11 (a) Normalized SPT blow count versus friction angle (adjusted from Hatanaka and Uchida [1996] to use 60% SPT efficiency instead of 78%) as measured from frozen samples; and (b) normalized CPT tip resistance versus drained triaxial friction angle [Kulhawy and Mayne 1990]. 29

Figure 2.12 Contours of state parameter (ψ) (for granular soils) on friction ratio (sleeve friction/tip resistance) versus normalized cone penetration resistance [Robertson 2012] classification chart. The zone numbers 1–9 in the chart correspond to soil descriptions provided by Robertson. Zones 5–7 correspond to granular soils. 30

Figure 2.13 An example of modulus reduction and stress-strain curves from Darendeli [2001], reference strain model, and hybrid procedure (PI = 20%, OCR = 1.5, σ'_0 = 100kPa, V_S = 135 m/sec, and (γ_1 = 0.1%). 33

Figure 2.14 Schematic illustration of constructing shear strength–adjusted modulus reduction curves [Yee et al. 2013]. 34

Figure 2.15 Calculation of damping ratio using the area of cyclic loops [Kramer 1996]....35

Figure 2.16 An example of standard deviation of soil damping for Quaternary soil (PI = 20, OCR = 1, and σ'_0 = 100 kPa). 38

Figure 2.17 An example of damping curves for a soil (PI = 0, OCR = 1, and σ'_0 = 100 kPa) from Masing rule [1926] and Darendeli [2001] model. 40

Figure 2.18 Schematic illustration of different viscous damping models (modified from Kwok et al. [2007]). 41

Figure 2.19 Comparison of computed spectra, amplification factors, and spectral shapes of predicted motions at La Cienaga site using equivalent-linear and nonlinear methods of analysis (adapted from Stewart and Kwok [2008]). 44

Figure 2.20 Pseudo-spectral acceleration ratios for predicted motions from equivalent-linear and nonlinear analyses plotted against strain index γ_{ind}. Results show that the ratios depart from unity at high frequencies, indicating problem with equivalent-linear analyses. Modified from Kim et al. [2014] by B. Kim (personal communication, 2014)....46

Figure 2.21 Variation of strain index values where PSA from equivalent-linear analysis are biased low relative to PSA from nonlinear analysis. The plot shows the space where equivalent-linear analyses are effectively unbiased relative to nonlinear analysis, and where increasing amount of bias are observed (modified from Kim et al. [2013]).....47

Figure 2.22 (a) Location of example site (downtown Los Angeles) marked on southern California fault map by Grant and Rockwell [2002]; and (b) UHS for 0.2%, 2%, and ~20% in 50-year hazard levels (rupture forecast model: UCERF2, GMPE: see Boore et al. [2014]).....49

Figure 2.23 Contours of $\rho(T_1, T_2)$ based on Baker and Jayaram [2008] relationships.....50

Figure 2.24 Two examples of CMS compatible with the 2% in 50-year UHS for the example site in downtown Los Angeles at matching periods of (a) 0.5 sec ($\overline{\mathbf{M}} = 6.7$, $\overline{R} = 6.8$ km, $\overline{\varepsilon} = 1.71$) and (b) 2.0 sec ($\overline{\mathbf{M}} = 6.9$, $\overline{R} = 11.0$ km, $\overline{\varepsilon} = 1.92$).....50

Figure 2.25 Conditional spectra compatible with the 2% in 50-year UHS at matching period of 2.0 sec for example site in downtown Los Angeles.....51

Figure 2.26 Disaggregation of the 2% in 50-year hazard for 2 sec PSA for the example site for a reference site condition of 760 m/sec. 54

Figure 2.27 CMS-based target spectrum and PSA for 11 selected and scaled motions. Part (a) is Approach 1, using a range of periods (0.01–10 sec). Part (b) is Approach 2, using a single matching period at 2.0 sec.....60

Figure 2.28 Examples of mean amplification plots using input motions selected and scaled to a single hazard level using input motions scaled and selected per Approaches 1 and 2 in Section 2.5.3. One fit is based on constraining f_2 and f_3, from an empirical model (SS14 = Seyhan and Stewart [2014]). The second fit is based on constraining f_1 from weak motion GRA results and f_3 from SS14. The effect of $\Delta D_{\min}$ is also shown for the weak-motion GRA constraint.....61

Figure 2.29 Example mean amplification values from GRA and mean fit using Equation (2.21) with f_3 fixed at 0.1g. Dashed line shows truncation at weak motion amplification level.....63

Figure 2.30 Interpolation for calculating f_1 and f_2 values based on semi-empirical model and GRA-based values of f_1 and f_2 at six periods. For f_1, the semi-empirical model is taken as the sum of V_{S30}-based term ($\ln F_{lin}$) from Eq. 6 of BSSA14 and basin depth term F_{z1} from Eq. 9 of BSSA14. Basin depth of z_1 = 4.2 km was used for the site location in Figure 2.22. For f_2, the semi-empirical model is taken as term f_2 in Eq. 8 from BSSA14.....65

Figure 3.1 Velocity profiles and soil properties for three sites investigated by Li and Assimaki [2011]: (a) Obregon Park (CE.K400), (b) Los Angeles-La Cienega Geotechnical Array, (c) El Centro-Hwy8/Meloland Overpass (data from Nigbor et al. [2001]).....71

Figure 3.2 Contribution of different sources of variability to site amplification variability for La Cienega site [Li and Assimaki 2011]. 72

Figure 3.3 Velocity profile of the Sylmar County Hospital (SCH) site in southern California [Gibbs et al. 1999]. 73

Figure 3.4 Contribution of different sources of variability to ϕ_{lnY} for SCH site [Rathje et al. 2010]. 74

Figure 3.5 Schematic illustration of Turley Flat vertical arrays and the velocity profile of Valley Center site [Kwok et al. 2008]. 75

Figure 3.6 Standard deviation of amplification function and its different components for Turkey Flat site during Parkfield earthquake [Kwok et al. 2008].....76

Figure 3.7 V_S profile of the two sites studied by Bazzurro and Cornell [2004b]. 77

Figure 3.8 Average contribution of randomizing soil properties in $\phi_{\ln Y}$ [Bazzurro and Cornell 2004b]. 78

Figure 3.9 Bias in prediction of surface PSA from KiK-net Japanese data, Between-site standard deviation of residuals, and Within-site standard deviation of residuals [Kaklamanos et al. 2013].....80

Figure 3.10 Components of standard deviation of site amplification using analyses of Taiwan ground motion data [Lin et al. 2011]. 81

Figure 3.11 Different components of standard deviation of site amplification obtained from KiK-net data [Rodrigues-Marek et al. 2011]. 82

Figure 3.12 Standard deviation of between-site residuals (ϕ_{S2S}) from different regions (from Rodriguez-Marek et al. [2013].....84

Figure 3.13 Standard deviation of between-site residuals (ϕ_{S2S}) calculated from Atkinson [2006]. 84

Figure 3.14 Synthesis of standard deviations of site amplification obtained from simulation-based studies. 85

Figure 3.15 Synthesis of $\phi_{\ln Y}$ results obtained from data-based studies. 86

Figure 3.16 Difference between simulation-based studies and data-based studies on $\phi_{\ln Y}$ 86

Figure 3.17 Standard deviation of between-site residuals (ϕ_{S2S}). Discrete symbols are regional results from Rodriguez-Marek et al. [2013]. Other studies identified in legend. 87

Figure 4.1 Snapshot of '*XY* Plots' EXCEL spreadsheet used for developing amplification function when x_{IMref} is defined over narrow range of amplitudes. Parameters f_2 and f_3 are constrained from empirical model. 90

Figure 4.2 Snapshot of '*XY* Plots' EXCEL spreadsheet used for developing amplification function when x_{IMref} is defined over narrow range of amplitudes and weak motion (elastic) site amplification is specified. Parameters f_1 and f_3 are constrained from empirical model. 91

Figure 4.3 Snapshot of '*XY* Plots' EXCEL spreadsheet used for developing amplification function when x_{IMref} is defined over wide range of amplitudes. Option for specifying weak motion (elastic) site amplification is provided (this can be turned off by specifying -999 for Y_{elas} in cell U4). 92

Figure 4.4 Snapshot of 'Interpolation' EXCEL spreadsheet used for interpolating site coefficients and transitioning the site amplification to empirical values beyond the site period. 94

Figure 4.5 A snapshot of 'APPROX_PSHA' EXCEL spreadsheet for implementing the results of GRA in PSHA using hybrid, modified hybrid, and convolution methods. 95

Figure 4.6 An example of calculated median response spectrum for M = 6.5, R = 20 km, Reference V_{S30} = 760 m/sec, basin depth = 100 m, f_1 = 0.5, f_2 = -0.6, f_3 = 0.1, $\phi_{\ln Y} = \phi_{S2S}$ =0.3, and single-site reduction facto r = 0.....96

Figure 4.7 Downtown Los Angeles site: (a) UHS for rock, soft-soil, and firm-soil sites for APE = 0.001025; (b) Hazard curves calculated from different methods for the soft-soil site for PGA and PSA (1 sec); (c) hazard curves calculated from different methods for the stiff-soil site; and (d) disaggregation of hazard for APE = 0.001025 for PSA (1 sec) for rock site, and (e) disaggregation of hazard for APE = 0.001025 for PSA (1 sec) for soft-soil site. 98

Figure 4.8 San Francisco site: (a) UHS for rock, soft soil, and firm soil sites for APE = 0.001025; (b) hazard curves calculated from different methods for the soft-soil site for PGA and PSA (1 sec); (c) hazard curves calculated from different methods for the stiff-soil site; (d) disaggregation of hazard for APE = 0.001025 for PSA (1 sec) for rock site; and (e) disaggregation of hazard for APE = 0.001025 for PSA (1 sec) for soft-soil site. 99

Figure 4.9 Sacramento site: (a) UHS for rock, soft-soil, and firm-soil sites for APE = 0.001025; (b) hazard curves calculated from different methods for the soft-soil site for PGA and PSA (1 sec); (c) hazard curves calculated from different methods for the stiff-soil site; and (d) disaggregation of hazard for APE = 0.001025 for PSA (1 sec) for rock site; and (e) disaggregation of hazard for APE = 0.001025 for PSA (1 sec) for soft-soil site. 100

Figure A.1 Soil profile and geotechnical information for the example site having soft-soil conditions. 119

Figure A.2 Peak ground acceleration and maximum shear strain profiles for the example site. The input motions for this case are selected and scaled for compatibility with a single hazard level (Approach 1 in Section 2.5.3).....120

1 Introduction and Literature Review

This research is directed at addressing three practical issues related to the analysis of site effects and their implementation in probabilistic seismic hazard analysis (PSHA):

1. When is the use of geotechnical one-dimensional (1D) ground response analysis (GRA) beneficial relative to the use of ergodic (i.e., not site-specific) empirical site terms?
2. When site response is estimated using GRA, what simple methods can be used to merge the GRA results with a PSHA for reference-rock sites?
3. When GRA is to be performed, what methods of analysis should be used and how should parameter uncertainties be accounted for?

In this report, we address the first and third questions through synthesis of findings from the literature. Our original contributions at this early stage of the work are focused on the second issue. Sections 1.1–1.3 below synthesizes relevant literature related to Questions 1 and 2. Subsequent chapters of this report provide recommendations for GRA protocols related to Question 3 (Chapter 2), develop required standard deviation terms for GRA implementation (Chapter 3), and describe preliminary versions of relatively robust and simplified analytical tools for GRA implementation in PSHA (Chapter 4). Chapter 5 summarizes our findings and provides recommendations for future work.

1.1 ACCURACY OF 1D GROUND RESPONSE ANALYSIS

It is widely assumed by geotechnical engineers that performing GRA will improve the accuracy of predicted ground motions relative to the use of median predictions from empirical ground motion prediction equations (GMPEs) with their site terms. In this context, implies the use of models limited to 1D shear-wave propagation through horizontal layers. Such analyses can capture impedance, nonlinear, and resonance effects.

However, while site response can include important contributions from the wave propagation mechanics simulated in GRA, site response as a whole is considerably more complex. True site response represents the difference between ground motions for a given site condition and what would have occurred had the site had a reference condition (typically rock with a particular V_{S30}). Processes that can control site response in this context include surface waves, basin effects (including focusing and basin edge-generated surface waves), and topographic effects. Because GRA only simulates a portion of the physics controlling site response, there should be no surprise that it is not always effective at accurately predicting site effects.

In this section, we review two studies that have investigated the accuracy of site response predictions using GRA procedures. Baturay and Stewart [2003] considered ground surface recordings at well-characterized sites in California. Thompson et al. [2012] considered vertical array recordings from Kiban-Kyoshin network (KiK-net) sites in Japan.

1.1.1 California Surface Records: Baturay and Stewart [2003]

The goal of this study was to investigate potential benefits of equivalent-linear (EL) 1D GRA compared to empirical site terms in GMPEs. This was undertaken by comparing observations to predictions. The observations were 134 recorded ground surface motions from 68 sites. All sites have surface instruments. Predictions were based on a rock GMPE combined with empirical site factors and a rock GMPE combined with site-specific GRA results.

The GMPE used in the calculations was the Abrahamson and Silva [1997] rock relationship. The empirical site amplification factors that were used are based on surface geologic conditions as given by Stewart et al. [2003]. The ground response analyses were performed using EL methods implemented in the program SHAKE91 [Idriss and Sun 1992]. Input ground motions for the GRA consisted of recordings from sites having geologic conditions similar to those at the base of the geotechnical profile (typically rock). The input motions were selected from events having similar source and path characteristics to those at the soil recording site (hence, different input suites were selected for each soil recording). The ensemble of inputs used for a particular GRA preserved record-to-record variability but was adjusted (as needed) to match the shape of a target spectrum consisting of the rock GMPE median plus the applicable event term.

The results for some examples of different sites and different events are shown in Figure 1.1. In most cases, GRA predicts the surface spectrum better than alternative of a GMPE combined with a generic site term. However, there are cases of large bias. For example, the Saturn School site recording from the 1994 Northridge earthquake substantially exceeds all predictions (including GRA). This strongly negative bias is likely caused by strong path and site effects not considered in the predictions. The site is in a deep sedimentary basin, which can produce complex site effects.

Residuals were computed as the difference of natural logs (observation minus prediction) for each recording and prediction method. The mean and standard deviation of residuals are plotted for different site categories in Figure 1.2, where GRA results are seen to be practically unbiased for spectral periods $T < \sim 1$ sec in well-populated site categories (NEHRP C and D), but they underestimate the ground motion at longer periods. Based on the standard deviation of the residuals (Figure 1.2), GRA reduced dispersion at soft sites for $T < \sim 1$ sec, but these reductions are not apparent for stiff-soil sites nor at long periods (for any site condition).

In summary, the result from the Baturay and Stewart [2003] work indicate improved predictions relative to generic site terms for soft sites (especially the Hlm category) having large impedance contrasts within the profiles. The relative effectiveness of the GRA predictions is most clearly illustrated by the reduced standard deviation of residuals for Hlm sites at short periods.

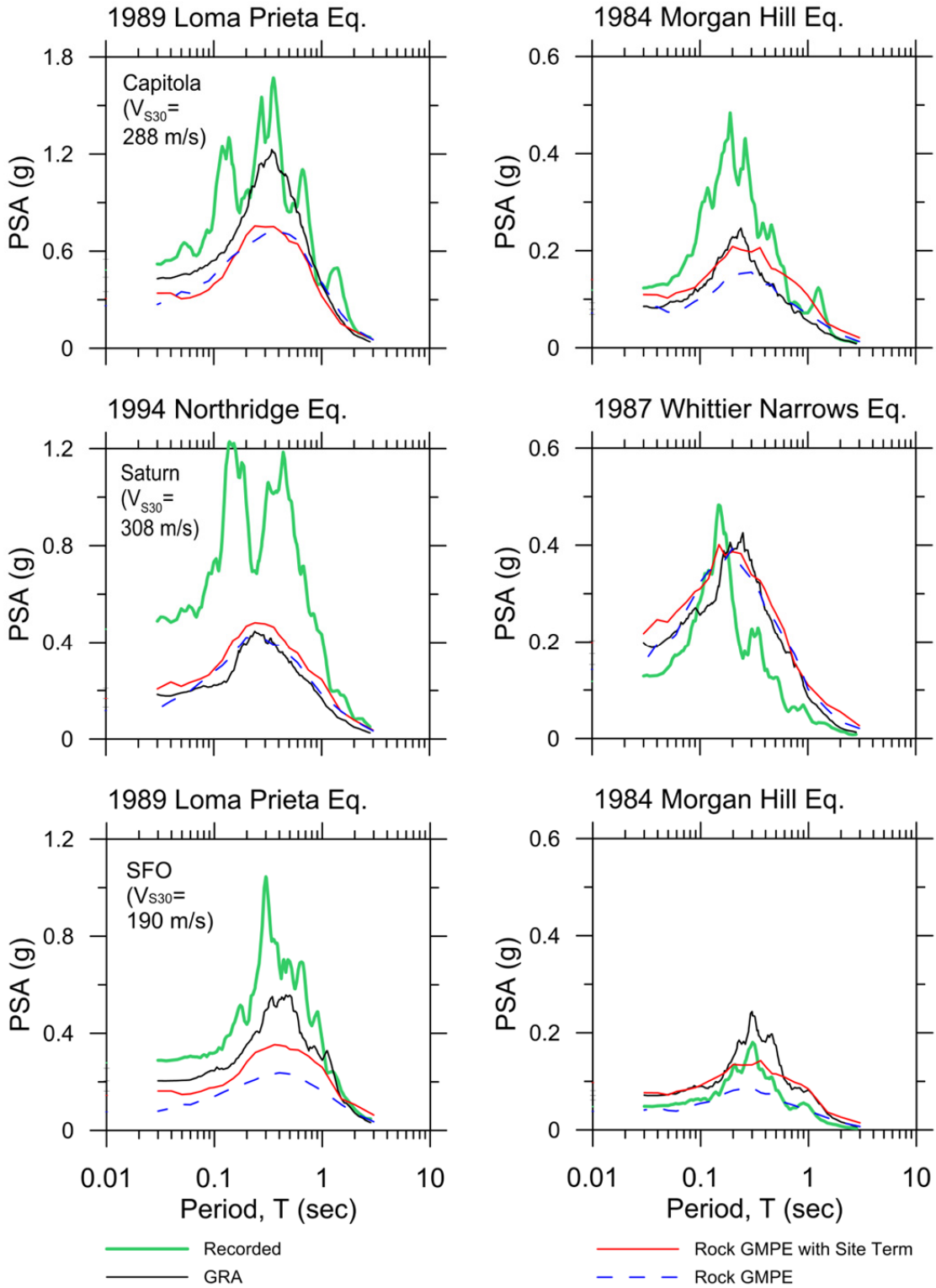

Figure 1.1 **Comparison of recorded spectra to two sets of predictions: rock GMPE with empirical amplification factors and rock GMPE with GRA [Baturay and Stewart 2003]; rock GMPE spectrum is also shown.**

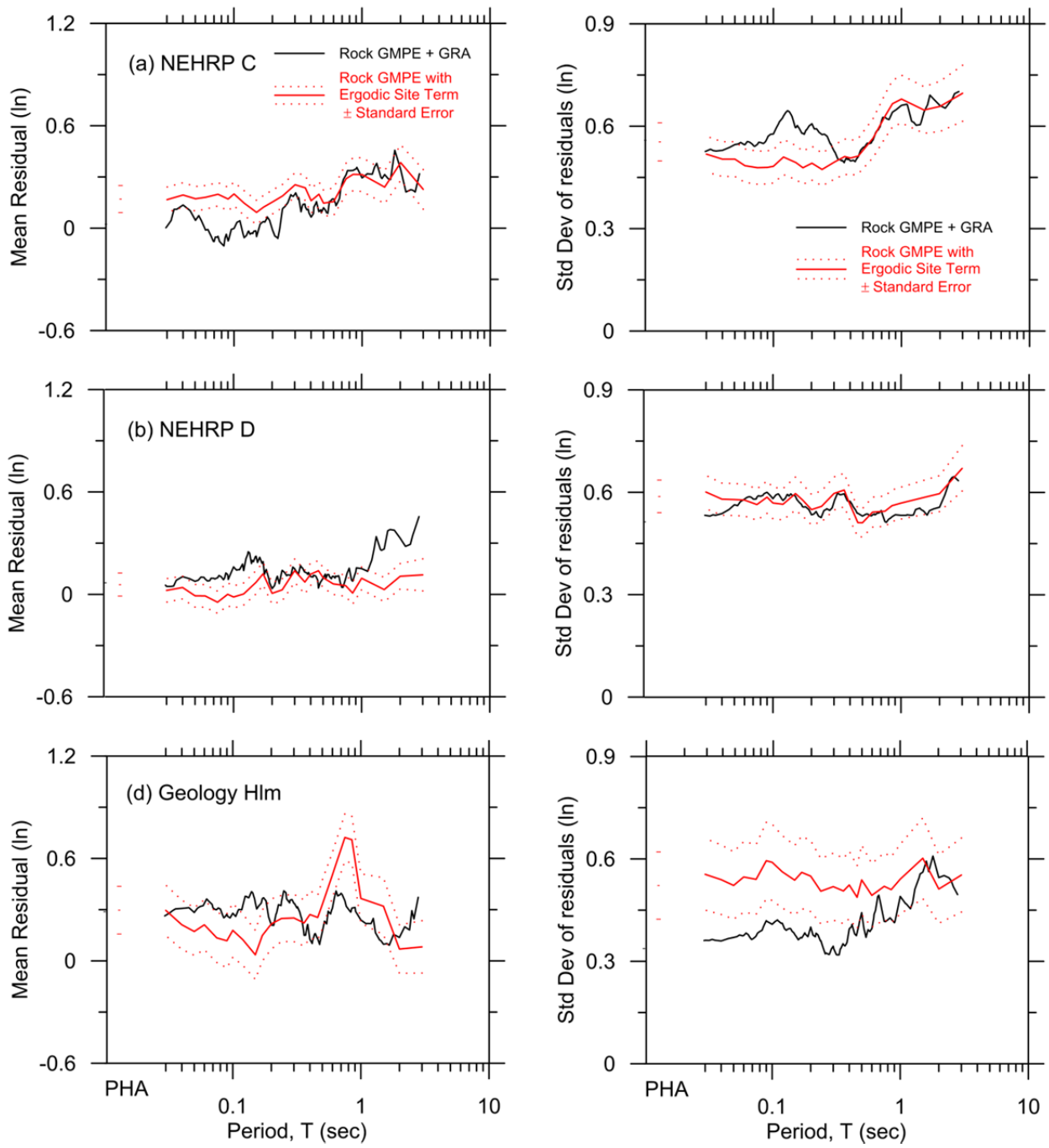

Figure 1.2 **Prediction residuals and their standard deviations for NEHRP C, D, and Hlm sites (Holocene lacustrine or marine geology); modified from Baturay and Stewart [2003].**

1.1.2 Japan Vertical Array Data: Thompson et al. [2012]

Thompson et al. [2012] studied 100 KiK-net sites in Japan in order to assess the variability in site amplification and the performance of linear 1D GRA. These sites have recorded a large number of surface and downhole (in rock) recordings. The presence of multi-depth records enables the

calculation of empirical transfer functions directly from surface $G(f,x_1)$ and downhole $G(f,x_2)$ amplitude spectra:

$$H(f) = \frac{G(f,x_1)}{G(f,x_2)} \tag{1.1}$$

where $H(f)$ is the empirical transfer function. For GRA, they used the program NRATTLE [Boore 2005], which performs linear GRA using quarter-wavelength theory. In order to minimize the potential for nonlinear effects, only records having a ground surface peak ground acceleration (PGA) < 0.1*g* were selected.

Empirical transfer functions were computed with Equation (1.1) using available data meeting certain selection requirements. In total, 3714 records from 1573 earthquakes were considered for the 100 KiK-net sites using. The mean and 95% confidence intervals were computed across all selected recordings at a given site, with the example results (for two sites) given in Figure 1.3; transfer functions from the quarter-wavelength GRA are also shown in Figure 1.3. Figure 1.3(a) provides an example of poor fit between the data and GRA whereas Figure 1.3(b) shows a good fit. Goodness-of-fit was quantified using Pearson's sample correlation coefficient (r); a value of $r = 0.6$ taken as the threshold for good fit. The corresponding r values for the two sites in Figure 2.3 are 0.10 for the poor fit site and 0.79 for the good fit site.

Looking across the 100 sites, only 18 had a good fit of GRA to the data per the $r > 0.6$ criterion. This suggests a surprisingly low rate of satisfactory results (18%). To provide insight into possible causes of these misfits, suites of SASW tests were performed in the vicinity of selected accelerographs. Dispersion curves (phase velocity versus frequency) for the two example sites are shown in Figure 1.3. The results show that there is a large degree of variability in the dispersion curves for the poor-fit site and consistency in the dispersion curves for the good-fit site. These and other similar results for additional sites indicate that geologic complexity, as reflected by spatial variability in the Rayleigh wave velocity structure, may correlate to the accuracy of GRA prediction. More complex geologic structure would be expected to produce three-dimensional (3D) site effects that are not captured by GRA.

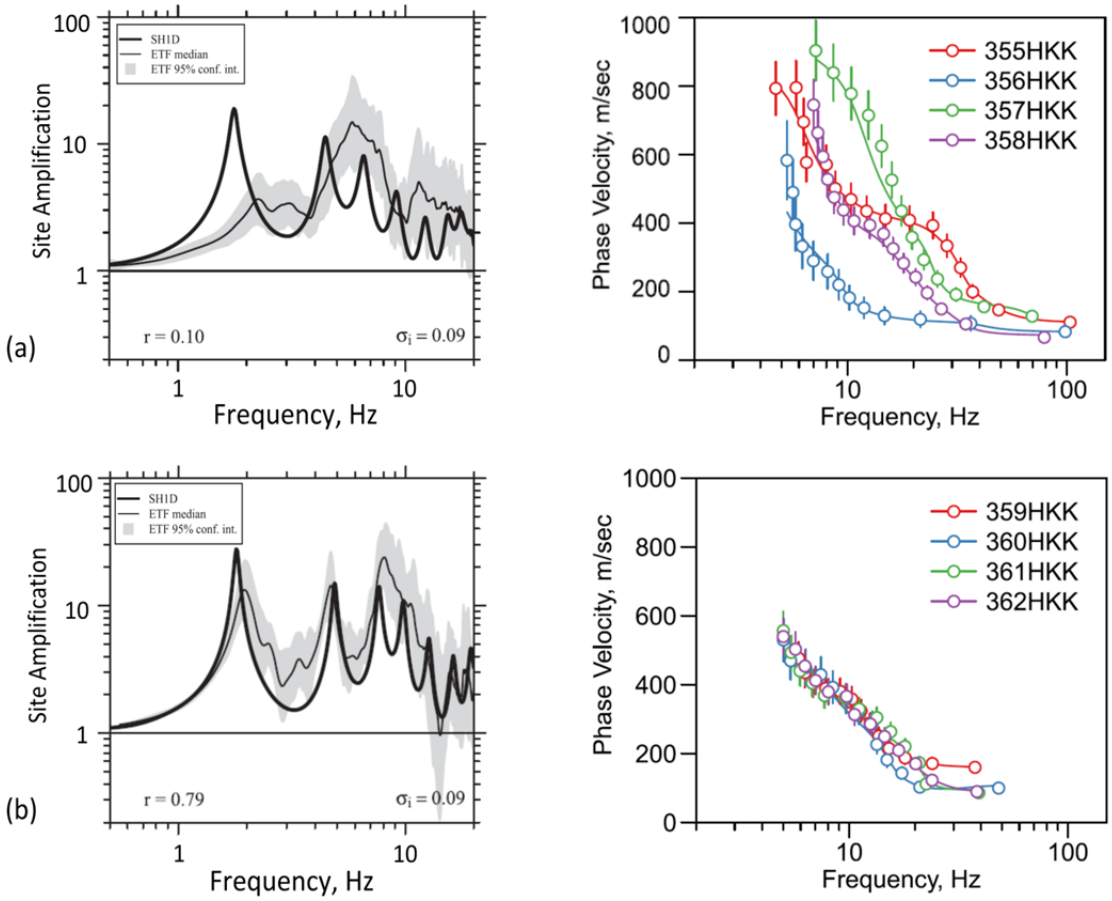

Figure 1.3 **Surface-to-downhole transfer functions indicating site amplification effects from data (marked as ETF) and GRA (marked as SH1D). Part (a) provides an example of poor fit. Part (b) shows good fit. The right side of the figure shows dispersion curves from four SASW tests conducted in the vicinity of the sites [Thompson et al. 2012].**

1.2 MERGING RESULTS OF GRA WITH PSHA

Ground response analyses are deterministic computations of site response phenomena given certain input parameters. The results of these calculations are typically merged in some way with a probabilistically-derived ground motion hazard for rock site conditions. This section describes several ways of combining these analysis results. Both probabilistically robust and simplified methods are considered. In Chapter 4 we apply these methods and provide recommendations on their application. This section focuses on presentation of the methods, with relatively limited examples drawn from the literature.

1.2.1 Site-Specific Nonlinear Ground Motion Amplification Function

Ground response analysis results will generally provide levels of amplification for a particular intensity measure (IM) that depend on the strength of the input. For example, if the input motion is weak (peak acceleration of 0.001*g*), peak ground acceleration (PGA) amplification might for

example be 2.0 for a particular site and input motion, whereas a strong input might produce de-amplification (i.e., PGA amplification < 1.0). Moreover, even for a given input motion amplitude, there can be considerable scatter in the computed site amplification due to variations in the input motion frequency content and variations in the dynamic soil properties that might be considered in GRA runs. As an example, Figure 1.4 shows computed levels of PGA amplification (denoted as Y) in natural log units. The amplification Y is computed from the difference between the ground surface IM (denoted Z) and input motion IM (denoted X):

$$\ln Y = \ln Z - \ln X \tag{1.2}$$

The trend of the site amplification with input motion amplitude ($Y|X$) can be represented by a regression fit through the analysis results. As shown in Figure 1.4, this can be accomplished with a linear relationship (as recommended by Bazzurro and Cornell [2004a]) or a nonlinear relationship. The linear relationship has the form:

$$\ln \overline{Y}(f) = c_1 + c_2 \ln\left(x_{IMref}\right) \tag{1.3}$$

where the overbar on Y indicates mean amplification, c_1 and c_2 are regression coefficients, and x_{IMref} represents the amplitude of shaking for the reference site condition. Parameter c_2 is particularly important, as it represents the effects of nonlinearity; it is typically negative. Parameter x_{IMref} can take several forms: it is an intensity measure that can be defined at the same frequency as $\overline{Y}(f)$ or using an alternative IM (PGA is typical). Moreover, depending on the application, it may be defined as the median of the IM given a controlling magnitude and distance, or computed using hazard analysis (in which case it is usually larger than the median).

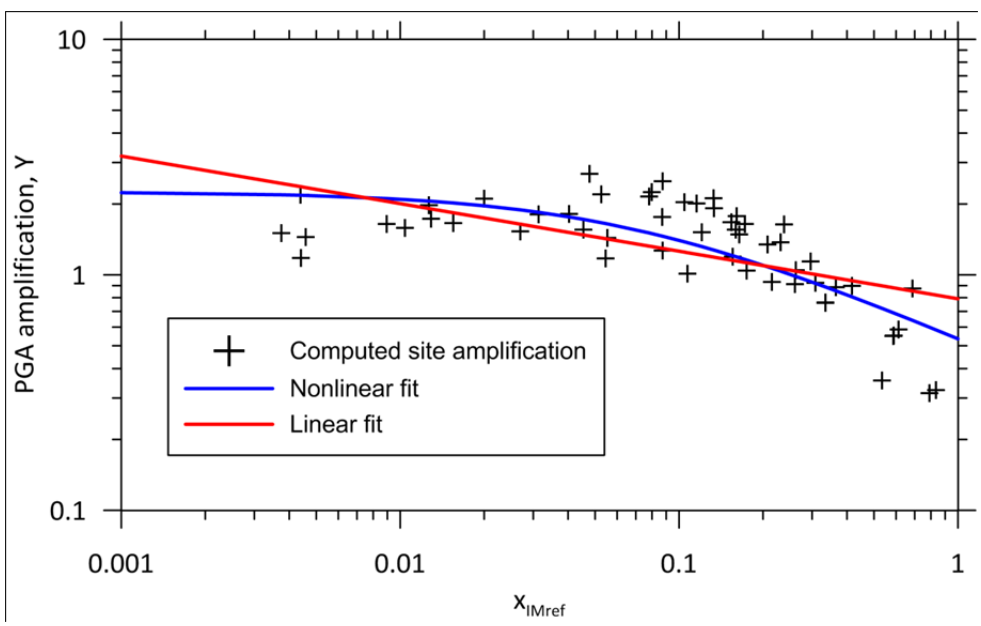

Figure 1.4 **Intensity measure amplification levels from individual GRAs (symbols) and fit curves. A downward slope in the fit curves illustrates the effects of nonlinearity.**

Equation (1.3) can be non-physical for low values of input X, where the amplification should converge towards a flat (zero slope) trend corresponding to linear conditions. Equation (1.3) cannot capture this condition. To overcome this difficulty, an alternative nonlinear expression that has been used for a number of applications is recommended. An expression used by Abrahamson and Silva [1997] and Goulet et al. [2007] is as follows:

$$\ln \overline{Y}(f) = f_1^{'} + f_2^{'} \ln\left(x_{IMref} + f_3^{'}\right) \tag{1.4}$$

We modify Equation (1.4) to make the term inside the logarithm function dimensionless, as follows:

$$\ln \overline{Y}(f) = f_1 + f_2 \ln\left(\frac{x_{IMref} + f_3}{f_3}\right) \tag{1.5}$$

Equation (1.5) matches the form used by Seyhan and Stewart [2014] (who took x_{IMref} as the median PGA). The parameters in Equations (1.4) and (1.5) can be related to each other. We expand the right side of Equation (1.5) as follows:

$$f_1 + f_2 \ln\left(\frac{X(f) + f_3}{f_3}\right) = f_1 + f_2\left[\ln\left(x_{IMref} + f_3\right) - \ln\left(f_3\right)\right] = f_1 + f_2 \ln\left(x_{IMref} + f_3\right) - f_2 \ln\left(f_3\right) \tag{1.6}$$

Equating the right side of Equation (1.6) to Equation (1.4), we find:

$$f_3 = f_3^{'} \tag{1.7}$$

$$f_2 = f_2^{'} \tag{1.8}$$

$$f_1 = f_1^{'} + f_2 \ln\left(f_3\right) = f_1^{'} + f_2^{'} \ln\left(f_3^{'}\right) \tag{1.9}$$

$$f_1^{'} = f_1 - f_2 \ln\left(f_3\right) \tag{1.10}$$

Adopting the form of the equation in Equation (1.5), f_2 represents nonlinearity, f_1 represents weak motion (linear) amplification, and f_3 represents the level of reference site ground shaking below which the amplification converges towards a linear (constant) upper limit. Fits through the GRA results using Equations (1.3) and (1.5) are shown in Figure 1.4. The linear fit can be established using linear least squares regression in logarithmic space [ln(Y) versus ln(x_{IMref})]. The analysis is somewhat more involved in the case of the nonlinear fit, which is addressed further in Chapter 4.

The standard deviation of ground motions is equally important as the mean for probabilistic applications. At issue for the present problem is the within-event standard deviation of the ground surface motion evaluated from GRA (ϕ_{lnZ}) given the standard deviation of the input (ϕ_{lnX}) and of the amplification (ϕ_{lnY}). For the case of a linear (in log units) amplification relationship as in Equation (1.3), Bazzurro and Cornell [2004a] derived the following relationship:

$$\phi_{\ln Z} = \sqrt{(c_2 + 1)^2 \phi_{\ln X}^2 + \phi_{\ln Y}^2} \tag{1.11}$$

Note that when the site response is strongly nonlinear (strongly negative c_2), ϕ_{lnZ} will often be reduced relative to ϕ_{lnX}. This is a real physical phenomenon that is observed in recordings (e.g., Boore et al. [2014]).

When the site amplification is represented through the nonlinear relationship given in Equation (1.4), the standard deviation can be shown to be [Goulet et al. 2007]:

$$\phi_{\ln Z} = \sqrt{\left(\frac{f_2' x}{x + f_3'} + 1\right)^2 \phi_{\ln X}^2 + \phi_{\ln Y}^2} \tag{1.12}$$

The expression can be used with site amplification from Equation (1.5) by replacing f_2' with f_2 and f_3' with f_3. As described further in Chapter 3, further modifications to Equation (1.12) can, in principal, be implemented to account for the effects of reduced uncertainty associated with site-to-site aleatory variability.

1.2.2 Hybrid Method

The hybrid method is the most convenient and widely used approach for implementing GRA results with rock hazard [Cramer 2003]. In this method, we simply multiply the rock motion from a hazard curve at the desired exceedance probability level by the mean amplification conditional on that rock motion. In log units, this is addition and can be expressed as:

$$\ln(z) = \ln(x) + \ln\left(\overline{Y} \middle| x_{IMref}\right) \tag{1.13}$$

where x is the IM on rock (from the rock hazard curve), z is the surface motion, and $\overline{Y}$ is the mean value returned by the amplification function for input motion x_{IMref}. The amplification function depends on rock motion x_{IMref} as described in the previous section. This method is referred to as "hybrid" because it combines a probabilistic rock motion with deterministic site amplification.

When x and z represent the same IM (e.g., both are PSA at a given oscillator frequency f, and the amplification is PSA amplification at that frequency), x_{IMref} can be replaced with x in Equation (1.13). This choice of x_{IMref} is particularly convenient, because the ground motion level used in the site amplification function is known from the hazard analysis. When x_{IMref} is defined using a different IM, it must be computed from the hazard analysis result x (and its disaggregation). In this case, x_{IMref} can be conceptualized as the most likely value of the reference *IM* (e.g., PGA) on rock, given the hazard estimate of the IM of interest (x).

For this case of x and x_{IMref} representing different IMs, we compute x_{IMref} from the epsilon of the rock motion (ε_{lnx}, obtained from disaggregation) and knowledge of the correlation coefficient between epsilons for different IMs ($\rho_{lnIMref\text{-}lnX}$) [Baker and Jayaram 2008]. This can be accomplished by adapting the well-known conditional mean spectrum (CMS) methodology of Baker and Cornell [2006] to the present problem. Under this approach, we recognize that the

natural log of x_{IMref} is the sum of its mean value ($\ln \bar{X}_{IMref}$) and its appropriate number of standard deviations above the mean.

$$\ln x_{IMref} = \ln \bar{X}_{IMref} + \bar{\varepsilon}_{IMref} \sigma_{IMref} \tag{1.14}$$

The mean and standard deviation in Equation (1.4) are computed from a GMPE using the same mean magnitude and distance found from disaggregation of x. That disaggregation also provides a mean epsilon for x, denoted $\bar{\varepsilon}_{\ln x}$. The mean epsilon for the reference IM can be related to the epsilon for x using the correlation coefficient between the epsilons for these two IMs [Baker and Jayaram 2008]:

$$\bar{\varepsilon}_{IMref} = \bar{\varepsilon}_{\ln x} \rho_{\ln IMref - \ln X} \tag{1.15}$$

For example, in the case of the reference IM (x_{IMref}) being PGA and the IM for x being 1.0-sec pseudo-spectral acceleration (PSA), the correlation coefficient is denoted as $\rho_{\ln PGA\text{-}\ln PSA(1.0)}$ and is equal to 0.57 [Baker and Jayaram 2008].

One drawback to the hybrid approach is that standard deviation terms used in the hazard integral are those for rock, which are not generally appropriate for soil sites as indicated in Section 1.2.1. Another problem is that the controlling sources for soil sites will often be somewhat different from those for rock (typically with greater contributions from more distant sources). These effects are not accounted for in the hybrid approach, because the rock hazard is undergoing a simple (deterministic) modification for site effects. Figure 1.5 illustrates the difference between fully probabilistic soil hazard curves (derived using a soil GMPE) and soil hazard curves derived using the hybrid approach (rock GMPE combined with deterministic site term, taken as the site term from the GMPE). These results, originally presented by Goulet and Stewart [2009], show the hybrid approach produces lower hazard estimates than the more correct fully probabilistic approach.

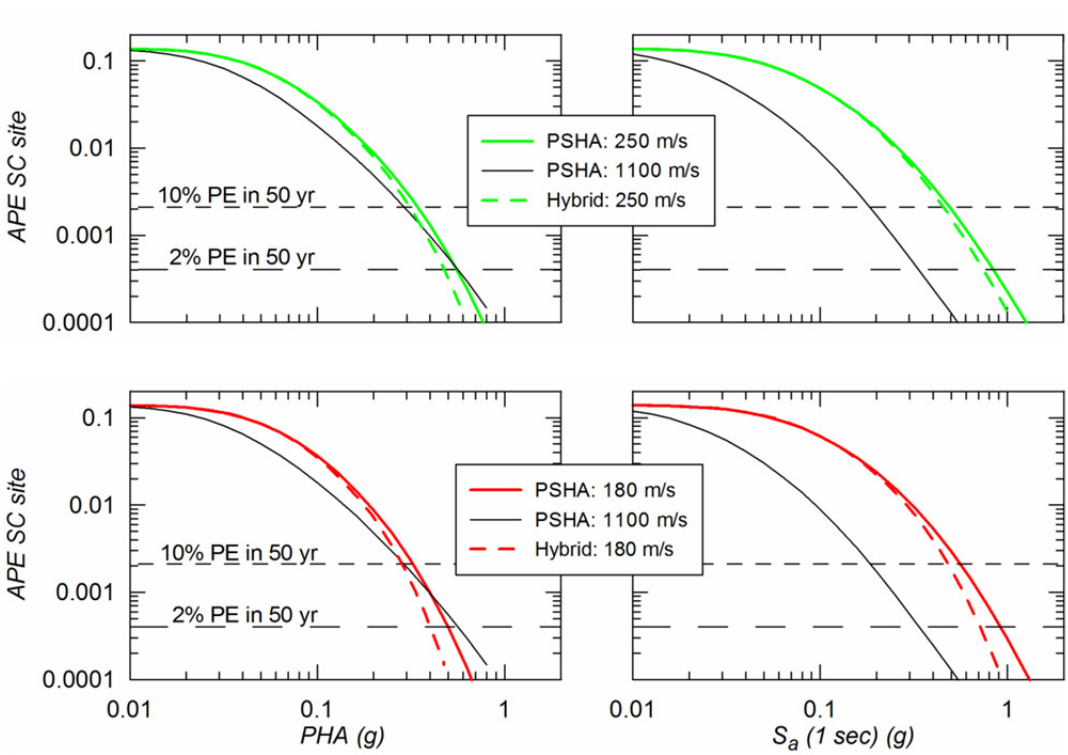

Figure 1.5 **Hazard curves for PGA as derived using fully probabilistic approach (labeled PSHA) and hybrid approach for sites with V_{S30} = 250 and 180 m/sec. The results indicate underestimation of hazard at long return periods with the hybrid method [Goulet and Stewart 2009].**

In addition to the factors mentioned previously, another important reason for the discrepancies in the hazard curves shown in Figure 1.5 is the value of x_{IMref} used within the site amplification function. In the hybrid approach, x_{IMref} is taken from the rock hazard curve and hence has non-zero, generally positive, epsilon ($\bar{\varepsilon}_{\ln x}$ or $\bar{\varepsilon}_{IMref}$). In the PSHA approach using GMPE-based site terms, a mean value of x conditional on M, R, etc. is typically used for x_{IMref} (i.e., epsilon is taken as zero). At long return periods, the larger values of x_{IMref} from the hybrid approach produce greater nonlinearity, which in turn lower the hazard curves.

1.2.3 Modified Hybrid Approach

A modification of the hybrid method was proposed by Goulet and Stewart [2009] in which the value of x_{IMref} used in the amplification function is taken as a mean value ($\bar{\varepsilon}_{IMref} = 0$). Under this approach, the soil ground motion (z) is computed from the rock motion at the desired hazard level (x) as:

$$\ln(z) = \ln(x) + \ln\left(\bar{Y} \middle| \bar{X}_{IMref}(\mathbf{M}, R)\right) \tag{1.16}$$

where the mean amplification $\overline{Y}$ is conditioned on the mean reference site ground motion $\overline{X}_{IMref}$ for the magnitude and distance found from disaggregation. The effectiveness of this approach is examined in Chapter 4.

1.2.4 Modifying the Hazard Integral

The hazard integral used in PSHA (e.g., see Reiter [1990] and McGuire [1995]) includes a term expressing the probability of exceeding site ground motion level z given an event has occurred with magnitude **M** and site-source distance R. For our soil site condition, this exceedance probability is written as $P(Z > z|\mathbf{M}, R)$. The calculation of this probability requires a probability distribution function (taken as log-normal) and its moments (median $\overline{Z}$ and standard deviation σ_{lnZ}). These moments can be readily computed given a rock GMPE (providing $\overline{X}$ and σ_{lnX}) and a site amplification function (providing $\overline{Y}$ and σ_{lnY}). The mean for the soil site condition is obtained as:

$$\ln \overline{Z} = \ln \overline{X} + \ln \overline{Y} \tag{1.17}$$

The standard deviation σ_{lnZ} is obtained from the expressions given in Section 1.2.1 [Equations (1.3). (1.4), or (1.5)]. Note that the within-event standard deviation (ϕ) needs to be combined with the between-event standard deviation (τ) through the square root of sum of variances. This conceptually simple approach is complex in practice because hazard analyses cannot be completed with pre-coded GMPEs, instead requiring editing of the hazard code.

1.2.5 Convolution Method

Bazzurro and Cornell [2004a] recommended a convolution method for combining a nonlinear site amplification function with a rock hazard curve to estimate a soil hazard curve. The principal advantage of this approach relative to the hybrid approach is that uncertainties in the site amplification function are directly incorporated into the analysis (only the mean amplification is used in the hybrid methods).

The convolution is performed as follows:

$$P(Z > z) = \int_0^\infty P\left(Y > \frac{z}{x} \mid x_{IMref}\right) f_X(x)\, dx \tag{1.18}$$

in which $f_X(x)$ is the absolute value of the slope of the hazard curve and all other terms are as defined previously. The probability $P\left(Y > z/x \mid x_{IMref}\right)$ requires an assumed probability density function (taken as log-normal) and the mean and standard deviation of the amplification function ($\ln \overline{Y}$ and ϕ_{lnY}). The mean amplification function is as given in Equations (1.3), (1.4) or (1.5). The standard deviation of the amplification (ϕ_{lnY}) function can be derived in various ways as described further in Chapter 3. As originally described by Bazzurro and Cornell [2004a], x_{IMref} is taken as x, although the approach can in principal be extended for alternate IMs for x_{IMref} using

the procedures given in Equations (1.14) and (1.15). The time interval corresponding to the exceedance probability from Equation (1.18) matches that for the rock hazard curve.

The principal drawbacks of the convolution method are similar to those for the hybrid approach:

- The hazard calculation is based on the standard deviation of the rock motion and cannot account for changes (generally reductions) associated with nonlinear site response.
- The distribution of sources and epsilons controlling the hazard are based on those for rock site conditions. The relative contributions of different sources will generally change for soil sites, which are not taken into account in this analysis.
- The typical limitations of 1D analysis (e.g., at long periods) will cause bias when this method of analysis is implemented.

The principal advantage of the convolution method relative to the hybrid method is that it accounts for uncertainty in the site amplification function.

2 Protocols for Performing Ground Response Analyses and Interpretation of Results

2.1 INTRODUCTION

In this chapter, we review some considerations in performing one-dimensional ground response analyses (1D GRA) for the purpose of estimating site effects. We emphasize the selection of required soil dynamic properties and their uncertainties (Sections 2.2–2.3), the use of equivalent-linear versus nonlinear methods of analysis (Section 2.4), input motion selection (Section 2.5), and developing a site amplification function based on the analysis results.

This chapter emphasizes GRA, which is recognized as one component of site response effects that may also be affected by surface topography and deep basin structure. Impacts of these other site response effects are discussed briefly in Section 1.1. This chapter is intended to build upon a guidelines document for ground response analysis by NCHRP [2012] entitled *Practices and Procedures for Site-Specific Evaluations of Earthquake Ground Motions*. Interested readers are referred to that report for background on the topic. We emphasize some of the most important features of that document and relevant results of more recent work.

2.2 DYNAMIC SOIL PROPERTIES: BACKBONE CURVE

Whether equivalent-linear or nonlinear, GRA require the specification of input parameters describing the backbone curve and soil damping characteristics. This section emphasizes those parameters related to the backbone curve, while Section 2.3 is focused on damping relations.

The backbone curve describes the nonlinear shear stress-strain behavior of a soil element. Figure 2.1 shows an example backbone curve, which can be viewed as representing the monotonic stress-strain response for a non-degrading soil, or as the envelope of peaks of cyclic stress-strain loops for a cyclically sheared specimen. The backbone curve is generally defined by three types of parameters:

1. The initial (or maximum) shear modulus, $G_{\max}$, which is related to the shear-wave velocity V_S as $G_{\max} = \rho\left(V_S\right)^2$;
2. The variation of normalized secant shear modulus with the amplitude of cyclic shear strain (γ_c), typically referred to as a modulus reduction curve $\left(G/G_{\max} - \gamma_c\right)$; and

3. The maximum value of shear stress, which is the shear strength (τ_{ff} = shear stress on the failure plane at failure).

The following subsections describe procedures for developing each of these input parameters and for defining their uncertainty. The definitions of uncertainty are based on data compilations in the literature (i.e., we assume that a sufficiently large volume of data from which to define uncertainty distributions is not available for most sites, although when such data is available, it would supersede the recommendations on uncertainty provided here).

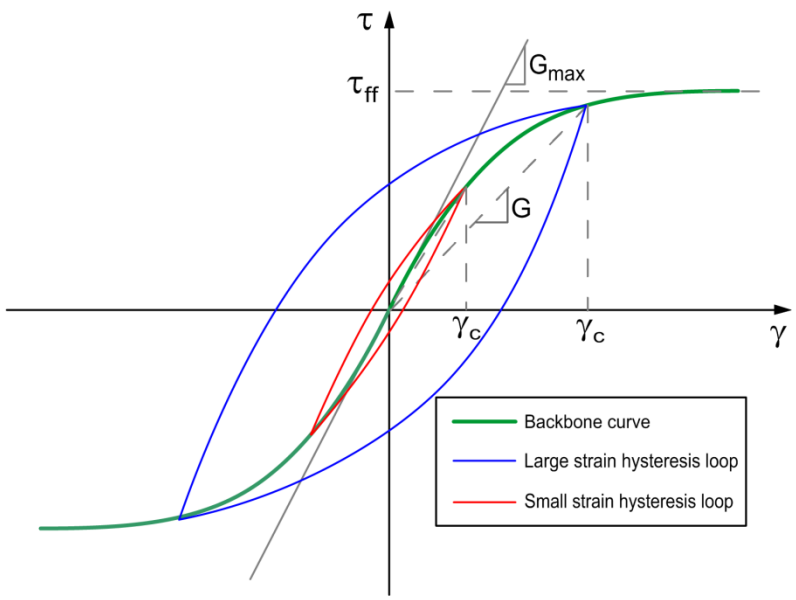

Figure 2.1 Schematic illustration of backbone curve and small strain and large strain hysteresis loops. G_{max} is the maximum (small strain) shear modulus, *G* is the secant shear modulus for a given strain level, and τ_{ff} is the shear stress at failure.

2.2.1 Shear-Wave Velocity Profile and its Uncertainty

Shear-wave velocity (V_S) should be measured using appropriate techniques, which may include surface wave methods, suspension logging, downhole testing, and cross-hole testing. Remi-based techniques (e.g., Louie [2001]) should be avoided due to potential for bias, particularly at depth [Cox and Beekman 2011]. Although numerous techniques exist for estimating V_S from penetration resistance [e.g., Robertson (2009) for CPT and Brandenberg et al. [2010] for SPT], these should not be used for GRA applications, for which results can be very sensitive to small variations in V_S that can only be reliably evaluated using high-quality measurements.

Shear-wave velocity (V_S) profiles measured with the above techniques represent averaged velocities over variable length scales. Suspension logging provides a highly localized measurement adjacent to a borehole at 1m vertical spacing. Downhole and cross-hole methods measure V_S over longer length scales corresponding to the source-receiver separation distances, which are typically on the order of meters to tens of meters. All of these borehole-based methods

have shortcomings near the ground surface, in most cases being considered reliable for depths greater than 3–5 m. At great depth, suspension logging is generally preferred because it requires only one borehole and maintains a consistent source-receiver distance regardless of depth. Surface wave methods can sample much larger dimensions (comparable to the wavelength) and are most reliable at shallow depths.

Regardless of the geophysical technique employed, when multiple V_S profiles are measured at different locations, the V_S profiles will in general not match. These variations in measured velocities, when based on reliable geophysical methods, represent the variability of the geologic structure. Such variations are always present to varying degrees and affect the variability in site response as described in Section 1.1. If the variations in V_S can be measured at a site using multiple profiles, a mean and standard deviation of V_S can be quantified on a site-specific basis. This is desirable because such a characterization would presumably reflect the local geologic conditions. However, in many cases only a single profile is available, which is generally assumed to represent the mean. In such situations, it is necessary to estimate other statistical properties of the V_S distribution (standard deviation and correlation coefficient) using relationships derived for other sites and presented in the literature. Because these relationships are relatively generic, they will not necessarily reflect well the local geologic conditions.

One such set of statistical relations are given by Toro [1995] and are based on 513 shear-wave velocity profiles in California and 44 profiles from the Savannah River site in Georgia, U.S. For a given depth, V_S is assumed to be log-normally distributed with a depth-dependent standard deviation ($\sigma_{\ln V_S}$). As shown in Figure 2.2, values of $\sigma_{\ln V_S}$ are provided for 'generic' and 'site-specific' applications.

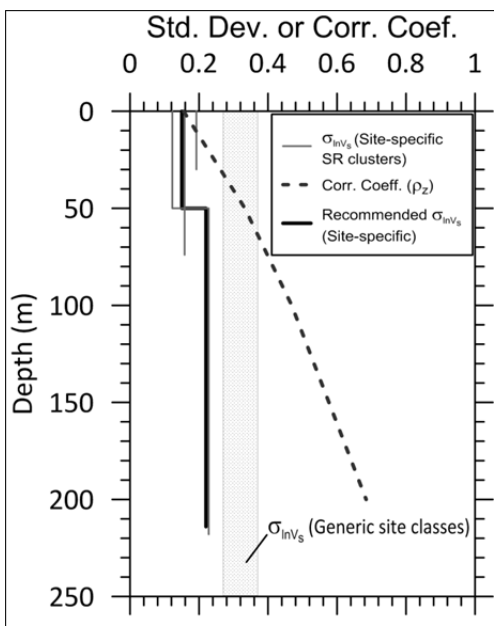

Figure 2.2 Variation of standard deviation and correlation coefficient of V_S with depth for generic and site-specific conditions (adapted from Toro [1995]).

The generic results in Figure 2.2 apply for horizontal separation distances between profiles on the order of several hundred meters to a few kilometers, whereas for site-specific the separation distances range from 2 to 800 m. The generic $\sigma_{\ln V_S}$ is based on statistics for many sites within NEHRP [Dobry et al. 2000] or Geomatrix [Chiou et al. 2008] site classes–they are intended for use with generic mean V_S profiles for each site class. As shown in Figure 2.2, the generic $\sigma_{\ln V_S}$ values for each of the site classes fall within a relatively narrow range from 0.27–0.37. Toro [1995] provides site-specific $\sigma_{\ln V_S}$ values based on clusters of V_S profiles for eight sites (three from Savannah River, Georgia; five from California). Of the clusters considered by Toro [1995], only the three from Savannah River sites have at least 10 profiles. We consider these cluster statistics to be the most reliable information on $\sigma_{\ln V_S}$ from Toro [1995], which we plot in Figure 2.2. A representative value through these three profiles is also shown, which is 0.15 from 0–50 m depth and 0.22 at greater depths. These values are recommended for sites where geologic variability is anticipated to be small, typically in areas of low topographic relief and far from contacts between adjoining geologic units on surface geology maps. As a site specific value of $\sigma_{\ln V_S}$, it is intended for use with a site-specific V_S profile. A depth-dependent model for interlayer correlation of V_S is also given in Figure 2.2.

The Toro [1995] model has been widely used for V_S randomization in GRA studies (e.g., Kottke and Rathje [2008]), in part because it is the only model available. In this randomization approach, a particular realization of shear-wave velocity is given as:

$$V_S(i) = \exp\left(\ln\left[V_{S0}(i)\right] + Z_i \sigma_{\ln Vs}\right) \tag{2.1}$$

in which $V_S(i)$ is the shear-wave velocity in the ith layer, and $V_{S0}(i)$ is the baseline (median) value. Parameter Z_i is a realization of a standard normal distribution for layer *i* that is computed as follows:

$$Z_i = \rho_{1L} Z_{i-1} + \varepsilon_i \sqrt{1 - \rho_{1L}{}^2} \quad \textit{and} \quad Z_1 = \varepsilon_1 \tag{2.2}$$

where Z_{i-1} is the corresponding realization of a standard normal distribution for the previous layer, and ε_i is a separately (and randomly) sampled standard normal variate for layer *i* having zero mean and unit standard deviation. In general the standard deviation used with ε_i can be taken, as appropriate, from the generic or site-specific results in Figure 2.2. Kottke and Rathje [2008] provide generic values of $\sigma_{\ln V_S}$ in the program STRATA, but arguably the site-specific values of $\sigma_{\ln V_S}$, shown in Figure 2.2, are preferred when a site-specific V_S profile is available, and the geologic variability across the site is modest (as described above).

Parameter ρ_{1L} is the interlayer correlation coefficient, which is computed from a depth-dependent correlation (ρ_z) and a layer thickness correlation (ρ_t):

$$\rho_{1L}(z,t) = [1 - \rho_z(z)]\,\rho_t(t) + \rho_z(z) \tag{2.3}$$

$$\rho_z(z) = \begin{cases} \rho_{200}\left[\dfrac{z+z_0}{200+z_0}\right]^b & z \le 200\,\text{m} \\ \rho_{200} & z > 200\,\text{m} \end{cases} \tag{2.4}$$

$$\rho_t(t) = \rho_o \exp\left(\frac{-t}{\Delta}\right) \tag{2.5}$$

where ρ_{200}, z_0, b, ρ_o, and Δ are model parameters, z = depth, and t = layer thickness. The parameters, given in Table 2.1, depend on site condition as represented by NEHRP site category or Geomatrix site class (A-B are rock and shallow soil, and C-D are soil). Also shown in Table 2.1 are the category-specific generic values of $\sigma_{\ln V_S}$. The correlation coefficient model presented in Equations (2.3)–(2.5) is based on the generic profile statistics. A correlation coefficient model based on site-specific cluster statistics has not been developed to our knowledge.

Table 2.1 Model parameters for velocity profile uncertainty for generic site classes [Toro 1995]. NEHRP site classes defined in Dobry et al. [2000]; Geomatrix site categories defined in Chiou et al. [2008].

Parameter	Generic Site Classes					
	Geomatrix A and B	Geomatrix C and D	NEHRP B	NEHRP C	NEHRP D	NEHRP E
σ_{lnVs}	0.46	0.38	0.36	0.27	0.31	0.37
ρ_o	0.96	0.99	0.95	0.97	0.99	0.00
Δ	13.1	8.0	3.4	3.8	3.9	5.0
ρ_{200}	0.96	1.00	0.42	1.00	0.98	0.50
z_o	0.0	0.0	0.0	0.0	0.0	0.0
b	0.095	0.160	0.063	0.293	0.344	0.744

2.2.2 Modulus Reduction and its Uncertainty

(a) Material Specific Testing

Modulus reduction $\left(G/G_{\max}\right)$ versus shear-strain curves (MR curves) can be measured on a site- and material-specific basis using dynamic laboratory testing or estimated using empirical correlations. When measured in the laboratory, typically either cyclic simple shear or resonant column/torsional shear (RCTS) apparatuses are used. In many cases, cyclic simple shear tests encounter difficulty in measuring small strain properties [Doroudian and Vucetic 1995], but are quite effective for evaluating large strain response (including shear failure conditions). RCTS devices often provide the opposite capabilities, with relatively good small strain measurements but a limited ability to induce large strain response. Regardless of device, what these tests provide are hysteretic stress-strain curves from which secant moduli and soil damping can be evaluated. To compute modulus reduction, the secant modulus at a particular strain level is

divided by G_{max}, which is typically taken from a loop developed on the same specimen when sheared at very small strains. It is often the case that these $G_{\max}$ values are much lower than would be expected from *in situ* V_S testing. For the case of clays sampled using relatively high-quality samplers, these differences have been postulated to result from pseudo-overconsolidation from secondary compression [Trudeau et al. 1974], which is lost in sampling. If these disturbance effects can be assumed to be consistent across strain levels, normalization by a laboratory-based $G_{\max}$ is appropriate.

(b) Literature

When material-specific test results are unavailable, MR curves can be estimated from relationships in the literature. A number of 'classical' MR curves have seen widespread use in geotechnical engineering practice, including Seed and Idriss [1970] (generic curves for clay and sand), Iwasaki et al. [1978] (overburden-dependent curves for sand), and Vucetic and Dobry [1991] (PI-dependent curves for clay). As an example, Figure 2.3 shows the PI-dependent MR curves from Vucetic and Dobry [1991] (damping curves are also shown, which are discussed further in Section 2.3). While each of these models has substantially contributed to our knowledge of dynamic soil behavior, recent models are based on more extensive testing, making them a better choice for contemporary GRA.

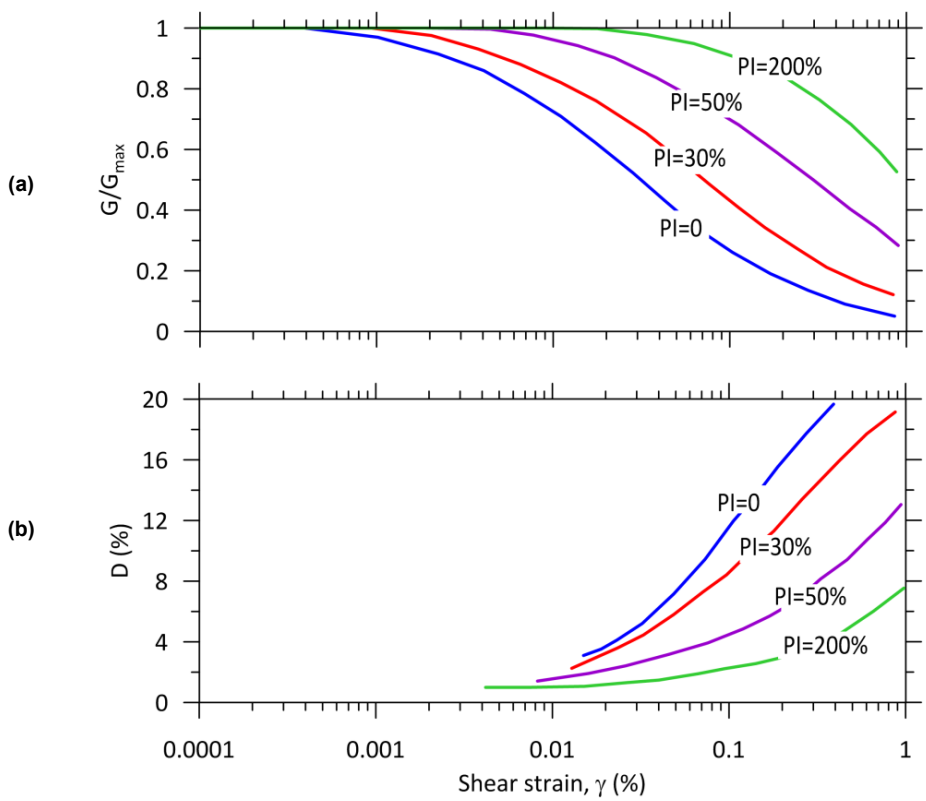

Figure 2.3 **(a) Modulus reduction and (b) damping curves for soils with different plasticity indexes [Vucetic and Dobry 1991].**

Contemporary models for MR curves are based on a hyperbolic function for the backbone curve:

$$\frac{G(\gamma)}{G_{\max}} = \frac{1}{1+\left(\frac{\gamma}{\gamma_r}\right)^{\alpha}} \tag{2.6}$$

The regression parameters in these models are γ_r, referred to as a pseudo-reference shear strain, and curvature coefficient α. As shown in Figure 2.4, both have physical meaning: γ_r is the level of shear strain for which $G/G_{\max} = 0.50$; α describes the steepness of the MR curve about γ_r These parameters are dependent on the soil properties (e.g., PI and C_u) and mean effective stress (σ_0'). While a MR curve using Equation (2.6) can be readily plotted and used over a wide strain range, and this is indeed common practice, the regression parameters are typically based on data that extends to maximum strains of about 0.1–0.3% [Darendeli 2001]. As discussed further in Section 2.2.3, the model is not reliable for larger strains, especially when the shear strength of the soil is approached.

Table 2.2 summarizes the MR attributes of models that utilize the function in Equation (2.6) (selected model coefficients in Tables 2.3–2.4). All of these models were developed from RCTS testing using many samples. As indicated in the table, the Darendeli [2001] model applies to generic soil materials (sand, silt, and clay), but is superseded for relatively coarse-grained granular soils (gravels and sands having mean grain size D_{50} > ~ 0.3 mm) by Menq [2003]. The Zhang et al. [2005] model also applies to mineral (non-organic) soils but was derived entirely from tests on samples from the South Carolina region; therefore, its more general applicability is unknown. A simplified version of the Darendeli [2001] model was prepared by Roblee and Chiou [2004] in which γ_r and α are tabulated on the basis of soil categories defined by fines content and plasticity as given in Table 2.5. Referred to as the GeoIndex model, the tabulated γ_r and α values are given in Table 2.6 and plotted versus depth in Figure 2.5.

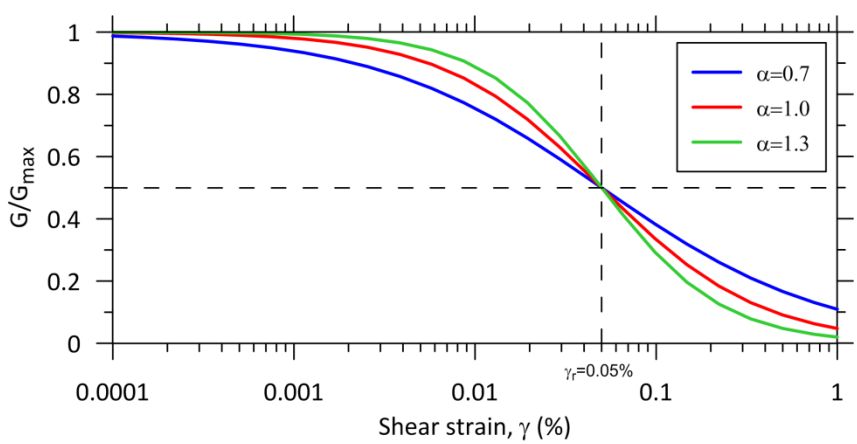

Figure 2.4 Illustration of pseudo reference strain γ_r and effect of α on the shape of modulus reduction curves.

Table 2.2 Summary of attributes of hyperbolic MR curve models from literature.

Reference	Model for γ_r	Model for α	Soil types considered	Applicable strain range
Darendeli [2001][1]	$\gamma_r(\%) = (\phi_1 + \phi_2 + PI \times OCR^{\phi_3}) \times (\sigma_0'/p_a)^{\phi_4}$	$\alpha = \phi_5$	Generic (110 samples from 20 sites)	0.0001–0.5%
Menq [2003][2]	$\gamma_r(\%) = 0.12 \times C_u^{\phi_1} \times (\sigma_0'/p_a)^{\phi_2}$	$\alpha = 0.86 + 0.1 \times \log(\sigma_0'/p_a)$	Granular with D_{50} > ~ 0.3 mm (59 reconstituted specimens)	0.0001–0.6%
Roblee and Chiou [2004]	From table GeoIndex model parameters	From table GeoIndex model parameters	Clay, sand and silt (154 samples from 28 sites)	0.0001–4.0%
Zhang et al. [2005][3]	$\gamma_r(\%) = \gamma_{r1}^{\ k} \ (\sigma_0'/p_a)^k$		Mineral soils in South Carolina (122 samples)	0.0001–0.3%
	Quaternary:	Quaternary:		
	$\gamma_{r1} = 0.011PI + 0.0749$	$\alpha = 0.0021PI + 0.834$		
	$k = 0.316e^{-0.0142PI}$	Residual/saprolite:		
	Residual/saprolite:	$\alpha = 0.0043PI + 0.794$		
	$\gamma_{r1} = 0.0009PI + 0.0385$	Tertiary and older:		
	$k = 0.42e^{-0.0456PI}$	$\alpha = 0.0043PI + 0.794$		
	Tertiary and older:	$\alpha = 0.0009PI + 1.026$		
	$\gamma_{r1} = 0.0004PI + 0.0311$			
	$k = 0.316e^{-0.011PI}$			
Choi [2008]	$\gamma_r(\%) = 0.046(\sigma_0'/p_a)^{0.46}$	$\alpha = -0.298\log_{10}(\gamma_r) + 0.656$	Bandelier Tuff, Pajarito Plateau, NM (38 samples)	0.0001–0.04 %

[1] See Table 2.3 for parameters.
[2] See Table 2.4 for parameters.
[3] γ_{r1} is γ_r at $\sigma_0' = p_a$.

Table 2.3 Parameters for Darendeli [2001] model for modulus reduction.

Parameter	Value
ϕ_1	0.0352
ϕ_2	0.001
ϕ_3	0.3246
ϕ_4	0.3483
ϕ_5	0.92

Table 2.4 Parameters for Menq [2003] model for modulus reduction.

Parameter	Value
ϕ_1	-0.6
ϕ_2	0.382

Table 2.5 GeoIndex soil classes [Roblee and Chiou 2004].

GeoIndex Abbreviation	GeoIndex Soil Description	Passing #200	Plasticity Index
1–PCA	Primarily Coarse –All Plasticity Values	<=30%	All
2–FML	Fine-Grained Matrix–Lower Plasticity	>30%	<=15%
3–FMH	Fine-Grained Matrix–Higher Plasticity	>30%	>15%

Table 2.6 GeoIndex model parameters for modulus reduction [Roblee and Chiou 2004].

GeoIndex Class	1-PCA Soil		2-FML Soil		3-FMH Soil	
Depth (m)	γ_r	α	γ_r	α	γ_r	α
0–10	0.032	0.85	0.057	0.9	0.085	0.98
10–20	0.044	0.85	0.065	0.9	0.097	0.98
20–40	0.061	0.85	0.074	0.9	0.111	0.98
40–80	0.085	0.85	0.085	0.9	0.126	0.98
80–160	0.130	0.85	0.130	0.9	0.130	0.98
>160	0.200	0.85	0.200	0.9	0.200	0.98

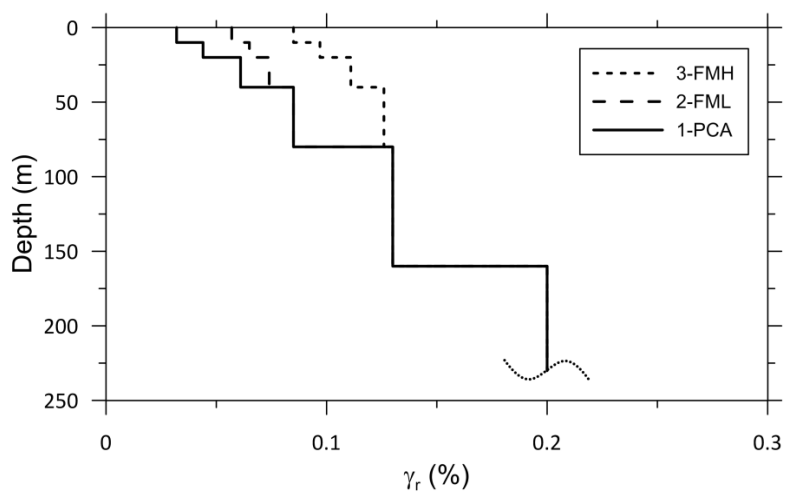

Figure 2.5 Effect of depth on reference shear strain (γ_r) for different categories of soils [Roblee and Chiou 2004].

For rock materials, soil MR curves are recommended when the rock is relatively soft (e.g., Tertiary materials with V_S < ~ 900 m/sec). For relatively hard rock, the available data is remarkably sparse; the only information currently available is for welded Tuff materials investigated by Choi [2008].

Figure 2.6 shows the variation of γ_r with confining stress for sand materials with varying uniformity coefficient C_u [Menq 2003], clay materials for varying PI [Darendel, 2001] and a Tuff material [Choi 2008]. Note that as γ_r increases, the dynamic soil behavior becomes linear over a wider range of shear strains. Accordingly, the trends in Figure 2.6 indicate that each of these material types (sand, clay, and rock) become more linear as confining stress increases. The results also show the well-known trend of increasing linearity as soil plasticity increases.

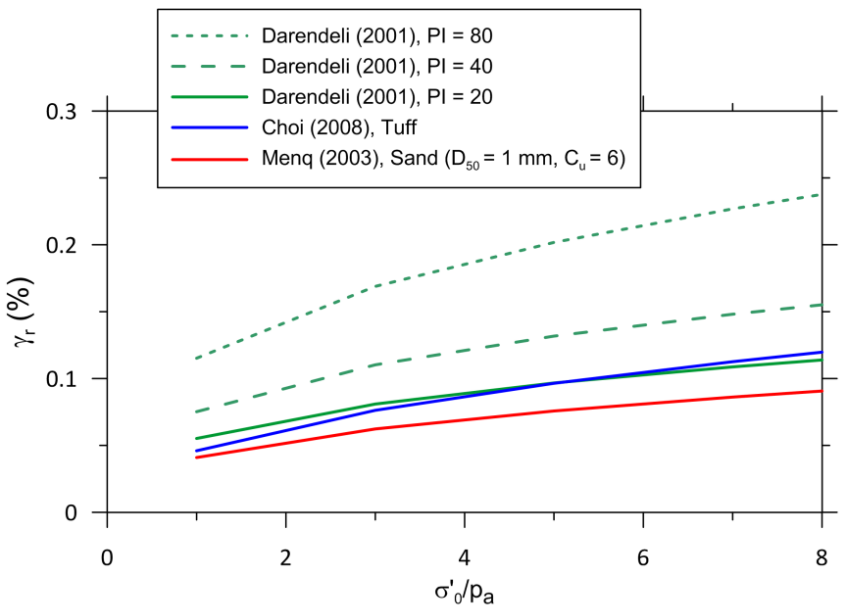

Figure 2.6 Variation of reference shear strain (γ_r) versus confining stress (σ'_0/p_a) for different models.

(c) Uncertainty in Modulus Reduction Curves

Darendeli [2001] and Zhang et al. [2008] analyzed the dispersion characteristics of the datasets used to develop their MR models. Figure 2.7 shows the range of the data that was considered in by Darendeli [2001] in their model development. Whereas there is very little uncertainty in modulus reduction at small shear strains, there is substantial uncertainty in modulus reduction behavior at strains large enough for $G/G_{\max}$ to be less than 1.0.

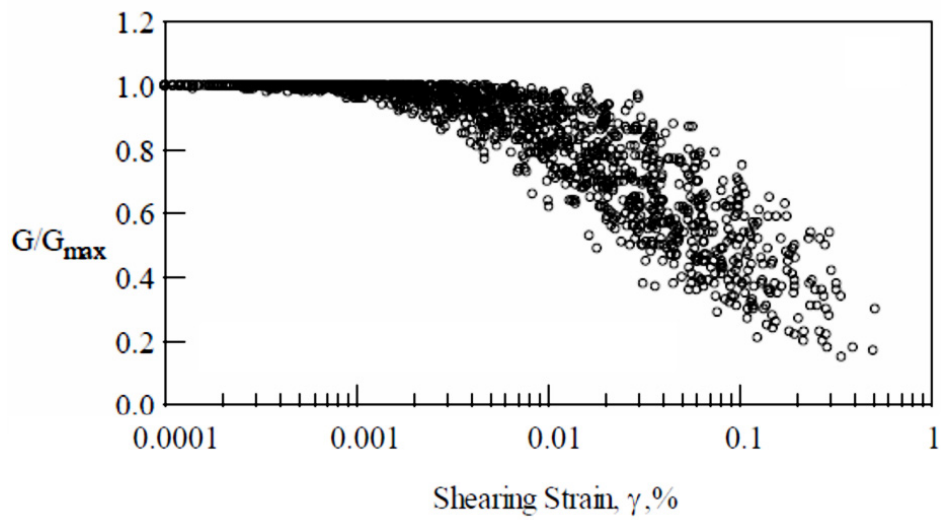

Figure 2.7 The data for normalized modulus from the resonant column and torsional shear tests (from Darendeli [2001]).

Darendeli [2001] assumed a normal distribution for the soil nonlinear properties at a given level of strain. The standard deviations of these normal distributions (σ_{NG}) are provided as equations (given below) that employ the independent variable of mean modulus reduction, as follows:

$$\sigma_{NG} = 0.015 + 0.16\sqrt{0.25 - \left(\overline{G/G_{\max}} - 0.5\right)^2} \tag{2.7}$$

$$G/G_{\max}(\gamma) = \overline{G/G_{\max}}(\gamma) + \varepsilon_1 \sigma_{NG} \tag{2.8}$$

where ε_1 is an uncorrelated standard normal variate (zero mean, standard deviation of unity). Figure 2.8 shows an example mean MR curve and its standard deviation.

Zhang et al. [2008] do not present equations for the standard deviation of modulus reduction. Instead, they provide standard errors for model coefficients and describe a methodology (referred to as the point estimate method) by which these standard errors can be propagated through the recommended equations for the mean of MR by Zhang et al. [2005]. As a result, their σ_{NG} values vary with the independent variables controlling MR, including geology (Quaternary, residual/saprolite, Tertiary and older), PI, and overburden stress. Their sensitivity studies show that uncertainty in k and γ_{r1} control σ_{NG}. Figure 2.9 shows an example of σ_{NG} as a function of MR for the case of Quaternary soils. The Darendeli uncertainty is also shown for comparison. Whereas the Darendeli model for σ_{NG} is symmetric about MR = 0.5, the Zhang et al. results are skewed towards larger values at lower MR, peaking near MR = 0.25. Uncertainty is minimized at the limits of the distribution (MR = 0 and 1).

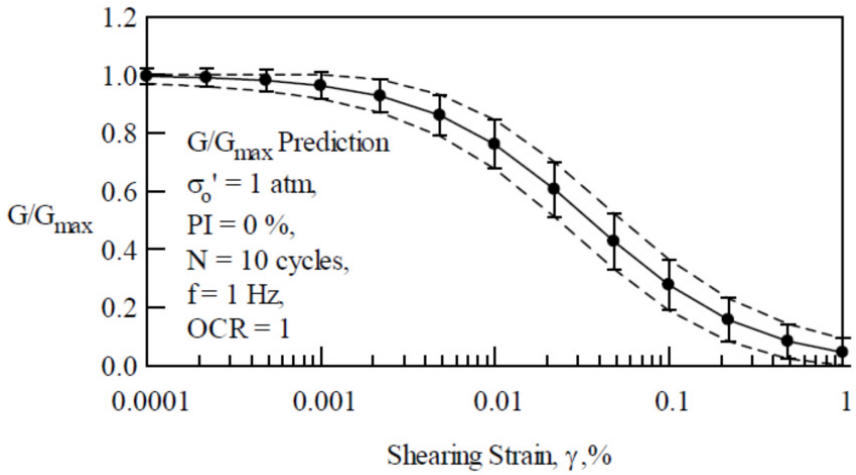

Figure 2.8 **An example of the mean and standard deviation of modulus reduction curves [Darendeli 2001].**

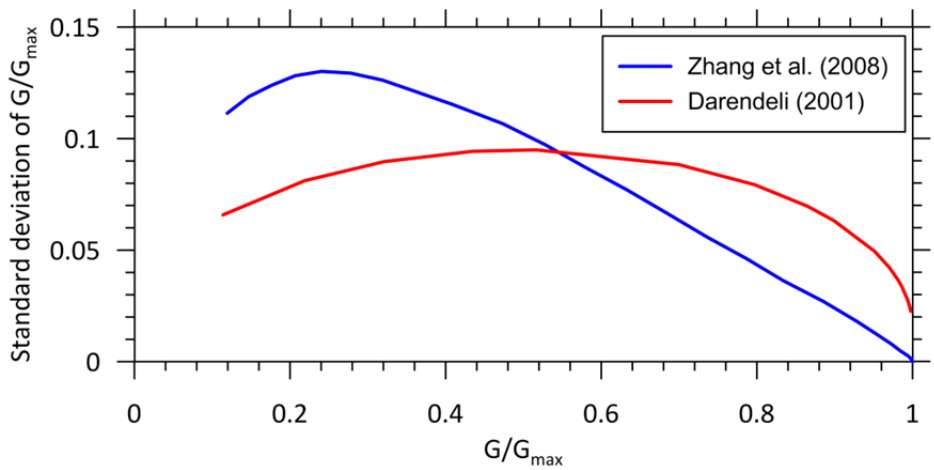

Figure 2.9 **Standard deviation of G/G_{max} for a Quaternary soil (OCR = 1.0, PI = 20 and σ'_0 = 100 kPa from Darendeli [2001] and Zhang et al. [2008] models. Values below G/G_{max} of 0.1 are not shown due to lack of data for those large strain levels.**

2.2.3 Constraining Backbone Curve at Large Strains using Shear Strength

When ground response problems involve the development of large strains at some depth (or range of depths), difficulties are encountered with the use of the MR curves described in the preceding section because they do not account for the shear strength of the soil. One common situation where this occurs is for soft soils (e.g., normally or lightly over-consolidated clays, and medium and loose sands) and strong levels of ground motion. As an example, Figure 2.10 shows a backbone curve derived using the Darendeli [2001] model for a clay soil with PI = 20, OCR = 2, and V_S = 180 m/sec. Using strength normalization concepts [Ladd 1991], the undrained shear strength ratio (without allowing for strain rate or cyclic degradation effects) would be expected to be approximately $s_u/\sigma'_0 = 0.44$ for this material, whereas the strength ratio implied by the

Darendeli model is 0.35. The underprediction of stresses at large strains that occurs in this case can have significant implications for site response, as shown in several previous studies [Yee et al. 2013; Afacan 2014].

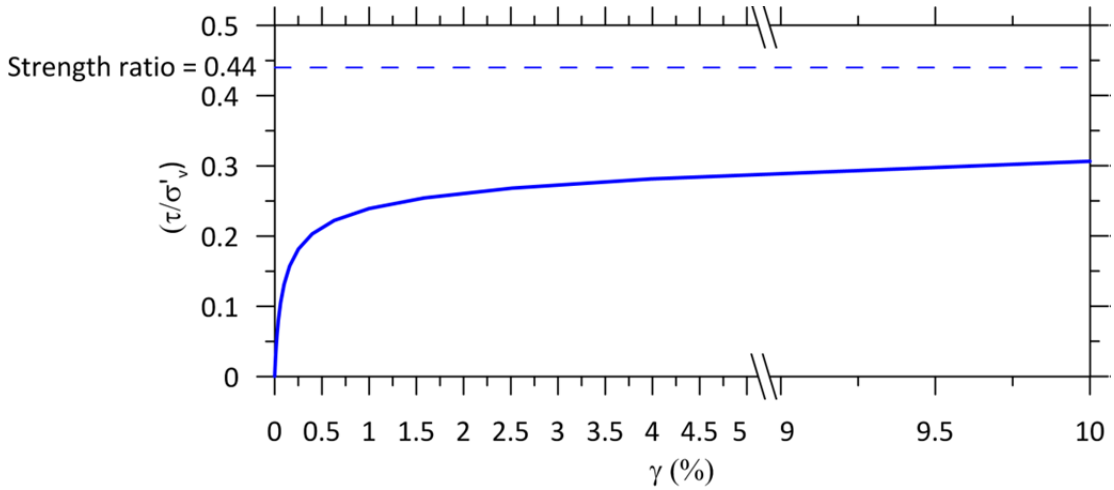

Figure 2.10 Backbone curve and strength ratio derived from Darendeli [2001] model for an example soil with PI = 20, OCR = 2, and V_S = 180 m/sec.

In this section, we briefly describe shear strength measurement, describe uncertainties in measured or estimated strengths, and review a recent method for combining MR curves with shear strength to obtain hybrid backbone curves.

(a) Shear Strength Evaluation

Numerous publications describe the non-trivial subject of shear strength estimation for seismic applications (e.g., Blake et al. [2002]; Boulanger and Idriss [2006]). Here we provide a brief synthesis of good practice in the evaluation of shear strength for seismic applications.

The analysis of shear strength begins by considering the potential for cyclic strength degradation from pore pressure development (i.e., liquefaction of sands and cyclic softening of clays). Procedures for these analyses are given in Boulanger and Idriss [2008]. If a material is found to be subject to significant cyclic degradation, an effective stress analysis of ground response is needed, which is beyond the scope of this document.

If significant cyclic strength degradation is not expected, then more 'traditional' total stress methods (or undrained strength analyses; see Ladd [1991]) are appropriate. An important point in this regard is that if the soil is below the ground water table, the shear strength that should be used for seismic analysis is the undrained shear strength. The undrained strength is used for seismic analysis even if a drained strength was found to be critical for non-seismic applications. Above the ground water table, if the saturation is sufficiently low that significant pore pressure generation is not expected (this can be safely assumed to be the case if the saturations are below 90%), then drained shear strengths can be used.

For clayey materials, undrained strengths can be measured using *in situ* vane shear testing, or with sampling and undrained testing in the laboratory. Sampling should occur with a thin walled tube sampler (Shelby tube or similar) and not with a "California-type" thick-walled

driven sampler, which produces excessive soil disturbance. Shear strength testing should be accompanied with consolidation testing to evaluate the pre-consolidation pressure $\left(\sigma'_p\right)$ and over-consolidation ratio $\left(\mathrm{OCR} = \sigma'_p / \sigma'_0\right)$. Details on various laboratory testing methods are provided elsewhere (see Ladd [1991] and Blake et al. [2002]). If shear strength test results are not available, shear strengths can often be estimated as follows [Ladd 1991]:

$$s_u / \sigma'_0 = S \times \mathrm{OCR}^m \tag{2.9}$$

where s_u / σ'_0 is the undrained shear strength ratio. Prior experience has shown that for many clays $S \sim 0.2–0.25$ and $m \sim 0.8$ [Ladd 1991].

Undrained shear strengths measured in the field or laboratory usually have times to shear failure that are approximately 20–30 minutes. Because clayey soils have rate-dependent shear strengths, and the strain rate during earthquake applications is much faster than that applied during typical testing, a correction to the measured shear strengths for rate effects can be applied. Sheahan et al. [1996] evaluated rate effects on shear strength using undrained direct simple shear tests at various, relatively slow, strain rates. The fastest rates in these tests corresponded approximately to the typical 20–30 minute time to failure. These results suggested an approximately 4.5–9.5% increase in strength for each log cycle increase in strain rate for clays with OCR < 8. If this rate effect is extrapolated to faster rates compatible with seismic loading, the factor applied to typical undrained shear strength measurements is in the range of 1.2–1.4. This rate correction is approximate for several reasons: it represents an extrapolation to fast strain rates (the original measurements were based on slower rates) and it applies for low OCR materials subjected to simple shear stress paths (its applicability for higher OCRs and other stress paths is unknown). The application of the rate effect correction to shear strength should also be made with due consideration of possible cyclic softening effects [Boulanger and Idriss 2006] associated with cyclic degradation. These softening effects can reduce the undrained shear strength substantially, so the rate correction should only be made when softening is not anticipated.

For sandy soils, whether above or below the ground water table (assuming no liquefaction), shear strength is typically expressed using the friction angle ϕ'. Because of excessive soil disturbance in sand by sampling, friction angles are typically evaluated using correlations with penetration resistance in lieu of sampling and strength testing in the laboratory. There are two types of these correlations: those that correlate ϕ' directly with penetration resistance (from CPT or SPT), and those that take friction angle as the sum of a critical state friction angle (related to mineralogy) and the differential between the peak and critical state friction angle (related to state parameter, which in turn is related to penetration resistance and effective stress). Figure 2.11 shows direct correlations of overburden-normalized penetration resistance to friction angle provided by Hatanaka and Uchida [1996] (using SPT) and Kulhawy and Mayne [1990] (using CPT). The Hatanaka and Uchida [1996] relation provides similar result to the familiar Terzaghi et al. [1996] relation, but has the advantage of showing the data and having a defined aleatory variability.

The preferred method for evaluating ϕ' is as follows:

$$\phi' = \phi_c + \left(\phi' - \phi_c\right) \tag{2.10}$$

Angle ϕ_c (critical state friction angle) is principally a function of mineralogy and gradation and ranges from about 30–35° [Negussey et al. 1988] for typical quartz sands. The difference between peak friction angle and critical state friction angle $\left(\phi' - \phi_c\right)$ has been related to state parameter $\left(\Psi\right)$ as [Jeffries and Been 2006]:

$$\begin{aligned} \Psi < 0 \qquad & \phi' - \phi_c = -48 \times \Psi \\ \Psi \geq 0 \qquad & \phi' - \phi_c = 0 \end{aligned} \tag{2.11}$$

The state parameter, in turn, can be evaluated from penetration resistance and *in situ* confining stress. A number of relations for this appear in the literature, one example of which is shown in Figure 2.12 [Robertson 2012].

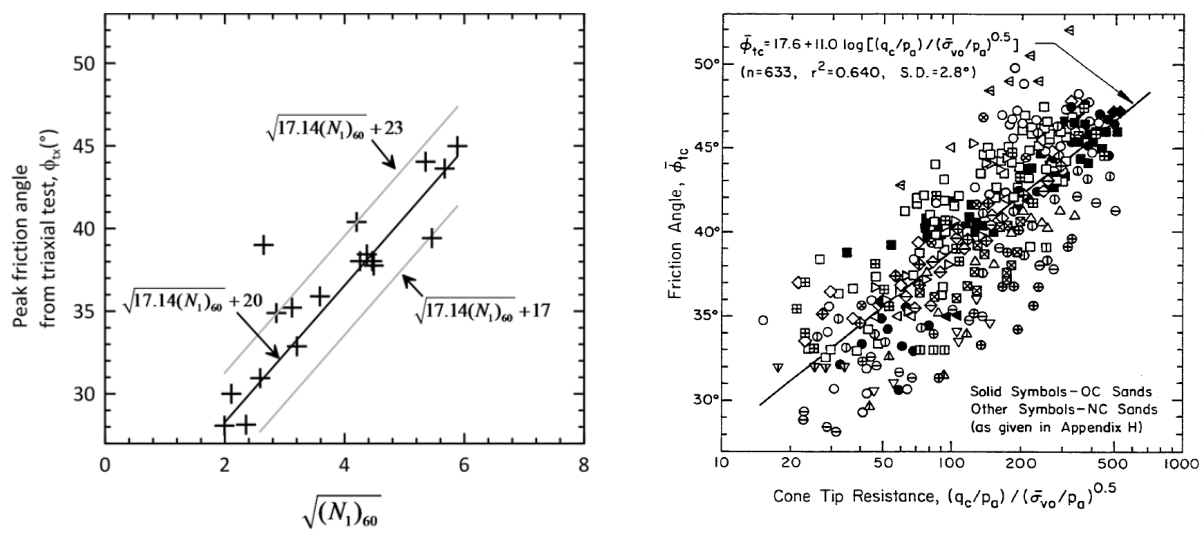

(a) (b)

Figure 2.11 (a) Normalized SPT blow count versus friction angle (adjusted from Hatanaka and Uchida [1996] to use 60% SPT efficiency instead of 78%) as measured from frozen samples; and (b) normalized CPT tip resistance versus drained triaxial friction angle [Kulhawy and Mayne 1990].

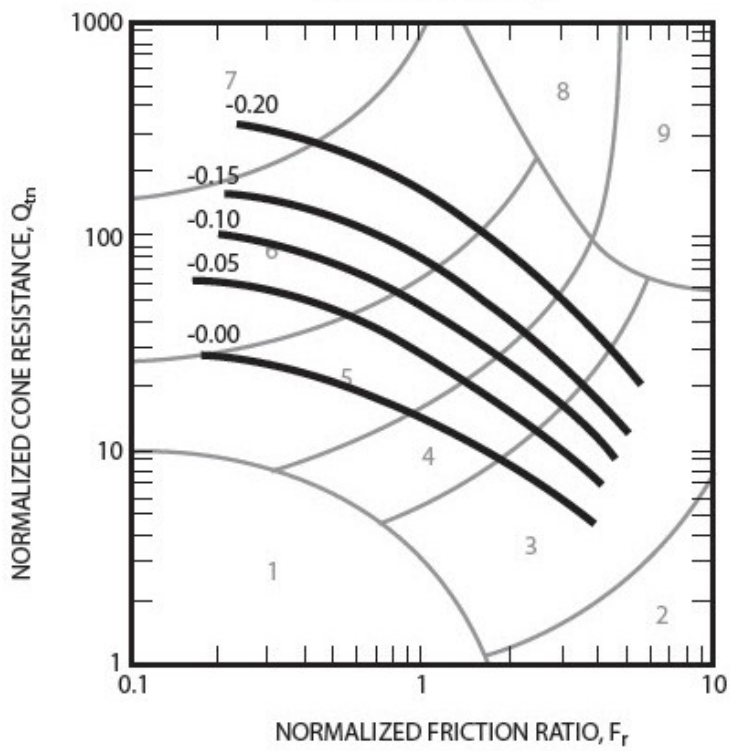

Figure 2.12 Contours of state parameter (ψ) (for granular soils) on friction ratio (sleeve friction/tip resistance) versus normalized cone penetration resistance [Robertson 2012] classification chart. The zone numbers 1–9 in the chart correspond to soil descriptions provided by Robertson. Zones 5–7 correspond to granular soils.

(b) Shear Strength Uncertainty

For clayey soils, there are several sources of uncertainty that can significantly affect shear strength evaluation:

- *In situ* OCR: The measurement of pre-consolidation pressures from consolidation curves is subject to potentially substantial uncertainties, especially when samples are significantly disturbed (e.g., Holtz et al. [2011]). The uncertainty in OCR directly affects uncertainty in strength ratio [via Equation [2.9]).
- Sample disturbance: Aside from its effect on OCR uncertainty, sample disturbance contributes considerable uncertainty to shear strength measurements, especially when unconsolidated-undrained testing is employed. Disturbance causes a conservative bias of unknown size to strengths evaluated using UU test methods. This source of uncertainty can be overcome by using in situ testing (vane shear) or CU test methods in which specimens are first consolidated to the virgin compression line before the onset of undrained shear [Ladd 1991].

- Rate effects: As mentioned in Section 2.2.3a, rate effects are estimated to increase undrained shear strengths in clays for seismic loading conditions. However, this range is highly uncertain because the test data upon which it is based do not extend to fast (seismic) loading rates, the effects of compositional factors (such as plasticity) are poorly understood, and it could in some cases be offset by cyclic softening effects.

Ideally, each of these sources of uncertainty should be considered in a site-specific analysis of shear strength. If such an evaluation cannot be undertaken for a given project, shear strength uncertainties from the literature (e.g., Jones at al. [2002]) can be applied to the non-rate corrected shear strength, as shown in Table 2.7. The uncertainties shown in Table 2.7 should be increased by about 20% for seismic applications to account for uncertainties in rate effects. If shear strength is not measured but is estimated using S and m values from the literature [Equation (2.9)], uncertainties in these parameters (as given by Ladd [1991]) should be taken into account along with the uncertainty in OCR and rate effects.

For sandy soils, the principal sources of uncertainty are the estimation of friction angle from penetration resistance (standard deviation of about 3°, as shown in Figure 2.11) and the penetration resistance itself, which will often exhibit considerable scatter from borehole-to-borehole (or sounding-to-sounding with CPT data) and with depth within a layer. The scatter of the penetration resistance reflects geological conditions related to sediment deposition, and should be evaluated on a site-specific basis.

Table 2.7 COV valued of inherent variability of soil shear strength parameters (from Jones et al. [2002]).

Property (units)	Soil Type	No. of Data Groups	No. of Tests Per Group		Property Value		Property COV (%)		Note
			Range	Mean	Range	Mean	Range	Mean	
$\phi(°)$	Sand	7	29–136	62	35–41	37.6	5–11	9	a
	Clay, silt	12	5–51	16	9–33	15.3	10–56	21	
	Clay, silt	9	*	*	17–41	33.3	4–12	9	
	*	20	*	*	*	*	*	12.6	d
$\tan\phi$	Clay, silt	4	*	*	0.24–0.69	0.509	6–46	20	a
	Clay, silt	3	*	*	*	0.615	6–46	23	
	Sand	13	6–111	45	0.65–0.92	0.744	5–14	9	a
	*	7	*	*	*	*	*	11.3	d
$\phi(°)$	Sand	*	*	*	*	*	2–5	*	b
	Gravel	*	*	*	*	*	7	*	c
	Sand	*	*	*	*	*	12	*	
S_u [1] (kPa)	Fine-grained	38	2–538	101	–412	100	6–56	33	a
S_u [2] (kPa)	Clay, Silt	13	14–82	33	15–363	276	11–49	22	
S_u [3] (kPa)	Clay	10	12–86	47	130–713	405	18–42	32	
S_u [4] (kPa)	Clay	42	24–124	48	8–638	112	6–80	32	
	*	38	*	*	*	*	*	33.8	c
S_u [5] (kPa)	Clay	*	*	*	*	*	5–20	*	b
S_u [6] (kPa)	Clayey silt	*	*	*	*	*	10–30	*	
c[7]	*	*	*	*	*	*	40	*	c
S_u/σ'_{v0} [8]	Clay	*	*	*	*	*	*	40	d
S_u/σ'_{v0}	Clay	*	*	*	*	*	5–15	*	b

[1]Unconfined compression test; [2]Unconsolidated-undrained triaxial compression test.; [3]Consolidated isotropic undrained triaxial compression test; [4]Laboratory test not reported; [5]Triaxial test.; [6,7]No information on how the uncertainty was derived; and [8]Vane shear test.
Notes: (a) Phoon and Kulhawy [1999]; (b) Lacasse and Nadim [1996]; (c) Harr [1987]; and (d) Kulhawy [1992].

(c) Extending Backbone Curve to Large Strains in Consideration of Shear Strength

The classical approach for forcing a hyperbolic stress-strain curve to a limiting shear stress corresponding to shear strength τ_{ff} is to replace γ_r in Equation (2.6) with reference shear strain $\gamma_{ref} = \tau_{ff} / G_{\max}$ and set curvature parameter $\alpha = 1$ [Hardin and Drnevich 1972]. Reference strain γ_{ref} should not to be confused with pseudo-reference shear strain γ_r used in empirical MR curves. As shown in Figure 2.13, the problem with this approach is that it does not capture well the shape of the MR curve at small strains (i.e., well below the failure strain).

To overcome this problem, Yee et al. [2013] developed a hybrid model in which a user-defined MR curve is used at small strains below a limiting value $(\gamma < \gamma_1)$. As shown in Figure 2.14, for larger strains $(\gamma > \gamma_1)$, a classical reference strain approach is used but for a set of axes that begins at strain γ_1 and corresponding stress τ_1; the modulus at point (γ_1, τ_1) matches the tangent modulus from the user-defined MR curve at strain γ_1. Hence this approach takes as input the parameters required to specify a MR curve (γ_r and α) along with shear strength τ_{ff}. The matching strain γ_1 is also user-specified and its selection depends on α: when $\alpha < 1$ (the most common case), γ_1 should be selected such that τ_1 is well below the shear strength (e.g., $\tau_1 / \tau_{ff} < 0.3$), otherwise, when $\alpha > 1$ α, γ_1 should not exceed γ_r. The hybrid approach of Yee et al. is implemented in a spreadsheet that accompanies this report.

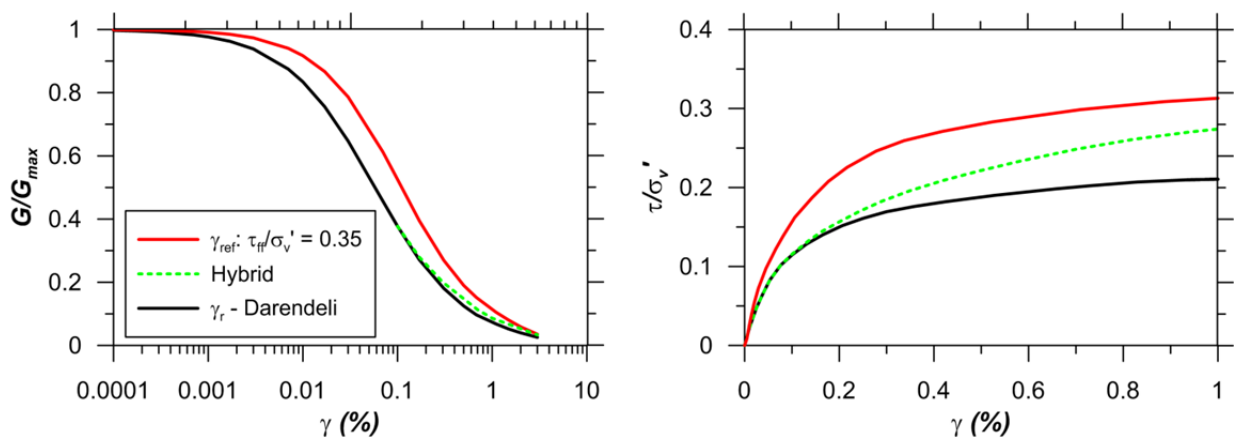

Figure 2.13 An example of modulus reduction and stress-strain curves from Darendeli [2001], reference strain model, and hybrid procedure (PI = 20%, OCR = 1.5, σ_0' = 100kPa, V_S = 135 m/sec, and (γ_1 = 0.1%).

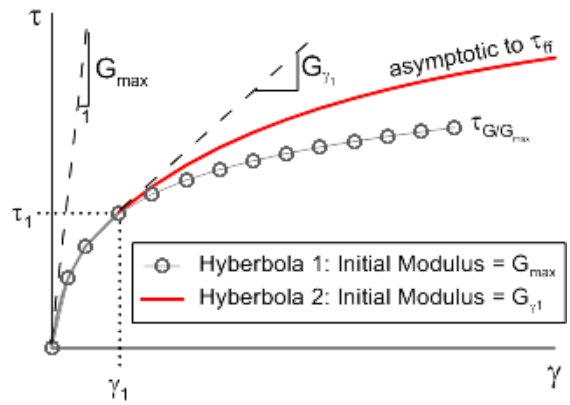

Figure 2.14 Schematic illustration of constructing shear strength–adjusted modulus reduction curves [Yee et al. 2013].

2.2.4 Software Implementation of Backbone Curves

Most EL GRA routines compute the ordinates of the backbone curve from user-defined $G_{\max}$ (or shear-wave velocity and mass density) and a series of strain–$G/G_{\max}$ points on a user-specified MR curve. Hence, any MR curve shape is admissible, including the hybrid model described in the previous section.

Conversely, most implementations of nonlinear codes (e.g., DEEPSOIL [Hashash 2012] and DMOD [Matasovic 1992]) require the backbone curve to follow a hyperbolic shape compatible with the MR curve function in Equation (2.6). This requirement is applied to facilitate the evaluation of unload-reload soil behavior in cyclic loading, but it does not allow for implementation of more complex backbone curve shapes such as those produced by the hybrid model from the previous section. As an approximation, in DEEPSOIL a hyperbola can be fit to a more complex user-specified backbone curve [Zheng et al. 2010]. An exception is OpenSees [McKenna and Fenves 2001] in which a user-specified backbone curve is allowed. However, the benefits of this flexibility must be weighed against some limitations in the damping model, as described further in the following section. Future versions of DEEPSOIL will modify the backbone curve formulation to allow the incorporation of shear strength in a manner similar to that of Yee et al. [2013], in that small-strain behavior will be maintained as that produced by a hyperbolic MR curve.

2.3 DYNAMIC SOIL PROPERTIES: DAMPING

As soil is cyclically sheared, slippage between soil grains and the complex interactions between solid and fluid phases produces a lag in time between the application of stress and development of the resulting strains. This behavior causes the characteristic stress-strain loops depicted in Figure 2.1, the area within which can be converted to damping ratio that is dependent on strain amplitude [depicted in Figure 2.3(b)]. Because this damping ratio is often found to be nearly independent of loading frequency within the frequency range of interest, it is commonly referred to as hysteretic.

In this section, we describe approaches for evaluating strain-dependent hysteretic soil damping using lab test results (Section 2.3.1) and describe its implementation in computer codes for ground response analysis (see Section 2.3.2). This section is concluded by reviewing some analyses of vertical array data that challenge whether laboratory-based damping should be used as-is for application to field conditions (see Section 2.3.3).

2.3.1 Evaluation of Strain-Dependent Damping

(a) Material Specific Testing

The same test procedures described in Section 2.2.1a for modulus reduction $\left(G/G_{\max}\right)$ versus shear-strain curves (MR curves) are used to evaluate damping versus strain curves. Figure 2.15 shows how the area within the stress-strain curve is converted to a damping ratio. The same device- and sample disturbance-related considerations described previously apply equally to the measurement of damping. Small-strain damping can be particularly difficult to capture in lab testing, requiring specialized equipment that can control and measure stress and strain responses for very small-strain conditions.

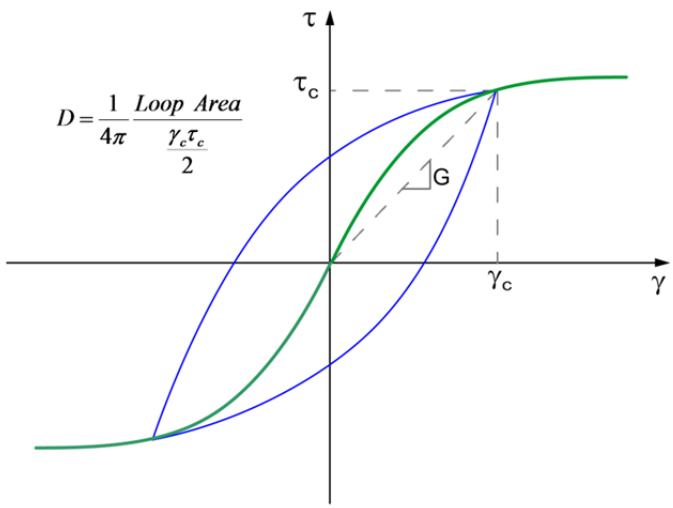

Figure 2.15 Calculation of damping ratio using the area of cyclic loops [Kramer 1996].

(b) Literature

When material-specific test results are unavailable, damping curves can be estimated from empirical equations from the same literature proving MR curves. Damping is usually taken as the sum of small strain damping $\left(D_{\min}\right)$ and a function of $G/G_{\max}$:

$$D(\gamma) = D_{\min} + f\left(\frac{G(\gamma)}{G_{\max}}\right) \tag{2.12}$$

Table 2.8 summarizes the regression functions for the two terms on the right side of Equation (2.12), and selected model coefficients are in Tables 2.9–2.11. In the case of the Darendeli

[2001] and Menq [2003] models, the regression equations modify the damping from the use of Masing rules [Masing 1926] (D_M).

Table 2.8 Summary of attributes of hyperbolic soil damping models from literature.

Reference	Model for D_{min}	Model for D-D_{min}	Soil types considered	Applicable strain range
Darendeli [2001][1]	$D_{\min} = \left(\phi_6 + \phi_7 \times \mathrm{PI} \times \mathrm{OCR}^{\phi_8}\right) \times \sigma_0'^{\phi_9} \times \left[1 + \phi_{10} \ln(freq)\right]$	$D(\gamma) - D_{\min} = b \times D_M(\gamma) \times \left(G(\gamma)/G_{\max}\right)^{0.1}$ $b = \phi_{11} + \phi_{12} \times \ln(N)$	Generic (110 samples from 20 sites)	0.0001–0.5%
Menq [2003][2]	$D_{\min} = \phi_3 \times C_u^{\phi_4} \times D_{50}^{\phi_5} \times \left(\sigma_0'/p_a\right)^{\phi_6}$	Same as Darendeli [2001]	Granular (59 reconstituted specimens)	0.0001–0.6%
Roblee and Chiou [2004]	From Table 2.11	Same as Darendeli [2001]	Clay, sand and silt (154 samples from	0.0001–4.0%
Zhang et al. [2005]	$D_{\min} = D_{\min 1}\left(\sigma_0'/p_a\right)^{-k/2}$ $D_{\min 1} = a(PI) + b$ a=0.008 b=0.82	$D(\gamma) - D_{\min} = 10.6(G/G_{\max})^2 - 31.6(G/G_{\max}) + 21.0$	Mineral soils in South Carolina (122 samples)	0.0001–0.3%
Choi [2008]	$D_{\min} = 119e^{-0.0026\gamma_t}$ γ_t = material density	$D(\gamma) - D_{\min} = C\left(\gamma/\gamma_D\right)^{a_D}$ $\gamma_D = 0.038(\sigma_0/p_a)^{0.54}$ $a_D = -0.545\log_{10}\gamma_D + 0.337$	Bandelier Tuff, Pajarito Plateau, NM (38 samples)	0.0001–0.04%

[1] See Table 2.9 for parameters.
[2] See Table 2.10 for parameters.

Darendeli [2001] presented an approximate method for computing Masing damping D_M from the γ_r and α parameters describing the shape of the backbone curve. To begin, the Masing damping for the case of $\alpha = 1$ is computed as follows:

$$D_{M,\alpha=1}(\gamma)[\%] = \frac{100}{\pi}\left[4\frac{\gamma - \gamma_r \ln\left(\frac{\gamma+\gamma_r}{\gamma_r}\right)}{\frac{\gamma^2}{\gamma+\gamma_r}} - 2\right] \tag{2.13}$$

Damping D_M for values of $\alpha \neq 1$ is then computed as:

$$D_M = c_1\left(D_{M,\alpha=1}\right) + c_2\left(D_{M,\alpha=1}\right)^2 + c_3\left(D_{M,\alpha=1}\right)^3 \tag{2.14a}$$

$$c_1 = 0.2523 + 1.8618\alpha - 1.1143\alpha^2 \tag{2.14b}$$

$$c_2 = -0.0095 - 0.0710\alpha + 0.0805\alpha^2 \tag{2.14c}$$

$$c_3 = 0.0003 + 0.0002\alpha - 0.0005\alpha^2 \tag{2.14d}$$

In the case of the Roblee and Chiou [2004] GeoIndex model, coefficients $D_{\min}$ and b are given as a function of depth listed in Table 2.11.

Table 2.9 Parameters for Darendeli [2001] model for soil damping.

Parameter	Value
ϕ_6	0.8005
ϕ_7	0.0129
ϕ_8	-0.1069
ϕ_9	-0.2889
ϕ_{10}	0.2919
ϕ_{11}	0.6329
ϕ_{12}	-0.0057

Table 2.10 Parameters for Menq [2003] model for soil damping.

Parameter	Value
ϕ_3	0.55
ϕ_4	0.1
ϕ_5	-0.3
ϕ_6	-0.08
ϕ_{11}	0.6329
ϕ_{12}	-0.0057

Table 2.11 GeoIndex model parameters for damping [Roblee and Chiou 2004].

Depth (m)	$D_{\min}$	b
0-10	1.30	1.62
10-20	1.15	1.62
20-40	1.02	1.62
40-80	0.90	1.62
80-160	0.80	1.62
>160	0.70	1.62

(c) Uncertainty in Damping Curves

Darendeli [2001] and Zhang et al. [2008] analyzed the dispersion characteristics of the datasets used to develop their damping models. Unlike modulus reduction, there is uncertainty in damping values across the full range of shear strains.

Darendeli [2001] provides a model for the natural log standard deviation of soil damping as follows:

$$\sigma_{\ln D} = 0.0067 + 0.78\sqrt{\bar{D}(\%)} \tag{2.15}$$

where $\bar{D}$ is the mean damping from Equation (2.12) when implemented with the component models in Table 2.8. Figure 2.16 shows an example mean and standard deviation of strain dependent damping using the Darendeli [2001] model.

As with MR uncertainty, Zhang et al. [2008] do not present equations for the standard deviation of damping. Their $\sigma_{\ln D}$ values vary with the independent variables used in the Zhang et al. [2005] mean model. Figure 2.16 compares the Zhang et al. [2008] standard deviation computed from the point estimate method for a Quaternary soil. The two models given similar uncertainties for $D_{\min}$, but at larger strains, the Zhang et al. value of $\sigma_{\ln D}$ peaks near $\gamma_c = 0.05\%$ whereas the Darendeli $\sigma_{\ln D}$ monotonically increases with γ_c.

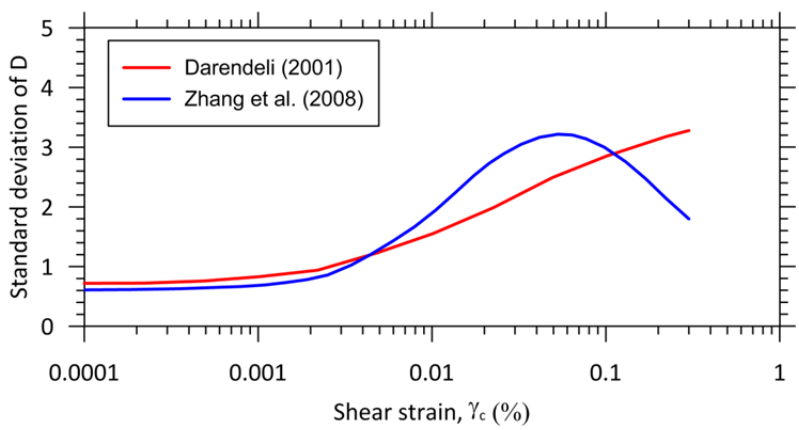

Figure 2.16 An example of standard deviation of soil damping for Quaternary soil (PI = 20, OCR = 1, and σ_0' = 100 kPa).

Because damping and modulus reduction are correlated, a randomization scheme for evaluating these properties can proceed as follows (modified from Darendeli [2001]):

$$D(\gamma) = \bar{D}(\gamma) + \rho_{D,NG}\varepsilon_1\sigma_{\ln D} + \sqrt{1-\rho^2{}_{D,NG}\varepsilon_2\sigma_{\ln D}} \tag{2.16}$$

where ε_1 and ε_2 are uncorrelated random variables with zero mean and unit standard deviation. Parameters ε_1 and ε_2 are used for randomizing $G/G_{\max}$ and damping, respectively. Parameter $\rho_{D,NG}$ is the strain-dependent correlation coefficient. Correlation coefficient is a measure of

linear correlation between the two variables $G/G_{\max}$ and D. The correlation is negative in this case, meaning that increases in $G/G_{\max}$ tend to produce decreases in D. Kottke and Rathje [2008] recommend taking $\rho_{D,NG} = -0.5$ to account for these effects.

2.3.2 Damping Implementation in GRA

(a) Equivalent-Linear Analysis

As described in the introduction to this section, soil damping as measured in cyclic laboratory tests is approximately hysteretic, meaning that energy is dissipated within each loading-unloading cycle. As described further by Kramer [1996], EL methods implement soil damping as equivalent viscous damping. Like the shear modulus, equivalent viscous damping is constant throughout the ground motion duration for a given soil layer. The implementation of strain-dependent equivalent viscous damping in EL analyses has no practical constraints with respect to the shape of the curve. Any $D-\gamma$ relationship derived from empirical methods or material-specific testing can be entered as user-defined points.

(b) Nonlinear Analysis

In nonlinear analysis, the backbone curve, in combination with unload-reload rules, controls the shape of cyclic loops such as those shown in Figure 2.1, which in turn controls the level of soil damping for a given strain level. Hence, a critical issue in the implementation of a given $D-\gamma$ relationship is the degree to which the unload-reload rules used in a nonlinear GRA procedure can reproduce the trend in the $D-\gamma$ data. One common problem in this regard is that most unload-reload rules will produce zero damping at very small strains where the backbone curve is linear. This is often overcome by including viscous damping elements within the soil constitutive model. These two issues (unload-reload rules, viscous damping formulation) are discussed in NCHRP [2012]; a brief review of key points is provided in the following paragraphs.

The classical approach for constructing cyclic loops, representing the unload-reload soil behavior, is the Masing rules [1926] and extended Masing rules [Vucetic 1990; Pyke 1979]. In this approach, the shape of the unloading and reloading portions of the cyclic loops matches that of the backbone curve (factored by two to account for positive and negative strains). As shown in Figure 2.17, Masing rules produce levels of damping that are too low at small strains (approaching zero) and too large at large strains. To overcome the large-strain problem, alternative unload-reload rules have been proposed, which typically 'pinch' the hysteresis curves relative to those from Masing rules, thus making them thinner. Philips and Hashash [2009] and Assimaki et al. [2000] provide alternative methods for performing this pinching, with the objective of producing hysteretic damping levels matching target $D-\gamma$ curves. The only nonlinear code available in practice that implements such procedures is DEEPSOIL. Other widely used codes (DMOD [Matasovic 1992], OpenSees [Ragheb 1994; Parra 1996; Yang 2000; and McKenna and Fenves 2001], TESS [Pyke 2000], SUMDES [Li et al. 1992]) use Masing rules or variants thereof [Stewart et al. 2008].

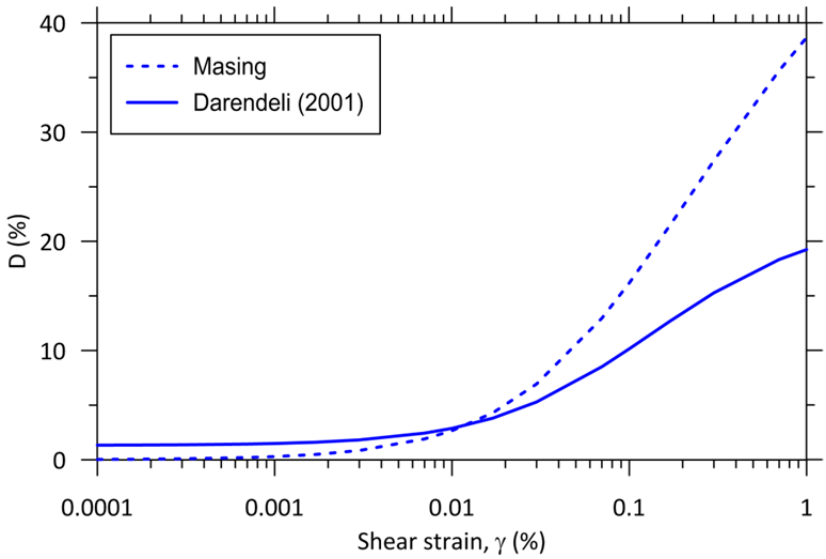

Figure 2.17 An example of damping curves for a soil (PI = 0, OCR = 1, and σ_0' = 100 kPa) from Masing rule [1926] and Darendeli [2001] model.

The need for some form of viscous damping in a time-domain solution of a nonlinear dynamic response problem occurs for many applications (site response, structural response, etc.). The classical approach to applying viscous damping is through the use of various types of Rayleigh damping. In Rayleigh damping, a damping matrix is computed either as proportional to the stiffness matrix alone or as a linear combination of the stiffness and mass matrices for the system. The former approach produces a linear variation of damping ratio with frequency and hence, can only match a target damping level at a single frequency as shown in Figure 2.18; this is referred to as simplified Rayleigh damping. The later approach, referred to as full Rayleigh damping and also shown in Figure 2.18, has a more complex shape and matches the target damping ratio at two frequencies. Kwok et al. [2007] tested both schemes against exact frequency-domain solutions for idealized viscoelastic site conditions, providing recommendations on the matching frequencies that should be used for full Rayleigh damping (simplified Rayleigh damping tends to overdamp high frequencies and its use is discouraged) and showing that the target viscous damping level should be taken as $D_{\min}$. A shortcoming of all Rayleigh damping formulations is that the target damping level is not achieved except at matching frequencies; Philips and Hashash [2009] describe a procedure for numerically producing frequency-independent viscous damping. This procedure is implemented in DEEPSOIL [Hashash 2012] only.

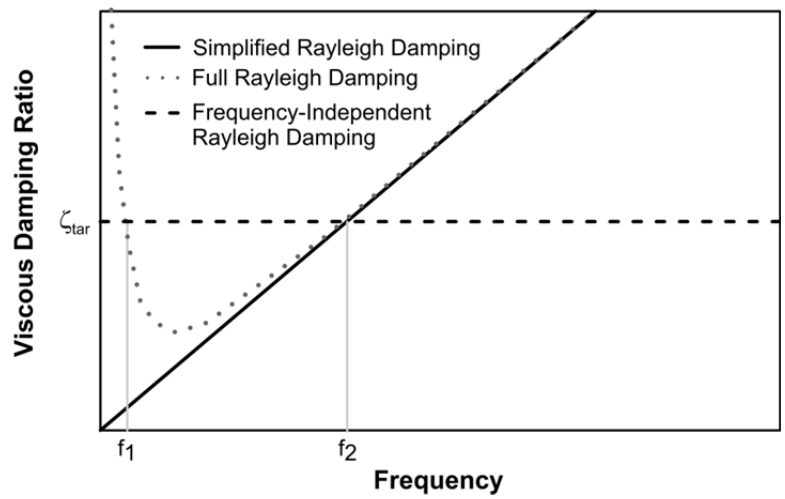

Figure 2.18 Schematic illustration of different viscous damping models (modified from Kwok et al. [2007]).

2.3.3 Application of Laboratory-Based Soil Damping for Field Conditions

Any soil property derived from laboratory testing of small-scale soil elements should be critically considered with respect to its applicability for field conditions. For example, in Section 2.2.2a, it was noted that V_S measured in the field will generally be incompatible with $G_{\max}$ measured in the laboratory on soil samples from the same site. This discrepancy can arguably be accepted due to the normalization of shear modulus by $G_{\max}$, provided that the sample disturbance effects responsible for the field-to-laboratory discrepancy influence both moduli similarly. The question considered here is whether the laboratory-based damping measurement is applicable to field conditions. Although damping ratio like $G/G_{\max}$ is also a normalized quantity, several factors might be expected to produce field-to-lab discrepancies: (1) potential sample disturbance effects on the shape of the stress-strain loops measured in the laboratory; and (2) wave scattering effects present under field conditions that cannot be captured with laboratory element testing. The potential significance of these effects is poorly understood, but the few studies that have considered this problem are reviewed below.

For a study to be useful in the present context, the data must be from vertical arrays, high-quality V_S measurements should be available (to minimize uncertainty in that critical parameter), and the GRA predictions should utilize, or at least consider as one alternative, laboratory-based estimates of soil damping. Studies meeting these criteria that have found misfits between data and GRA predictions are Tsai and Hashash [2009], Elgamal et al. [2001], and Yee et al. [2013]. Tsai and Hashash [2009] used vertical array data from the Lotung, Taiwan, (soft silts) and La Cienega, California, (soft clay) arrays in a neural network based inverse analysis to extract soil properties. Because their analyses were not constrained by model-based assumptions of soil behavior, they hold the potential to provide insights into *in situ* soil behavior. However, the approach does have the potential to map-modeling errors unrelated to soil behavior (e.g., lack of 1D response) into inverted soil properties. Shear-wave velocity models were slightly adjusted from data in the "learning" process and stress-strain loops were extracted. Modulus reduction and damping curves were then computed from the loops, which demonstrate stronger

nonlinearity than laboratory-based curves (i.e., lower modulus reduction and higher damping). The observation of higher damping is also in agreement with system identification results obtained from Lotung data by Elgamal et al. [2001]. Yee et al. [2013] analyzed vertical array data from the Kashiwazaki, Japan, Service Hall Array site (stiff deep soil) under relatively weak and strong shaking conditions. The weak motion data showed that $D_{\min}$ should be increased by 2–5% for GRA results to adequately capture observations. When these elevated damping levels were used with strong-motion data, the GRA predictions were satisfactory. These three studies provide some (admittedly anecdotal) evidence that the damping mobilized in the field is higher than that represented by the small-strain portion of laboratory $D-\gamma$ curves (i.e., the $D_{\min}$ value). The available data does not suggest any problem with the nonlinear ($D-D_{\min}$) portion of these curves.

Several additional studies meet the criteria described in the previous section but did not identify a need for increasing the laboratory-based soil damping. Stewart and Kwok [2008] report on the results of a multi-investigator project in which GRA analyses, using parameter selection protocols similar to those described previously in this chapter, were tested against the best available vertical array data not involving soil liquefaction (because the codes are for total stress analysis). The arrays utilized were a series of stiff-soil sites in Japan (KiK-net), the Lotung array in Taiwan, the La Cienega array in California, and the Turkey Flat array in California (shallow, stiff soil). At the Turkey Flat site [Kwok et al. 2008], peak velocities from the 2004 **M** 6.0 Parkfield earthquake were in the range of 7–8 cm/sec and calculated peak ground strains were as large as 10^{-2}%. Predicted and observed acceleration histories at the surface and at intermediate depth were consistent, thus indicating that no adjustment to the laboratory-based $D-\gamma$ curves is needed. At the other sites considered, observed ground motions had some misfits relative to the data, but not in a manner that could be explained by errors in the damping model. The lack of a damping-related misfit in these cases may have resulted from a combination of shallow soil profiles for which damping effects are relatively small (Turkey Flat and KiK-net sites) and strain levels that, while modest, are large enough for the $D-D_{\min}$ component to dominate relative to the $D_{\min}$ component. Analyses of damping misfit are best undertaken using weak motion data.

Given the uncertainty surrounding this issue, we consider that the potential for soil sites to have additional damping beyond laboratory-based values to be a source of epistemic uncertainty. As such, it is good practice to treat the additional damping to be added to $D_{\min}$ as a parameter to be varied in sensitivity studies. Given currently available information, a range of about zero to 5% would seem to be appropriate.

2.4 EQUIVALENT-LINEAR VERSUS NONLINEAR METHODS OF ANALYSIS

We assume the reader to have a basic working knowledge of EL and NL methods of GRA. A literature review and summary of these methods of analysis are given in NCHRP [2012]. Aspects of these methods that are particularly relevant for the present discussion are:

- Equivalent-linear methods use time-invariant secant moduli (G) and damping (D) in each soil layer, which enables a closed form solution of the differential wave equation

assuming linear soil behavior. These methods are iterative so that the G and D used for a layer are compatible with the computed level of shear strain γ.

- Nonlinear methods solve the equation of motion for a multi-degree-of-freedom system in the time domain. This requires assembling appropriate mass, stiffness, and damping matrices. Because the solution uses time-stepping algorithms to solve the equation of motion, the soil properties can modulate with time as the severity of shaking changes.

The EL methods of analysis are more efficient than NL analysis, both from the standpoint of developing input parameters (the only damping input required for EL analysis is $D-\gamma$ curves) and shorter computation times. For this reason, an issue that is commonly faced during GRA is whether EL analyses are sufficient or whether more costly NL analyses are required. In this section, we address this issue from two perspectives: (1) if EL and NL analyses are already completed, how can differences in the results be interpreted to evaluate potential shortcomings of the EL results?; and (2) on what basis can differences be anticipated *a priori* to guide the development of an appropriate analysis plan?

In order to be meaningful, any comparison of EL and NL analysis results must utilize identical input motions and soil properties. The manner by which input motions should be specified is discussed in Section 2.5. Some particular pitfalls related to specification of soil properties that have affected previous comparisons between NL versus EL methods (e.g., Silva et al. [2000] include: (1) mismatched soil damping ($D-\gamma$) curves due to the use of laboratory-based models for EL and Masing-type unload-reload rules for NL analysis; (2) the application of simplified or full Rayleigh viscous damping formulations in NL analysis, which are incompatible with the frequency-independent damping used in EL analysis; and (3) lack of appropriate consideration of shear strength to constrain backbone curves at large strain, especially for EL analyses. All of these issues can be addressed with proper specification of dynamic soil properties and other input parameters following the guidelines in Sections 2.2–2.3. The recommendations given in the following section are based on a small subset of the literature in which consistency of input motions and dynamic soil properties was enforced, so that the differences can be attributed solely to the different solution algorithms for the EL and NL analyses.

2.4.1 Judging Differences between Equivalent-Linear and Nonlinear Analysis Results

A number of validation studies, in which vertical array data are compared to predictions from EL and NL GRA, have shown general consistency between the two methods of analysis [Stewart et al. 2008; Kwok et al. 2008; Assimaki and Li 2012; and Kaklamanos et al. 2013]. However, such analyses are most often performed for conditions involving relatively modest levels of shear strain, typically well below the pseudo reference strain γ_r.

More meaningful insight into the differences between EL and NL ground motion predictions can be made when the analyses are performed for relatively strong shaking levels that induce large strains. Figure 2.19 presents EL–NL comparisons for both relatively modest and very strong levels of shaking. The analyses are for a soft clay site having a vertical array (La Cienega, California) using recorded ground motions of modest amplitude from a 2001 **M** 4.2

earthquake (left side) and simulated strong ground motions for a near-field **M** 7.5 earthquake (right side). The figure shows geometric mean horizontal component pseudo-acceleration response spectra (PSA) and spectral shapes (PSA/PGA). Further details on the input parameters and other details of the analysis are given in Stewart and Kwok [2008].

As shown in the bottom frames of Figure 2.19, the EL and NL spectral shapes are similar for the 2001 input motion that induces relatively low strain but are significantly different for the large amplitude simulated motions. For the large-strain simulation, the spectral shapes at low periods (< ~0.2 sec) from EL analyses are flatter and have less period-to-period fluctuations than those from NL analyses. To provide insight into which result is more compatible with observation, the spectral shape from a GMPE is shown for the **M** 7.5 (large strain) case [Campbell and Bozorgnia 2008]. The GMPE spectral shape is very similar to those from NL analyses, suggesting that the EL shape is unrealistic. This problem with EL analysis is also mentioned by Kaklamanos et al. [2013], who evaluated a large amount of KiK-net vertical array data in Japan. These features of EL analysis result from large strains producing high damping that is applied across the full ground motion duration. In reality, the large damping only occurs during a limited time period associated with arrival of the strongest shear waves; that portion of the record will not necessarily control the short-period portions of the response spectrum. As a result, some portions of the time series and hence, the spectrum, are overdamped by the EL analysis. This is overcome by NL procedures in which soil properties modulate with time as the strength of shaking changes.

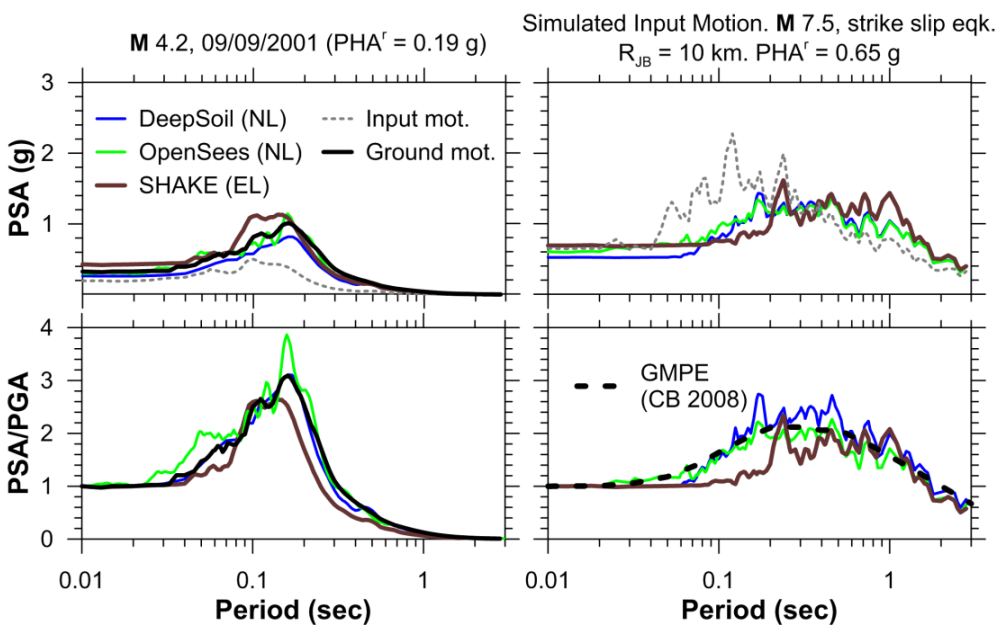

Figure 2.19 Comparison of computed spectra, amplification factors, and spectral shapes of predicted motions at La Cienaga site using equivalent-linear and nonlinear methods of analysis (adapted from Stewart and Kwok [2008]).

On the basis of the results shown in Figure 2.19 and similar results obtained for many other sites in the authors' experience, we recommend that the EL and NL spectra be plotted together, along with normalized spectra PSA/PGA. When the EL results show a long tail of flat spectral ordinates, as in the right side of Figure 2.19, the EL results should be considered to be in error, and their use for prediction of ground response is not recommended; NL analyses are preferred in such cases. It is also good practice to plot computed peak accelerations and shear strains as a function of depth. Difficulties of the type shown in Figure 2.19 will typically occur when maximum strains $\gamma_{\max}$ are large over some depth interval in the profile (i.e., $\gamma_{\max} >\sim 0.5-1.0\%$ in the authors' experience; Kaklamanos et al. [2013] suggest that EL analyses are problematic for $\gamma_{\max} >\sim 0.1-0.4\%$).

Even for cases where NL analyses are to be used, corresponding EL analyses should be undertaken. This facilitates comparisons of the type shown in Figure 2.19, which enables bug-checking the analysis results and inference of the severity of nonlinearity in the site response.

2.4.2 *A Priori* Evaluation of Conditions Leading to Different Equivalent Linear and Nonlinear Analysis Results

The guidelines for discriminating between EL and NL analyses in the prior section require that ground response analyses be performed to evaluate strain levels and response spectra for interpretation. This will be inconvenient for many applications, where an *a priori* assessment of conditions where EL analyses are permissible is desirable to efficiently plan the analysis program.

The problem of *a priori* discrimination of GRA results has been considered by Assimaki and Li [2012] and Kim et al. [2013, 2014]. Assimaki and Li [2012] focused principally on the difference between linear viscoelastic (LIE) and NL analysis results, which they found to be related to the input motion amplitude and V_{S30}. Kim et al. [2013; 2014] extended this work by focusing on differences between EL and NL analysis results. Both studies considered 24 sites with well-characterized geotechnical conditions (described by Baturay and Stewart [2003]) having widely varying geologic conditions with V_{S30} ranging from 142 to 692 m/sec). In addition, Kim et al. [2013; 2014] considered sites in the Mississippi Embayment in the Central U.S. A diverse set of simulated input motions were applied having varying amplitudes, durations, and frequency contents. The goal of these analyses was to identify conditions where the EL and NL analysis results have divergent spectral ordinates (response spectra and Fourier amplitude spectra).

Results of these calculations are given as ratios of PSA ordinates ($\mathrm{PSA}^{EL}/\mathrm{PSA}^{NL}$) or Fourier amplitudes ($\mathrm{FA}^{EL}/\mathrm{FA}^{NL}$). Figure 2.20 shows the trend of PSA ratios from many analyses for sites and input motions in the central and eastern U.S. against strain index, defined as follows:

$$\gamma_{\mathrm{ind}} = \frac{\mathrm{PGV}^{r}}{V_{S30}} \tag{2.17}$$

where PGV^r is the peak velocity of the outcropping input motion used in GRA (use of the RotD50 component of velocity is recommended; see Boore [2010]). Note that γ_{ind} can be computed without performing GRA as it depends only on properties of the V_S profile and input motion. Strain index was found to more strongly correlate to variations in EL and NL results than a series of other parameters that included the peak acceleration and peak velocity of the input motion, among others. Kim et al. [2014] shows that both sets of ratios follow similar trends, but that Fourier amplitude ratios are more consistent between regions (e.g., eastern versus western U.S.) due to the saturation of PSA at high frequencies.

Kim et al. [2013; 2014] judged the divergence between EL and NL analyses to be significant when the trend of results like those shown in Figure 2.20 depart from unity by amounts greater than about 10–30%. Based on this criterion, there are no significant differences between EL and NL analyses for periods > ~ 0.7 sec. As shown in Figure 2.21, for shorter periods, EL are considered unreliable (biased) for $\gamma_{\text{ind}} >\sim 0.1-0.4\%$; for these conditions, NL analyses are preferred.

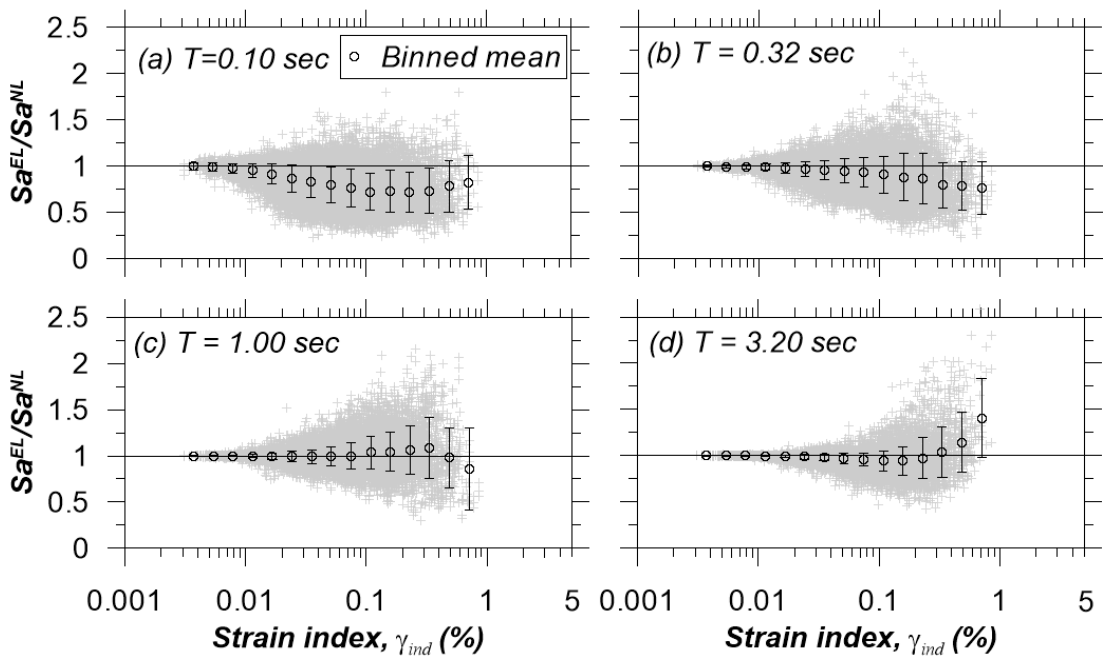

Figure 2.20 **Pseudo-spectral acceleration ratios for predicted motions from equivalent-linear and nonlinear analyses plotted against strain index γ_{ind}. Results show that the ratios depart from unity at high frequencies, indicating problem with equivalent-linear analyses. Modified from Kim et al. [2014] by B. Kim (personal communication, 2014).**

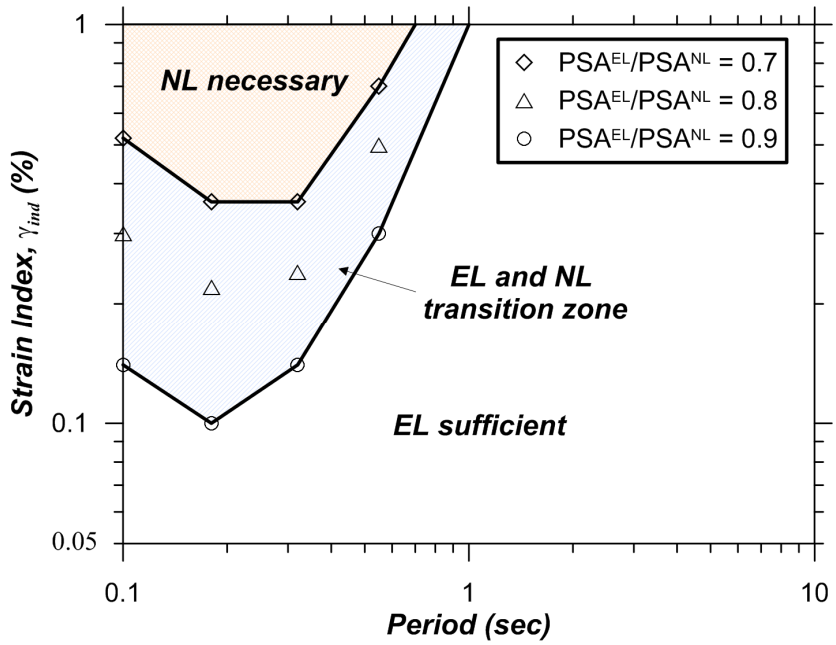

Figure 2.21 **Variation of strain index values where PSA from equivalent-linear analysis are biased low relative to PSA from nonlinear analysis. The plot shows the space where equivalent-linear analyses are effectively unbiased relative to nonlinear analysis, and where increasing amount of bias are observed (modified from Kim et al. [2013]).**

2.5 INPUT MOTION SELECTION

This section addresses critical issues associated with the development of input time series for use in GRA. Three principal factors affecting this process are: (1) definition of the target spectrum (or spectra) for the reference site condition; (2) the selection of ground motion time series that are compatible with the target; and (3) the use of ground motion scaling or spectral matching of selected time series to adjust them for compatibility with the target spectra. These issues are discussed in the three subsections that follow. The discussion provided here to a large extent mirrors recommendations provided for recent revisions of Chapter 16 in BSSC [2015], as described by Haselton et al. [2014–in review].

Both the target spectra and ground motion time series are evaluated for *reference site conditions*, which are defined as those conditions below the geotechnical layers being analyzed in GRA. Those layers are often rock for geotechnical profiles where rock is reached by the site exploration. However, for deep basin sites, the reference condition will often be firm soil at depth within the profile. For any selected reference site condition, input ground motions should be specified in GRA codes as outcropping and used with an underlying half-space having a V_S compatible with the reference site condition (assuming the selected recordings were recorded on the ground surface; details in Kwok et al. [2007]).

Because amplification functions are defined over a range of acceleration amplitudes, an important decision to be made in this process is whether to consider multiple hazard levels,

which will produce multiple levels of ground motion demand. The minimum is to consider only a single hazard level, corresponding to the design conditions being considered for the site.

2.5.1 Target Spectra

(a) Definition and Hazard Levels

Target spectra are defined as the pseudo-acceleration response spectra representing ground shaking demands for the reference site condition below the geotechnical layers being considered in GRA. Although building code applications use a maximum direction spectrum, denoted RotD100 by Boore [2010], we recommend that target spectra be defined for the component-median condition of RotD50. This is the ground motion definition considered in GMPEs (e.g., in the NGA-West 2 models and Bozorgnia et al. [2014], and is preferred here because the maximum component motions would produce potentially unconservatively large nonlinear responses).

Most engineering applications have a defined hazard level for which ground motions are to be evaluated. For new buildings, hazard analyses are nominally performed for ground motion intensity measures having a 2% in 50-year probability of exceedance. For California bridges, the Caltrans Seismic Design Criteria, Appendix B, [2013] requires that a 5% in 50-year hazard level is used. At a minimum, target spectra representing the design-basis hazard level should be used for the specification of input motions. However, if only this single hazard level is used, site amplification values Y (using nomenclature from Section 1.2.1) will only be defined for a narrow range of input motion amplitude X. Because amplification functions need to be defined over a range of acceleration amplitudes (e.g., Figure 1.4), it is desirable when feasible to consider multiple hazard levels providing widely variable input ground motion demand levels. Based on work performed to date, it appears that if the exceedance rate from hazard analysis for the design condition is λ_{des}, additional rates of $10\times\lambda_{\text{des}}$ and $0.25\times\lambda_{\text{des}}$ will provide a suitable range for most applications.

(b) Target Defined as Uniform Hazard Spectra or Modifications Thereof

For most applications, design ground motions are defined as Uniform Hazard Spectra (UHS), which are created by enveloping PSA values having a given probability of exceedance. The UHS ordinates at any period are not associated with a given earthquake, but rather represent the composite contributions of many magnitude-distance and ground motion realization combinations. The UHS will generally be a conservative target spectrum if used for ground motion selection and scaling, especially for large and rare ground motions, unless the site does not experience significant nonlinear ground response. This conservatism results from the fact that the spectral ordinates across the multiple periods that define a UHS are unlikely to all occur in a single ground motion realization [Bommer et al. 2000; Naeim and Lew 1995; and Reiter 1990].

In the building code, the risk-targeted maximum considered earthquake spectrum (MCE_R spectrum) has similarities to the UHS. The MCE_R spectrum is modified from the UHS with a risk coefficient to produce a 1% collapse risk in 50 years [Luco et al. 2007] and, for sites near active faults, it is capped at a lower-amplitude deterministic ground motion level. The use of the MCE_R spectrum is referred to as Method I in BSSC [2015] [Haselton et al. 2014].

Figure 2.22 shows an example site in southern California along with uniform hazard spectra computed using OpenSHA [Field et al. 2003] for a 2% in 50-year hazard level and two other rates. The reference site condition used in these calculations is V_{S30} = 760 m/sec and differential basin depth $\delta_{z1} = 0$ m.

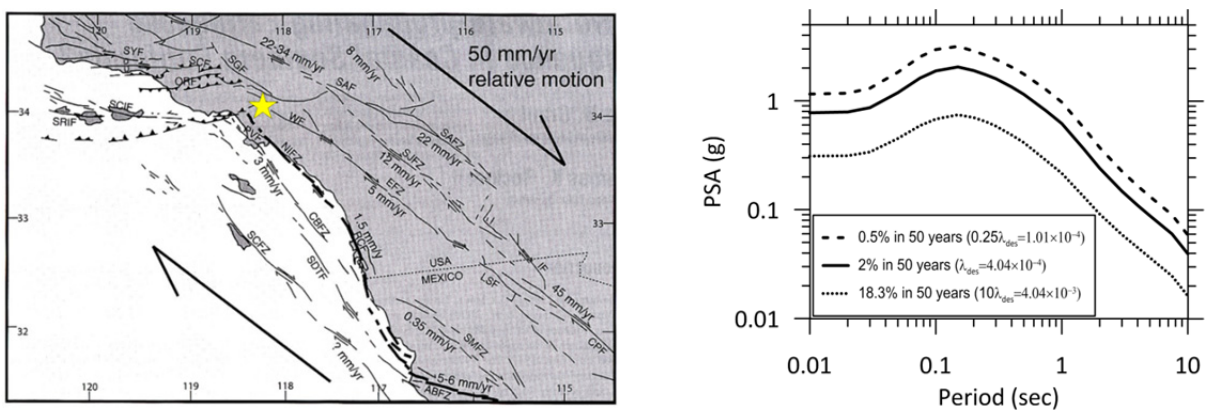

(a) (b)

Figure 2.22 (a) Location of example site (downtown Los Angeles) marked on southern California fault map by Grant and Rockwell [2002]; and (b) UHS for 0.2%, 2%, and ~20% in 50-year hazard levels (rupture forecast model: UCERF2, GMPE: see Boore et al. [2014]).

(c) Scenario Target Spectra

Scenario spectra represent ground shaking conditions that are compatible with the ordinate of the UHS at a period of interest but which have spectral shapes that are more physically realizable. As such, they comprise alternative target spectra to the UHS or MCE_R. Common definitions of scenario spectra are the conditional mean spectrum (CMS) and scenario spectra (CS).

The CMS conditions the spectrum calculation on the spectral acceleration at a target period, and then computes the mean spectral acceleration values for other periods (e.g., Baker and Cornell [2006]; Baker [2011]; and Al Atik and Abrahamson [2010]). The CMS is calculated as follows:

$$\mu_{\ln Sa(T_i)|\ln Sa(T^*)} = \mu_{\ln Sa}(\mathbf{M}, R, V_{S30}, T_i) + \rho(T_i, T^*)\varepsilon(T^*)\sigma_{\ln Sa}(\mathbf{M}, R, V_{S30}, T_i) \qquad (2.18)$$

where T_i is the spectral period, T^* is the matching period (e.g., for structural analysis it can be the first fundamental period of the structure), **M**, R, and $\varepsilon(T^*)$ are mean magnitude, distance, and epsilon from disaggregation of the hazard for PSA(T^*), μ_{lnSa} and $\sigma_{lnSa}(T_i)$ are the natural log mean and standard deviation of PSA at T_i, and $\rho(T_i, T^*)$ is the correlation coefficient between the epsilon at the matching period (T^*) and epsilon at T_i. Contours of $\rho(T_1,T_2)$ are shown in Figure 2.23 [Baker and Jayaram 2008].

Figure 2.24 shows example CMS, compatible with the 2% in 50-year UHS, for the site in Figure 2.22a. The CMS are computed at periods of 2.0 sec and 0.5 sec. Tools for the computation of CMS are available at the PEER-NGA website (*http://peer.berkeley.edu/nga/*) or with tools at the web site of Baker research group (*www.stanford.edu/~bakerjw*).

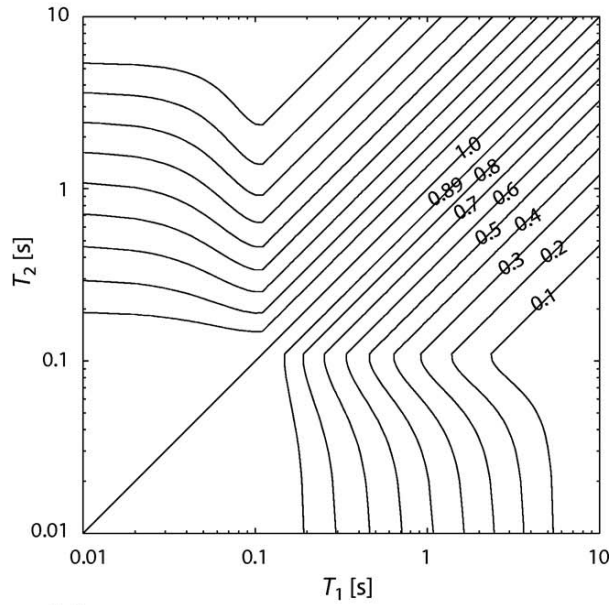

Figure 2.23 Contours of ρ (T_1, T_2) based on Baker and Jayaram [2008] relationships.

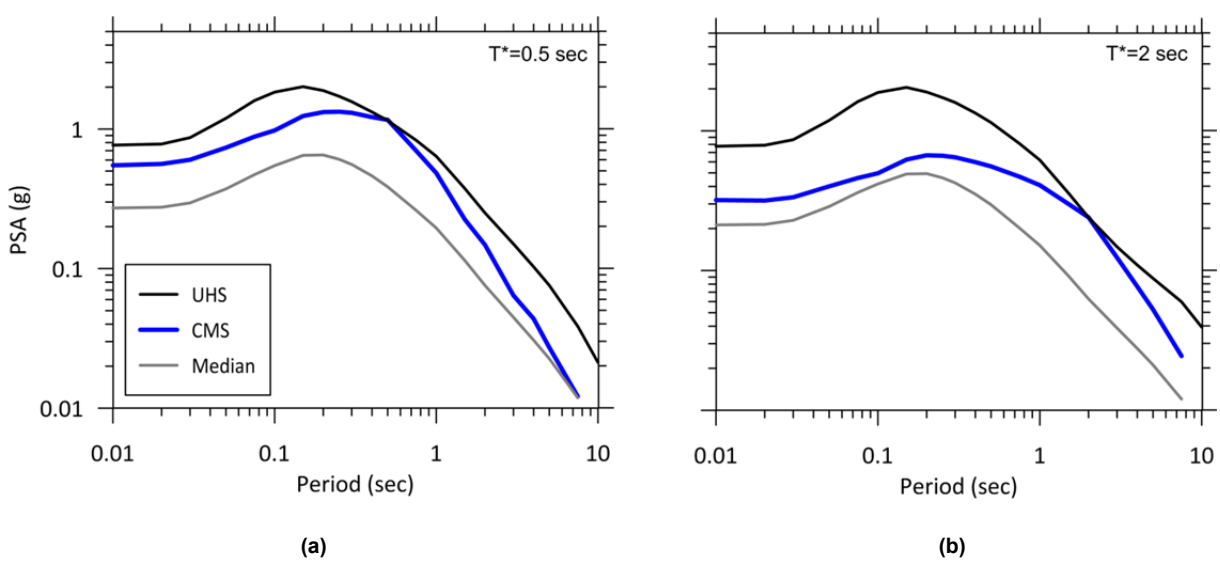

Figure 2.24 Two examples of CMS compatible with the 2% in 50-year UHS for the example site in downtown Los Angeles at matching periods of (a) 0.5 sec ($\overline{\mathbf{M}}$ = 6.7, $\overline{R}$ = 6.8 km, $\overline{\varepsilon}$ =1.71) and (b) 2.0 sec ($\overline{\mathbf{M}}$ = 6.9, $\overline{R}$ = 11.0 km, $\overline{\varepsilon}$ = 1.92).

The CMS is a mean spectrum and as such does not capture spectral variability. A comparable target that considers variability is the conditional spectrum (CS). The conditional mean and conditional mean ± 1.0 conditional standard deviation spectra for the 2.0 sec matching period are shown in Figure 2.25. The conditional standard deviation used in these calculations is given as Baker [2011]:

$$\sigma_{\ln Sa(T_i)|\ln Sa(T^*)} = \sigma_{\ln Sa}(\mathbf{M}, R, V_{S30}, T_i)\sqrt{1-\rho(T_i, T^*)^2} \tag{2.19}$$

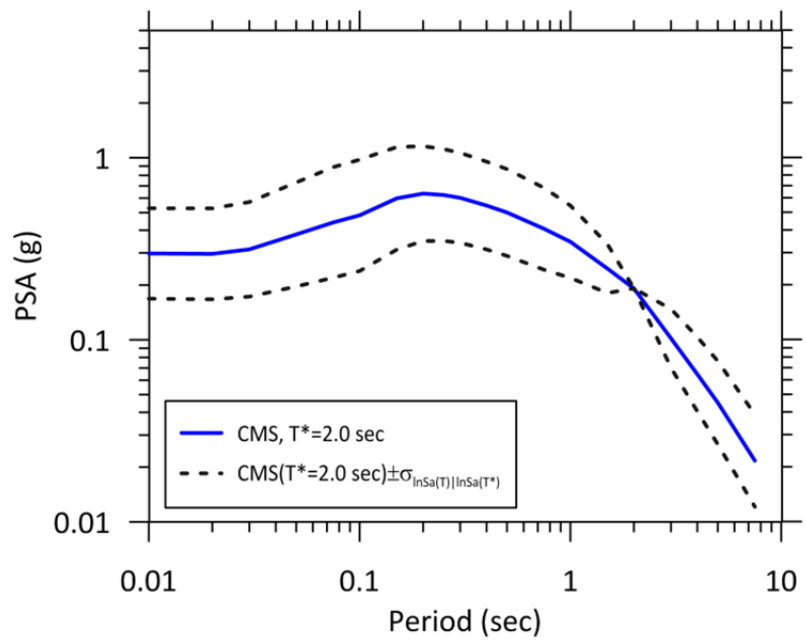

Figure 2.25 Conditional spectra compatible with the 2% in 50-year UHS at matching period of 2.0 sec for example site in downtown Los Angeles.

The use of CMS or CS as target spectra is denoted as Method II in BSSC [2015]. The following procedure can be used to develop site-specific scenario target spectra (modified from Haselton et al. [2014]):

1. Select two or more matching periods that correspond to periods of vibration that significantly contribute to the dynamic response of the system under consideration (building, bridge, or other). This will include a period near the system's fundamental mode periods (e.g., an average of the two horizontal direction periods, if they are relatively similar), or perhaps an extended period to account for inelastic period lengthening. For the case of bridges, periods should be selected that correspond to dominate vibration modes along and perpendicular to the bridge alignment (i.e., longitudinal and transverse modes). For sites having a strong impedance contrast, an additional matching period near the site period may also be considered.
2. For each selected matching period, perform a site-specific deaggregation to identify dominate magnitude-distance-epsilon (**M**-*R*-ε) scenarios. Such de-

aggregations can be performed using the USGS Deaggregation website (*http://geohazards.usgs.gov/deaggint/2008/*). For each matching period and corresponding epsilon develop a CMS or CS scenario spectrum using Equation (2.18) and, if CS, Equation (2.19). The PEER Ground Motion Selection website (*http://peer.berkeley.edu/products/strong_ground_motion_db.html*) provides a convenient online tool for the generation of CMS spectra.

The principal difference between this procedure and Method II in Haselton et al. [2014] is our lack of enforcement of a "floor" in spectral ordinates (taken as a percentage of the UHS). The lack of need for a floor is because input motions for the present application are only being used to derive amplification functions, not final response spectra for design.

2.5.2 Ground Motion Time Series Selection

(a) Number of Records

In general applications, the number of input motions used for a nonlinear response history analysis depends on whether the goals of the analysis are predictions of mean response or also quantification of the variability of response. For the present problem of nonlinear ground response, we require only the mean response. This is because the standard deviation of site response (σ_{lnY}) is derived separately, as described further in Chapter 3.

As described by Haselton et al. [2014], for Chapter 16 of BSSC [2015], eleven input motions were recommended, based prior work [FEMA 2012] showing that this number of motions provides mean response parameters that are within 30% at a 70% confidence level. For bridges, Caltrans prefers seven input motions, arguing that the modeling variability is sufficiently low to justify fewer motions (T. Shantz, *personal communication*, 2014). Seeking to balance precision with efficiency, and taking into consideration this precedent, we recommend the use of a minimum of seven, but preferably eleven, records from which to evaluate mean ground response at a single hazard level. If additional hazard levels are to be considered, as described in Section 2.5.1a, additional suites of seven or eleven records should generally be used. An exception is at low levels of input motions where the site response is effectively linear. For this condition, fewer records could be used, or a theoretical constraint on the level of amplification could be applied (as described further in Section 2.6).

A recorded ground motion is typically comprised of two horizontal components and one vertical component. For the present application, only horizontal records are of interest, and only a single component is required. This component is of arbitrary orientation for far-field sites; additional considerations apply to near-fault sites as explained further below.

(b) Differentiation of Near-Fault and Far-Field Sites

We define near-fault sites as having a reasonable probability of experiencing ground motions strongly influenced by rupture directivity effects. These effects can include large velocity pulses and polarization of ground motions such that the maximum direction of response is likely to be perpendicular to the fault strike. Any sites that are not near-fault are considered far field.

The potential for pulse-type ground motions affects ground motion selection, as described below. Ground motion polarization creates a potential for significantly stronger ground motions

in the fault-normal direction than in the fault-parallel direction, which in turn affects the levels of nonlinearity in site response. This issue is discussed further in Section 2.5.2d below.

Near-fault sites are located at close distance to the causative fault for an earthquake. Site-source distance can be evaluated from site-specific disaggregation at the periods of interest. Research to date suggests that pulses in high-amplitude ground motions are reasonably probable up to 10–20 km from the site [Shahi and Baker 2011] and that ground motion polarization in the fault-normal direction occurs for distances up to approximately 3–5 km [Watson-Lamprey and Boore 2007; Huang et al. 2008].

(c) Ground Motion Selection for Far-Field Sites

Traditional approaches required selected ground motions to have magnitudes, fault distances, source mechanisms, and site conditions that are roughly similar to those likely to cause the ground motion intensity level of interest, and not to explicitly consider spectral shape in ground motion selection. In many cases, however, response spectrum shape is the ground motion property most correlated with nonlinear response [Bozorgnia et al. 2010]. Accordingly, we consider spectral shape to be an important consideration when selecting input ground motions for GRA. When spectral shape is considered in the ground motion selection, the allowable range of magnitudes, distances, and site conditions can be relaxed so a sufficient number of ground motions with appropriate spectral shapes are available.

The selection of recorded motions occurs in two steps. Step 1 involves pre-selecting the ground motion records in the PEER NGA-West2 website (*http://peer.berkeley.edu/ngawest2/*) having reasonable magnitude, fault distance, source mechanisms, site conditions, and range of useable frequencies. In completing this pre-selection, it is permissible to use relatively liberal ranges because Step 2 involves selecting motions that provide good matches to a target spectrum (which implicitly accounts for many of the above issues). Note that the site condition used in Step 1 should be roughly compatible with that for the reference site condition presented below the geotechnical layers modeled by GRA.

Step 1 criteria for initial screening of ground motions are as follows:

- **Tectonic Regime:** Select recordings from the same tectonic regime as present at the site (typical choices are active crustal regions, stable continental regions, and subduction zones; Garcia et al. [2012]).
- **Magnitude and Distance:** These parameters are obtained from disaggregation of the hazard at a period of interest. Selecting ground motions having reasonably similar magnitude and distance is intended to provide generally compatible durations and spectral contents. Since spectral shape criteria are separately enforced in Step 2, the duration compatibility is the principal consideration. Duration is more related to magnitude than distance, so distance criteria need not be strict. Selecting a record set with a representative range of durations is especially important when modeling strength degrading systems.
- **Site Conditions:** Site conditions, typically represented by V_{S30}, exert a large influence on ground motions, but are already reflected in the spectral shape used in Step 2. For Step 1, reasonable limits on site conditions should be

imposed but should not be too restrictive as to unnecessarily limit the number of candidate motions.

- **Useable Frequency of the Ground Motion:** Only processed ground motion records should be considered for response history analysis. Processed motions have a usable frequency range and the most critical parameter is the lowest usable frequency. It is important to verify that the useable frequencies of the record (after filtering) accommodate the range of frequencies important to the nonlinear site response; this frequency (or period) range is discussed in the next section on scaling.

Considering the 2% in 50-year hazard level for the site in Figure 2.22, Figure 2.26 shows the disaggregation for 2-sec PSA. Based on this analysis, the controlling earthquake for this hazard level and earthquake is identified as $\overline{\mathbf{M}} = 6.9$ and $\overline{R} = 11.0$ km. Using the PEER NGA-West2 website (*http://peer.berkeley.edu/ngawest2/*) with **M** = 6.0 to 7.5, R_{JB} = 5–40 km and V_{S30} = 600 to 900 m/sec (representing reference rock conditions), we find the list of records given in Table 2.12.

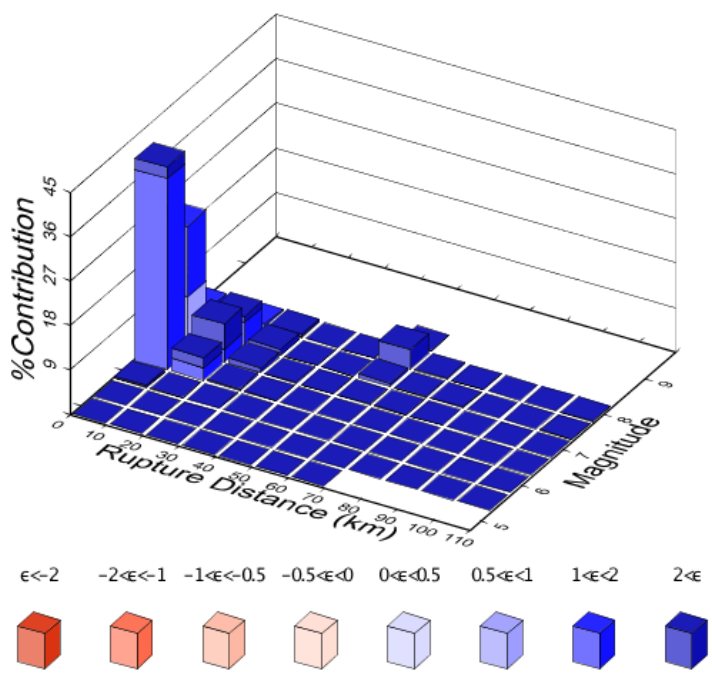

Figure 2.26 **Disaggregation of the 2% in 50-year hazard for 2 sec PSA for the example site for a reference site condition of 760 m/sec.**

Table 2.12 List of records from PEER website using Step I criteria for example site based on following criteria: 6.0 < M < 7.5, 5 km < R_{JB} < 40 km, and V_{S30} > 600 m/sec.

Record sequence number	M	R_{JB} (km)	Focal mechanism	V_{S30} (m/sec)	Minimum usable frequency (Hz)	PGA (*g*)	PGV (m/sec)	PSA (2.0 sec)(*g*)	ε (2.0)
63	6.6	36.5	Reverse	634	0.19	0.09	7.13	0.03	-1.19
71	6.6	37.7	Reverse	602	0.25	0.32	14.67	0.05	-0.24
72	6.6	23.8	Reverse	600	0.25	0.18	7.55	0.03	-1.13
73	6.6	34.0	Reverse	671	0.63	0.15	5.00	0.03	-1.00
80	6.6	32.1	Reverse	969	0.63	0.14	9.86	0.04	-0.74
87	6.6	15.2	Reverse	667	0.38	0.19	4.95	0.02	-1.70
285	6.9	24.8	Normal	650	0.11	0.15	29.99	0.24	1.97
296	6.2	26.5	Normal	650	0.41	0.05	4.06	0.02	-1.29
369	6.4	9.1	Reverse	648	0.25	0.16	15.93	0.15	1.27
454	6.2	15.6	Strike-slip	730	0.38	0.11	3.07	0.02	-1.53
455	6.2	25.3	Strike-slip	1428	0.20	0.08	2.75	0.02	-1.65
459	6.2	39.2	Strike-slip	663	0.16	0.27	26.78	0.07	0.32
511	6.1	21.8	Reverse-Oblique	680	0.38	0.12	4.62	0.01	-2.65
536	6.1	17.2	Reverse-Oblique	679	0.50	0.10	2.46	0.00	-3.91
537	6.1	17.8	Reverse-Oblique	659	0.63	0.13	3.71	0.00	-3.56
763	6.9	19.1	Reverse-Oblique	730	0.13	0.34	27.37	0.10	0.71
765	6.9	34.0	Reverse-Oblique	1428	0.08	0.43	32.70	0.11	0.86
769	6.9	39.0	Reverse-Oblique	663	0.16	0.16	13.89	0.16	1.36
775	6.9	20.7	Reverse-Oblique	621	0.13	0.05	7.34	0.06	-0.04
782	6.9	18.6	Reverse-Oblique	639	0.13	0.07	4.80	0.03	-1.00
791	6.9	18.2	Reverse-Oblique	609	0.06	0.07	10.80	0.07	0.21
801	6.9	23.0	Reverse-Oblique	672	0.04	0.28	25.65	0.08	0.42
809	6.9	15.6	Reverse-Oblique	714	0.13	0.37	11.90	0.04	-0.58
810	6.9	28.1	Reverse-Oblique	714	0.15	0.46	21.81	0.05	-0.35
934	6.5	30.3	Strike-slip	659	0.60	0.07	2.17	0.01	-2.72
989	6.7	25.4	Reverse	740	0.26	0.20	22.37	0.11	0.81
1011	6.7	23.6	Reverse	1223	0.18	0.14	12.20	0.04	-0.66
1012	6.7	21.2	Reverse	706	0.16	0.34	27.64	0.08	0.33
1020	6.7	31.5	Reverse	602	0.12	0.22	10.22	0.05	-0.32
1021	6.7	31.4	Reverse	600	0.12	0.08	6.06	0.03	-0.92
1023	6.7	26.0	Reverse	671	0.18	0.19	9.11	0.04	-0.47
1041	6.7	37.5	Reverse	680	0.50	0.19	6.49	0.02	-1.62
1091	6.7	22.4	Reverse	996	0.25	0.15	13.69	0.07	0.30
1111	6.9	17.3	Strike-slip	609	0.13	0.47	39.49	0.23	1.89
1126	6.4	21.1	Normal	650	0.75	0.16	7.73	0.05	-0.38
1613	7.1	22.4	Strike-slip	782	0.08	0.04	8.23	0.03	-0.92
1618	7.1	23.0	Strike-slip	638	0.08	0.15	11.83	0.03	-0.86
1633	7.4	25.2	Strike-slip	724	0.13	0.52	49.48	0.48	2.98

Record sequence number	M	R_{JB} (km)	Focal mechanism	V_{S30} (m/sec)	Minimum usable frequency (Hz)	PGA (*g*)	PGV (m/sec)	PSA (2.0 sec)(*g*)	ε (2.0)
1664	6.1	36.1	Reverse	602	1.20	0.01	0.30	0.00	-8.16
1787	7.1	13.9	Strike-slip	726	0.04	0.31	34.78	0.23	1.94
2622	6.2	37.9	Reverse	625	0.04	0.31	13.32	0.05	-0.19
2627	6.2	36.5	Reverse	615	0.07	0.38	44.14	0.12	0.99
2635	6.2	37.7	Reverse	672	0.13	0.09	8.58	0.11	0.83
2661	6.2	23.8	Reverse	653	0.10	0.13	19.94	0.18	1.54
2712	6.2	34.0	Strike-slip	665	0.05	0.09	8.11	0.07	0.16
2742	6.2	32.1	Strike-slip	665	0.06	0.11	12.38	0.07	0.22
2753	6.2	15.2	Strike-slip	804	0.05	0.06	2.71	0.02	-1.70
2820	6.2	24.8	Strike-slip	665	0.05	0.07	3.54	0.03	-1.24
2871	6.2	26.5	Strike-slip	665	0.20	0.05	6.56	0.04	-0.52
2873	6.2	9.1	Strike-slip	672	0.18	0.02	2.86	0.03	-1.17
2897	6.2	15.6	Strike-slip	653	0.06	0.04	9.68	0.07	0.19
2935	6.2	25.3	Strike-slip	665	0.06	0.07	5.24	0.02	-1.48
3008	6.2	39.2	Reverse	626	0.07	0.06	3.64	0.01	-2.93
3018	6.2	21.8	Reverse	602	0.06	0.07	4.86	0.03	-1.14
3022	6.2	17.2	Reverse	677	0.05	0.06	3.99	0.02	-1.88
3025	6.2	17.8	Reverse	643	0.06	0.04	4.89	0.05	-0.29
3334	6.3	19.1	Reverse	626	0.02	0.03	2.98	0.01	-2.60
3347	6.3	34.0	Reverse	677	0.04	0.03	2.95	0.02	-1.62
3472	6.3	39.0	Reverse	615	0.06	0.13	8.81	0.06	-0.08
3489	6.3	20.7	Reverse	714	0.04	0.05	8.38	0.10	0.79
3509	6.3	18.6	Reverse	653	0.04	0.06	8.90	0.14	1.20
3925	6.6	18.2	Strike-slip	940	0.01	0.15	11.09	0.07	0.25
3926	6.6	23.0	Strike-slip	694	0.04	0.24	9.67	0.04	-0.54
3932	6.6	15.6	Strike-slip	710	0.13	0.37	18.28	0.06	-0.12
3943	6.6	28.1	Strike-slip	617	0.08	0.22	15.30	0.10	0.68
3954	6.6	30.3	Strike-slip	967	0.04	0.20	15.67	0.12	0.95
4213	6.6	25.4	Reverse	655	0.08	0.39	25.39	0.22	1.85
4227	6.6	22.2	Reverse	653	0.05	0.17	8.65	0.05	-0.31
4231	6.6	23.6	Reverse	686	0.04	0.20	6.94	0.01	-2.55
4284	6.0	21.2	Strike-slip	621	0.38	0.14	6.96	0.02	-1.96
4472	6.3	31.5	Normal	613	0.04	0.09	6.20	0.03	-1.07
4475	6.3	31.4	Normal	638	0.13	0.02	2.34	0.02	-1.26
4485	6.3	26.0	Normal	650	0.10	0.01	0.75	0.01	-3.05
4503	6.3	37.5	Normal	613	0.03	0.03	2.95	0.03	-0.92
4841	6.8	16.3	Reverse	655	0.05	0.20	19.74	0.08	0.45
4842	6.8	22.4	Reverse	655	0.08	0.46	23.63	0.11	0.82
4843	6.8	17.3	Reverse	640	0.05	0.19	17.13	0.13	1.11
4844	6.8	21.1	Reverse	640	0.05	0.11	17.21	0.14	1.20
4845	6.8	22.4	Reverse	610	0.13	0.62	21.67	0.07	0.22

Record sequence number	M	R_{JB} (km)	Focal mechanism	V_{S30} (m/sec)	Minimum usable frequency (Hz)	PGA (*g*)	PGV (m/sec)	PSA (2.0 sec)(*g*)	ε (2.0)
4846	6.8	23.0	Reverse	606	0.08	0.31	25.89	0.09	0.57
4852	6.8	25.2	Reverse	606	0.09	0.23	15.77	0.11	0.90
4858	6.8	36.1	Reverse	640	0.06	0.22	20.70	0.15	1.35
4868	6.8	13.9	Reverse	655	0.10	0.34	34.81	0.11	0.91
4869	6.8	37.9	Reverse	640	0.06	0.16	12.51	0.09	0.53
4872	6.8	36.5	Reverse	640	0.09	0.14	19.80	0.18	1.56
5269	6.8	37.7	Reverse	655	0.04	0.05	4.70	0.05	-0.18
5472	6.9	23.8	Reverse	644	0.04	0.19	12.81	0.11	0.90
5474	6.9	34.0	Reverse	640	0.03	0.18	12.08	0.10	0.72
5483	6.9	32.1	Reverse	829	0.04	0.08	5.05	0.03	-0.80
5618	6.9	15.2	Reverse	826	0.03	0.27	24.87	0.30	2.30
5806	6.9	24.8	Reverse	655	0.24	0.20	23.26	0.40	2.72
5809	6.9	26.5	Reverse	655	0.24	0.25	14.72	0.17	1.51
5810	6.9	9.1	Reverse	655	0.19	0.16	29.88	0.20	1.72
5815	6.9	15.6	Reverse	655	0.10	0.20	16.58	0.30	2.28
5819	6.9	25.3	Reverse	640	0.10	0.34	7.92	0.02	-1.47
6928	7.0	39.2	Strike-slip	650	0.13	0.30	24.96	0.11	0.85
7087	6.3	21.8	Reverse	638	0.40	0.05	1.73	0.00	-3.76
8110	6.2	17.2	Reverse-Oblique	650	0.03	0.12	6.75	0.04	-0.65
8167	6.5	17.8	Reverse	1100	0.04	0.04	8.45	0.08	0.37

Step 2 criteria for final selection of ground motions are as follows [NIST 2011; Haselton et al., [2014]):

- **Spectral Shape:** The shape of the response spectrum should be the primary consideration when selecting ground motions. A good indicator of spectral shape is parameter $\varepsilon^{t}(T)$ at the period of interest (defined below).
- **Scale Factor:** A scale factor limit of approximately 0.25 to 4.0 is not uncommon.
- **Maximum Motions from a Single Event:** Although less important than spectral shape and scale factor, it is common to limit the number of motions from a single seismic event to three or four motions when possible.

In practice, the application of the Step 1 and 2 selection criteria are juxtaposed with scaling requirements–combined recommendations accounting for both aspects are given in Section 2.5.3.

The $\varepsilon^{t}(T)$ variable mentioned in the spectral shape bullet above is a metric of how different a given ground motion is from is expected based on a GMPE. This parameter has been

found to correlate strongly with spectral shape at period T and hence to be a good indicator of structural response [Baker and Cornell; 2006; Baker 2011]. For a given ground motion record, it is computed as:

$$\varepsilon^t(T) = \frac{\ln \mathrm{PSA}(T) - \mu_{\ln Sa}(\mathbf{M}, R, V_{S30}, T_i)}{\sigma_{\ln Sa}(\mathbf{M}, R, V_{S30}, T_i)} \tag{2.20}$$

where PSA*(T)* is the pseudo spectral acceleration at period T from the recording. Superscript 't' (for 'total residual') is used here so as to not confuse this parameter with the within-event residual as defined in Section 3.2.1. The present epsilon is a total residual (including within and between event components) that is normalized by the standard deviation, whereas ε in Chapter 3 [Equation (3.2)] is the within-event, non-normalized residual. A high ε^t (e.g., larger than 1) suggests a peaked spectral shape since neighboring periods are less likely to exceed the GMPE predicted median to the same degree as ε^t.

Using spectral shape considerations, 11 of the 99 records from Table 2.12 would be identified as roughly compatible with the disaggregation [$\varepsilon^t(T)$ = 1.5 to 2.3]. Figure 2.27 shows these records after scaling them to match the UHS (and CMS) at 2.0 sec period. The PEER web site enables record searches in which $\varepsilon^t(T)$ is a search parameter.

(d) Ground Motion Selection for Near-Fault Sites

For near-fault sites, a certain fraction of selected ground motions should exhibit pulse-like characteristics, while the remainder can be non-pulse records selected according to the standard process described above. The probability of experiencing pulse-like characteristics is dependent principally on (1) distance of site from fault; (2) fault type (e.g., strike slip or reverse); and (3) location of hypocenter relative to site, such that rupture occurs towards or away from the site.

Criteria (1) and (2) above are available from conventional disaggregation of PSHA. Criteria (3) can be computed as well in principle, but is not generally provided in a conventional hazard analysis. However, for the long ground motion return periods associated with typical design-basis ground motions, it is conservative and reasonable to assume that the fault rupture will be towards the site for the purposes of evaluating pulse probabilities. Empirical relations for evaluating pulse probabilities in consideration of these criteria are given in NIST [2011] and Shahi and Baker [2011].

Once the pulse probability is identified, the proper percentage of pulse-like records should be included in the ground motion selection. For example, if the pulse probability is 30% and eleven records are to be used, then three or four records in the set should exhibit pulse-like characteristics in at least one of the two horizontal components. The PEER Ground Motion Database can be used to identify records with pulse-type characteristics. The predominant period of the pulse is also an important selection criterion for pulse-like records and depends primarily on the magnitude of the event (which is known from disaggregation). Guidance on selection of ground motions with appropriate pulse periods can be found in Almufti et al. [2014].

2.5.3 Ground Motion Time Series Scaling

As indicated in Section 2.5.2c, it is often necessary to scale recorded ground motions in order to match the ground motion intensities associated with target spectra. In this context, scaling consists of simple multiplication of the time series by a constant (time-invariant) factor, which will increase its PSA by the same amount. Many applications in earthquake engineering utilize response spectral matching in addition to scaling, although this practice is not recommended for ground response applications.

The objective of ground motion selection and scaling is a record suite that is generally compatible with the amplitude and frequency content of the target spectrum (from Section 2.5.1). This goal is usually much more readily accomplished for scenario target spectra (which have realistic spectral shapes) than for UHS (which do not). Ground motion scaling procedures for direct structural application (e.g., BSSC [2015] as described by Haselton et al., [2014]) include strict requirements regarding the period range over which scaled motions must approximately match a target spectrum. These requirements are enforced because the scaled motions are used directly to evaluate structural performance. The present application for nonlinear ground response is different in that the input motions are being used to define a nonlinear site amplification function, which is then combined with the reference site ground motions to estimate ground surface motions. For this reason, it is not strictly necessary for input motions to match the target over a period range. Some variability in the input motions is actually desirable, as it provides a broader range of points with which to constrain the $Y|X$ amplification function.

With this in mind, two approaches for the coupled tasks of ground motion selection and scaling are considered to be suitable for GRA applications. The distinction between the approaches is that the first provides a more formal match of the record suite to the target spectrum (in a manner similar to structural applications), whereas the second matches the target at a given period but does not enforce matching elsewhere. These approaches can be summarized as follows:

- **Approach 1–enforced matching of target over period range**: Ground motions are selected and scaled such that as an ensemble their median matches the target spectrum over a defined period range. In BSSC [2015] Chapter 16, this period range is taken from $0.2T$–$2.0T$, where T is the elastic first mode period of a structure. In ground response applications, a similar range based on the period of the structural system that is the subject of the overall ground motion analysis will generally be important. It is also possible for this selection process to consider a defined uncertainty as in the conditional spectra (CS) approach. Approach 1 requires relatively sophisticated record search algorithms as implemented in the PEER web site[1] using procedures developed by Jarayam et al. [2011].
- **Approach 2–matching target at single period**: Ground motions are selected in consideration of spectral shape (as described in Step 2 of 2.5.2c) and scaled

[1] This approach can be implemented by choosing "Scaled option," uploading the target spectrum, activating "Scaling" option, choosing a period range (e.g., 0.1–1 sec), and applying default weights over the period range.

such that their PSA at a selected period matches the target spectrum at that period. If spectral shape is appropriately considered, for example through the use of $\varepsilon^t(T)$, general compatibility is likely but is not formally enforced.

For the example site shown in Figure 2.22, PSA for motions selected using Approaches 1 and 2 are shown in Figure 2.27. Both approaches provide a range of PGA^r for the motions selected as compatible with a hazard level, but this range is much larger for Approach 2. The utilization of GRA results derived from these motions to fit an amplification model is the subject of Section 2.6.

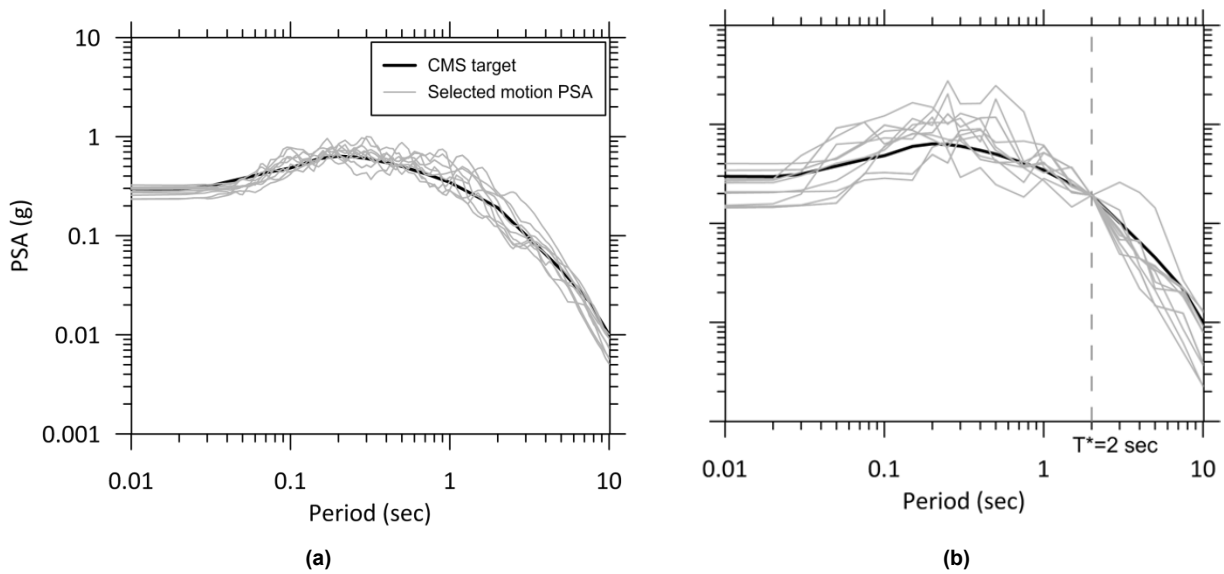

Figure 2.27 CMS-based target spectrum and PSA for 11 selected and scaled motions. Part (a) is Approach 1, using a range of periods (0.01–10 sec). Part (b) is Approach 2, using a single matching period at 2.0 sec.

2.6 FITTING GROUND RESPONSE ANALYSIS RESULTS TO SITE AMPLIFICATION FUNCTION $Y|X$

Section 1.2 described how a mean site amplification function is utilized to merge the results of ground response analysis (GRA) with the ground motion hazard for a reference site condition. The mean site amplification function was expressed as [Seyhan and Stewart 2014]:

$$\ln \overline{Y}(f) = f_1 + f_2 \ln\left(\frac{x_{IMref} + f_3}{f_3}\right) \tag{2.21}$$

where the overbar on Y indicates mean amplification, x_{IMref} is the reference site ground motion amplitude used as the driver of nonlinearity, f_2 represents nonlinearity, f_1 represents weak-motion (linear) amplification and f_3 represents the level of reference site ground shaking below which the amplification converges towards a linear (constant) upper limit.

In this section, we provide recommendations on the derivation of coefficients f_1, f_2, and f_3. The process by which these coefficients are derived depends on whether GRA are performed for input motions selected and scaled for compatibility with a single hazard level or multiple hazard levels, as described in Section 2.5.1a.

2.6.1 Input Motions Derived for Single Hazard Level

When the reference site ground motions are derived for a single hazard level, usually that prescribed for design purposes, values of amplification Y are computed for a relatively narrow range of x_{IMref}. Two examples of such site amplification results are shown in Figure 2.28 using ground motion selection and scaling Approaches 1 and 2 from Section 2.5.3. These site amplifications were derived for an example site, the characteristics of which are provided in Appendix A. In both cases, the range of x_{IMref} is sufficiently narrow that it is not possible to establish parameters f_1, f_2, and f_3 from regression. As a result, some parameters must be constrained through independent means and others set based on the site-specific GRA results.

One such approach is to constrain parameters f_2 and f_3 from an appropriate V_{S30}-dependent site amplification model such as the semi-empirical model of Seyhan and Stewart [2014]. In this case, parameter f_1 would be set based on the data, producing the fit shown Figure 2.28. The approach allows site-specific features related to profile impedance and possible resonance effects to be captured in the amplification function, although the level of nonlinearity is based on a global average from the site amplification model. Practically identical fits are obtained using analysis results based on Approaches 1 or 2; the fit in Figure 2.28 is based on Approach 1 results.

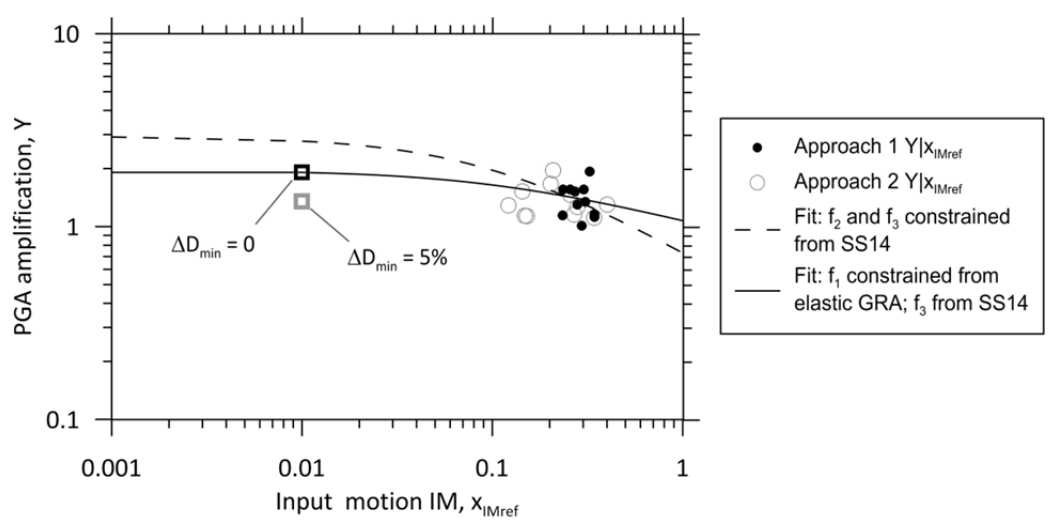

Figure 2.28 Examples of mean amplification plots using input motions selected and scaled to a single hazard level using input motions scaled and selected per Approaches 1 and 2 in Section 2.5.3. One fit is based on constraining f_2 and f_3, from an empirical model (SS14 = Seyhan and Stewart [2014]). The second fit is based on constraining f_1 from weak motion GRA results and f_3 from SS14. The effect of ΔD_{min} is also shown for the weak-motion GRA constraint.

An alternative approach is to run the GRA for very weak input motions (e.g., PGA^r of 0.01*g* or lower). Site amplification values from these analyses provide a constraint on weak motion amplification, which can be coupled with results at the design hazard level to compute regression coefficients. Results of calculations of this type are also shown in Figure 2.28 and for high-frequency IMs are quite sensitive to whether small strain damping ($D_{\min}$) is increased for field conditions as discussed in Section 2.3.3. To produce a satisfactory fit, we have found that the weak motion amplification cannot be assigned at $x_{IMre} = 0$. Limited trials have shown that when the IM used to drive nonlinearity is PGA, the weak motion amplification can be assigned at $x_{IMref} = 0.01g$. In this case, Equation (2.21) describes the amplification for $x_{IMref} > 0.01g$, and for weaker motions, a fixed amplification at the following level is used:

$$\ln \overline{Y}(f) = f_1 + f_2 \ln\left(\frac{0.01 + f_3}{f_3}\right) \tag{2.22}$$

Even with this weak motion constraint, it is typically necessary to set f_3 based on a site amplification model. A value of $f_3 = 0.1g$ is often effective (when x_{IMref} is based on PGA) and is used in Figure 2.28. Note that there is a trade-off between f_3 and f_2 when weak motion amplification is constrained in this manner; if f_3 is increased, f_2 will become more strongly negative. As is evident from the example in Figure 2.28, a good deal of judgment is associated with developing site parameters when GRA are performed for a single hazard level.

We consider both of the above approaches for deriving amplification functions from GRA results at a single hazard level to be equally viable. Variations in computed hazard that would occur from the use of both approaches are a sensible reflection of epistemic uncertainty associated with not performing GRA over a wide range of input motions.

2.6.2 Input Motions Derived for Multiple Hazard Levels

When site amplification is computed over a wide range of input motion amplitudes, in principle, parameters f_1, f_2, and f_3 can be established directly from regression. A spreadsheet included with this report performs this calculation (described in Chapter 4). It is often helpful in these analyses to constrain f_3 at a typical value that depends on the IM used for x_{IMref}; 0.1*g* works well for PGA. Figure 2.29 shows an example fit of this type. Table 2.13 lists values of fit parameters f_1, f_2, and f_3 from this approach and the more approximate methods in Section 2.6.1. The results in Table 2.13 highlight the tendency of the amplification model in Equation (2.21) to produce weak motion amplification (f_1) values that are larger than those computed from weak motion GRA. This can be overcome by truncating the amplification from Equation (2.21) at a specified weak motion value, as shown by the dashed line in Figure 2.29.

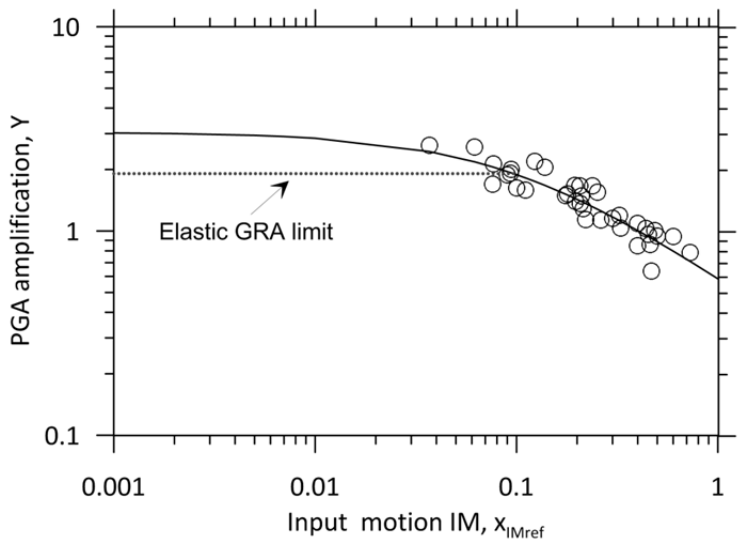

Figure 2.29 Example mean amplification values from GRA and mean fit using Equation (2.21) with f_3 fixed at 0.1*g*. Dashed line shows truncation at weak motion amplification level.

Table 2.13 Parameters for mean amplification equation for PGA obtained from different approaches

Approach	Constrained parameters	f_1	f_2	f_3
Single hazard level	f_2 , f_3	1.07	-0.58	0.1
	f_1 , f_3	0.67	-0.25	0.1
Multiple hazard level	f_3	1.13	-0.66	0.1

2.6.3 Variations across Periods

It will often be cumbersome to perform the fitting operations for parameters f_1, f_2, and f_3 for all of the periods used to construct a response spectrum. In lieu of this, it is possible for the analyst to compute these parameters for a selected number of periods over the range where GRA results are considered valid (usually this would be periods up to the site period). With these values established, additional values at intermediate periods can be interpolated in a way that captures the trends in the data while mimicking known trends from semi-empirical models (such as SS14). This interpolation can be evaluated as follows:

1. Compute the coefficient residuals for f_i (e.g., f_1, f_2, f_3), which are the differences between the GRA-based values (f_i^{GRA}) and the values from a semi-empirical model (f_i^{emp}):

$$\varepsilon^{f_i}(T_j) = f_i^{GRA}(T_j) - f_i^{emp}(T_j) \tag{2.23}$$

Index j is for the discrete number of periods where GRA results are regressed to evaluate parameters f_1, f_2, and f_3 (j = 1 to 6 in the example below). The semi-empirical values for f_i are available for many periods, whereas f_i^{GRA} are available for only a few periods.

A detail in the calculation of the coefficient residuals in Equation (2.23) is the IM used for x_{IMref}. Because SS14 use PGA for x_{IMref}, if f_i^{GRA} are similarly defined using PGA for x_{IMref}, the coefficient residuals are taken as the simple differences in Equation (2.23). When x_{IMref} is defined using an IM other than PGA, parameter f_3^{GRA} is mismatched from f_3^{emp} (f_1 and f_2 are unaffected[2]). For f_3, this can be corrected as follows:

$$\varepsilon^{f_3}(T_j) = f_3^{GRA}(T_j) - \frac{\ln \bar{X}_{IMref}\left(\bar{\mathbf{M}}, \bar{R}\right)}{\ln \overline{\mathrm{PGA}}_{ref}\left(\bar{\mathbf{M}}, \bar{R}\right)} f_3^{emp}(T_j) \tag{2.24}$$

where $\ln \bar{X}_{IMref}\left(\bar{\mathbf{M}}, \bar{R}\right)$ and $\ln \overline{\mathrm{PGA}}_{ref}\left(\bar{\mathbf{M}}, \bar{R}\right)$ are GMPE mean IMs for the reference site condition using $\bar{\mathbf{M}}$ and $\bar{R}$ from disaggregation.

2. For periods T_j, f_i^{GRA} is used directly without modification.
3. For periods $T \neq T_j$, f_i^{GRA} is interpolated by taking the sum of the empirical estimate f_i^{emp} and the weighted average of the residuals from Equation (2.23) for the nearest periods where GRA results are available:

$$f_i^{GRA}(T) = f_i^{emp}(T) + w_1 \varepsilon^{f_i}(T_1) + w_2 \varepsilon^{f_i}(T_2) \tag{2.25}$$

In Equation (2.25), period T_1 is the first period less than T for which GRA results are available, and T_2 is similarly the first larger period with GRA results. Weights w_1 and w_2 are based on the log differences between periods and are computed as:

$$w_1 = \frac{\log\left(T_2/T\right)}{\log\left(T_2/T_1\right)} \tag{2.26}$$

$$w_2 = \frac{\log\left(T/T_1\right)}{\log\left(T_2/T_1\right)} \tag{2.27}$$

[2] Simple algebraic manipulation will show that multiplying x_{IMref} and f_3 by a common factor (representing the IM ratio of GMPE means) will not change the ratio inside the logarithm in Equation (2.21), hence f_1 and f_2 are unchanged.

Figure 2.30 shows f_1 and f_2 values interpolated using this procedure for our example site (V_{S30} = 197 m/sec). In this example, GRA were used to compute f_1 and f_2 at six periods, and the above approach was used for other periods up to about 0.65 sec. A transition to the semi-empirical model is applied for long periods as described further below.

The complexity associated with Equation (2.24) for parameter f_3 is seldom required, because this parameter is usually fixed and not directly regressed from GRA results. Our recommendation is to take f_3 as 0.1g when x_{IMref} is PGA, and as the product of 0.1g and a reasonable ratio of reference IM median values as estimated from GMPEs [similar to the subtracted term on right side of Equation (2.24) otherwise].

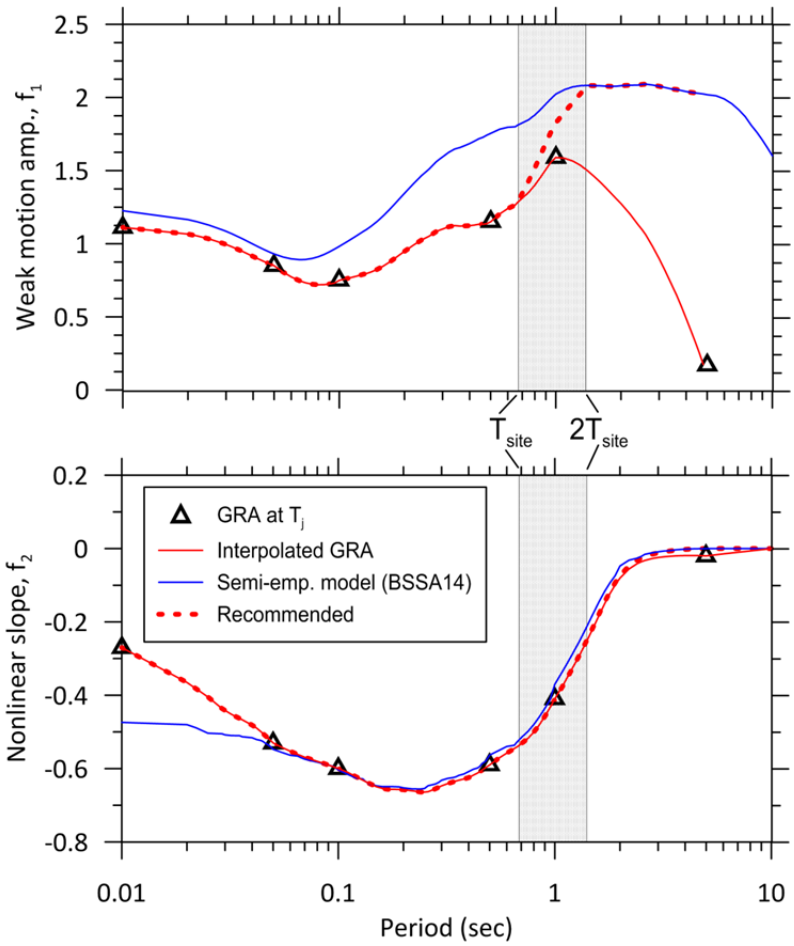

Figure 2.30 **Interpolation for calculating f_1 and f_2 values based on semi-empirical model and GRA-based values of f_1 and f_2 at six periods. For f_1, the semi-empirical model is taken as the sum of V_{S30}-based term ($\ln F_{lin}$) from Eq. 6 of BSSA14 and basin depth term $F_{\delta z1}$ from Eq. 9 of BSSA14. Basin depth of z_1 = 4.2 km was used for the site location in Figure 2.22. For f_2, the semi-empirical model is taken as term f_2 in Eq. 8 from BSSA14.**

At periods beyond the site period (T_{site}), GRA results have been found to be deficient in their ability to predict site response, as described in Section 1.1. For this reason, at periods greater than about two times the site period in the GRA model, we recommend that site amplification be taken from semi-empirical models, preferably including a basin term when applicable depth parameters are known.

As shown in Figure 2.30, differences between coefficients for the example site are negligible for nonlinear slope parameter f_2, but are quite significant for weak motion amplification f_1. For periods between T_{site} and $2T_{site}$, we propose the use of a transition zone from GRA-based parameters f_i^{GRA} for $T < T_{site}$ to semi-empirical model based parameters f_i^{mod} for $T > 2T_{site}$. If the site in question does not have a well-defined first-mode period, T_{site} can be taken as the period of the soil medium above the halfspace in the GRA model.

The proposed procedures for evaluation of model parameters across the transition zone are as follow:

1. For $T < T_{site}$, use $f_i = f_i^{GRA}$.
2. For $T_{site} < T < 2T_{site}$, use interpolated values:

$$f_i(T) = f_i^{GRA}(T) \times \frac{\log\left(2T_{site}/T\right)}{\log(2)} + f_i^{\mathrm{mod}}(T) \times \frac{\log\left(T/T_{site}\right)}{\log(2)} \tag{2.27}$$

3. For $T > 2T_{site}$, use $f_i = f_i^{\mathrm{mod}}$.

Results of these analyses are shown in Figure 2.30. The procedure produces a smooth transition between the period ranges where GRA and semi-empirical models control the site parameters.

3 Dispersion of Site Amplification and its Implementation in Probabilistic Seismic Hazard Analysis

3.1 INTRODUCTION

Site amplification is quantified by amplification factors (Y), which represent the ratio of a ground motion intensity measure on the ground surface (Z) to the intensity measure (IM) on the reference condition (typically rock), X:

$$Y = \frac{Z}{X} \text{ or } \ln Y = \ln(Z) - \ln(X) \tag{3.1}$$

The implementation of site amplification factors in probabilistic seismic hazard analyses (PSHA) requires knowledge of Y, which is typically taken as log-normally distributed. The standard deviation of Y (denoted ϕ_{lnY}) contributes to the within-event dispersion of earthquake ground motions, which is commonly denoted as ϕ. Chapter 2 described several sources of variability in site amplification, including uncertainty in shear-wave velocity profiles, modulus reduction and damping curves, and input motions. All of these factors are thought to contribute to ϕ_{lnY}, along with more complex features of site response related to geologic structure and other factors that are difficult to quantify.

A second standard deviation term that is important to consider in the present context, where site-specific GRA are being incorporated into PSHA, is the between-site standard deviation (denoted ϕ_{S2S}). This dispersion term contributes to the within-event standard deviation provided by GMPEs (ϕ), in which site response effects for the many sites contributing to the dataset are captured only through a relatively generic, V_{S30}-based site term. The use of such a site term in the GMPEs comprises the classical ergodic approach, in which site-specific effects are not included beyond the global-average site amplification that is associated with the site's V_{S30}. The commensurate lack of knowledge of site-specific effects comprises epistemic uncertainty that contributes to ϕ. When a proper site-specific analysis is performed, the extra knowledge that is gained reduces the epistemic uncertainty in the mean site amplification, which in turn can be used to justify reductions in ϕ. That reduction is implemented using ϕ_{S2S}, as explained in Section 3.2 below.

In Section 3.2, we describe the general components of ground motion variability, which include ϕ_{S2S} and ϕ_{lnY} along with terms related to path and source variability. Section 3.3 describes the estimation of site amplification variability (ϕ_{lnY}) from simulations using results found in the literature, while Section 3.4 presents an evaluation of both ϕ_{S2S} and ϕ_{lnY} using analyses of array data in the literature. The chapter is concluded in Section 3.5 with preliminary recommendations for values of both standard deviation terms.

3.2 COMPONENTS OF GROUND MOTION VARIABILITY

3.2.1 Ground Motion Components Expressed in GMPE Framework

Earthquake ground motions are affected by source, path, and site effects, each of which has corresponding terms in GMPEs. Each of those terms may be systematically in error for a particular earthquake source, wave path, and site. Provided sufficient data exists, those systematic component errors can be estimated through mixed effects methods of residuals analysis (e.g., Pinheiro et al. [2013]). A general expression to help visualize such effects is as follows (adapted from Al Atik et al. [2010]):

$$\ln z_{ij} = \left(\mu_{\ln Z}\right)_{ij} + \eta_{Ei} + \eta_{Pi,j} + \eta_{Sj} + \varepsilon_{ij} \tag{3.2}$$

where z_{ij} represents a recorded ground motion for site i and event j, $(\mu_{lnZ})_{ij}$ represents the mean from a GMPE (in natural log units), and η_{Ei}, $\eta_{Pi,j}$, and η_{Sj} represent event, path, and source terms, respectively. The term ε_{ij} represents the remaining residual when each of the above systematic biases are removed.

Each of the event, path, and source terms has corresponding standard deviations. Following the notation introduced by Al Atik et al. [2010], the standard deviation of between-event terms, between-path terms, and between-site terms are denoted τ, ϕ_{P2P}, and ϕ_{S2S}, respectively. The remaining aleatory standard deviation (of the ε_{ijk} term) is often taken as ϕ_{lnY}, although this term may represent sources of within-event aleatory variability beyond the site amplification (e.g., some path effects are included). The total standard deviation can then be computed as:

$$\sigma = \sqrt{\tau^2 + \phi_{P2P}^2 + \phi_{S2S}^2 + \phi_{\ln Y}^2} \tag{3.3}$$

The three 'phi-squared terms' in Equation (3.3) sum to ϕ^2, which is the total within-event variance.

3.2.2 Ground Motion Components Relative to Predictions from GMPE with Location-Specific Site Factors

When a site-specific analysis of ground motion amplification is available, it is combined with a GMPE applied for reference rock conditions to estimate ground motions. In this case, Equation (3.2) is re-written as:

$$\ln z_{ij} = \left(\mu_{\ln X}\right)_{ij} + \eta_{Ei} + \eta_{Pi,j} + \ln \overline{Y}_{ij} + \varepsilon_{ij} \tag{3.3}$$

Equation (3.4) is identical to Equation (3.2) from the prior section, except that the GMPE-based mean ground motion for soil (μ_{lnZ}, which includes a generic site term) has been replaced with a GMPE-based mean ground motion for rock (μ_{lnX}) and site-term η_{Sj} has been replaced with mean location-specific site amplification, $\ln \overline{Y}_{ij}$. Note that Equation (3.4) only applies for an unbiased site term for the conditions at site *j*. If the site term has bias, then an additional η_{Sj} term would be required, although presumably the numerical value of that term would be smaller (in an absolute value sense) than its value in Equation (3.2)

As we have seen in Section 1.2.1, when a site-specific nonlinear amplification function is combined with a rock GMPE, the within-event variance is the sum of the site amplification variance ($\phi^2_{\ln Y}$) and the within-event reference rock site variance reduced for effects of site response nonlinearity [Equation (1.12)]. As in Section 3.2.1, the within-event reference rock site variance from a GMPE includes contributions from path-to-path and site-to-site variability (site amplification variability is assumed to be negligible, as the site response for reference rock conditions will typically be null or very nearly so). While there can be no doubt that rock sites exhibit considerable site-to-site variability, by undertaking a site specific analysis, it is expected that this source of variance is reduced. If the site response were perfectly represented by the mean amplification function $\overline{Y}_{ij}$ (including both the soil and rock components of the site), the site-to-site contribution to the variance would be eliminated. Under such conditions, the within-event component of ground motion variability can be adapted from Equation (1.12) as:

$$\phi = \sqrt{\left(\frac{f_2 x}{x + f_3} + 1\right)^2 \phi^2_{P2P} + \phi^2_{\ln Y}} = \sqrt{\left(\frac{f_2 x}{x + f_3} + 1\right)^2 \left(\phi^2_{\ln X} - \phi^2_{S2S}\right) + \phi^2_{\ln Y}} \tag{3.4}$$

This form of the within-event standard deviation function would be appropriate when the site amplification is derived from on-site recordings (e.g., from a vertical array). On the other hand, when the site amplification is computed by models such as GRA, we cannot be sure that $\overline{Y}$ is unbiased and that site-to-site variability is eliminated. Under these conditions, it is convenient to re-write Equation (3.5) as:

$$\phi = \sqrt{\left(\frac{f_2 x}{x + f_3} + 1\right)^2 \left(\phi^2_{\ln X} - F\phi^2_{S2S}\right) + \phi^2_{\ln Y}} \tag{3.5}$$

where F ranges from zero to one. A value of F = 0 indicates no confidence that the site amplification factors remove site-specific effects beyond the capability of generic site terms in GMPEs (this is the case in Section 3.2.1). A value of F = 1 corresponds to the ideal conditions in which site-to-site variability is completed removed. The appropriate values for F are not known when a GRA is used to estimate site factors. We discuss this matter further in the recommendations (Section 5.2.1).

3.3 ESTIMATING UNCERTAINTY IN SITE AMPLIFICATION FROM SIMULATIONS

One way of quantifying the uncertainty in site amplification (ϕ_{lnY}) is to perform a suite of ground response analyses that capture the effects of different sources of variability by introducing random realizations of input parameters, running analyses for different combinations of the realizations, and obtaining the probability distribution of results (i.e., the log mean and standard deviation of site amplification). Sources of variability that can be captured in this manner using 1D GRA are variable input motions, randomness in V_S profiles, randomness in modulus reduction and damping (MRD) curves, and model-to-model variability. Because they require the use of ground motion data, sources of variability that cannot be investigated are the effects of epistemic uncertainty associated with limitations of the 1D assumption. These include effects of 3D geological structure and surface waves.

In this section, four studies are summarized that have produced results that allow the estimation of ϕ_{lnY}. These studies provide insight into the factors controlling ϕ_{lnY} and provide estimates of ϕ_{lnY} that can be subsequently compared to those evaluated from ground motion data. Table 3.1 summarizes the sources of variability considered in the four studies.

Table 3.1 Sources of variability considered in simulation-based studies of ϕ_{lnY}.

Study	Input motion	Velocity profile	MRD curves	Model to model variability
Li and Assimaki [2011]	No[1]	Yes	Yes	No
Rathje et al. [2010]	Yes	Yes	Yes	No
Kwok et al.[2008]	No	Yes	Yes	Yes
Bazzurro and Cornell [2004b]	Yes	Yes	Yes	No

[1]Input motion variability not considered together with other sources of variability, but is considered as a stand-alone source of ground motion variability.

3.3.1 Li and Assimaki [2011]

As indicated in Table 3.1, Li and Assimaki investigated the effect of variability in V_S profiles and MRD curves on the results of 1D GRA. Their analyses were undertaken using the downhole array sites Obregon Park (CE.K400), Los Angeles-La Cienega Geotechnical Array, and El Centro-Hwy8/Meloland Overpass. We summarize here their results for the La Cienega site. Velocity profiles based on suspension logging for the three sites are shown in Figure 3.1.

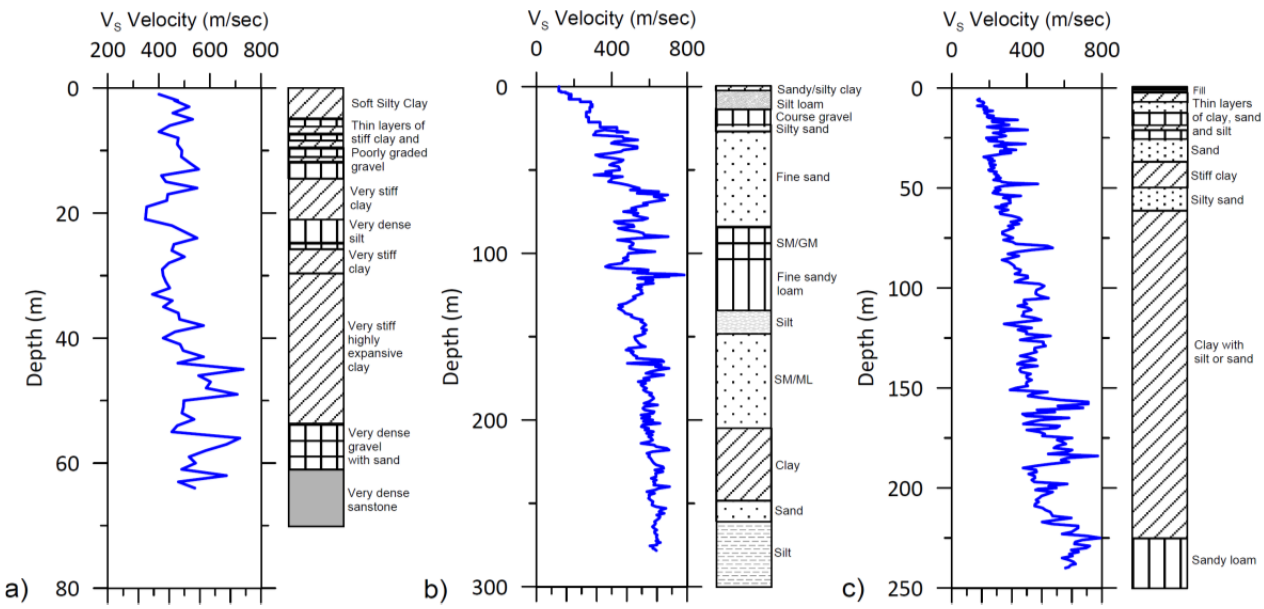

Figure 3.1 Velocity profiles and soil properties for three sites investigated by Li and Assimaki [2011]: (a) Obregon Park (CE.K400), (b) Los Angeles-La Cienega Geotechnical Array, (c) El Centro-Hwy8/Meloland Overpass (data from Nigbor et al. [2001]).

Measured values of velocity were used as the base value. Uncertainty in the velocity profiles was evaluated using the Toro [1995] model for generic site conditions (see Section 2.2.1). For MRD curves, they used the generic relationships given by Darendeli [2001], which are taken as the baseline or median modulus reduction or damping ratio relationships. They also used Darendeli [2001] relationships for capturing variability in modulus reduction and damping ratio [described in Section 2.2.2(c) and 2.3.1(b)].

For input motions, they used simulated accelerographs obtained from a finite source dynamic rupture model [Liu et al. 2006]. Both weak and strong ground shaking conditions were considered. Ground response analyses were performed using an 'in-house' nonlinear code (not generally available outside of the investigators' university). As documented by Assimaki et al. [2008], the code has some similarities to DEEPSOIL [Hashash 2012] in that it uses the monotonic constitutive law by Matasovic and Vucetic [1995]. In lieu of the Masing rules, it uses a modified hysteretic formulation by Muravskii [2005] capable of matching target MRD curves.

To investigate a particular source of variability (e.g., V_s), all other factors were held constant and analyses were performed across a suite of the variable parameter. For the example of considering V_s variability, a particular input motion would be used with mean MRD curves; two simulated input motions representing weak and strong motion conditions were selected. Figure 3.2 shows standard deviations in site amplification computed in this manner for different sources of input variability for the La Cienega site. Their results are intended to show that the factors contributing to the uncertainty in site amplification are different for weak and strong shaking conditions. For weak motion conditions, V_s variability dominates the total variability, whereas for strong shaking both V_s and MRD variability contribute significantly. The standard

deviation results shown in Figure 3.2 do not unambiguously demonstrate these findings because V_S and MRD variability were not partitioned for both the weak and strong motion cases in the Li and Assimaki [2011] paper. Nonetheless, the relatively high dispersions for the strong-motion cases can speculatively be associated with an increased effect of MRD variability for this condition. It also can be seen that the standard deviation drops at periods longer than the site period. This feature is somewhat characteristic of site response variabilities computed from GRA and is discussed further below.

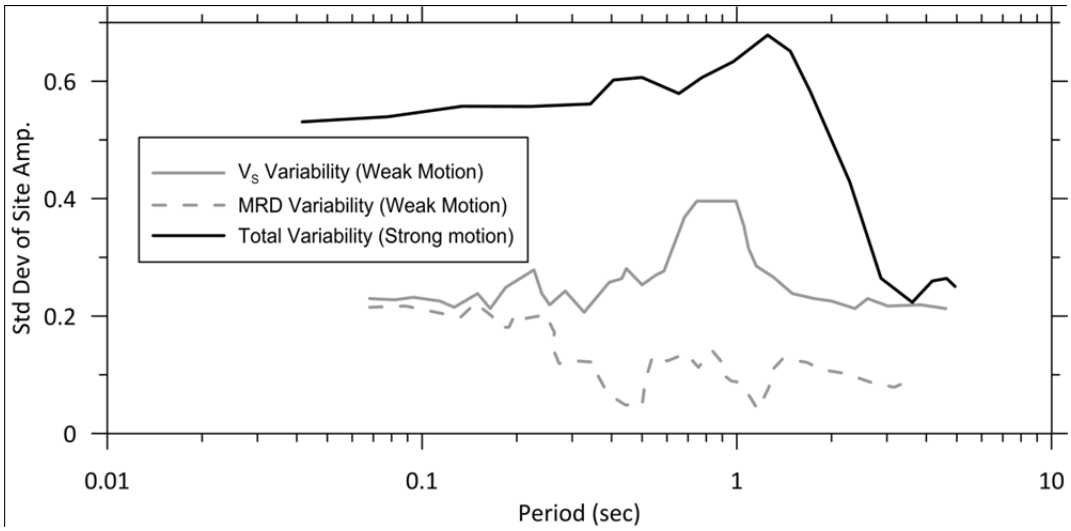

Figure 3.2 Contribution of different sources of variability to site amplification variability for La Cienega site [Li and Assimaki 2011].

3.3.2 Rathje et al. [2010]

Rathje et al. [2010] investigated the effect of soil property (V_S profile and MRD) variability as well as the variability in input motion for a deep alluvium site (Sylmar County Hospital, SCH). The velocity profile for the site is shown in Figure 3.3 (from Gibbs et al. [1999]).

The GRA were performed using the program STRATA [Kottke and Rathje 2009], which performs EL analyses with the input motion represented by time series or a response spectrum. In the case of a response spectral representation of input, random vibration theory is used to convert between Fourier spectra and response spectra in combination with assumed white noise phase. STRATA has built-in capabilities for randomizing the velocity profile using the Toro [1995] method and the MRD curves using the relationships given by Darendeli [2001]. Note that these are the same soil property randomization methods used by Li and Assimaki [2011].

The soil property randomization by Rathje et al. [2010] used the built-in capabilities in STRATA. The V_S variability departed slightly from the Toro [1995] recommendations by using a fixed value with respect to depth of $\sigma_{\ln V} = 0.2$. Input motions were provided as time series, which were matched to a target spectrum from the Abrahamson and Silva [1997] rock GMPE (**M** 6.5 and R_{rup} = 20 km). Suites of 5, 10, and 20 motions were selected and scaled to fit the target spectrum.

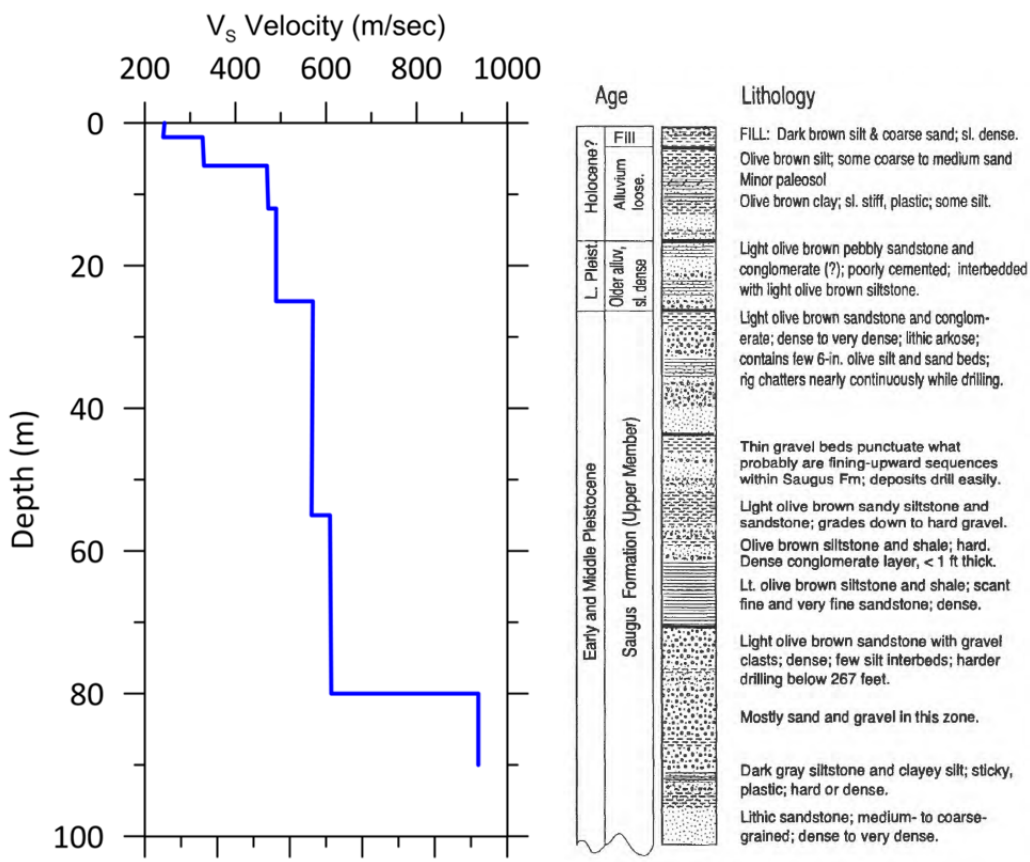

Figure 3.3 Velocity profile of the Sylmar County Hospital (SCH) site in southern California [Gibbs et al. 1999].

As shown in Figure 3.4, GRA were performed initially considering only input motion variability, then V_s variability was added, and finally MRD variability was added. The standard deviation of site amplification was computed at each stage as shown in Figure 3.4. The most important source of variability in this case was the input motions, followed by the V_s profile variability. As with the La Cienega site investigated by Li and Assimaki, the standard deviation for SCH initially rises with period, reaches a peak near or just before the site period, and falls beyond the site period.

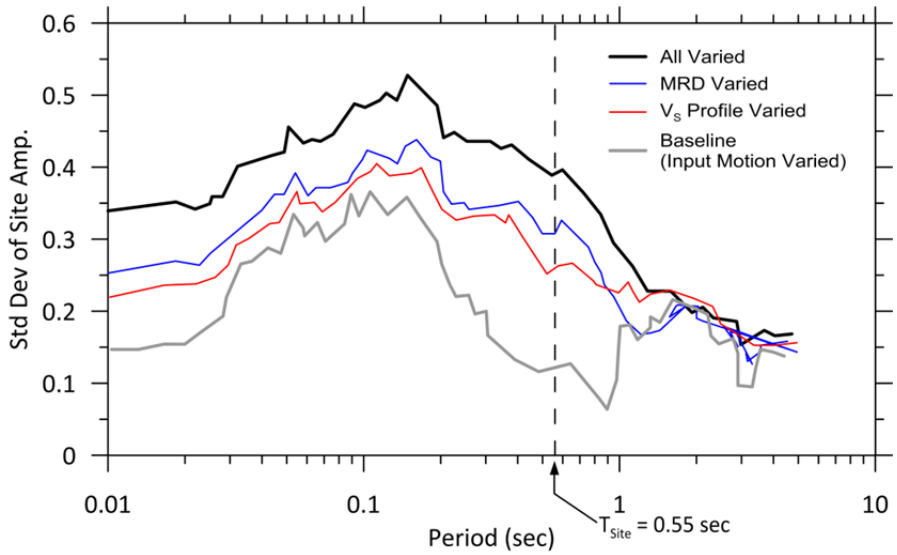

Figure 3.4 Contribution of different sources of variability to ϕ_{lnY} for SCH site [Rathje et al. 2010].

3.3.3 Kwok et al. [2008]

Kwok et al. [2008] investigated the site response at the Turkey Flat vertical array site during the 28 September 2004 Parkfield earthquake (**M** 6.0). They performed a number of EL and NL analyses for the site, and studied the effect of uncertainty in the *Vs* profile, MRD curves, and the effect of using different programs for the analyses. Because they used the motions recorded in the Parkfield event, ground motion input variability was not considered.

The Turkey Flat strong motion array and the velocity profile of the site are shown in Figure 3.5. The Valley Center vertical array was used, which has surface (V1) and bedrock (D3) instruments. The D3 record was used as input.

As shown in Figure 3.5, variability in the V_s profile is based on multiple measurements, and corresponds to a coefficient of variation (comparable to $\sigma_{\ln V}$) of about 0.2. In the GRA, V_S profile variability was captured using the first order second moment (FOSM) method [Cornell 2003; Melchers 1999] in which three profiles corresponding to mean and mean $\pm\sqrt{3}\sigma$ conditions are used. The standard deviation of the surface motion is computed from the weighted variance of the GRA results, using weights of two-thirds for the mean and one/sixth for the mean $\pm\sqrt{3}\sigma$ profiles. The generic relations by Darendeli [2001] were used for the mean and variation of MRD; MRD variability was also implemented in the GRA using the FOSM approach.

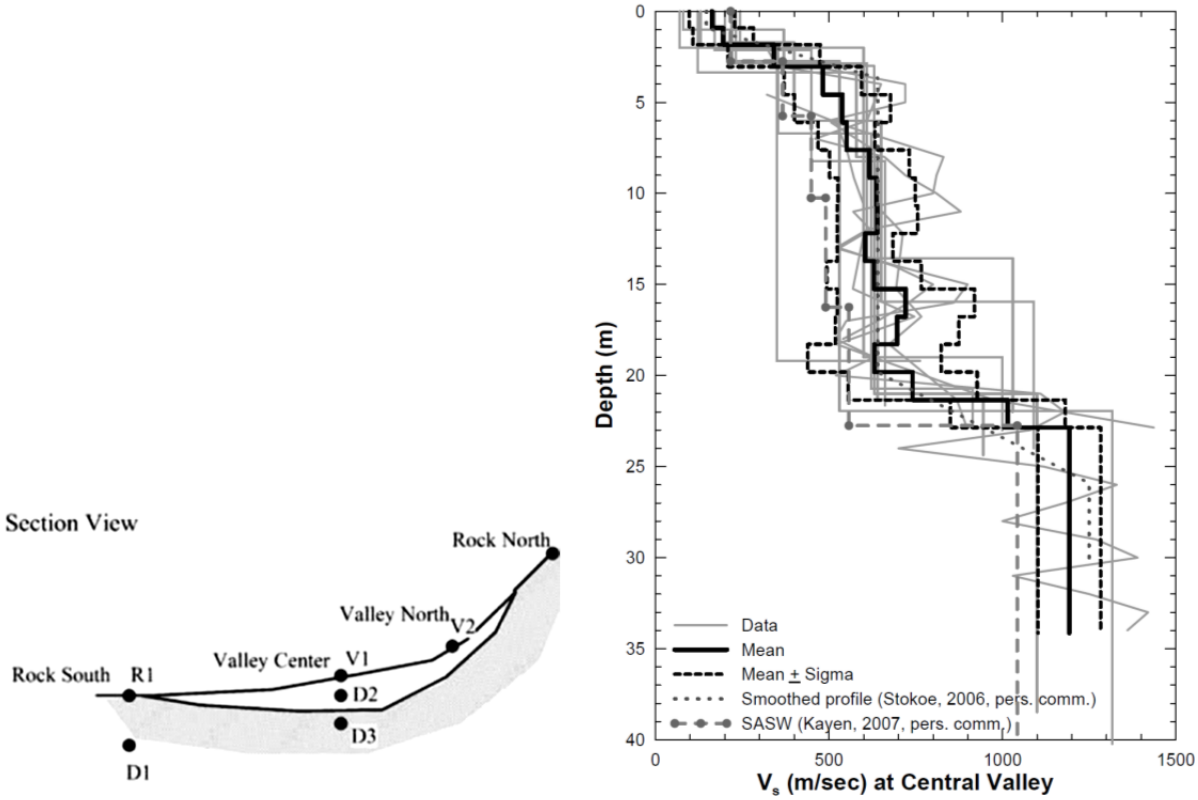

Figure 3.5 Schematic illustration of Turley Flat vertical arrays and the velocity profile of Valley Center site [Kwok et al. 2008].

Model-to-model variability was captured by running the GRA using six different programs for mean soil conditions: SHAKE04 [Youngs 2004], D-MOD_2 [Matasovic 2006], DEEPSOIL [Hashash and Park 2001; 2002, Park and Hashash 2004], TESS [Pyke 2000], OpenSees [Ragheb 1994; Parra 1996; Yang 2000; and McKenna and Fenves 2001], and SUMDES [Li et al. 1992].

Figure 3.6 shows the standard deviation of the surface motion for the various sources of variability. Because a single input motion was used, this ground motion dispersion matches the site amplification dispersion. The largest contributor is from V_S variability followed by model-to-model variability and MRD variability. The general trend of the site amplification dispersion with period matches those from the La Cienega and SCH sites (increase to just before site period, then decrease).

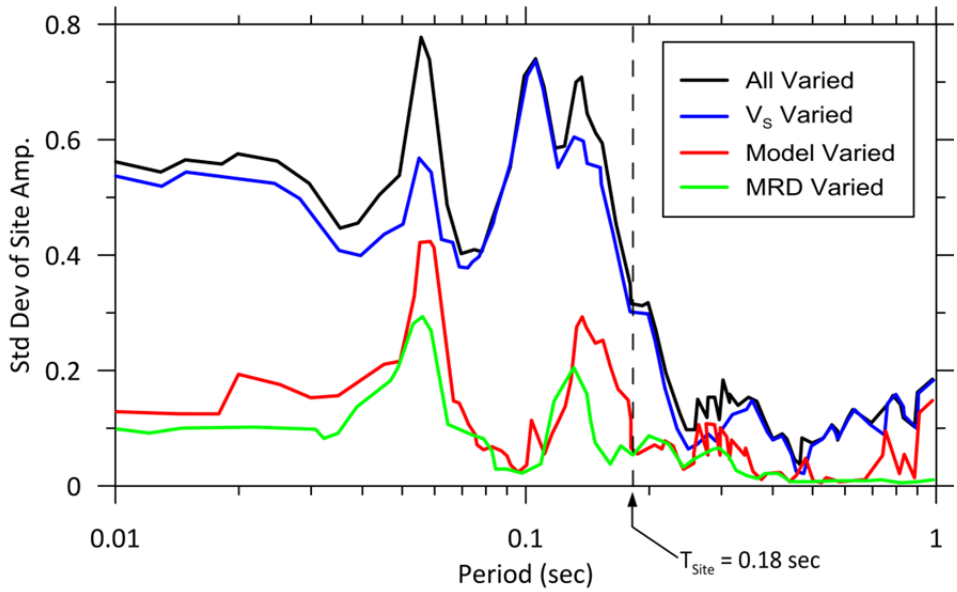

Figure 3.6 Standard deviation of amplification function and its different components for Turkey Flat site during Parkfield earthquake [Kwok et al. 2008].

3.3.4 Bazzurro and Cornell [2004b]

Bazzurro and Cornell [2004b] investigated parameters affecting amplification functions (such as earthquake magnitude, distance, peak ground acceleration on rock, and rock spectral acceleration). As part of that study, they also investigated the effect of uncertainty in input motion and soil parameters on the variability of the amplification function $(\phi_{\ln Y})$.

They considered two off-shore sites comprised predominantly of sandy and clayey soils, with the V_S profiles shown in Figure 3.7. Ground response analyses were performed using the finite element program SUMDES [Li et al. 1992], which is a nonlinear code with effective stress analysis and pore pressure generation capabilities.

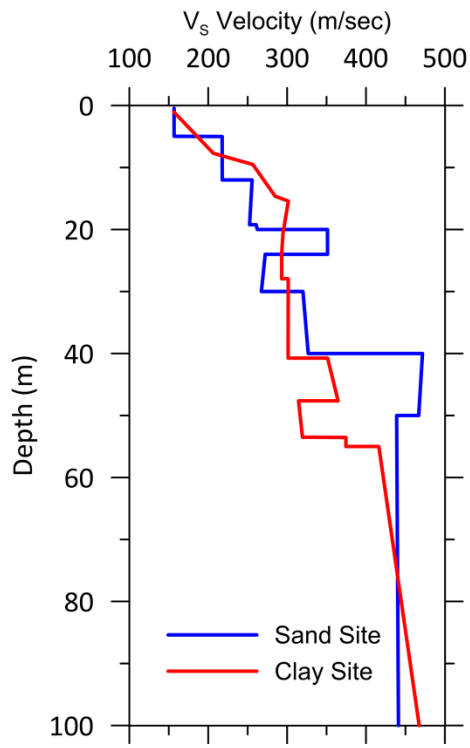

Figure 3.7 ***V_S* profile of the two sites studied by Bazzurro and Cornell [2004b].**

Variability in soil properties was captured by randomizing the coefficient of permeability (π_0), shear and compression viscous damping ratios at 1Hz (ξ_s and ξ_c), the coefficient of lateral earth pressure at rest (K_0), $G_{\max}$, the soil friction angle (ϕ), and the shear strain value at $G/G_{\max} = 0.64$ $(\gamma_{64\%})$. These variables are considered as log-normally distributed, and the standard deviation for ξ_s, ξ_c, K_0, and $G_{\max}$ is assumed 0.25, 0.1 for ϕ, 0.35 for $\gamma_{64\%}$, and 0.7 for π_0. Because the standard deviation for G_{max} is 0.25, the standard deviation for V_S is 0.125, which is less than the values used in the other studies described above (approximately 0.2). The spatial correlation between soil layers was defined by a first-order auto-regressive model, with correlation coefficient equal to 0.58 [Toro 1995].

The GRA were performed considering input parameter variability only, input motion variability only, and with the two sources of variability combined. Figure 3.8 shows the resulting values of $\phi_{\ln Y}$, which are consistent for both sites. The input motion variability is much larger than that from variability in soil properties (which is especially small in this case due to the low $\sigma_{\ln V}$ value). The relative impact of different sources of variability for weak and strong ground motions was not considered (more effect of MRD variability might be expected for stronger shaking).

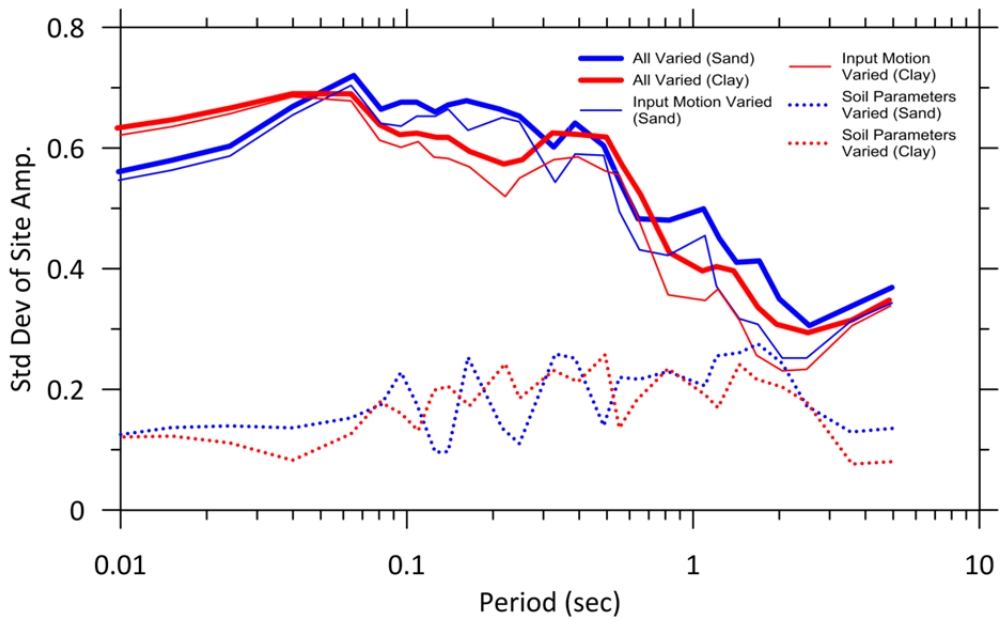

Figure 3.8 Average contribution of randomizing soil properties in $\phi_{\ln Y}$ [Bazzurro and Cornell 2004b].

3.4 ESTIMATING UNCERTAINTY TERMS FROM RECORDED GROUND MOTION DATA

For sites having ground motion recordings from multiple earthquake events, it is possible to interpret event-to-event variations in ground motions in such a way that site response variability (akin to ϕ_{lnY}) can be estimated. There are two general ways that this has been evaluated. One way of studying variability in site amplification is by analysis of residuals of a predictive model [Equation (3.2)]. The second approach, which requires vertical array data, evaluates site amplification empirically and compiles the relevant statistics directly from the observations. Neither approach requires performing GRA, but GRA has been used in some of the predictive models considered in residuals analysis.

We discuss three studies pertaining to the quantification of $\phi_{\ln Y}$. Kaklamanos et al. [2013] and Lin et al. [2011] analyze data using a residuals analysis approach. Rodriguez-Marek et al. [2011] develop models and analyze residuals as well, but their inference of $\phi_{\ln Y}$ is actually a direct interpretation of vertical array data. Thompson et al. [2012] have also directly interpreted site amplification statistics using vertical array data, but because they use Fourier amplitudes the results are not discussed here.

Kaklamanos et al. [2013] and Lin et al. [2011] also quantify site-to-site variability (ϕ_{S2S}) through partitioning of residuals [Equations (3.2) and (3.3)]. Additional studies investigating single-site standard deviation by Rodriguez-Marek et al. [2013] and Atkinson [2006] can be used to evaluate ϕ_{S2S} as described below.

Each of these studies is summarized below. We explain in each case how we have obtained estimates of $\phi_{\ln Y}$ and/or ϕ_{S2S} from the results presented in the respective papers.

3.4.1 Kaklamanos et al. [2013]

Kaklamanos et al. [2013] investigated site effects and their dispersion using the residuals analysis approach. They considered vertical array data from the KiK-net downhole array in Japan. The predicted motions to which data are compared consist of the downhole recording modified by a 1D ground response analysis. Referring to Equation (3.4), the downhole record represents the sum (in natural log units) of the mean rock motion (μ_{lnX}), the event term (η_{Ei}), and the path term ($\eta_{Pi,j}$). The site term is assumed to be zero for the downhole motion:

$$\ln x_{ij} = \left(\mu_{\ln X}\right)_{ij} + \eta_{Ei} + \eta_{Pi,j} \tag{3.6}$$

If the computed mean site response from model k is denoted $\ln \overline{Y}_{ijk}$, then residuals are computed as:

$$R_{ijk} = \ln z_{ij} - \left(\ln x_{ij} + \ln \overline{Y}_{ijk}\right) + c_k + \eta_{Sjk} + \varepsilon_{ijk} \tag{3.7}$$

where z_{ij} represents the surface recording, c_k is the mean residual when the source, path, and modeled site effects are accounted for, η_{Sjk} is a site term, and ε_{ijk} represents the remaining residual having a mean of zero. The site term η_{Sjk} represents the mean residual for site j relative to the predictions of model k. The standard deviation of η_{Sjk} and ε_{ijk} can be taken as ϕ_{S2S} and $\phi_{\ln Y}$, respectively. However, it should be recognized that the value of ϕ_{S2S} from this analysis is relative to a ground motion prediction method that includes site-specific GRA; as such, ϕ_{S2S} would be expected to be smaller than from an ergodic site term (e.g., from a GMPE).

The KiK-net vertical array records considered by Kaklamanos et al. [2013] include a large number of weak and strong motions, including records from the Tohoku earthquake on 11 March 2011. Their database includes 3720 records from 1122 events at 100 stations; 204 of the records have a PGA of more than 0.3g at the surface.

Ground response analyses were performed using linear and equivalent linear methods. Linear analyses were performed using the program NRATTLE, which uses the Thomson-Haskell matrix method [Thomson 1950]. Equivalent-linear analyses were performed using SHAKE [Schnabel et al. 1972; Idriss and Sun 1992; and Ordóñez 2010]. The GRA utilized seismic velocities (V_p and V_s) available from the NIED web site (*http://www.bosai.go.jp/e/).* Mass density ρ was estimated from V_p. For the linear analyses, an optimization process was undertaken to estimate quality factor Q, which is related to soil damping as $\xi=1/(2Q)$. In the EL analysis, MRD relationships by Zhang et al. [2005] were used. Residuals were computed from the results of the analyses (ln data minus ln model), which were then partitioned as given in Equation (3.8).

Figure 3.9 shows the model bias c_k and the standard deviation terms $\phi_{\ln Y}$ and ϕ_{S2S}. The bias is relatively large for both linear and EL methods. This misfit is not surprising given the large misfits between GRA and a similar dataset as identified by Thompson et al. [2012]. Standard deviation term $\phi_{\ln Y}$ is flat with period, whereas ϕ_{S2S} is more variable and generally larger than $\phi_{\ln Y}$.

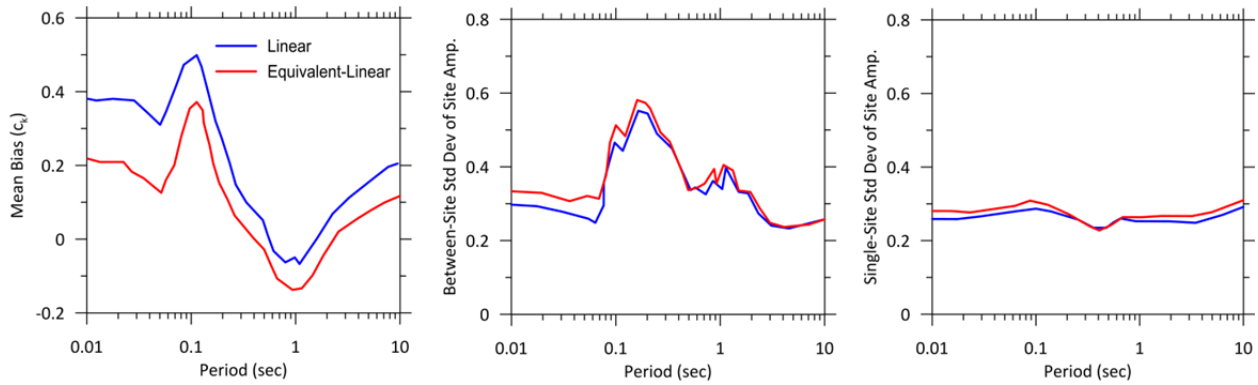

Figure 3.9 Bias in prediction of surface PSA from KiK-net Japanese data, Between-site standard deviation of residuals, and Within-site standard deviation of residuals [Kaklamanos et al. 2013].

3.4.2 Lin et al. [2011]

Lin et al. [2011] investigated source, path, and site effects and their dispersion using the residuals analysis approach. They considered surface recordings from the TSMIP strong-motion network in Taiwan [Liu et al. 1999; Shin and Teng 2001]. The predicted motions to which data are compared are from a region-customized GMPE (modified version of Chiou and Youngs [2008]). For this process, they used 4756 surface recordings from 64 shallow earthquakes recorded at 285 sites. Only stations with at least ten recordings were considered and each station has a V_{S30} value from either suspension logging or inference from proxy methods.

Residuals were partitioned into components matching the form of Equation (3.2), except that the event term (η_{Ei}) was separated into two components as:

$$\eta_{Ei} = \eta_{SRi} + \eta_{E0i} \tag{3.8}$$

where η_{SRi} is the mean event term for the cluster of earthquakes at the location of the ith event, and η_{E0i} is the event term after removing η_{SRi}.

Standard deviations were computed from the partitioned residuals; Figure 3.10 shows the different components, including site-to-site and within-site terms for six spectral periods. The $\phi_{\ln Y}$ results have a flat trend with period (similar to Kaklamanos et al. [2013]). The site-to-site variability (ϕ_{S2S}) exceeds $\phi_{\ln Y}$ and has more period dependence. It is somewhat surprising that ϕ_{S2S} values from this work, which used an ergodic site term, are smaller than those from Kaklamanos et al. [2013], which used site-specific GRA. The opposite would generally be expected, although we recognize that different datasets were considered.

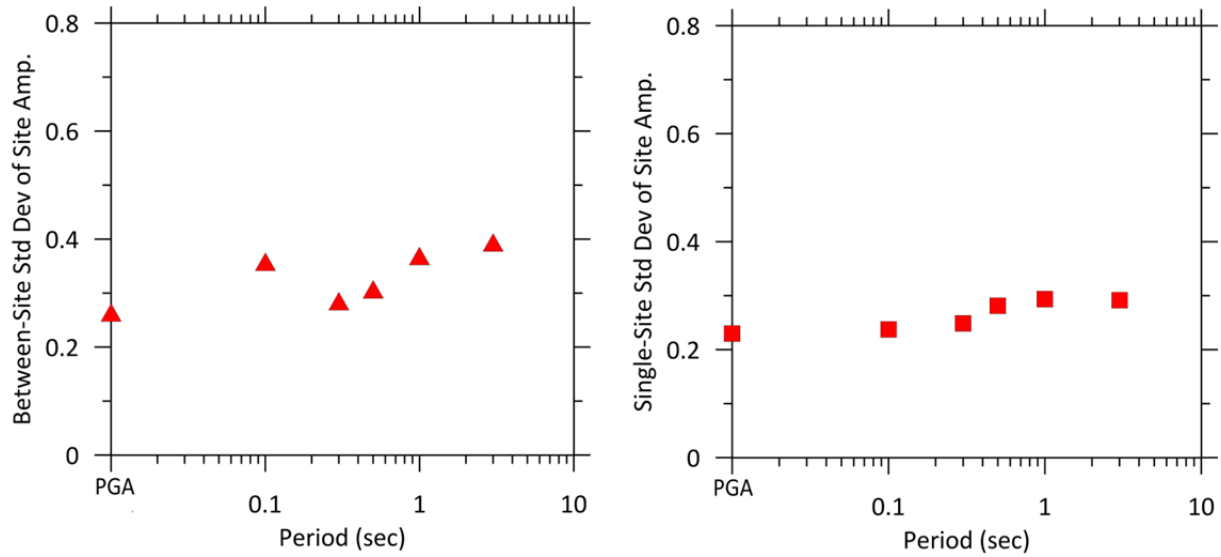

Figure 3.10 Components of standard deviation of site amplification using analyses of Taiwan ground motion data [Lin et al. 2011].

3.4.3 Rodriguez-Marek et al. [2011]

Similar to Lin et al. [2011], in this study ground motion residuals were partitioned to evaluate applicable standard deviation terms. Rodriguez-Marek et al. [2011] utilized KiK-Net vertical array data from Japan, which enabled site amplification and its standard deviation to be evaluated more directly than is possible from analysis of surface records only. Only stations with at least ten recordings were considered.

Ground motion predictions are based on a GMPE developed for the KiK-Net data that can be used to predict either the borehole or the surface recordings. We denote the means from this relationship as $(\mu_{lnX})_{ij}$ and $(\mu_{lnZ})_{ij}$ for downhole and surface locations, respectively, to be consistent with notation elsewhere in this document. Following Equation (3.2), residuals were partitioned into components using the borehole and surface recordings as follows:

$$\text{Borehole residual: } R_{ij}^{X} = \ln x_{ij} - \left[\left(\mu_{\ln X} \right)_{ij} + \eta_{Ei} + \eta_{Sij} \right] + \varepsilon_{ij} \tag{3.9}$$

$$\text{Surface residual: } R_{ij}^{Z} = \ln z_{ij} - \left[\left(\mu_{\ln Z} \right)_{ij} + \eta_{Ei} + \eta_{Sij} \right] + \varepsilon_{ij} \tag{3.10}$$

Note that a path-to-path term was not included in the residuals partitioning. The KiK-net data allows for direct inference of the site amplification:

$$\ln y_{ij} = \ln z_{ij} - \ln x_{ij} = \left(\mu_{\ln Z} \right)_{ij} - \left(\mu_{\ln X} \right)_{ij} + R_{ij}^{Y} \tag{3.11}$$

Equation (3.12) can be used to compute amplification residuals R_{ij}^{Y} from the data. This represents a direct analysis of site amplification statistics without the use of an underlying site response model. These residuals can be partitioned by mixed-effects analysis as:

$$R_{ij}^{Y} = \eta_{Sj}^{Y} + \varepsilon_{ij}^{Y} \tag{3.12}$$

The term η_{Sj}^{Y} represents the mean of the amplification residual for site *j,* and ε_{ij}^{Y} represents the remaining residual. The standard deviation of η_{Sj}^{Y} is taken as ϕ_{S2S} and the standard deviation of ε_{ij}^{Y} as $\phi_{\ln Y}$. (Note that $\phi_{\ln Y}$ cannot be estimated from the standard deviation of ε_{ij} in Equation (3.2) because path-to-path variability was not considered in the partitioning of residuals.) The two components of standard deviation of site amplification are shown in Figure 3.11. As before, $\phi_{\ln Y}$ is seen to have a relatively flat trend with respect to period, and ϕ_{S2S} values are both higher and more variable with period.

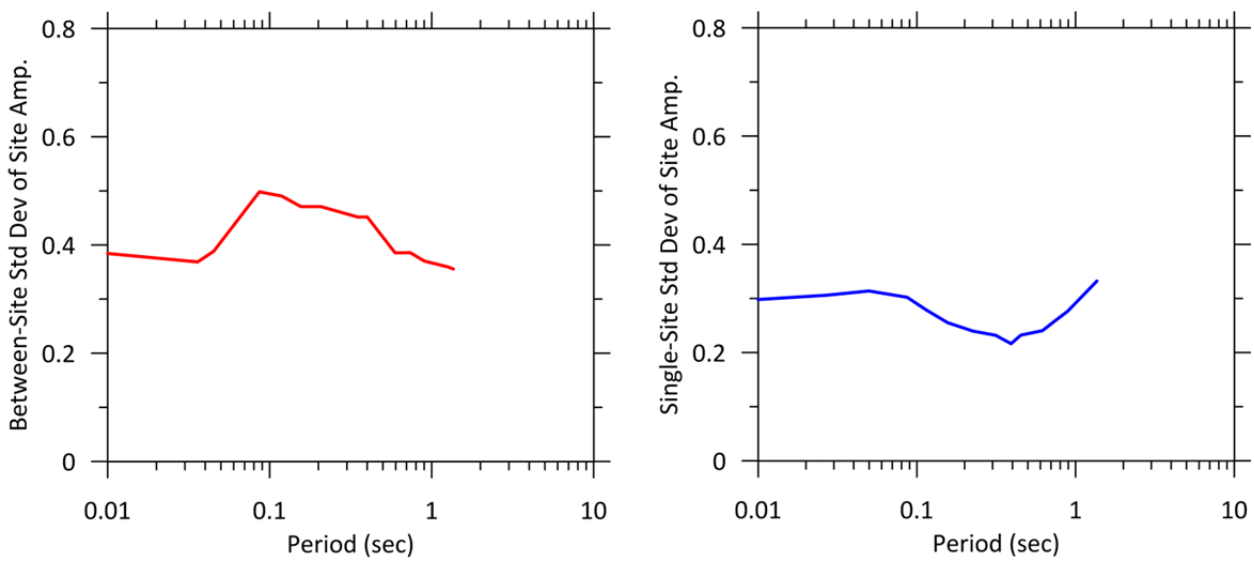

Figure 3.11 Different components of standard deviation of site amplification obtained from KiK-net data [Rodrigues-Marek et al. 2011].

3.4.4 Rodriguez-Marek et al. [2013]

In this study, Rodriguez-Marek et al. [2013] describe partially non-ergodic PSHA in which repeatable effects of site response at a single site are evaluated, thus allowing the site-to-site variance to be removed from the within-event standard deviation. The resulting aleatory variability is often referred to as the single-station standard deviation of the surface motion. If the repeatable site effect is evaluated from multiple recordings at the site, it is expressed as term η_{Sj} in Equation (3.2). In this case, the total site effect is the sum of the ergodic site term and η_{Sj}. If the site effect is evaluated from GRA, it is expressed as term $\ln \overline{Y}_{ij}$ in Equation (3.4).

Rodriguez-Marek et al. [2013] have utilized ground motion data from many events and sites in the following regions: California, Japan, Taiwan, Turkey, and Switzerland. Records were selected having **M** > 4.5 and R_{rup} < 200 km. For each region, an appropriate GMPE is selected

and residuals are computed. Table 3.2 presents details on the datasets and reference GMPEs by region.

Residuals for a given region are partitioned in a manner similar to Equation (3.2), but the path term (η_{Pij}) is not computed because it was not the focus of the paper. Accordingly, the residuals were partitioned as:

$$R_{ij} = \eta_{Ei} + \eta_{Sj} + \varepsilon_{ij} \tag{3.13}$$

By not including the η_{Pij} term, path-to-path variations are included in the ε_{ij} term. The site-to-site standard deviation (ϕ_{S2S}) could be evaluated form the η_{Sj} terms, but this was not compiled. Rather, the authors computed the total standard deviation σ and the single-station standard deviation, σ_{ss}:

$$\sigma = \sqrt{\phi^2 + \tau^2} \tag{3.14}$$

$$\sigma_{ss} = \sqrt{\phi_{ss}^2 + \tau^2} \tag{3.15}$$

Total standard deviation σ in general has the components shown in Equation (3.3), whereas σ_{ss} is missing the ϕ_{S2S} component. Since Rodriguez-Marek et al. compile the σ_{ss} and σ terms, ϕ_{S2S} can be readily evaluated as:

$$\phi_{S2S} = \sqrt{\phi^2 - \phi_{ss}^2} \tag{3.16}$$

Table 3.2 Datasets and GMPEs utilized for the regions considered by Rodriguez-Marek et al. [2013].

Region	No. of records used	GMPE used as the predictive model
California	1635 (1627 for *T*=1 sec)	Chiou and Youngs [2008]
Japan	1834	Discussed in Rodriguez-Marek et al. [2011]
Taiwan	4062 (4052 for *T*=1 sec and 3733 for *T*=3 sec)	Chiou and Youngs [2008] with slight revision
Turkey	145	Akkar and Çağnan [2010] with slight revision
Switzerland	28 (19 for PGA)	Discussed in Douglas [2010]

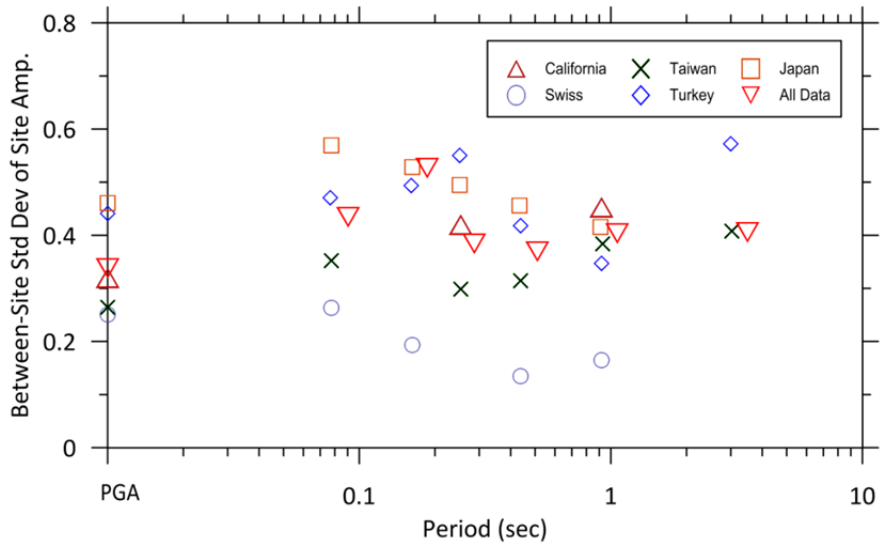

Figure 3.12 Standard deviation of between-site residuals (ϕ_{S2S}) from different regions (from Rodriguez-Marek et al. [2013].

3.4.5 Atkinson [2006]

Atkinson [2006] introduced the concept of customizing a GMPE for a single site as well as the term 'single station sigma'. Her work, which was similar in scope to the subsequent work of Rodriguez-Marek et al. [2013], utilized a much smaller dataset of 21 stations in the Los Angeles area; GMPE residuals were computed with and without site-specific terms (η_{Sj}). Using Equation (3.17), values of ϕ_{S2S} can be computed from the total standard deviation (ϕ) and single-station standard deviation (ϕ_{ss}), with the results shown in Figure 3.13. These standard deviations are much lower than those from other studies, which may have resulted from the small size of the dataset.

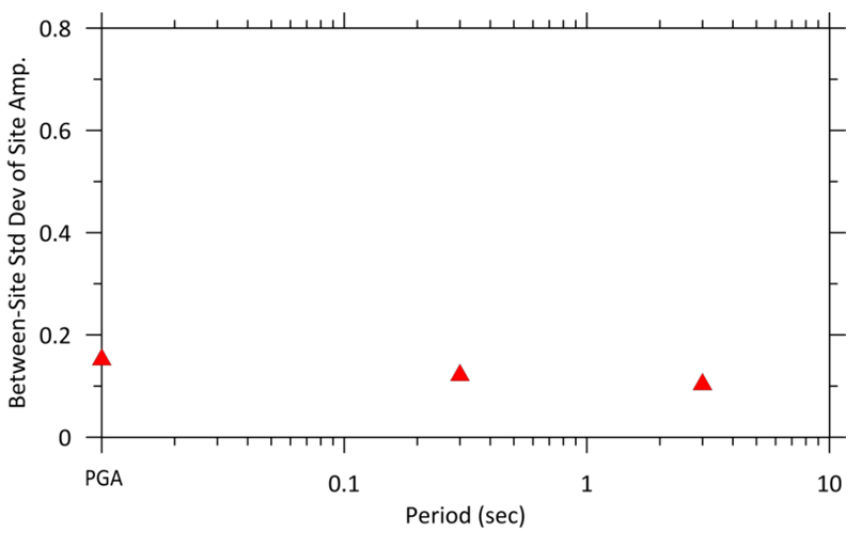

Figure 3.13 Standard deviation of between-site residuals (ϕ_{S2S}) calculated from Atkinson [2006].

3.5 SYNTHESIS OF FINDINGS

3.5.1 Standard Deviation of Site Amplification ($\sigma_{\ln Y}$)

In Section 3.3, we presented sets of results for computed standard deviations in site amplification for five different sites. Note that we do not refer to these standard deviations as $\sigma_{\ln Y}$ as in the data-based studies, because in some cases input motion variability was considered whereas in others it was not. Nonetheless, these five sets of results, plotted together in Figure 3.14, exhibit some common characteristics. The standard deviations at short periods have values ranging from 0.35 to 0.65, which then gradually increase with period towards a maximum value just before the site period. For periods greater than the site period, standard deviations decreases markedly with period. This decrease of standard deviation beyond the site period is most pronounced when input motion variability is not considered [Kwok et al. 2008; Li and Assimaki 2011], but it is present to some extent in all of the results.

Results for $\phi_{\ln Y}$ from data-based studies are summarized in a single plot in Figure 3.15. Results of the three studies are remarkably consistent across the period range of 0.01 to about 3.0 sec, generally falling within the range of 0.23–0.30. This consistency is found despite significant differences in the manner by which the $\phi_{\ln Y}$ values were computed. In particular, Kaklamanos et al. [2013] and Rodriguez-Marek et al. [2011] evaluated site response effects and $\phi_{\ln Y}$ relatively directly, whereas Lin et al. [2011] used surface records for which other effects (non-site) may affect the residuals from which $\phi_{\ln Y}$ was computed.

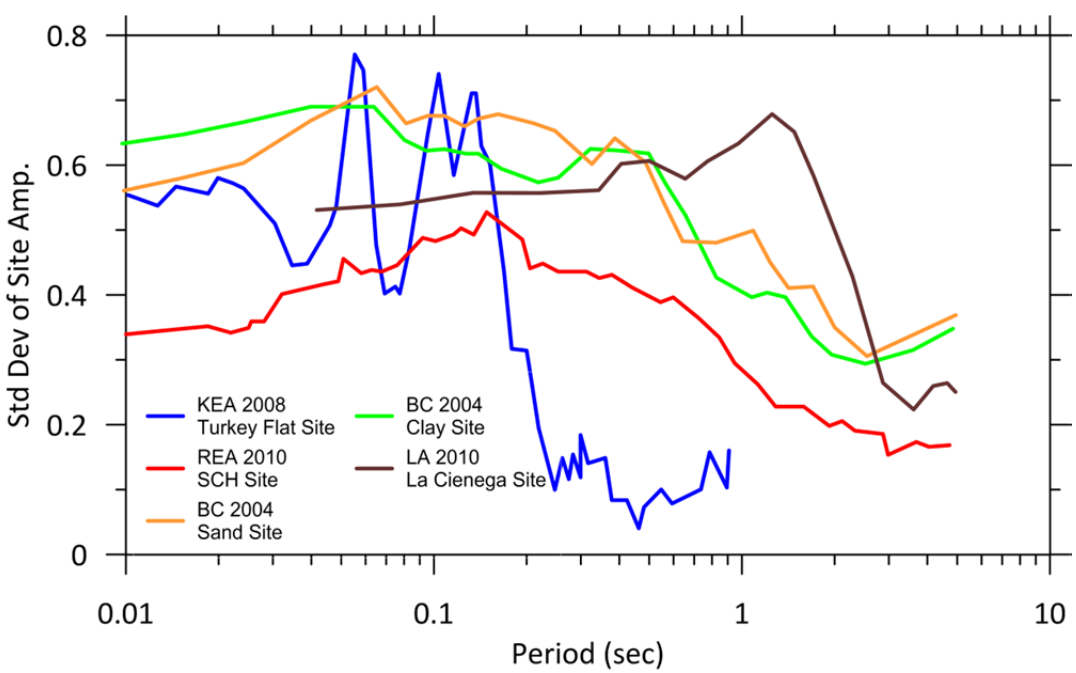

Figure 3.14 Synthesis of standard deviations of site amplification obtained from simulation-based studies.

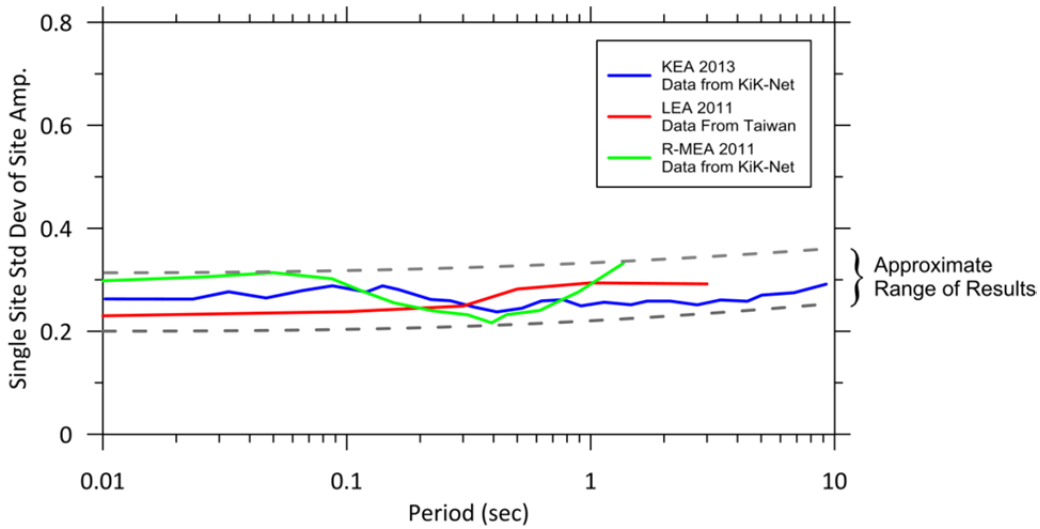

Figure 3.15 Synthesis of $\phi_{\ln Y}$ results obtained from data-based studies.

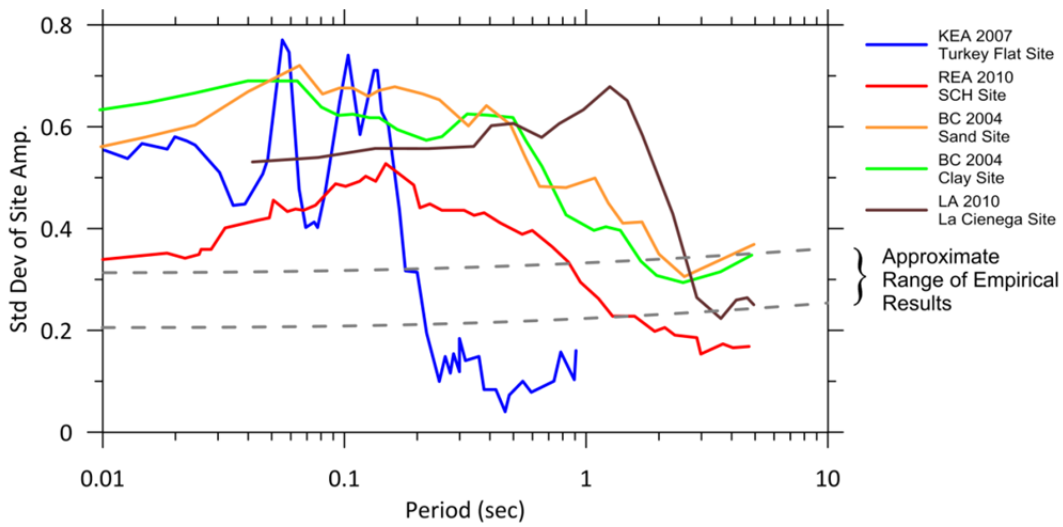

Figure 3.16 Difference between simulation-based studies and data-based studies on $\phi_{\ln Y}$.

Figure 3.16 replots the simulation-based studies with the approximate band of results from data-based studies. The trends are significantly different from these two groups. First, the simulation-based studies overestimate $\phi_{\ln Y}$ at short periods, which could potentially result from over-randomization of the V_S profiles, MRD curves, or (in some cases) input motions. Because the overestimation of $\phi_{\ln Y}$ at short periods occurs for both weak and strong motions, the cause is not likely related to over-randomization of the MRD curves (which do not affect significantly ground motion prediction for weak motions). Moreover, because the overestimation occurs for studies that did not consider input motion variability, it appears that the overestimation of $\phi_{\ln Y}$ at short periods is likely due principally to over-randomization of the V_S profiles. In light of these findings, it would be worthwhile to re-visit the randomization scheme provided by Toro [1995].

Another difference in the standard deviation terms produced by the two categories of studies is underestimation of $\phi_{\ln Y}$ at long periods (beyond the site period) by the simulations. At these long periods, seismic quarter-wavelengths become long relative to the profile thickness, so there is little site response and hence little variability in site response. As discussed in Section 1.2.1, in reality there are significant site effects at these long periods, which are associated with physical processes that are not captured by 1D GRA, such as surface waves and various basin effects. Variability in those processes control long-period $\phi_{\ln Y}$ from data-based studies.

Given the significant differences observed between simulation-based and data-based site amplification dispersion, and the apparent causes of the simulation results, we recommend avoiding the use of the simulation-based dispersion results. We recommend using $\phi_{\ln Y} = 0.23 - 0.30$ over the period range of 0 to 3.0 sec.

3.5.2 Standard Deviation of Site-to-Site Variability (σ_{S2S})

Figure 3.17 summarizes available results for ϕ_{S2S}. There are two independent sets of results for each of Japan, Taiwan, and California, and one set for the other regions. The Japan results (from Rodriguez-Marek et al. [2013] and Kaklamanos et al. [2013]) are generally consistent for periods > 0.1 sec. At shorter periods, the Kaklamanos et al. results have lower values of ϕ_{S2S}, which would be expected given their use of site-specific analysis (what is somewhat surprising is that the values are not much lower in the Kaklamanos et al. study). The Taiwan results (from Rodriguez-Marek et al. [2013] and Lin et al. [2011]) are consistent over the full period range. The California results (from Rodriguez-Marek et al. [2013] and Atkinson [2006]) are inconsistent, with the Atkinson results being much lower (possibly due to a small dataset).

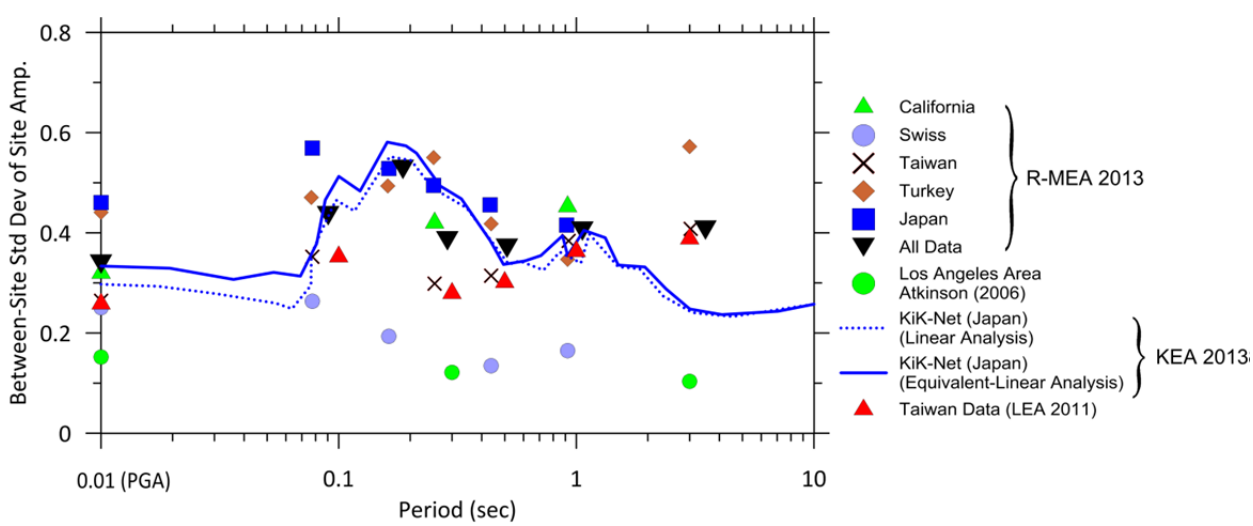

Figure 3.17 Standard deviation of between-site residuals (ϕ_{S2S}). Discrete symbols are regional results from Rodriguez-Marek et al. [2013]. Other studies identified in legend.

Looking across all the results for ϕ_{S2S}, there is a large degree of regional variability. Accordingly, there is substantial epistemic uncertainty in assigning an appropriate value of ϕ_{S2S} for a given application region. Moreover, given the results of the Kaklamanos et al. [2013] study in Japan, there is some question as to whether performing site-specific GRA can be used as justification for using a within-event standard deviation (i.e. taking $F = 1$ in Equation (3.6). This issue is discussed further in Chapter 5 on future work.

4 Implementation and Testing of Methods for Merging Ground Response Analysis Results in PSHA

4.1 INTRODUCTION

In previous chapters of this report, we have described methods of implementing ground response analysis (GRA) results into probabilistic seismic hazard analyses (PSHA (see Chapter 1), presented recommendations for performing GRA (Chapter 2), and provided guidance on quantifying uncertainties related to site effects that are required for PSHA (Chapter 3).

To facilitate practical application of these recommendations, we present in Section 4.2 EXCEL spreadsheets for critical steps in the analysis process. These spreadsheets include the regression of mean amplification functions (as described in Chapter 2) and the various GRA-into-PSHA approaches described in Chapter 1. Section 4.3 describes the most sophisticated implementation, in which a site-specific amplification function is used in PSHA, which has been implemented in a local version of OpenSHA [Field et al. 2003]. A more permanent implementation on the main code for OpenSHA is pending.

This chapter concludes by testing and comparing results from alternate simplified methods of implementing GRA results in PSHA (hybrid, modified hybrid, and convolution) with the more rigorous result of implementing site-specific amplification functions with a GMPE in the hazard integral. The comparisons reveal conditions where the relatively simplified methods perform well and where they exhibit bias.

4.2 SPREADSHEET ROUTINES

4.2.1 Fitting the Mean Amplification Function

When GRA are used to estimate site amplification in the manner described in Chapter 2, they produce a series of discrete results, consisting of frequency-dependent amplification Y given input motion amplitude x_{IMref}. When multiple input motions are used, along with multiple realizations of uncertain soil properties, a 'cloud' of x_{IMref}-Y results is obtained that is fit with a mean amplification function of the following form:

$$\ln \overline{Y}(f) = f_1 + f_2 \ln\left(\frac{x_{IMref} + f_3}{f_3}\right) \tag{4.1}$$

In Section 2.6, we described various approaches for fitting Equation (4.1) given practical limitations on the size of the data cloud, which may necessitate constraining some of the fit parameters (f_1, f_2, and f_3). We have developed EXCEL spreadsheets to perform the $Y|x_{IMref}$ curve fitting using these alternate approaches. The spreadsheets are included as an electronic supplement (*http://apps.peer.berkeley.edu/publications/peer_reports/reports_2014/electronic-supplement-2014-16.zip*).

(a) Input Motion from a Single Hazard Level

The background for this fitting approach is presented in Section 2.6.1, which applies when input motions are defined for a single hazard level and hence, span a relatively narrow range of x_{IMref}. This requires significant external constraint of parameters in Equation (4.1).

In spreadsheet 'XY Plots' and tab 'f_2 and f_3 constrained', we fit Equation (4.1) with f_2 and f_3 constrained empirically [Seyhan and Stewart 2014]; hence only f_1 is regressed from the GRA results. A spreadsheet snapshot is shown in Figure 4.1. GRA results are entered in Columns A and B. The applicable period and V_{S30} for calculating f_2 and f_3 from the empirical model are given in cells P2 to P3. The fit value of f_1 is then given in cell P5 and the GRA-based and SS14-based amplification functions are tabulated and plotted.

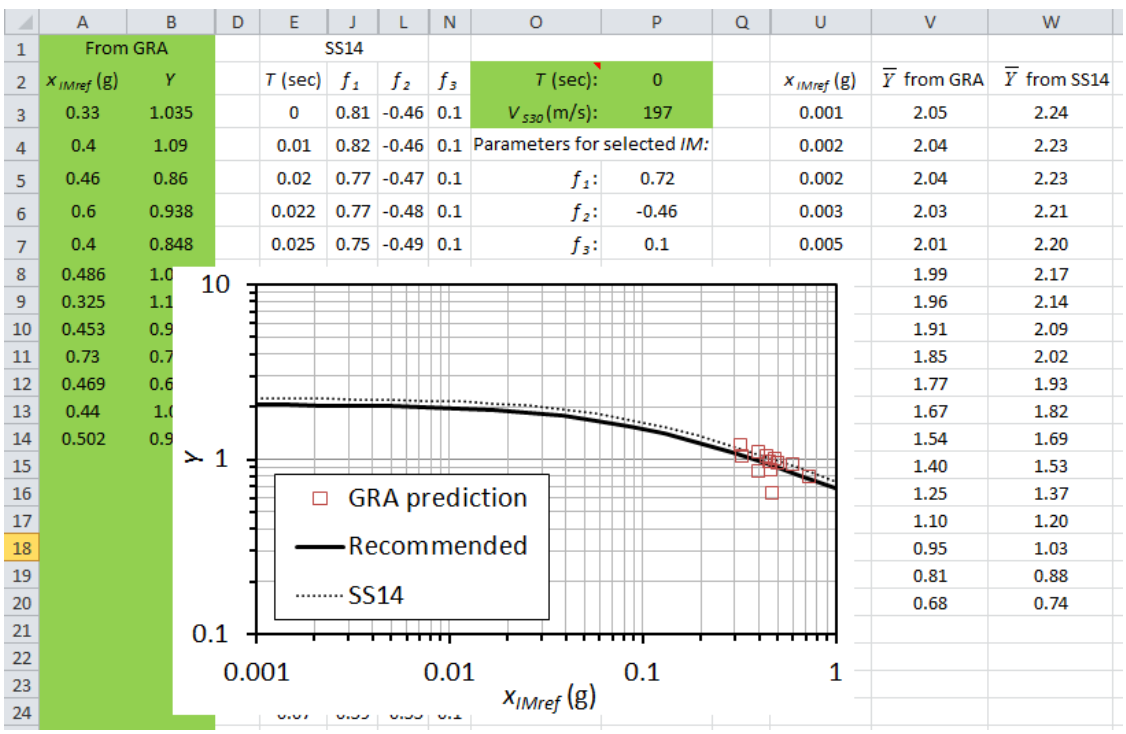

Figure 4.1 **Snapshot of '*XY* Plots' EXCEL spreadsheet used for developing amplification function when x_{IMref} is defined over narrow range of amplitudes. Parameters f_2 and f_3 are constrained from empirical model.**

In the spreadsheet 'XY Plots' and tab 'f_1 and f_3 constrained' we consider the alternate approach described in Section 2.6.1 in which weak-motion amplification is specified in addition to GRA results for the single hazard level. This approach requires the user to enter the weak motion amplification Y_{elas} and assign it to an appropriate x_{IMref} amplitude (0.01g was recommended in Section 2.6.1 when x_{IMref} is defined in terms of PGA). Figure 4.2 shows a spreadsheet snapshot that is formatted similarly to that in Figure 4.1, but which also includes these two additional inputs in cells P4 to P5. The spreadsheet is computing both f_1 and f_2 in this case; the results are given in cells P6 and P7. The resulting fit is displayed as before along with the SS14 model.

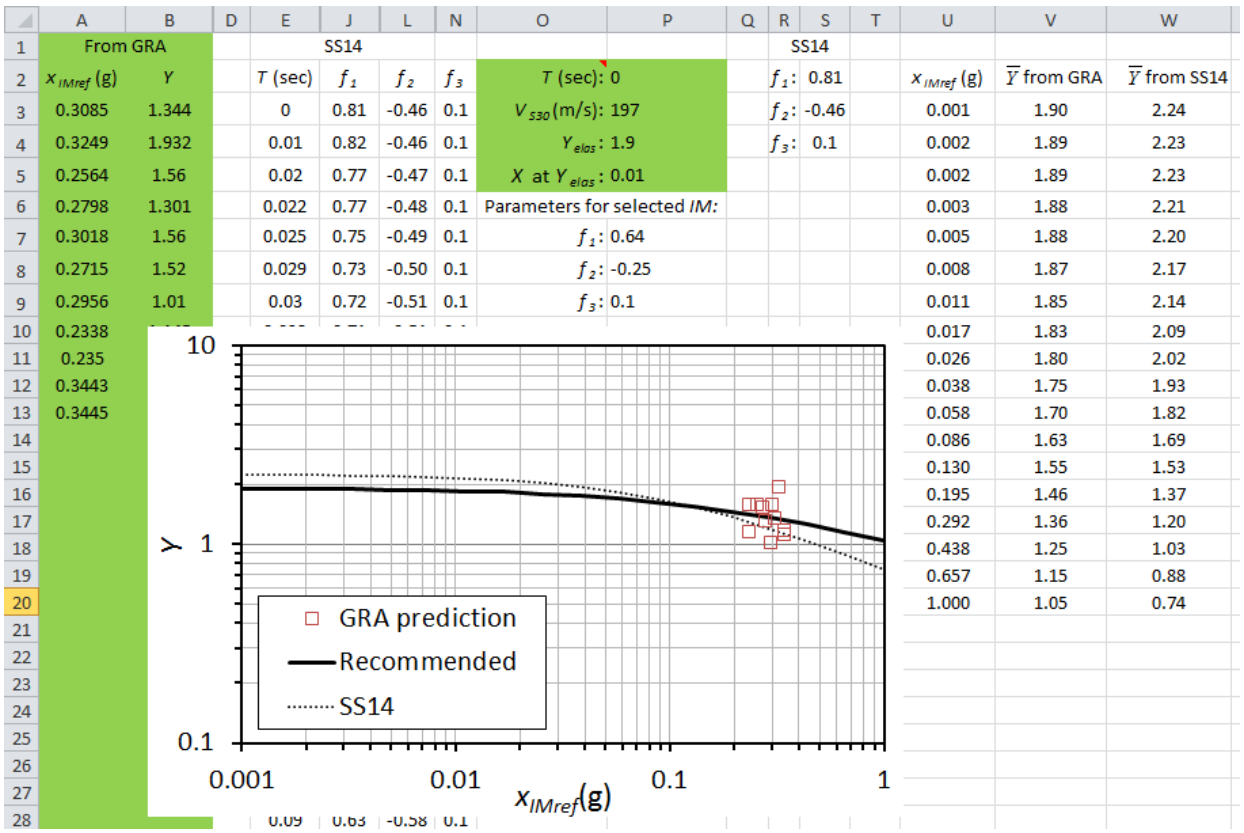

Figure 4.2 Snapshot of '*XY* Plots' EXCEL spreadsheet used for developing amplification function when x_{IMref} is defined over narrow range of amplitudes and weak motion (elastic) site amplification is specified. Parameters f_1 and f_3 are constrained from empirical model.

(b) Input Motions from Multiple Hazard Levels

The background for this fitting approach is presented in Section 2.6.2, which applies when input motions are defined for multiple hazard levels and hence, span a broad range of x_{IMref}. In principal all three regression parameters can be fit simultaneously, but our experience has been that f_3 is poorly constrained by this process and should be pre-set by the user and manipulated to provide a good visual fit. A default value of f_3=0.1g is used here for the case of x_{IMref} defined using PGA.

To compute f_1 and f_2 with f_3 fixed, we define parameter x'_{IMref} as follows:

$$x'_{IMref} = \left(\frac{x_{IMref} + f_3}{f_3} \right) \tag{4.2}$$

and then re-write Equation (4.1) as:

$$\ln Y(f) = f_1 + f_2 \ln x'_{IMref} \tag{4.3}$$

where $\ln Y$ and $\ln x'_{IMref}$ are known for each data point. Linear regression is then performed to calculate f_1 and f_2. This approach is implemented in spreadsheet '*XY* Plots' and tab 'f_3 constrained'. A spreadsheet snapshot is shown in Figure 4.3. The spreadsheet is organized in a similar manner to that in Figure 4.2, with the difference generally being that more input results are provided in Columns A and B. This spreadsheet also includes an option to constrain weak motion amplification at Y_{elas}; if used, the amplification will be truncated at this value. This can be turned off by setting Y_{elas} to -999, in which case no truncation is applied.

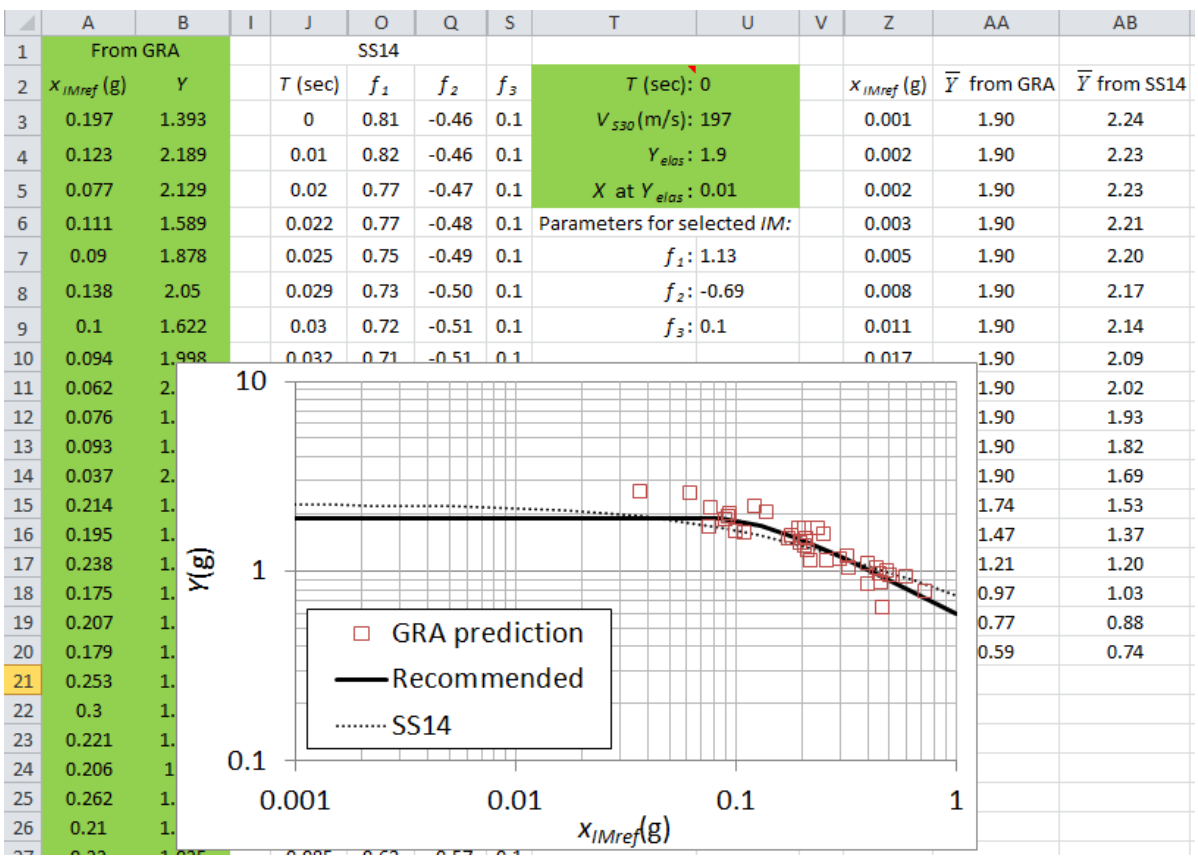

	A	B	I	J	O	Q	S	T	U	V	Z	AA	AB
1	From GRA				SS14								
2	x_{IMref} (g)	Y		T (sec)	f_1	f_2	f_3	T (sec):	0		x_{IMref} (g)	$\bar{Y}$ from GRA	$\bar{Y}$ from SS14
3	0.197	1.393		0	0.81	-0.46	0.1	V_{S30} (m/s):	197		0.001	1.90	2.24
4	0.123	2.189		0.01	0.82	-0.46	0.1	Y_{elas}:	1.9		0.002	1.90	2.23
5	0.077	2.129		0.02	0.77	-0.47	0.1	X at Y_{elas}:	0.01		0.002	1.90	2.23
6	0.111	1.589		0.022	0.77	-0.48	0.1	Parameters for selected *IM:*			0.003	1.90	2.21
7	0.09	1.878		0.025	0.75	-0.49	0.1	f_1:	1.13		0.005	1.90	2.20
8	0.138	2.05		0.029	0.73	-0.50	0.1	f_2:	-0.69		0.008	1.90	2.17
9	0.1	1.622		0.03	0.72	-0.51	0.1	f_3:	0.1		0.011	1.90	2.14
10	0.094	1.998		0.032	0.71	-0.51	0.1				0.017	1.90	2.09
11	0.062	2.										1.90	2.02
12	0.076	1.										1.90	1.93
13	0.093	1.										1.90	1.82
14	0.037	2.										1.90	1.69
15	0.214	1.										1.74	1.53
16	0.195	1.										1.47	1.37
17	0.238	1.										1.21	1.20
18	0.175	1.										0.97	1.03
19	0.207	1.										0.77	0.88
20	0.179	1.										0.59	0.74
21	0.253	1.											
22	0.3	1.											
23	0.221	1.											
24	0.206	1											
25	0.262	1.											
26	0.21	1.											

Figure 4.3 **Snapshot of '*XY* Plots' EXCEL spreadsheet used for developing amplification function when x_{IMref} is defined over wide range of amplitudes. Option for specifying weak motion (elastic) site amplification is provided (this can be turned off by specifying -999 for Y_{elas} in cell U4).**

4.2.2 Interpolation of Site Parameters over a Range of Periods

As described in Section 2.6.3, for practical reasons it is desirable to evaluate parameters $f_1 - f_3$ for a limited number of periods and interpolate for other intermediate periods. In this section we implement the procedure described in Section 2.6.3 in spreadsheet 'Interpolation'. The values of $f_1 - f_3$ established using the routines from the prior section are entered in column A-D along with the corresponding periods. Because the interpolation is guided by empirical models, including basin effects, it is necessary to specify V_{S30} (in m/sec) and basin depth differential δ_{z1} (in km) in cells H2 and H4. If basin depth is unknown, δz_1 should be given as the default value of zero. Site period T_{site} is given in cell H3; the coefficients $f_1 - f_3$ will be computed so as to transition to empirical values at periods longer than T_{site}. If this feature is not desired, T_{site} can be given as a large value (> 10 sec).

After entering all of the input parameters in the green cells, the interpolation is completed by clicking the 'Calculate' button. The site coefficients are tabulated for a large number of periods in Columns X, Z, and AA, and plotted.

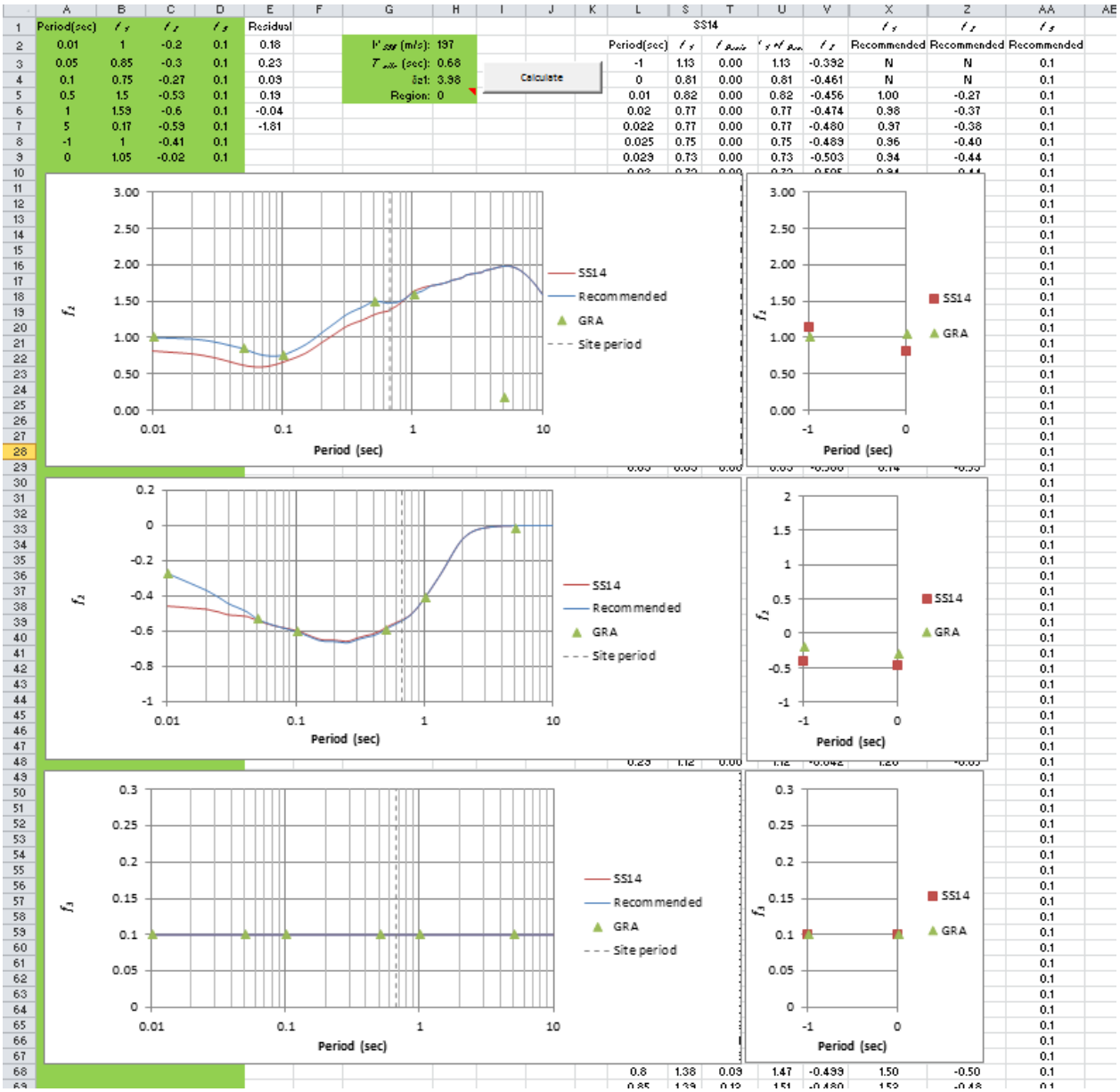

Figure 4.4 **Snapshot of 'Interpolation' EXCEL spreadsheet used for interpolating site coefficients and transitioning the site amplification to empirical values beyond the site period.**

4.2.3 Simplified Methods for Merging GRA with PSHA

Section 1.2 described three simplified approaches for merging the site amplification function from GRA with PSHA for a rock site condition. These were the hybrid approach (Section 1.2.2), modified hybrid approach (Section 1.2.3), and convolution approach (Section 1.2.5).

The 'APPROX_PSHA' EXCEL spreadsheet implements all three approaches. As shown in the screen shot in Figure 4.5, PSHA results for the period of interest are entered in Columns A and B. Disaggregation results are required for situations where the IM for which reference-site

hazard is computed (x) does not match the IM used for x_{IMref}. The IM of interest and the IM used to drive nonlinearity are identified in cells E8 and E9–(use 0 for PGA, -1 for PGV; otherwise, positive real values will be interpreted as the PSA oscillator period). The GRA-based site amplification coefficients are entered in cells E2 to E6.

The spreadsheet requires disaggregation results $\overline{\mathbf{M}}$ and $\overline{R}$ when the IM used for x does not match that for x_{IMref} (for all methods) and for the modified hybrid method generally. These results can be entered for user-selected probability levels in the cells below the label 'Disaggregation results' (Cols D-F). The first probability level (PE) (in cell D14), should be the hazard level of interest (e.g., 5% in 50 years). Additional probability levels are needed to define an approximate hazard curve from the modified hybrid method.

After entering the input variables in the designated cells (in green), the user clicks on the 'Calculate' button. All three analyses are performed simultaneously and hazard ordinates are tabulated and plotted.

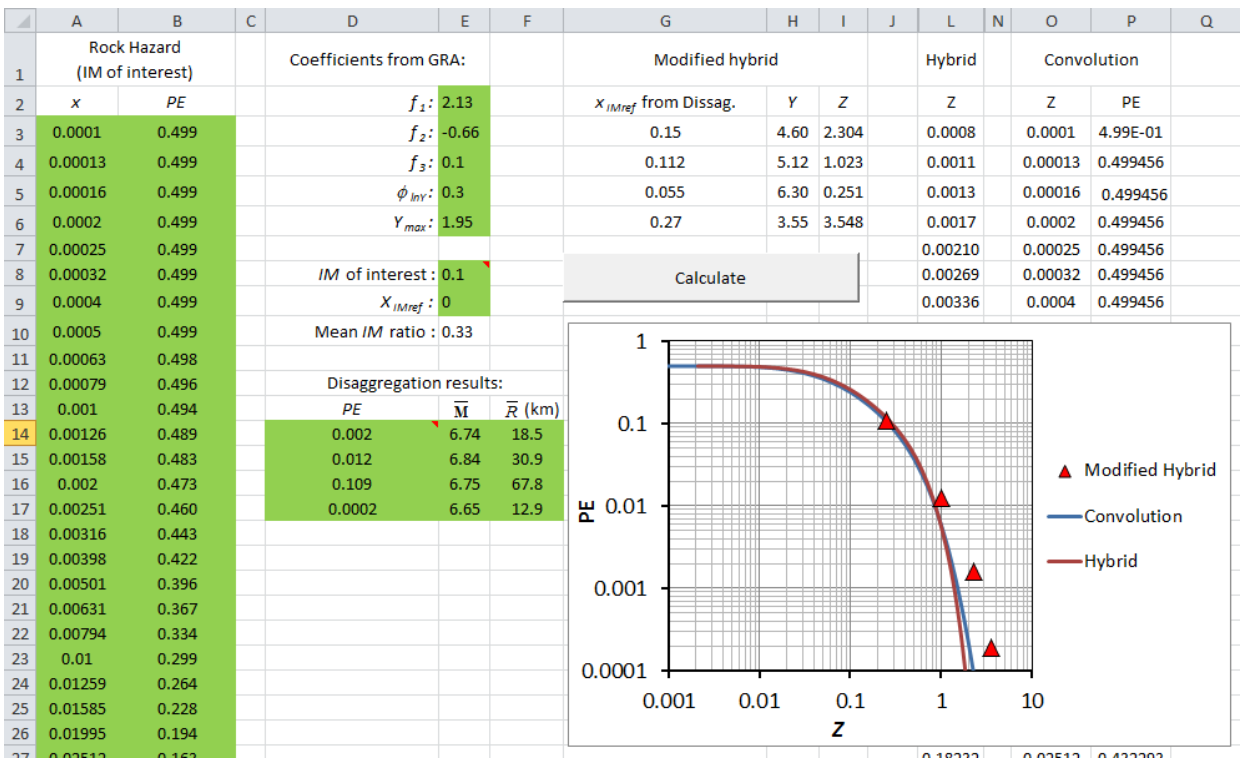

	A	B	C	D	E	F	G	H	I	J	L	N	O	P	Q
1	Rock Hazard (IM of interest)			Coefficients from GRA:			Modified hybrid				Hybrid		Convolution		
2	x	PE		f_1:	2.13		x_{IMref} from Dissag.	Y	Z		Z		Z	PE	
3	0.0001	0.499		f_2:	-0.66		0.15	4.60	2.304		0.0008		0.0001	4.99E-01	
4	0.00013	0.499		f_3:	0.1		0.112	5.12	1.023		0.0011		0.00013	0.499456	
5	0.00016	0.499		ϕ_{lnY}:	0.3		0.055	6.30	0.251		0.0013		0.00016	0.499456	
6	0.0002	0.499		Y_{max}:	1.95		0.27	3.55	3.548		0.0017		0.0002	0.499456	
7	0.00025	0.499									0.00210		0.00025	0.499456	
8	0.00032	0.499		IM of interest :	0.1		Calculate				0.00269		0.00032	0.499456	
9	0.0004	0.499		X_{IMref} :	0						0.00336		0.0004	0.499456	
10	0.0005	0.499		Mean IM ratio :	0.33										
11	0.00063	0.498													
12	0.00079	0.496		Disaggregation results:											
13	0.001	0.494		PE	$\overline{\mathbf{M}}$	$\overline{R}$ (km)									
14	0.00126	0.489		0.002	6.74	18.5									
15	0.00158	0.483		0.012	6.84	30.9									
16	0.002	0.473		0.109	6.75	67.8									
17	0.00251	0.460		0.0002	6.65	12.9									
18	0.00316	0.443													
19	0.00398	0.422													
20	0.00501	0.396													
21	0.00631	0.367													
22	0.00794	0.334													
23	0.01	0.299													
24	0.01259	0.264													
25	0.01585	0.228													
26	0.01995	0.194													

Figure 4.5 **A snapshot of 'APPROX_PSHA' EXCEL spreadsheet for implementing the results of GRA in PSHA using hybrid, modified hybrid, and convolution methods.**

4.3 OPENSHA IMPLEMENTATION

The most robust manner by which ground response analyses can be implemented within PSHA is to modify the mean and standard deviation within the hazard integral. Equations for the modification of the mean are given in Section 1.2.4. Equations for standard deviation are given in Section 1.2.1 [Equation (1.12)]; considerations related to the aleatory uncertainty model,

including reduction of the within-event standard deviation for nonlinearity and non-ergodic site response, are given in Chapter 3.

These procedures are implemented in a local version of the open-source Java-based online software package OpenSHA [Field et al. 2003]. We are working with the OpenSHA developer team to implement these procedures on the public version. A screen shot of the local version user interface is given in Figure 4.6.

In the current, local, implementation, reference site hazard is computed for a specified V_{S30} (e.g., 760 m/sec) using the Boore et al. [2014] GMPE. Subsequent versions should allow for any suitable GMPE to be selected. Site amplification is given by Equation (4.1), so user-specified values of $f_1 - f_3$ are provided. Additional user parameters are ϕ_{lnY}, ϕ_{S2S}, and reduction factor for single-site analysis, F (discussed in Section 3.2.2). The current OpenSHA implementation assumes that x_{IMref} is based on the IM of PGA.

Once the reference site GMPE and site amplification function are specified, the full suite of hazard analysis functionality in OpenSHA can be implemented including the UHS calculator, hazard curve calculator and disaggregation calculator.

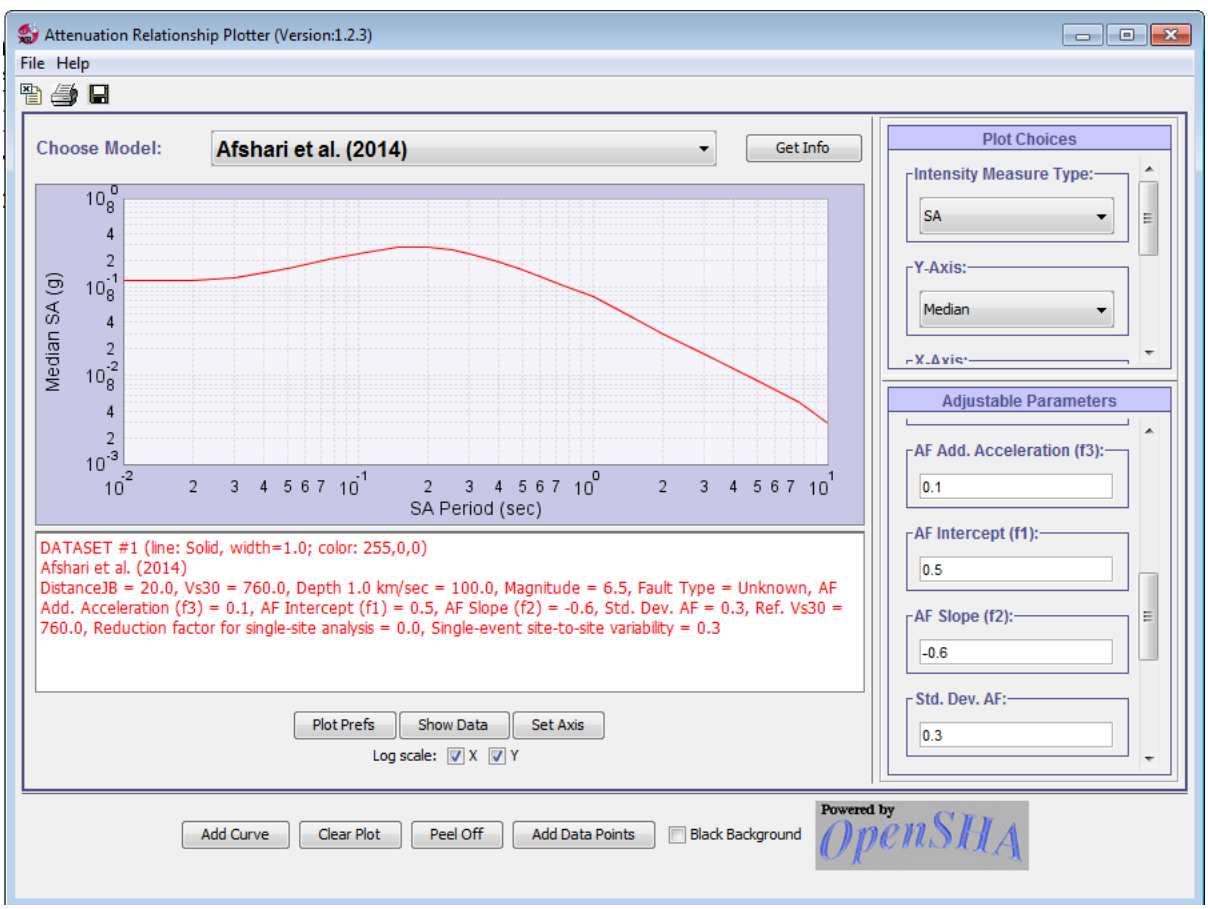

Figure 4.6 **An example of calculated median response spectrum for M = 6.5, *R* = 20 km, Reference V_{S30} = 760 m/sec, basin depth = 100 m, f_1 = 0.5, f_2 = -0.6, f_3 = 0.1, $\phi_{\ln Y}$ = ϕ_{S2S} =0.3, and single-site reduction facto r = 0.**

4.4 COMPARATIVE ANALYSES OF GRA IMPLEMENTATION METHODS

In this section, we compare hazard curves and uniform hazard spectra obtained from the approximate procedures with those obtained using the relatively robust implementation within the hazard integral. Calculations are performed for the locations in Table 4.1, namely downtown Los Angeles (I-10/I-110), San Francisco (Hwy-101/I-80), and Sacramento (Hwy-50/Hwy-99). The San Francisco site hazard is dominated by the nearby San Andreas fault. The Los Angeles site has a combination of hazard from local faults and the somewhat more distant San Andreas fault. The Sacramento site has relatively low-hazard. For each location, we consider two site conditions: (1) the soft-soil site condition illustrated in Appendix A and considered previously in Section 2.5 (V_{S30} =197 m/sec); and (2) is for relatively firm soils (V_{S30} = 300 m/sec), for which we use default site amplification parameters from SS14. In this section, all disaggregation results and UHS plots are calculated for probability of exceedance of 5% in 50 years (APE = 0.001025).

For each site in Table 4.1, we present the following results in Figures 4.7–4.9: (a) UHS developed using fully probabilistic implementations in OpenSHA for the rock, firm-soil, and soft-soil site conditions; (b) for the firm-soil site, hazard curves for PGA and 1.0-sec PSA developed using approximate and fully probabilistic methods; (c) same as (b) but for soft-soil site condition; (d) 1.0-sec PSA disaggregation results for the rock site condition; and (e) same as for (d) but for soft-soil site condition. The hazard curves plotted in Parts (b) and (c) are evaluated for the limiting cases of the site response remaining fully ergodic (F=0) and reliably site-specific (F=1).

Table 4.1 Sites investigated for comparative study of GRA implementation methods.

Site	Location	PGA		PSA (1 sec)	
		$\overline{\mathbf{M}}$	$\overline{R}$ (km)	$\overline{\mathbf{M}}$	$\overline{R}$ (km)
Downtown LA	34.021°N, 118.163°W	6.69	12.92	6.73	11.39
San Francisco	37.461°N, 122.242°W	7.34	6.84	7.55	5.65
Sacramento	38.333°N, 121.282°W	6.58	65.23	6.75	73.62

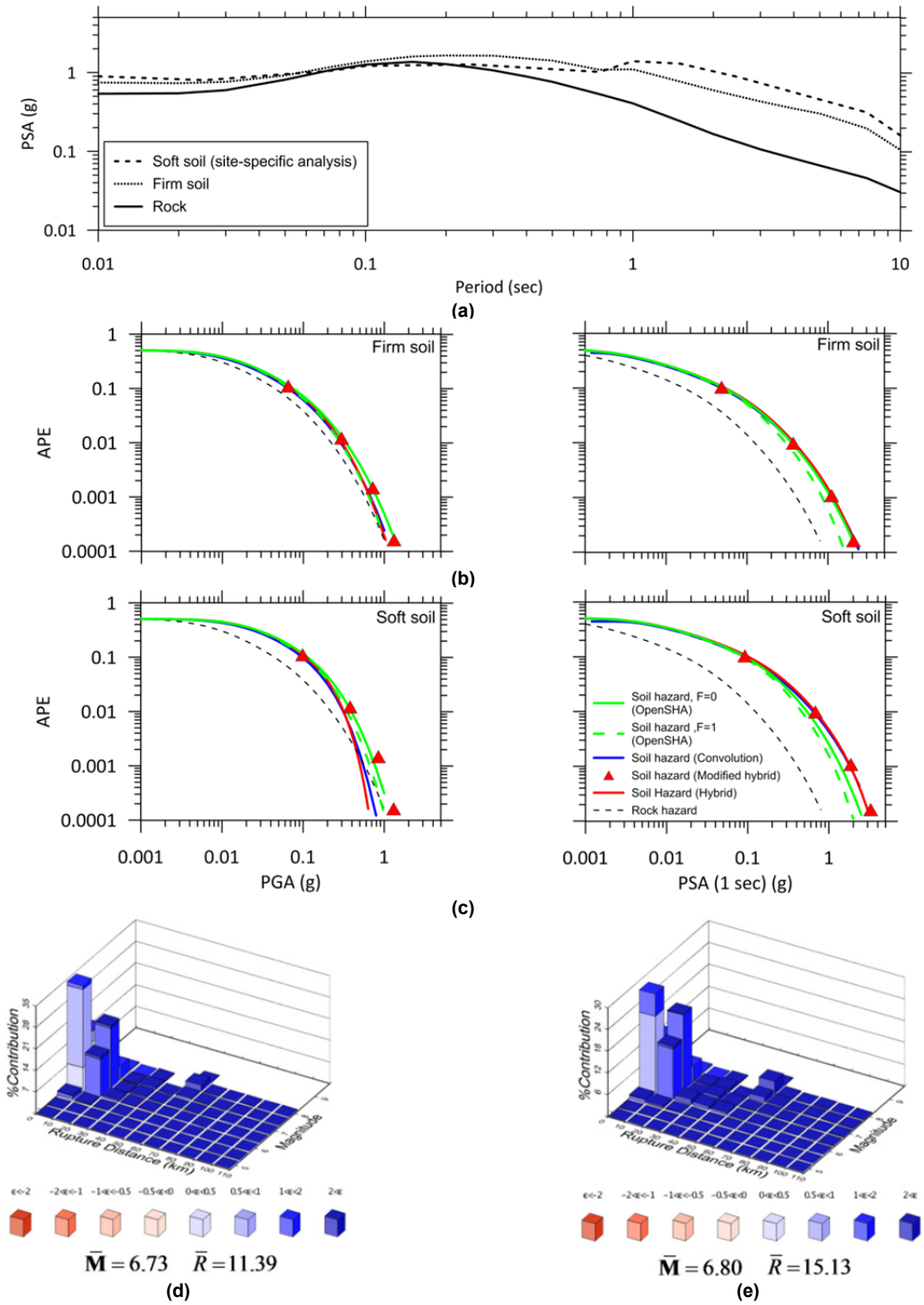

Figure 4.7 Downtown Los Angeles site: (a) UHS for rock, soft-soil, and firm-soil sites for APE = 0.001025; (b) Hazard curves calculated from different methods for the soft-soil site for PGA and PSA (1 sec); (c) hazard curves calculated from different methods for the stiff-soil site; and (d) disaggregation of hazard for APE = 0.001025 for PSA (1 sec) for rock site, and (e) disaggregation of hazard for APE = 0.001025 for PSA (1 sec) for soft-soil site.

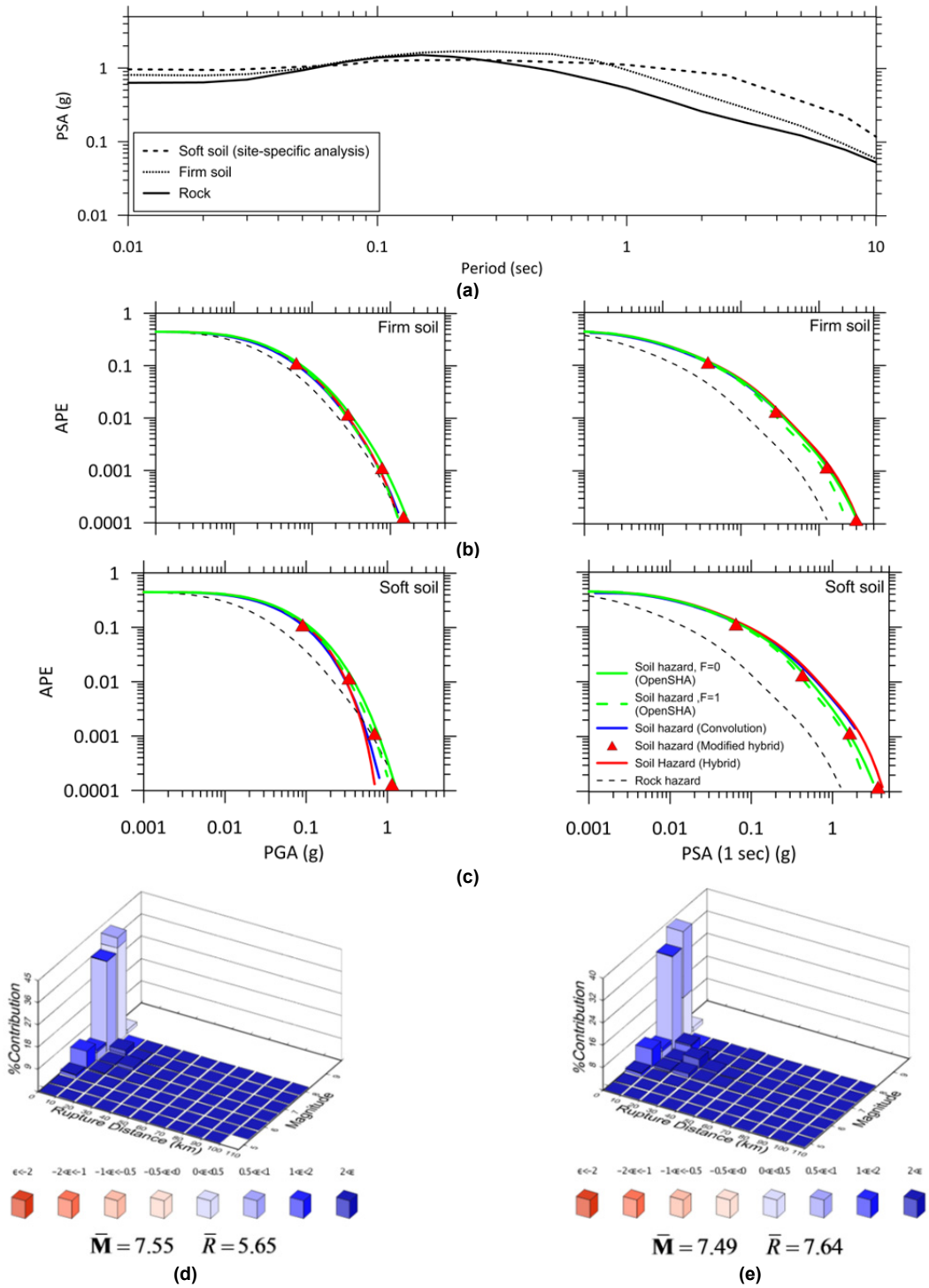

Figure 4.8 San Francisco site: (a) UHS for rock, soft soil, and firm soil sites for APE = 0.001025; (b) hazard curves calculated from different methods for the soft-soil site for PGA and PSA (1 sec); (c) hazard curves calculated from different methods for the stiff-soil site; (d) disaggregation of hazard for APE = 0.001025 for PSA (1 sec) for rock site; and (e) disaggregation of hazard for APE = 0.001025 for PSA (1 sec) for soft-soil site.

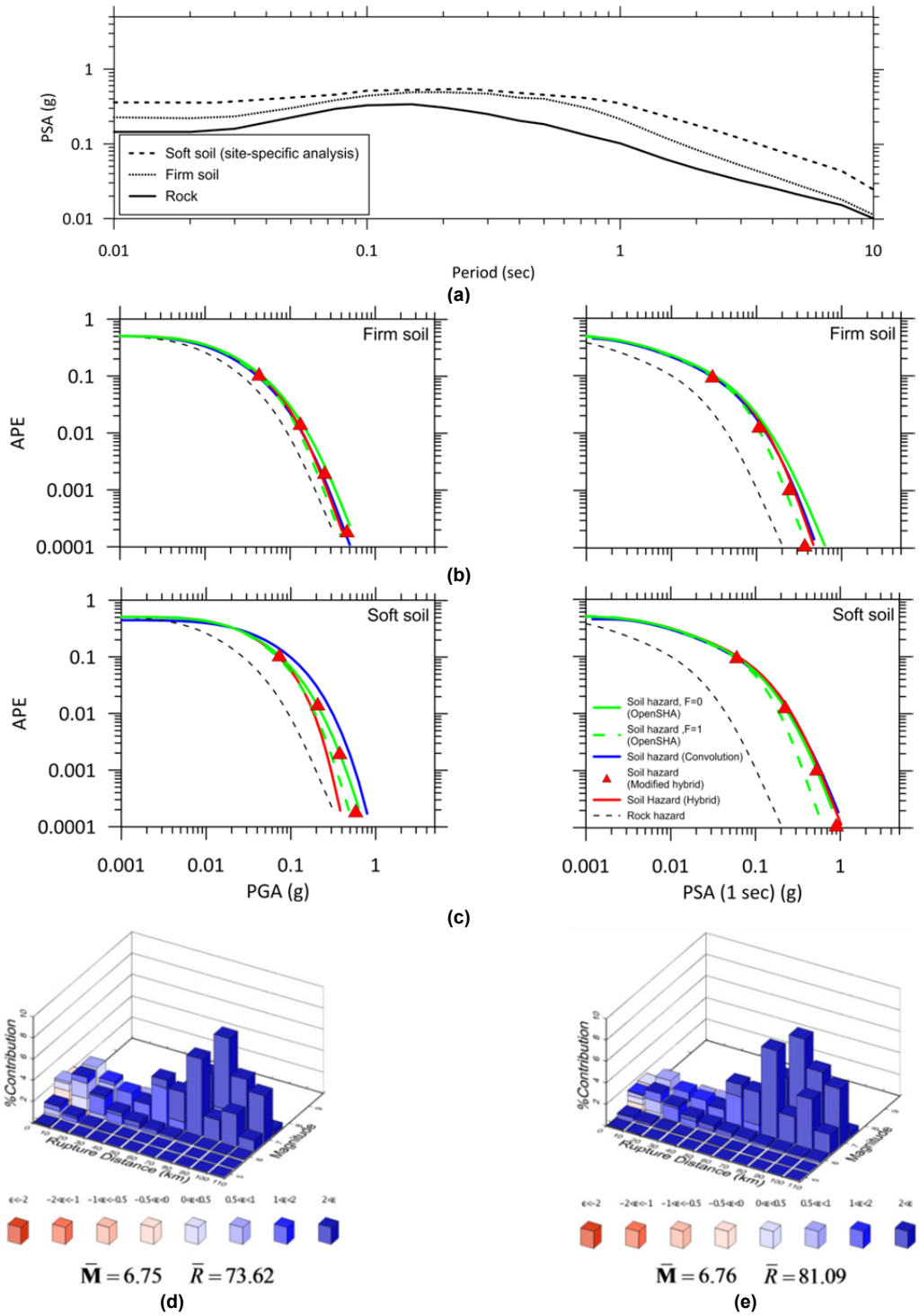

Figure 4.9 Sacramento site: (a) UHS for rock, soft-soil, and firm-soil sites for APE = 0.001025; (b) hazard curves calculated from different methods for the soft-soil site for PGA and PSA (1 sec); (c) hazard curves calculated from different methods for the stiff-soil site; and (d) disaggregation of hazard for APE = 0.001025 for PSA (1 sec) for rock site; and (e) disaggregation of hazard for APE = 0.001025 for PSA (1 sec) for soft-soil site.

Examining first the UHS, we note that the firm soil site has broadly increased hazard relative to reference rock, whereas the soft-soil site has only modest amplification (and for some periods, de-amplification) at short periods but substantial amplification at long periods. The long period amplification is controlled by GRA up to the site period of about 1–2 sec, and is then dominated by the empirical models, which include basin effects. The relatively large basin-related amplification is what prevents a peak in the spectrum at the site period.

The fully probabilistic hazard curves show the expected sensitivity to whether the ergodic assumption is allowed to be relaxed by taking $F > 0$, which reduces within event standard deviation ϕ by the corresponding fraction of ϕ_{S2S}. Using $F = 1$ reduces the ground motions (relative to $F = 0$) by amounts ranging from 10 to 30% for PGA and 10 to 40% for 1.0-sec PSA at the target hazard level of APE = 0.001025.

Looking next at the simplified methods for developing hazard curves, we find for the firm soil site condition modest method-to-method variability. In most cases, the results are close to those for the fully probabilistic method with $F = 0$, and the sensitivity to F is greater than the variability between approximate methods. We believe that this lack of sensitivity to the approximate methods is caused by the relatively modest nonlinearity for the firm-soil site condition.

In the case of the soft-soil site condition, the approximate methods produce biased hazard estimates. For the relatively high-hazard Los Angeles and San Francisco locations, PGA hazard is underestimated by the hybrid and convolution approaches and 1.0-sec PSA hazard is overestimated. The underestimation of PGA hazard is caused principally by x_{IMref} in the site amplification function being taken as the value from the rock hazard curve (which has positive epsilon), which produces a stronger nonlinear effect than in the PSHA (where x_{IMref} is a mean value). For 1.0-sec PSA, the nonlinear considerations are relatively minor, and the overestimation is caused by differences in the standard deviation terms. Even without ergodic adjustments, the within-event standard deviation is reduced for soft soils as compared to rock [Equation (1.12)]; this adjustment affects the PSHA results but is not considered in the approximate methods. These differences in standard deviation are also present at short periods, but are overwhelmed by the nonlinear bias described previously. Trends similar to these were observed previously by Goulet and Stewart [2009].

In the case of the relatively low-hazard Sacramento site, the trends for the soft-soil site are more complex for PGA hazard (the long-period trends are similar to those for the coastal sites). In this case, nonlinearity is less severe due to weaker reference rock shaking levels, while the standard deviation differences persist. The net effect is an underestimation by the hybrid method and overestimation by the convolution method for PGA hazard.

In each case where the hybrid and convolution methods exhibit bias (principally for the soft-soil site condition), the modified hybrid approach provides results closer to the fully probabilistic PSHA. The relatively good match is to the ergodic PSHA results ($F = 0$); the approximate methods cannot accommodate relaxation of the ergodic assumption ($F > 0$).

Finally, the disaggregation results show that the controlling sources are modestly different for rock and soft-soil site conditions. Softer sites attract greater contributions to hazard from relatively distant sources, which for the Los Angeles and Sacramento locations increases

$\bar{\mathbf{M}}$ and $\bar{R}$. These differences are not present for the San Francisco site, which is close to a large source (San Andreas fault).

Based on these results, our recommendation is to use fully probabilistic implementations of nonlinear site amplification functions whenever practical, to ensure appropriate treatment of standard deviation terms and the most accurate hazard curves and de-aggregation results. When this is not possible, the modified hybrid approach provides the best results and is recommended.

5 Summary and Conclusions

5.1 SCOPE OF WORK

The scope of work for the project described in this report entailed (1) evaluating the effectiveness of one-dimensional ground response analysis (1D GRA) based on interpretation of research results in the literature; (2) identifying, and as needed, further developing approaches for merging site-specific GRA results with the results of probabilistic seismic hazard analysis (PSHA) (hazard curves or uniform hazard spectra) for a reference site condition, and (3) developing guidelines for performing GRA, with an emphasis on recommended input parameters and their uncertainties. Each of these scope items was addressed through a process involving careful literature review, discussions with appropriate experts (including project review panel and others noted in acknowledgements), synthesis and further development of the technical material (as needed), and the preparation of this report.

Scope Item 1 is addressed in Chapter 1. The limited available work on the effectiveness of GRA has involved interpretation of ground motion records from California and Japan. The California data that was considered involves surface instruments, whereas the study of Japanese data utilized vertical arrays. Both studies provided statistically robust evaluations of the effectiveness of GRA.

Scope Item 2 is addressed in Chapters 1, 3, and 4. In Chapter 1, methods for merging site-specific GRA with reference site hazard analyses are identified from suitable studies in the literature. These methods include fully probabilistic methods in which GRA results replace the site term in the ground motion prediction equations (GMPEs) used in the hazard integral, and more simplified methods in which PSHA is not directly performed for the soil condition. These simplified methods are referred to as hybrid, modified hybrid, and convolution approaches.

Implementation of these methods requires the use of two standard deviation terms for a given intensity measure (IM): (1) the standard deviation representing the uncertainty in the site amplification, $\phi_{\ln Y}$; and (2) the contributions of site-to-site variability to the within-event variability of a GMPE. The within-event variability for ground motion on a soil site condition is denoted $\phi_{\ln Z \quad D-\gamma}$, and the contribution of site-to-site variability to that standard deviation is denoted ϕ_{S2S}. In Chapter 3, we synthesize and interpret appropriate literature to support the development of recommendations regarding $\phi_{\ln Y}$ and ϕ_{S2S}. In Chapter 4 we implement procedures for merging GRA with PSHA, applying the applicable standard deviation terms, and perform comparative analyses for example sites. Based on these analyses, we develop

recommended best practices. Computational tools are developed to assist users in implementing these methods.

Scope Item 3 is addressed in Chapter 2 through a comprehensive literature review, drawing heavily upon the experience of the authors, review panel, and others. Methods of computation for GRA are not emphasized, being available in other reference documents. We present recommendations on the following critical issues: (1) selection or measurement of applicable soil properties describing (for a given depth) the backbone curve and damping, including dispersion of those properties; (2) under what conditions nonlinear versus equivalent-linear methods of analysis should be used; (3) selection and scaling of appropriate input motions; and (4) interpretation of GRA results to develop functions representing the variation of mean amplification of an IM given the strength of the ground motion on the reference site condition.

5.2 SUMMARY OF RECOMMENDATIONS

5.2.1 Value of Site-Specific Site Response

When site response is evaluated in an ergodic sense (i.e., through the use of site terms in GMPEs), a global average site response is applied, conditional on the site parameter (typically V_{S30}). This global average site response is likely to be in error for any particular site. If the level of error can be identified and used to adjust the ergodic model, the ground motion analysis becomes more accurate (i.e., bias is removed), and the dispersion of the predicted ground motions is reduced. Therefore, it should be understood that a site-specific evaluation of site response is practically always useful. The question is how that evaluation should be undertaken.

One option is to instrument the site, record earthquakes, and perform residuals analyses of the data relative to GMPEs in such a way that the bias term (denoted η_S in Section 3.2) can be defined. The site response in this case then becomes the sum (in natural log units) of η_S and the site term from the GMPE (although there may be some challenges in applying this with confidence for strong shaking conditions where the site response becomes highly nonlinear). Because the site response is truly site specific, ϕ_{S2S} can be removed from the within-event variability, which is akin to setting $F = 1$ in Equation (3.6).

The principal issue addressed in this study is whether, in the absence of recordings from a site of interest, geotechnical GRA provides a suitable basis for estimating site-specific site response. The available literature provides admittedly mixed results in this regard. As described in Section 1.1, an early study of California data [Baturay and Stewart 2003] found generally favorable results (GRA provides unbiased estimates of site response for short oscillator periods and uncertainty is reduced relative to the use of ergodic site terms). On the other hand, a recent study using downhole data from Japan [Thompson et al. 2012] found that GRA provides a poor fit to observed transfer functions for a significant majority of sites. In short, the former study supports of the use of GRA, especially for conditions where resonance effects may occur (i.e., sites having strong impedance contrasts), whereas the later effectively does not support the use of GRA.

This fundamental issue remains unresolved. We comment further on this in our recommendations for future work in Section 5.3.

5.2.2 Merging GRA with Hazard Analysis Results for Reference Site Condition

A summary of the steps involved in performing GRA is given in Section 5.2.3. This section summarizes findings and recommendations related to how the results of such analyses can be combined with PSHA results for a reference site condition (usually rock) to provide a nearly or approximately hazard-consistent ground motion for the actual (typically soil) site condition.

Effectively three attributes of site amplification are needed to merge GRA with PSHA for a given IM. First, an expression for the mean amplification is needed, which should allow for the possible effects of material nonlinearity. This expression is given in Equation (1.5) and has three coefficients (f_1, f_2, and f_3). Second, because its associated variance directly contributes to the within-event variability for the soil site condition, ($\phi_{\ln Y}$), the standard deviation of site amplification, is needed. Third, the contribution of site-to-site variability to the within event standard deviation (ϕ_{S2S}) is needed if the analyst wishes to reduce the within-event standard deviation under the assumption that the computed site response is at least partially non-ergodic.

The mean amplification function in Equation (1.5) is regressed from the GRA results, expressed as computed site amplification versus some measure of the intensity of shaking on the reference site condition. The mechanics of obtaining the coefficients for various practical conditions (e.g., the range of intensities for which GRA results were obtained, the range of oscillator periods for which PSHA results are required) are provided in Sections 2.6 and 4.2.1–4.2.2.

The standard deviation of the site amplification computed directly from GRA is considered unreliable—it is generally too high below the fundamental site period and too low above. For this reason, we recommend the use of $\phi_{\ln Y}$ inferred from ground motion data analysis as described in Section 3.4, which indicates remarkable consistency (between-periods and between-studies) at $\phi_{\ln Y} \approx 0.3$. This level of consistency is not found with ϕ_{S2S}, which appears to exhibit regional variations and variations across periods (see Section 3.5.2). Once values for these standard deviation terms are selected, the applicable standard deviation for the soil site condition can be obtained using Equation (3.6). A significant consideration in this regard is whether the site response computed from GRA is non-ergodic. This is currently unknown and falls within the realm of engineering judgment: that judgment can be exercised through alternate values of parameter F in Equation (3.6) (ergodic implies $F = 0$, full non-ergodic requires $F = 1$).

Armed with a mean amplification function and the applicable standard deviation terms, the most robust merging of GRA with PSHA requires replacement of the site term in a GMPE with the mean amplification function, and the use of that modified GMPE in the hazard integral. As described in Section 4.3, we have developed a local version of OpenSHA [Field et al. 2003] that can perform such calculations. This type of implementation is preferred because it properly handles modified standard deviation terms, which produces the most accurate hazard analysis results (i.e., hazard curves and uniform hazard spectra). This implementation also accounts for site effects in the disaggregation.

When implementation of GRA within the hazard integral is not considered practical, then the reference site (usually rock) hazard curves are modified using the mean site amplification function and (in some cases) $\phi_{\ln Y}$. Among the various options for this modification described in Section 1.2, the method having the least bias relative to the probabilistic approach is modified

hybrid. As described in Section 1.2.3, this method involves modifying the reference site ground motion for a point on the hazard curve using the mean site amplification. What differentiates modified hybrid method from the hybrid method, is that the hybrid method takes the amplitude of the rock motion from the hazard curve, whereas modified hybrid method uses the mean reference site ground motion for the controlling magnitude and distance (as evaluated from disaggregation). Convolution approaches can also be applied (see Section 1.2.5), but will produce biased hazard estimates. Hybrid methods are not recommended. Spreadsheet solutions for these approximate methods have been developed and are described in Section 4.2.

5.2.3 Guidelines for Performing GRA

Our recommended guidelines for performing GRA assume basic proficiency by the analyst in the use of EL) and nonlinear (NL) methods of analysis, e.g., as given by NCHRP [2012]. For such analysts, the principal issues that must be addressed in application are evaluation of mean or 'best estimate' dynamic soil properties and their uncertainties, deciding when to use EL versus NL methods of analysis, and selection and scaling of appropriate input motions. Those issues are addressed in detail in Sections 2.1–2.5, with a brief synopsis here. The interpretation of the results in terms of amplification functions is given in Section 2.6 and is summarized in Section 5.2.2.

(a) Soil Properties

For each depth interval in a discretized soil column, dynamic soil properties are needed to describe the shape of the backbone (i.e., shear stress versus shear strain, τ–γ) curve and the relationship between hysteretic damping ratio and shear strain ($D-\gamma$ curves). In principal, backbone curves can be described by a small-strain shear-wave velocity (V_S), mass density, and modulus reduction ($G/G_{\max}$) versus shear-strain curve. In principal, all of these quantities can be measured, but often in practice the $G/G_{\max}-\gamma$ and $D-\gamma$ curves are evaluated from empirical models. Shear-wave velocity profiles should always be based on suitable *in situ* measurements for GRA applications. When empirical models for $G/G_{\max}-\gamma$ and $D-\gamma$ curves are used, difficulties are encountered for sites that mobilize large strains, requiring the use of shear strength as an addition parameter explicitly considered in the analysis. Sections 2.2–2.3 provide recommendations for the measurement and (in the case of $G/G_{\max}-\gamma$ and $D-\gamma$ curves) estimation of these critical soil properties. Guidelines for uncertainty quantification for V_S, $G/G_{\max}$, D, and shear strength are also provided based on recommendations found in the literature.

The modeling of soil damping presents some particular challenges that go beyond the selection of appropriate $D-\gamma$ curves derived from laboratory testing. As described in Section 2.3.2, there is some evidence in the literature that the small-strain damping value ($D_{\min}$) derived from lab tests may not suitably represent in situ conditions, which can involve more complex energy dissipation phenomena such as wave scattering. While not well resolved in the literature, some preliminary results suggest that additive levels of small strain damping generally in the range of zero to 5% may be required to fit field observations. Another set of challenges, specific to NL methods of GRA, is that $D-\gamma$ soil behavior associated with rules for unload-reload

stress-strain cycles may provide a poor match to laboratory-based $D-\gamma$ relations. Moreover, because these unload-reload rules produce effectively zero damping at small strain, additional Rayleigh damping must be added to the model for numerical stability. Section 2.3.2 describes these issues and available solutions that are implemented in some NL analysis codes.

(b) Analysis Methods

Ground response problems involving small to moderate levels of shear strain are best analyzed with EL methods due to the simplicity of parameter selection and faster computation times when compared to NL analysis. However, as described in Section 2.4.1, for large-strain ground response problems, EL methods tend to over-damp portions of the ground motion. This motivates the use of more accurate NL analysis for those conditions. Section 2.4.1 describes how to detect the presence of over-damping and hence problematic results from EL analysis, using attributes of the pseudo-acceleration response spectral shape.

Section 2.4.2 provides recommendations on identifying *a priori* the conditions for which EL and NL analysis results are likely to be significantly different, which is useful when planning an analysis program. Nonlinear analyses are needed when the ratio of peak velocity (for reference rock) to V_{S30} (for the site of interest) exceeds certain thresholds that vary with oscillator period.

(c) Input Ground Motions

Most EL and NL computer programs for performing GRA require input acceleration time series (the exception is random vibration theory methods). Section 2.5 describes the process of ground motion selection and scaling, drawing upon best practices in this area for applications to structures. The process involves identification of target spectra appropriate for the hazard levels of interest, selecting records appropriate for those hazard levels, and scaling (or matching) the selected records to the target spectra.

Target spectra are defined for reference conditions (usually rock). A critical aspect of defining input ground motions is selection of one or more hazard levels (or return periods) for which motions are to be selected. Most projects have a defined hazard level that must be used for regulatory purposes, and the question then becomes whether additional hazard levels are to be considered. As explained in Section 2.5.1, the use of multiple hazard levels (providing ground motions weaker and stronger than the target) is recommended because it allows site amplification to be evaluated for a wide range of input amplitudes. An additional issue is the manner in which target spectra are defined, which is typically uniform hazard spectra (UHS) or scenario spectra having more physically realizable spectral shapes.

Once a target spectrum is identified, we recommend use of online search algorithms to identify compatible motions (details in Section 2.5.2). Spectral shape, which is well represented near a period of interest by parameter $\varepsilon^{i}(T)$ [Equation (2.20)], should be a principal consideration in ground motion selection, along with other factors such as magnitude, distance, and site condition. Near-fault sites require special considerations related to ground motion directionality and the presence of pulses in the time series. The process of selecting appropriate ground motions is repeated for each target spectrum that is being considered.

Finally, selected motions are scaled or modified to provide compatibility with the amplitude of the target spectrum (details in Section 2.5.3). Scaling involves simple multiplication

of the amplitude of the time series by a factor, which retains the natural spectral shape. Modification usually involves adjustment of records to match, within relatively narrow error limits, the target spectrum across a defined period range. We recommend the use of scaling over modification for GRA applications, because the desired product of the calculations is amplification functions for which some range of input motion amplitudes is desirable.

5.3 FUTURE WORK

The implementation of ground response analysis (GRA) in the manner described in this report would benefit substantially from future research addressing the following issues:

1. Effectiveness of 1D GRA at predicting observed site response. There is a fundamental discrepancy in the outcomes of prior research investigating this question, which is explained in Sections 1.1 and 5.2.1. In future work, available ground motion data from California and elsewhere can be utilized to investigate the effectiveness of GRA at predicting observed surface/downhole transfer functions from vertical arrays and observed site terms (η_S) from sites with large numbers of recordings. The work on surface/downhole transfer functions would reveal whether the relatively poor performance of GRA at Japanese sites is also observed in different geological environments, such as California. Analysis of the predictability of observed site terms (η_S) using GRA would address the question of whether an analytically-derived site amplification model can be considered non-ergodic.
2. Modulus reduction and damping models. When material-specific laboratory testing is not performed, we rely upon empirical models for modulus reduction and damping curves. Those empirical models, described in Sections 2.2–2.3, are based on databases that are not publically available. The models themselves are unpublished except for PhD dissertations. This is not an acceptable level of documentation and vetting for models having this level of practical importance. In future work, an appropriate database should be assembled and analyzed in a transparent manner to develop new modulus reduction and damping models that are then archived in the peer-reviewed literature. Ideally, these models should extend to large strains and include shear strength as a free parameter.
3. Models for shear-wave velocity uncertainty. At sites where GRA is to be performed, it is common for limited V_S profiling to be performed, and often only a single profile is available. Under such circumstances, uncertainty in the V_S profile can only be evaluated using data from other sites, where many V_S profiles were performed and models for the standard deviation and correlation coefficient of V_S were derived (see Section 2.2.1). At present, the only available models for these important parameters are contained in grey literature [Toro 1995] utilizing proprietary datasets that are now dated. As with the soil nonlinear curves, what is now needed is a compilation of data that is well documented and publically accessible, followed by analysis of that data and presentation of new models for standard deviation and correlation coefficient in the peer-reviewed literature.
4. OpenSHA implementation. As described in Section 4.3, our recommended procedures for full probabilistic implementation of GRA in PSHA are currently coded in a local version of OpenSHA that operates with a single GMPE [Boore et al. 2014]. Future work should

further advance this programming so that it can be used with any GMPE, and these procedures should be implemented in the public versions of the software disseminated online (*http://www.opensha.org/*).

5. Recommended values of ϕ_{S2S}. The standard deviation term representing the site-to-site contribution to within-event variability (ϕ_{S2S}) plays a very important role in defining the benefit of non-ergodic site response. This is because the within event variance is reduced by the square of ϕ_{S2S}, or some fraction thereof, as shown in Equation (3.6). As described in Section 3.5.2, previous studies investigating ϕ_{S2S} have found highly variable results, which introduce substantial epistemic uncertainty into the selection of an appropriate value of this important parameter. Given the significant divergence of prior research results, additional work is needed on this important topic.

References

Abrahamson N.A., Silva W.J. (1997). Empirical response spectral attenuation relations for shallow crustal earthquakes, *Seism. Res. Lett.,* 68(1): 94–127.

Afacan K.B. (2014). *Evaluation of Nonlinear Site Response of Soft Clay using Centrifuge Models*, PhD Thesis, Department of Civil Engineering, University of California, Los Angeles, CA.

Afacan K.B., Brandenberg S.J., Stewart J.P. (2014). Centrifuge modeling studies of site response in soft clay over wide strain range, ASCE, *J. Geotech. Eng.,* 140(2): 04013003.

Akkar S., Çagnan Z. (2010). A local ground-motion predictive model for Turkey and its comparison with other regional and global ground-motion models, *Bull. Seismol. Soc. Am.,* 100(6): 2978–2995.

Al Atik L., Abrahamson N.A. (2010). An improved method for nonstationary spectral matching, *Earthq. Spectra,* 26(3): 601–617.

Al Atik L., Abrahamson N., Bommer J.J., Scherbaum F., Cotton F., Kuehn N. (2010). The variability of ground motion prediction models and its components, *Seism. Res. Lett*., 81(5): 794–801.

Almufti I., Motamed R., Grant D.N., Willford M. (2014). Incorporation of velocity pulses in design ground motions for response history analysis using a probabilistic framework, *Earthq. Spectra* (in review).

Assimaki D., Kausel E., Whittle A.J. (2000). Model for dynamic shear modulus and damping for granular soils, ASCE, *J. Geotech. Eng.,* 126(10): 859–869.

Assimaki D., Li W. (2012). Site- and ground motion-dependent nonlinear effects in seismological model predictions, *Soil Dyn. Earthq. Eng*., 32(1): 143–151.

Assimaki D., Li W., Steidl J.M., Schmedes J. (2008). Quantifying nonlinearity susceptibility via site response modeling uncertainty at three sites in the Los Angeles Basin, *Bull. Seismol. Soc. Am*., 98(5): 2364–2390.

Atkinson G.M. (2006). Single-station sigma, *Bull. Seism. Soc. Am.*, 96(2): 446-455.

Baker J.W. (2011). Conditional mean spectrum: tool for ground motion selection, ASCE, *J. Struct. Eng.,* 137(3): 322–333.

Baker J.W., Cornell C.A. (2003). Uncertainty specification and propagation for loss estimation using FOSM methods, *Proceedings, 9th Int. Conf. on Applications of Statistics and Probability in Civil Engineering (ICASP9)*, San Francisco, California: Millpress., Rotterdam, Netherlands, 8pgs.

Baker J.W., Cornell C.A. (2006). Which spectral acceleration are you using?, *Earthq. Spectra*, 22(2): 293–312.

Baker J.W., Jayaram N. (2008). Correlation of spectral acceleration values from NGA ground motion models, *Earthq. Spectra*, 24(1): 299–317.

Baturay M.B., Stewart J.P. (2003). Uncertainty and bias in ground motion estimates from ground response analyses, *Bull. Seismol. Soc. Am.*, 93(5): 2025–2042.

Bazzurro P., Cornell C.A. (2004a). Nonlinear soil-site effects in probabilistic seismic-hazard analysis, *Bull. Seismol. Soc. Am.*, 94(6): 2110–2123.

Bazzurro P., Cornell C.A. (2004b). Ground motion amplification in nonlinear soil sites with uncertain properties, *Bull. Seismol. Soc. Am*., 94(6): 2090–2109.

Blake T.F., Hollingsworth R.A., Stewart J.P., eds. (2002). *Recommended Procedures for Implementation of DMG Special Publication 117 Guidelines for Analyzing and Mitigating Landslide Hazards in California*, Southern California Earthquake Center (SCEC), University of Southern California, Los Angeles, CA.

Bommer J.J., Scott S.G., Sarma S.K. (2000). Hazard-consistent earthquake scenarios, *Soil Dyn. Earthq. Eng.,* 19(4): 219–231.

Boore D.M. (2005). SMSIM-Fortran programs for simulating ground motions from earthquakes: version 2.3, a revision of *U.S. Geological Survey Open-File Report 96-80-A*, Menlo Park, CA.

Boore D.M. (2010). Orientation-independent non geometric-mean measures of seismic intensity from two horizontal components of motion*, Bull. Seismol. Soc. Am.,* 100(4): 1830–1835.

Boore D.M., Stewart J.P., Seyhan E., Atkinson G.M (2014). NGA-West 2 equations for predicting PGA, PGV, and 5%-damped PSA for shallow crustal earthquakes, *Earthq. Spectra*, 30(3): 1057–1085.

Brandenberg S.J., Bellana N., Shantz T. (2010). Shear wave velocity as a function of standard penetration test resistance and vertical effective stress at California bridge sites, *Soil Dyn. Earthq. Eng.,* 30(10): 1026–1035.

Boulanger R.W., Idriss I.M. (2006). Liquefaction susceptibility criteria for silts and clays, ASCE, *J. Geotech. Eng.,* 132(11): 1413–1426.

Boulanger R.W., Idriss I.M. (2008). Evaluation of cyclic softening in silts and clays, ASCE, *J. Geotech. Eng.,* 133(6): 641–652.

Bozorgnia Y., Abrahamson N.A., Al-Atik L., Ancheta T.D., Atkinson G.M., Baker J.W., Chiou B., Darragh R., Day S., Donahue J., Graves R.W., Gregor N., Hanks T., Idriss I.M., Kamai R., Kishida T., Kottke A., Rezaeian S., Rowshandel B., Seyhan E., Shahi S., Shantz T., Silva W., Spudich P., Stewart J.P., Watson-Lamprey J., Wooddell K. (2014). NGA-West2 research project, *Earthq. Spectra*, 30(3): 973–988.

Bozorgnia Y., Crouse C.B., Hamburger R.O., Klemencic R., Krawinkler H., Malley J.O., Moehle J.P., Naeim F., Stewart J.P. (2010). Guidelines for performance-based seismic design of tall buildings, *PEER Report No. 2010/05*, Pacific Earthquake Engineering Research Center, University of California, Berkeley, CA.

BSSC (2015). *NEHRP Recommended Seismic Provisions for New Buildings and Other Structures*, Building Seismic Safety Council, Federal Emergency Management Agency, Washington D.C, in press.

Campbell K.W., Bozorgnia Y. (2008). NGA ground motion model for the geometric mean horizontal component of *PGA*, *PGV*, *PGD*, and 5%-damped linear elastic response spectra for periods ranging from 0.01 to 10 *s*, *Earthq. Spectra,* 24(1): 139–171.

Caltrans (2013). *Seismic Design Criteria*, Version 1.7, California Department of Transportation, Sacramento, CA.

Chiou B.S.-J., Darragh R., Gregor N., Silva W. (2008). NGA project strong-motion database, *Earthq. Spectra,* 24(1): 23–44.

Chiou B.S.-J., Youngs R.R. (2008). An NGA model for the average horizontal component of peak ground motion and response spectra, *Earthq. Spectra*, 24(1): 173–215.

Choi W.K. (2008). *Dynamic Properties of Ash-Flow Tuffs*, PhD Thesis, Department of Civil Engineering, University of Texas, Austin, TX.

Cox B.R., Beekman A.N. (2011). Intramethod variability in ReMi dispersion measurements and V_S estimates at shallow bedrock sites, ASCE, *J. Geotech. Eng.,* 137(4): 354–362.

Cramer C.H., (2003). Site-specific seismic-hazard analysis that is completely probabilistic, *Bull. Seismol. Soc. Am*., 93(4): 1841–1846.

Darendeli M.B. (2001). Development of a New Family of Normalized modulus reduction and material damping curves, PhD Thesis, Department of Civil Engineering, University of Texas, Austin, TX.

Dobry R., Borcherdt R.D., Crouse C.B., Idriss I.M., Joyner W.B., Martin G.R., Power M.S., Rinne E.E., Seed R.B. (2000). New site coefficients and site classification system used in recent building seismic code provisions, *Earthq. Spectra,* 16(1): 41–67.

Doroudian M., Vucetic M. (1995). A direct simple shear device for measuring small-strain behavior, *ASTM Geotech. Testing J.*, 18(1): 69–85.

Douglas J. (2010). Comparisons of observations to predictions from selected ground-motion models for the PEGASOS refinement project (PRP), report prepared for the PEGASOS refinement project (PRP), *Internal Tech. Rept. TP2-TB-1050*, 19 October 2010.

Elgamal A., Lai T., Yang Z., He L. (2001). Dynamic soil properties, seismic downhole arrays and applications in practice, *Proceedings, 4th International Conference on Recent Advances in Geotechnical Earthquake Engineering and Soil Dynamics*, S. Prakash, ed., San Diego, CA.

Federal Emergency Management Agency, FEMA (2012). *Seismic Performance Assessment of Buildings, Volume I – Methodology and Volume II – Implementation Guide, FEMA P-58*, Washington, DC. Field E.H., Jordan T.H., Cornell C.A. (2003). OpenSHA: A developing community modeling environment for seismic hazard analysis, *Seism. Res. Lett.* 74(4): 406–419.

García D., Wald D.J., Hearne M.G. (2012). A global earthquake discrimination scheme to optimize ground-motion prediction equation selection, *Bull. Seismol. Soc. Am*. 102(1): 185–203.

Gibbs J.F., Tinsley J.C., Boore D.M., Joyner W.B. (1999). Seismic velocities and geological conditions at twelve sites subjected to strong ground motion in the 1994 Northridge, California earthquake: *A revision of OFR 96-740*, U.S. Geological Survey, Menlo Park, CA.

Goulet C.A., Stewart J.P. (2009). Pitfalls of deterministic application of nonlinear site factors in probabilistic assessment of ground motions *Earthq. Spectra*, 25(3): 541–555.

Goulet C.A., Stewart J.P., Bazzurro P., Field E.H. (2007). Integration of site-specific ground response analysis results into probabilistic seismic hazard analysis, *Proceedings, 4th International Conference on Earthquake Geotechnical Engineering,* Thessaloniki, Greece.

Grant L. B., Rockwell T. K. (2002). A northward propagating earthquake sequence in coastal southern California?, *Seism. Res. Lett.,* 73(4): 461–469.

Hardin B.O., Drnevich V.P. (1972). Shear modulus and damping in soils, *J. Soil Mech. and Found. Div.* 98(7): 667–692.

Harr M.E. (1987). *Reliability-Based Design in Civil Engineering*, McGraw-Hill Book Company.

Haselton C.B., Fry A., Baker J.W., Hamburger R.O., Whittaker A.S., Stewart J.P., Elwood K.J., Luco N., Hooper J.D., Charney F.A. (2014). Response history analysis for the design of new buildings: Part I - Development of Recommendations for the NEHRP Provisions and the ASCE/SEI 7 Standard, *Earthq. Spectra* (in review).

Hashash Y.M.A. (2012). *DEEPSOIL Version 5.1 User Manual and Tutorial*, University of Illinois at Urbana-Champaign, Urbana, IL.

Hashash Y.M.A., Park D. (2001). Non-linear one-dimensional seismic ground motion propagation in the Mississippi embayment, *Eng. Geol*., 62: 185–206.

Hashash Y.M.A., Park D. (2002). Viscous damping formulation and high frequency motion propagation in nonlinear site response analysis, *Soil Dyn. Earthq. Eng.*, 22(7): 611–624.

Hatanaka M., Uchida A. (1996). Empirical correlation between penetration resistance and internal friction angle of sandy soils, *Soils and Foundations,* 36(4): 1–9.

Holtz R.D., Kovacs W.D., Sheahan T.C. (2011). *An Introduction to Geotechnical Engineering*, 2nd Ed., Pearson Inc.: Uppersaddle River, New Jersey.

Huang Y., Whittaker A.S., Luco N. (2008). Maximum spectral demands in the near-fault region, *Earthq. Spectra,* 24(1): 319–341.

Idriss I.M., Sun J.I. (1992). *SHAKE91:* A computer program for conducting equivalent linear seismic response analyses of horizontally layered soil deposits, Center for Geotechnical Modeling, University of California, Davis, CA.

Iwasaki T., Tatsuoka F., Takagi Y. (1978). Shear modulus of sands under torsional shear loading, *Soils and Foundations,* 18(1): 39–56.

Jefferies M.G., Been K. (2006). *Soil Liquefaction – A Critical State Approach*, Taylor & Francis: New York, NY.

Jones A.L., Kramer S.L., Arduino P. (2002). Estimation of uncertainty in geotechnical properties for performance-based earthquake engineering, *PEER Report No. 2002/16*, Pacific Earthquake Engineering Research Center, University of California. Berkeley, CA.

Kaklamanos J., Bradley B.A., Thompson E.M., Baise L.G. (2013), Critical parameters affecting bias and variability in site-response analyses using KiK-net downhole array data, *Bull. Seismol. Soc. Am.*, 103(3): 1733–1749.

Kim B, Hashash Y.M.A., Kottke A., Assimaki D., Li W., Rathje E.M., Campbell K.W., Silva W.J., Stewart J.P. (2013). A predictive model for the relative differences between nonlinear and equivalent-linear site response analyses, *Transactions*, SMiRT-22, Division IV, San Francisco, CA.

Kim B, Hashash Y.M.A., Kottke A., Stewart J.P., Rathje E.M., Assimaki D., Li W., Campbell K.W., Silva W.J. (2014). Relative differences between nonlinear and equivalent-linear site response analyses (in review).

Kottke A., Rathje E.M. (2008). Technical manual for STRATA, *PEER Report No. 2008/10*, Pacific Earthquake Engineering Research Center, University of California, Berkeley, CA.

Kramer S.L. (1996). *Geotechnical Earthquake Engineering*, Prentice Hall, Inc.: New Jersey.

Kulhawy F.H., Mayne P.H. (1990). Manual on estimating soil properties for foundation design, *Report EL-6800*, Electric Power Research Institute (EPRI), Palo Alto, CA.

Kulhawy F.H. (1992). On the evaluation of static soil properties, ASCE, *Geotech. Special Publication,* 31: 95–115.

Kwok A.O.L., Stewart J.P., Hashash Y.M.A., Matasovic N., Pyke R., Wang Z., Yang Z. (2007). Use of exact solutions of wave propagation problems to guide implementation of nonlinear, time-domain ground response analysis routines, ASCE, *J. Geotech. Eng.,* 133(11): 1385–1398.

Kwok A.O.L., Stewart J.P., Hashash Y.M.A (2008). Nonlinear ground-response analysis of Turkey Flat shallow stiff-soil site to strong ground motion, *Bull. Seismol. Soc. Am*., 98(1): 331–343.

Lacasse S., Nadim F. (1996). Uncertainties in characterizing soil properties (plenary), Plenary lecture. In: Uncertainty in the Geologic Environment, From Theory to Practice, C. D. Shackelford, P. P. Nelson, and M. J. S. Roth, eds., *Proceedings, Uncertainty 96*, Madison, WI.

Ladd C.C. (1991). Stability evaluation during staged construction: The Twenty-Second Terzaghi Lecture, ASCE, *J. Geotech. Eng.,* 117(4): 537–615.

Li W., Assimaki D. (2011). Site and motion-dependent parametric uncertainty of site-response analyses in earthquake simulations, *Bull. Seismol. Soc. Am.*, 100(3): 954–968.

Li X.-S., Wang Z.-L., Shen C-.K. (1992). *SUMDES: A Nonlinear Procedure for Response Analysis of Horizontally-Layered Sites Subjected to Multi-Directional Earthquake Loading*, Department of Civil Engineering, University of California, Davis, CA.

Lin P.-S., Chiou B.S.-J., Abrahamson N., Walling M., Lee C.-T., Cheng C.-T. (2011). Repeatable source, site, and path effects on the standard deviation for ground-motion prediction, *Bull. Seismol. Soc. Am.* 101(5): 2281–2295.

Liu P.-S.., Archuleta R.J., Hartzell S.H. (2006). Prediction of broadband ground-motion time histories: Hybrid low/high-frequency method with correlated random source parameters, *Bull. Seismol. Soc. Am.,* 96(6): 2118–2130.

Liu K.-S., Shin T.-C., Tsai Y.-B. (1999). A free-field strong-motion network in Taiwan: TSMIP, *Terr. Atmos. Ocean. Sci.*, 10(2): 377–396.

Louie J.N. (2001). Faster, better: shear-wave velocity to 100 meters depth from refraction microtremor arrays, *Bull. Seismol. Soc. Am*., 91(2): 347–364.

Luco N., Ellingwood B.R., Hamburger R.O., Hooper J.D., Kimball J.K., Kircher C.A. (2007). Risk-targeted versus current seismic design maps for the conterminous United States, *Proceedings, SEAOC 2007 Convention*, Lake Tahoe, CA, pp. 163–175.

Masing G. (1926). Eigenspannungen and verfertigung beim messing, *Proceedings, 2nd International Congress on Applied Mechanics*, Zurich, Switzerland.

Matasovic N. (2006). *D-MOD_2: A Computer Program for Seismic Response Analysis of Horizontally Layered Soil Deposits, Earthfill Dams, and Solid Waste Landfills, User's Manual*, GeoMotions, LLC, Lacey, Washington.

Matasovic N. (1992). *Seismic Response of Composite Horizontally-Layered Soil Deposits*, Ph.D. Thesis, Department of Civil and Environmental Engineering, University of California, Los Angeles, CA.

Matasovic N., Vucetic M. (1995). Generalized cyclic degradation-pore pressure generation model for clays, ASCE, *J. Geotech. Eng.,* 121(1): 33–42.

McGuire R.K. (1995). Probabilistic seismic hazard analysis and design earthquakes: closing the loop, *Bull. Seismol. Soc. Am.*, 85(5): 1275–1284.

McKenna F., Fenves G.L. (2001). *The OpenSees Command Language Manual, Version 1.2.*, Pacific Earthquake Engineering Research Center, University of California, Berkeley, CA.

Melchers R.E. (1999). *Structural Reliability Analysis and Prediction*, John Wiley and Sons, Chichester. U.K.

Menq F.Y. (2003). *Dynamic Properties of Sandy and Gravelly Soils*, PhD Thesis, Department of Civil Engineering, University of Texas, Austin, TX.

Muravskii G. (2005). On description of hysteretic behavior of materials, *Int. J. Solids Struct*. 42: 2625–2644.

Naeim F., Lew M. (1995). On the use of design spectrum compatible time histories, *Earthq. Spectra* 11(1): 111–127.

NCHRP (2012). *Practices and Procedures for Site-Specific Evaluations of Earthquake Ground Motions, Synthesis 428* (N. Matasovic and Y.M.A. Hashash)*,* National Cooperative Highway Research Program, Transportation Research Board, Washington D.C.

Negussey D., Wijewickreme W.K.D., Vaid Y.P. (1988). Constant volume friction angle of granular materials, *Canadian Geotech. J.*, 26(1): 50-55.

Nigbor R.L., Diehl J., Swift J. (2001). Characterization of US Sites: ROSRINE 5B, *PEER Lifelines Research Project 2A01-Site Response*, presented at 2001 PEER Annual Meeting, Oakland, CA.

NIST (2011). Selecting and scaling earthquake ground motions for performing response-history analyses, *GCR 11–917–15*, National Institute of Standard and Technology, Department of Commerce, Gaithersburg, MD.

Ordóñez G.A. (2010). *SHAKE2000: A Computer Program for the 1-D Analysis of Geotechnical Earthquake Engineering Problems, User's Manual*, GeoMotions, LLC, Lacey, Washington.

Park D., Hashash Y.M.A. (2004). Soil damping formulation in nonlinear time domain site response analysis, *J. Earthq. Eng.*, 8(2): 249–274.

Parra E. (1996). *Numerical Modeling of Liquefaction and Lateral Ground Deformation including Cyclic Mobility and Dilation Response in Soil Systems*, PhD Thesis, Department of Civil and Environmental Engineering, Rensselaer Polytechnic Institute, Troy, NY

Phillips C., Hashash, Y.M.A. (2009). Damping formulation for nonlinear 1D site response analyses, *Soil Dyn. Earthq. Eng.*, 29(7): 1143–1158.

Phoon K., Kulhawy F.H. (1999). Characterization of geotechnical variability, *Canadian Geotech. J.* 36(4): 625–639.

Pinheiro J., Bates D., DebRoy S., Sarkar D., R Core Team (2013). *nlme: Linear and Nonlinear Mixed Effects Models*, R package version 3.1–107. 4.2.

Pyke R.M. (1979). Nonlinear soil models for irregular cyclic loadings, ASCE, *J. Geotech. Eng.,* 105(6): 715–726.

Pyke R.M. (2000). TESS users' manual, TAGA engineering software services, Lafayette, CA.

Ragheb A.M. (1994). *Numerical Analysis of Seismically Induced Deformations in Saturated Granular Soil Strata*, PhD Thesis, Department of Civil and Environmental Engineering, Rensselaer Polytechnic Institute, Troy, NY.

Rathje E.M., Kottke A.R., Trent W.L. (2010). Influence of input motion and site property variabilities on seismic site response analysis, ASCE, *J. Geotech. Eng.*, 136(4): 607−619.

Reiter L. (1990). *Earthquake Hazard Analysis*, Columbia University Press, New York.

Robertson P.K. (2009). Interpretation of cone penetration tests-a unified approach, *Canadian Geotech. J.* 46(11): 1337−1355.

Robertson P.K. (2012). Interpretation of in-situ tests- some insights, *Mitchell Lecture-ISC'4*, Brazil.

Roblee C., Chiou B. (2004). A proposed geoindex model for design selection of non-linear properties for site response analyses, *Proceedings, International Workshop on Uncertainties in Nonlinear Soil Properties and Their Impact on Modeling Dynamic Soil Response*, University of California, Berkeley, CA.

Rodriguez-Marek A., Montalva G.A., Cotton F., Bonilla F. (2011). Analysis of single-station standard deviation using the KiK-net data, *Bull. Seismol. Soc. Am.* 101(3): 1242−1258.

Rodriguez-Marek A., Montalva G.A., Cotton F., Bonilla F. (2013). A model for single-station standard deviation using data from various tectonic regions, *Bull. Seismol. Soc. Am.,* 103(6): 3149−3163.

Schnabel P.B., Lysmer J., Seed H.B. (1972). SHAKE: A computer program for earthquake response analysis of horizontally layered sites, *Report No. UCB/EERC-72/12*, Earthquake Engineering Research Center, University of California, Berkeley, CA.

Seed H.B., Idriss I.M. (1970). Soil moduli and damping factors for dynamic response analyses, *Report No. UCB/EERC-70-10*, Earthquake Engineering Research Center, University of California, Berkeley, CA.

Seyhan E., Stewart J.P. (2014). Semi-empirical nonlinear site amplification from NGA-West 2 data and simulations, *Earthq. Spectra* (in review).

Shahi S., Baker J.W. (2011). An empirically calibrated framework for including the effects of near-fault directivity in probabilistic seismic hazard analysis, *Bull. Seismol. Soc. Am.,* 101(2): 742−755.

Sheahan T.C., Ladd C.C., Germaine J.T. (1996). Rate-dependent undrained shear behavior of saturated clay, ASCE, *J. Geotech. Eng.,* 122(2): 99−108.

Shin T.C., Teng T.L. (2001). An overview of the 1999 Chi-Chi, Taiwan earthquake, *Bull. Seismol. Soc. Am.,* 91(5): 895−913.

Silva W.J., Darragh R.B., Gregor N., Martin G., Abrahamson N.A., Kircher C. (2000). Reassessment of site coefficients and near-fault factors for building code provisions, *Report to U.S. Geological Survey*, National Earthquake Hazards Reduction Program, Washington, D.C.

Stewart J.P., Kwok A.O. (2008). Nonlinear seismic ground response analysis: code usage protocols and verification against vertical array data, *ASCE Geotechnical Special Publication No. 181*, Geotechnical Engineering and Soil Dynamics IV, Sacramento, CA.

Stewart J.P., Kwok A.O., Hashash Y.M.A., Matasovic N., Pyke R., Wang Z., Yang Z. (2008). Benchmarking of nonlinear geotechnical ground response analysis procedures, *PEER Report No. 2008/04*, Pacific Earthquake Engineering Research Center, University of California, Berkeley, CA.

Stewart J.P., Liu A.H., Choi Y. (2003). Amplification factors for spectral acceleration in tectonically active regions, *Bull. Seism. Soc. Am*. 93: 332–352.

Terzaghi K., Peck R.B., Mesri G. (1996). *Soil Mechanics in Engineering Practice*, 3rd Edition, John Wiley & Sons, New York.

Thompson E.M., Baise L.G., Tanaka Y., Kayen R.E. (2012). A taxonomy of site response complexity, *Soil Dyn. Earthq. Eng.*, 41: 32–43.

Thomson W.T. (1950). Transmission of elastic waves through a stratified solid, *J. Appl. Phys.*, 21: 89–93.

Toro G.R. (1995). Probabilistic models of site velocity profiles for generic and site-specific ground-motion amplification studies, *Technical Report No. 779574*, Brookhaven National Laboratory, Upton, NY.

Trudeau P.J., Whitman R.V., Christian J.T. (1974). Shear wave velocity and modulus of a marine clay, *J. Boston Soc. Civil Engineers*, 61(1): 12–25.

Tsai C.C., Hashash Y.M.A. (2009). Learning of dynamic soil behavior from downhole arrays, ASCE*, J. Geotech. Eng.,* 135(6): 745–757.

Vucetic M. (1990). Normalized behavior of clay under irregular cyclic loading, *Canadian Geotech. J*., 27(1): 29–46.

Vucetic M., Dobry R. (1991). Effect of soil plasticity on cyclic response, ASCE*, J. Geotech. Eng.*, 117(1): 89–107.

Watson-Lamprey J.A., Boore D.M. (2007). Beyond Sa_{GMRotI}: conversion to Sa_{Arb}, Sa_{SN}, and Sa_{MaxRot}, *Bull. Seismol. Soc. Am*., 97(5): 1511–1524.

Yang Z. (2000). *Numerical Modeling of Earthquake Site Response including Dilation and Liquefaction*, PhD Thesis, Civil Engineering and Engineering Mechanics Department, Columbia University, New York, NY.

Yee E., Stewart J.P., Tokimatsu K. (2013). Elastic and large-strain nonlinear seismic site response from analysis of vertical array recordings, ASCE, *J. Geotech. Eng.,* 139(10): 1789–1801.

Youngs R.R. (2004). Software validation report for SHAKE04, Geomatrix Consultants, Oakland, CA.

Zhang J., Andrus R.D., Juang C.H. (2005). Normalized shear modulus and material damping ratio relationships, ASCE, *J. Geotech. Eng.*, 131(4): 453-464.

Zhang J., Andrus R.D., Juang C.H. (2008). Model uncertainty in normalized shear modulus and damping relationships, ASCE, *J. Geotech. Eng.*, 134(1): 24–36.

Zheng W., Hashash Y.M.A., Petersen M.M., Whittaker A.S. (2010). Site specific response analysis in the New Madrid seismic zone, In: S. Prakash, ed., *Proceedings, Fifth International Conference in Recent Advances in Geotechnical Earthquake Engineering and Soil Dynamics*, San Diego, CA.

Appendix A Soil Profile and GRA Results for the Example Site

For the soft-soil site used for the example calculations in Chapter 4, the geotechnical and geophysical logs are given in Figure A.1. For this example, equivalent-linear ground response analyses are performed in DEEPSOIL [Hashash 2012] for a number of input ground motions selected and scaled using different approaches discussed in Section 2.6. For the sandy, clayey silt, and soft silty marine clay, the Darendeli [2001] model is used for modulus reduction and damping curves. For the sand and sandstone layers, the Menq [2003] model is used for nonlinear curves. All layers are divided into sublayers having a thickness of 1 m. Input parameters for the analysis are given in Figure A.1. Figure A.2 shows an example of PGA and maximum shear strain profiles. These are based on analyses performed with a suite of input motions selected and scaled for compatibility with a target spectrum representing a single hazard level. The motions are scaled to the target in the manner described in Section 2.5.3 (Approach 1).

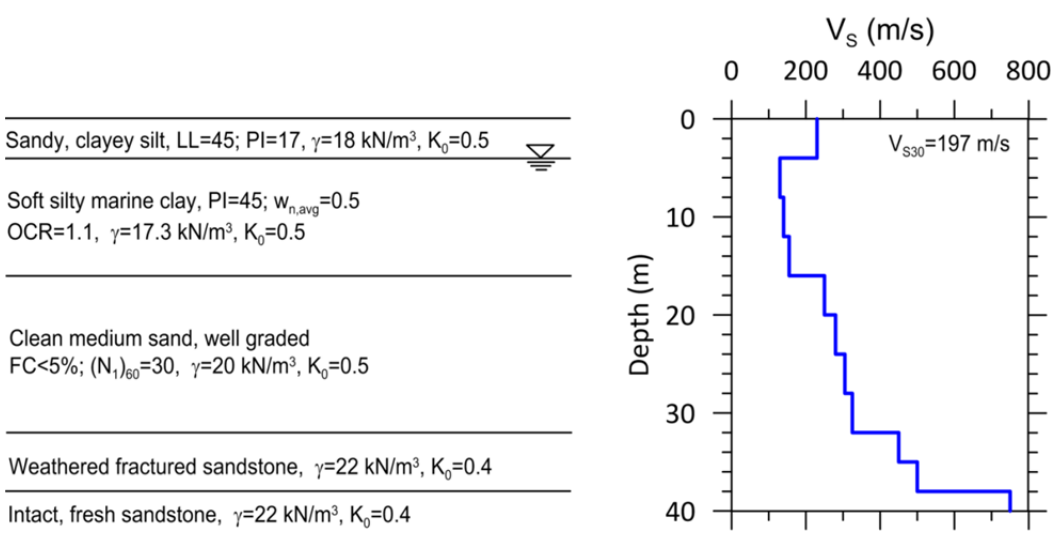

Figure A.1 Soil profile and geotechnical information for the example site having soft-soil conditions.

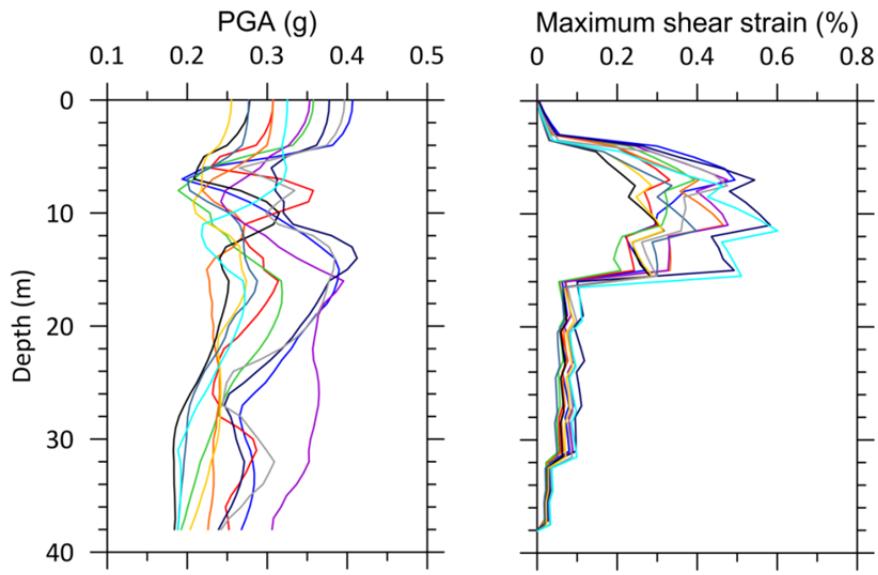

Figure A.2 **Peak ground acceleration and maximum shear strain profiles for the example site. The input motions for this case are selected and scaled for compatibility with a single hazard level (Approach 1 in Section 2.5.3).**

PEER REPORTS

PEER reports are available as a free PDF download from http://peer.berkeley.edu/publications/peer_reports_complete.html. Printed hard copies of PEER reports can be ordered directly from our printer by following the instructions at http://peer.berkeley.edu/publications/peer_reports.html. For other related questions about the PEER Report Series, contact the Pacific Earthquake Engineering Research Center, 325 Davis Hall mail code 1792, Berkeley, CA 94720. Tel.: (510) 642-3437; Fax: (510) 665-1655; Email: peer_editor@berkeley.edu

PEER 2014/16 *Guidelines for Performing Hazard-Consistent One-Dimensional Ground Response Analysis for Ground Motion Prediction.* Jonathan P. Stewart, Kioumars Afshari, and Youssef M.A. Hashash. October 2014.

PEER 2014/15 *NGA-East Regionalization Report: Comparison of Four Crustal Regions within Central and Eastern North America using Waveform Modeling and 5%-Damped Pseudo-Spectral Acceleration Response.* Jennifer Dreiling, Marius P. Isken, Walter D. Mooney, Martin C. Chapman, and Richard W. Godbee. October 2014.

PEER 2014/14 *Scaling Relations between Seismic Moment and Rupture Area of Earthquakes in Stable Continental Regions.* Paul Somerville. August 2014.

PEER 2014/13 *PEER Preliminary Notes and Observations on the August 24, 2014, South Napa Earthquake*. Grace S. Kang (Editor), Stephen A. Mahin (Editors). September 2014.

PEER 2014/12 *Reference-Rock Site Conditions for Central and Eastern North America: Part II – Attenuation (Kappa) Definition.* Kenneth W. Campbell, Youssef M.A. Hashash, Byungmin Kim, Albert R. Kottke, Ellen M. Rathje, Walter J. Silva, and Jonathan P. Stewart. August 2014.

PEER 2014/11 *Reference-Rock Site Conditions for Central and Eastern North America: Part I - Velocity Definition*. Youssef M.A. Hashash, Albert R. Kottke, Jonathan P. Stewart, Kenneth W. Campbell, Byungmin Kim, Ellen M. Rathje, Walter J. Silva, Sissy Nikolaou, and Cheryl Moss. August 2014.

PEER 2014/10 *Evaluation of Collapse and Non-Collapse of Parallel Bridges Affected by Liquefaction and Lateral Spreading*. Benjamin Turner, Scott J. Brandenberg, and Jonathan P. Stewart. August 2014.

PEER 2014/09 *PEER Arizona Strong-Motion Database and GMPEs Evaluation*. Tadahiro Kishida, Robert E. Kayen, Olga-Joan Ktenidou, Walter J. Silva, Robert B. Darragh, and Jennie Watson-Lamprey. June 2014.

PEER 2014/08 *Unbonded Pretensioned Bridge Columns with Rocking Detail*. Jeffrey A. Schaefer, Bryan Kennedy, Marc O. Eberhard, John F. Stanton. June 2014.

PEER 2014/07 *Northridge 20 Symposium Summary Report: Impacts, Outcomes, and Next Steps*. May 2014.

PEER 2014/06 *Report of the Tenth Planning Meeting of NEES/E-Defense Collaborative Research on Earthquake Engineering*. December 2013.

PEER 2014/05 *Seismic Velocity Site Characterization of Thirty-One Chilean Seismometer Stations by Spectral Analysis of Surface Wave Dispersion.* Robert Kayen, Brad D. Carkin, Skye Corbet, Camilo Pinilla, Allan Ng, Edward Gorbis, and Christine Truong. April 2014.

PEER 2014/04 *Effect of Vertical Acceleration on Shear Strength of Reinforced Concrete Columns.* Hyerin Lee and Khalid M. Mosalam. April 2014.

PEER 2014/03 *Retest of Thirty-Year-Old Neoprene Isolation Bearings.* James M. Kelly and Niel C. Van Engelen. March 2014.

PEER 2014/02 *Theoretical Development of Hybrid Simulation Applied to Plate Structures.* Ahmed A. Bakhaty, Khalid M. Mosalam, and Sanjay Govindjee. January 2014.

PEER 2014/01 *Performance-Based Seismic Assessment of Skewed Bridges.* Peyman Kaviani, Farzin Zareian, and Ertugrul Taciroglu. January 2014.

PEER 2013/26 *Urban Earthquake Engineering. Proceedings of the U.S.-Iran Seismic Workshop.* December 2013.

PEER 2013/25 *Earthquake Engineering for Resilient Communities: 2013 PEER Internship Program Research Report Collection.* Heidi Tremayne (Editor), Stephen A. Mahin (Editor), Jorge Archbold Monterossa, Matt Brosman, Shelly Dean, Katherine deLaveaga, Curtis Fong, Donovan Holder, Rakeeb Khan, Elizabeth Jachens, David Lam, Daniela Martinez Lopez, Mara Minner, Geffen Oren, Julia Pavicic, Melissa Quinonez, Lorena Rodriguez, Sean Salazar, Kelli Slaven, Vivian Steyert, Jenny Taing, and Salvador Tena. December 2013.

PEER 2013/24 *NGA-West2 Ground Motion Prediction Equations for Vertical Ground Motions.* September 2013.

PEER 2013/23 *Coordinated Planning and Preparedness for Fire Following Major Earthquakes.* Charles Scawthorn. November 2013.

PEER 2013/22 *GEM-PEER Task 3 Project: Selection of a Global Set of Ground Motion Prediction Equations.* Jonathan P. Stewart, John Douglas, Mohammad B. Javanbarg, Carola Di Alessandro, Yousef Bozorgnia, Norman A. Abrahamson, David M. Boore, Kenneth W. Campbell, Elise Delavaud, Mustafa Erdik and Peter J. Stafford. December 2013.

PEER 2013/21 *Seismic Design and Performance of Bridges with Columns on Rocking Foundations.* Grigorios Antonellis and Marios Panagiotou. September 2013.

PEER 2013/20 *Experimental and Analytical Studies on the Seismic Behavior of Conventional and Hybrid Braced Frames.* Jiun-Wei Lai and Stephen A. Mahin. September 2013.

PEER 2013/19 *Toward Resilient Communities: A Performance-Based Engineering Framework for Design and Evaluation of the Built Environment.* Michael William Mieler, Bozidar Stojadinovic, Robert J. Budnitz, Stephen A. Mahin and Mary C. Comerio. September 2013.

PEER 2013/18 *Identification of Site Parameters that Improve Predictions of Site Amplification.* Ellen M. Rathje and Sara Navidi. July 2013.

PEER 2013/17 *Response Spectrum Analysis of Concrete Gravity Dams Including Dam-Water-Foundation Interaction.* Arnkjell Løkke and Anil K. Chopra. July 2013.

PEER 2013/16 *Effect of hoop reinforcement spacing on the cyclic response of large reinforced concrete special moment frame beams.* Marios Panagiotou, Tea Visnjic, Grigorios Antonellis, Panagiotis Galanis, and Jack P. Moehle. June 2013.

PEER 2013/15 *A Probabilistic Framework to Include the Effects of Near-Fault Directivity in Seismic Hazard Assessment.* Shrey Kumar Shahi, Jack W. Baker. October 2013.

PEER 2013/14 *Hanging-Wall Scaling using Finite-Fault Simulations.* Jennifer L. Donahue and Norman A. Abrahamson. September 2013.

PEER 2013/13 *Semi-Empirical Nonlinear Site Amplification and its Application in NEHRP Site Factors.* Jonathan P. Stewart and Emel Seyhan. November 2013.

PEER 2013/12 *Nonlinear Horizontal Site Response for the NGA-West2 Project.* Ronnie Kamai, Norman A. Abramson, Walter J. Silva. May 2013.

PEER 2013/11 *Epistemic Uncertainty for NGA-West2 Models.* Linda Al Atik and Robert R. Youngs. May 2013.

PEER 2013/10 *NGA-West 2 Models for Ground-Motion Directionality.* Shrey K. Shahi and Jack W. Baker. May 2013.

PEER 2013/09 *Final Report of the NGA-West2 Directivity Working Group.* Paul Spudich, Jeffrey R. Bayless, Jack W. Baker, Brian S.J. Chiou, Badie Rowshandel, Shrey Shahi, and Paul Somerville. May 2013.

PEER 2013/08 *NGA-West2 Model for Estimating Average Horizontal Values of Pseudo-Absolute Spectral Accelerations Generated by Crustal Earthquakes.* I. M. Idriss. May 2013.

PEER 2013/07 *Update of the Chiou and Youngs NGA Ground Motion Model for Average Horizontal Component of Peak Ground Motion and Response Spectra.* Brian Chiou and Robert Youngs. May 2013.

PEER 2013/06 *NGA-West2 Campbell-Bozorgnia Ground Motion Model for the Horizontal Components of PGA, PGV, and 5%-Damped Elastic Pseudo-Acceleration Response Spectra for Periods Ranging from 0.01 to 10 sec.* Kenneth W. Campbell and Yousef Bozorgnia. May 2013.

PEER 2013/05 *NGA-West 2 Equations for Predicting Response Spectral Accelerations for Shallow Crustal Earthquakes.* David M. Boore, Jonathan P. Stewart, Emel Seyhan, Gail M. Atkinson. May 2013.

PEER 2013/04 *Update of the AS08 Ground-Motion Prediction Equations Based on the NGA-West2 Data Set.* Norman Abrahamson, Walter Silva, and Ronnie Kamai. May 2013.

PEER 2013/03 *PEER NGA-West2 Database.* Timothy D. Ancheta, Robert B. Darragh, Jonathan P. Stewart, Emel Seyhan, Walter J. Silva, Brian S.J. Chiou, Katie E. Wooddell, Robert W. Graves, Albert R. Kottke, David M. Boore, Tadahiro Kishida, and Jennifer L. Donahue. May 2013.

PEER 2013/02 *Hybrid Simulation of the Seismic Response of Squat Reinforced Concrete Shear Walls.* Catherine A. Whyte and Bozidar Stojadinovic. May 2013.

PEER 2013/01 *Housing Recovery in Chile: A Qualitative Mid-program Review.* Mary C. Comerio. February 2013.

PEER 2012/08 *Guidelines for Estimation of Shear Wave Velocity.* Bernard R. Wair, Jason T. DeJong, and Thomas Shantz. December 2012.

PEER 2012/07 *Earthquake Engineering for Resilient Communities: 2012 PEER Internship Program Research Report Collection.* Heidi Tremayne (Editor), Stephen A. Mahin (Editor), Collin Anderson, Dustin Cook, Michael Erceg, Carlos

Esparza, Jose Jimenez, Dorian Krausz, Andrew Lo, Stephanie Lopez, Nicole McCurdy, Paul Shipman, Alexander Strum, Eduardo Vega. December 2012.

PEER 2012/06 *Fragilities for Precarious Rocks at Yucca Mountain.* Matthew D. Purvance, Rasool Anooshehpoor, and James N. Brune. December 2012.

PEER 2012/05 *Development of Simplified Analysis Procedure for Piles in Laterally Spreading Layered Soils.* Christopher R. McGann, Pedro Arduino, and Peter Mackenzie–Helnwein. December 2012.

PEER 2012/04 *Unbonded Pre-Tensioned Columns for Bridges in Seismic Regions.* Phillip M. Davis, Todd M. Janes, Marc O. Eberhard, and John F. Stanton. December 2012.

PEER 2012/03 *Experimental and Analytical Studies on Reinforced Concrete Buildings with Seismically Vulnerable Beam-Column Joints.* Sangjoon Park and Khalid M. Mosalam. October 2012.

PEER 2012/02 *Seismic Performance of Reinforced Concrete Bridges Allowed to Uplift during Multi-Directional Excitation.* Andres Oscar Espinoza and Stephen A. Mahin. July 2012.

PEER 2012/01 *Spectral Damping Scaling Factors for Shallow Crustal Earthquakes in Active Tectonic Regions.* Sanaz Rezaeian, Yousef Bozorgnia, I. M. Idriss, Kenneth Campbell, Norman Abrahamson, and Walter Silva. July 2012.

PEER 2011/10 *Earthquake Engineering for Resilient Communities: 2011 PEER Internship Program Research Report Collection.* Eds. Heidi Faison and Stephen A. Mahin. December 2011.

PEER 2011/09 *Calibration of Semi-Stochastic Procedure for Simulating High-Frequency Ground Motions.* Jonathan P. Stewart, Emel Seyhan, and Robert W. Graves. December 2011.

PEER 2011/08 *Water Supply in regard to Fire Following Earthquake.* Charles Scawthorn. November 2011.

PEER 2011/07 *Seismic Risk Management in Urban Areas. Proceedings of a U.S.-Iran-Turkey Seismic Workshop.* September 2011.

PEER 2011/06 *The Use of Base Isolation Systems to Achieve Complex Seismic Performance Objectives.* Troy A. Morgan and Stephen A. Mahin. July 2011.

PEER 2011/05 *Case Studies of the Seismic Performance of Tall Buildings Designed by Alternative Means.* Task 12 Report for the Tall Buildings Initiative. Jack Moehle, Yousef Bozorgnia, Nirmal Jayaram, Pierson Jones, Mohsen Rahnama, Nilesh Shome, Zeynep Tuna, John Wallace, Tony Yang, and Farzin Zareian. July 2011.

PEER 2011/04 *Recommended Design Practice for Pile Foundations in Laterally Spreading Ground.* Scott A. Ashford, Ross W. Boulanger, and Scott J. Brandenberg. June 2011.

PEER 2011/03 *New Ground Motion Selection Procedures and Selected Motions for the PEER Transportation Research Program.* Jack W. Baker, Ting Lin, Shrey K. Shahi, and Nirmal Jayaram. March 2011.

PEER 2011/02 *A Bayesian Network Methodology for Infrastructure Seismic Risk Assessment and Decision Support.* Michelle T. Bensi, Armen Der Kiureghian, and Daniel Straub. March 2011.

PEER 2011/01 *Demand Fragility Surfaces for Bridges in Liquefied and Laterally Spreading Ground.* Scott J. Brandenberg, Jian Zhang, Pirooz Kashighandi, Yili Huo, and Minxing Zhao. March 2011.

PEER 2010/05 *Guidelines for Performance-Based Seismic Design of Tall Buildings.* Developed by the Tall Buildings Initiative. November 2010.

PEER 2010/04 *Application Guide for the Design of Flexible and Rigid Bus Connections between Substation Equipment Subjected to Earthquakes.* Jean-Bernard Dastous and Armen Der Kiureghian. September 2010.

PEER 2010/03 *Shear Wave Velocity as a Statistical Function of Standard Penetration Test Resistance and Vertical Effective Stress at Caltrans Bridge Sites.* Scott J. Brandenberg, Naresh Bellana, and Thomas Shantz. June 2010.

PEER 2010/02 *Stochastic Modeling and Simulation of Ground Motions for Performance-Based Earthquake Engineering.* Sanaz Rezaeian and Armen Der Kiureghian. June 2010.

PEER 2010/01 *Structural Response and Cost Characterization of Bridge Construction Using Seismic Performance Enhancement Strategies.* Ady Aviram, Božidar Stojadinović, Gustavo J. Parra-Montesinos, and Kevin R. Mackie. March 2010.

PEER 2009/03 *The Integration of Experimental and Simulation Data in the Study of Reinforced Concrete Bridge Systems Including Soil-Foundation-Structure Interaction.* Matthew Dryden and Gregory L. Fenves. November 2009.

PEER 2009/02 *Improving Earthquake Mitigation through Innovations and Applications in Seismic Science, Engineering, Communication, and Response. Proceedings of a U.S.-Iran Seismic Workshop.* October 2009.

PEER 2009/01 *Evaluation of Ground Motion Selection and Modification Methods: Predicting Median Interstory Drift Response of Buildings.* Curt B. Haselton, Ed. June 2009.

PEER 2008/10 *Technical Manual for Strata.* Albert R. Kottke and Ellen M. Rathje. February 2009.

PEER 2008/09 *NGA Model for Average Horizontal Component of Peak Ground Motion and Response Spectra.* Brian S.-J. Chiou and Robert R. Youngs. November 2008.

PEER 2008/08 *Toward Earthquake-Resistant Design of Concentrically Braced Steel Structures.* Patxi Uriz and Stephen A. Mahin. November 2008.

PEER 2008/07 *Using OpenSees for Performance-Based Evaluation of Bridges on Liquefiable Soils.* Stephen L. Kramer, Pedro Arduino, and HyungSuk Shin. November 2008.

PEER 2008/06 *Shaking Table Tests and Numerical Investigation of Self-Centering Reinforced Concrete Bridge Columns.* Hyung IL Jeong, Junichi Sakai, and Stephen A. Mahin. September 2008.

PEER 2008/05 *Performance-Based Earthquake Engineering Design Evaluation Procedure for Bridge Foundations Undergoing Liquefaction-Induced Lateral Ground Displacement.* Christian A. Ledezma and Jonathan D. Bray. August 2008.

PEER 2008/04 *Benchmarking of Nonlinear Geotechnical Ground Response Analysis Procedures.* Jonathan P. Stewart, Annie On-Lei Kwok, Yousseff M. A. Hashash, Neven Matasovic, Robert Pyke, Zhiliang Wang, and Zhaohui Yang. August 2008.

PEER 2008/03 *Guidelines for Nonlinear Analysis of Bridge Structures in California.* Ady Aviram, Kevin R. Mackie, and Božidar Stojadinović. August 2008.

PEER 2008/02 *Treatment of Uncertainties in Seismic-Risk Analysis of Transportation Systems.* Evangelos Stergiou and Anne S. Kiremidjian. July 2008.

PEER 2008/01 *Seismic Performance Objectives for Tall Buildings.* William T. Holmes, Charles Kircher, William Petak, and Nabih Youssef. August 2008.

PEER 2007/12 *An Assessment to Benchmark the Seismic Performance of a Code-Conforming Reinforced Concrete Moment-Frame Building.* Curt Haselton, Christine A. Goulet, Judith Mitrani-Reiser, James L. Beck, Gregory G. Deierlein, Keith A. Porter, Jonathan P. Stewart, and Ertugrul Taciroglu. August 2008.

PEER 2007/11 *Bar Buckling in Reinforced Concrete Bridge Columns.* Wayne A. Brown, Dawn E. Lehman, and John F. Stanton. February 2008.

PEER 2007/10 *Computational Modeling of Progressive Collapse in Reinforced Concrete Frame Structures.* Mohamed M. Talaat and Khalid M. Mosalam. May 2008.

PEER 2007/09 *Integrated Probabilistic Performance-Based Evaluation of Benchmark Reinforced Concrete Bridges.* Kevin R. Mackie, John-Michael Wong, and Božidar Stojadinović. January 2008.

PEER 2007/08 *Assessing Seismic Collapse Safety of Modern Reinforced Concrete Moment-Frame Buildings.* Curt B. Haselton and Gregory G. Deierlein. February 2008.

PEER 2007/07 *Performance Modeling Strategies for Modern Reinforced Concrete Bridge Columns.* Michael P. Berry and Marc O. Eberhard. April 2008.

PEER 2007/06 *Development of Improved Procedures for Seismic Design of Buried and Partially Buried Structures.* Linda Al Atik and Nicholas Sitar. June 2007.

PEER 2007/05 *Uncertainty and Correlation in Seismic Risk Assessment of Transportation Systems.* Renee G. Lee and Anne S. Kiremidjian. July 2007.

PEER 2007/04 *Numerical Models for Analysis and Performance-Based Design of Shallow Foundations Subjected to Seismic Loading.* Sivapalan Gajan, Tara C. Hutchinson, Bruce L. Kutter, Prishati Raychowdhury, José A. Ugalde, and Jonathan P. Stewart. May 2008.

PEER 2007/03 *Beam-Column Element Model Calibrated for Predicting Flexural Response Leading to Global Collapse of RC Frame Buildings.* Curt B. Haselton, Abbie B. Liel, Sarah Taylor Lange, and Gregory G. Deierlein. May 2008.

PEER 2007/02 *Campbell-Bozorgnia NGA Ground Motion Relations for the Geometric Mean Horizontal Component of Peak and Spectral Ground Motion Parameters.* Kenneth W. Campbell and Yousef Bozorgnia. May 2007.

PEER 2007/01 *Boore-Atkinson NGA Ground Motion Relations for the Geometric Mean Horizontal Component of Peak and Spectral Ground Motion Parameters.* David M. Boore and Gail M. Atkinson. May. May 2007.

PEER 2006/12 *Societal Implications of Performance-Based Earthquake Engineering.* Peter J. May. May 2007.

PEER 2006/11 *Probabilistic Seismic Demand Analysis Using Advanced Ground Motion Intensity Measures, Attenuation Relationships, and Near-Fault Effects.* Polsak Tothong and C. Allin Cornell. March 2007.

PEER 2006/10 *Application of the PEER PBEE Methodology to the I-880 Viaduct.* Sashi Kunnath. February 2007.

PEER 2006/09 *Quantifying Economic Losses from Travel Forgone Following a Large Metropolitan Earthquake.* James Moore, Sungbin Cho, Yue Yue Fan, and Stuart Werner. November 2006.

PEER 2006/08 *Vector-Valued Ground Motion Intensity Measures for Probabilistic Seismic Demand Analysis*. Jack W. Baker and C. Allin Cornell. October 2006.

PEER 2006/07 *Analytical Modeling of Reinforced Concrete Walls for Predicting Flexural and Coupled–Shear-Flexural Responses*. Kutay Orakcal, Leonardo M. Massone, and John W. Wallace. October 2006.

PEER 2006/06 *Nonlinear Analysis of a Soil-Drilled Pier System under Static and Dynamic Axial Loading.* Gang Wang and Nicholas Sitar. November 2006.

PEER 2006/05 *Advanced Seismic Assessment Guidelines.* Paolo Bazzurro, C. Allin Cornell, Charles Menun, Maziar Motahari, and Nicolas Luco. September 2006.

PEER 2006/04 *Probabilistic Seismic Evaluation of Reinforced Concrete Structural Components and Systems.* Tae Hyung Lee and Khalid M. Mosalam. August 2006.

PEER 2006/03 *Performance of Lifelines Subjected to Lateral Spreading.* Scott A. Ashford and Teerawut Juirnarongrit. July 2006.

PEER 2006/02 *Pacific Earthquake Engineering Research Center Highway Demonstration Project.* Anne Kiremidjian, James Moore, Yue Yue Fan, Nesrin Basoz, Ozgur Yazali, and Meredith Williams. April 2006.

PEER 2006/01 *Bracing Berkeley. A Guide to Seismic Safety on the UC Berkeley Campus.* Mary C. Comerio, Stephen Tobriner, and Ariane Fehrenkamp. January 2006.

PEER 2005/16 *Seismic Response and Reliability of Electrical Substation Equipment and Systems.* Junho Song, Armen Der Kiureghian, and Jerome L. Sackman. April 2006.

PEER 2005/15 *CPT-Based Probabilistic Assessment of Seismic Soil Liquefaction Initiation.* R. E. S. Moss, R. B. Seed, R. E. Kayen, J. P. Stewart, and A. Der Kiureghian. April 2006.

PEER 2005/14 *Workshop on Modeling of Nonlinear Cyclic Load-Deformation Behavior of Shallow Foundations.* Bruce L. Kutter, Geoffrey Martin, Tara Hutchinson, Chad Harden, Sivapalan Gajan, and Justin Phalen. March 2006.

PEER 2005/13 *Stochastic Characterization and Decision Bases under Time-Dependent Aftershock Risk in Performance-Based Earthquake Engineering.* Gee Liek Yeo and C. Allin Cornell. July 2005.

PEER 2005/12 *PEER Testbed Study on a Laboratory Building: Exercising Seismic Performance Assessment.* Mary C. Comerio, editor. November 2005.

PEER 2005/11 *Van Nuys Hotel Building Testbed Report: Exercising Seismic Performance Assessment.* Helmut Krawinkler, editor. October 2005.

PEER 2005/10 *First NEES/E-Defense Workshop on Collapse Simulation of Reinforced Concrete Building Structures.* September 2005.

PEER 2005/09 *Test Applications of Advanced Seismic Assessment Guidelines.* Joe Maffei, Karl Telleen, Danya Mohr, William Holmes, and Yuki Nakayama. August 2006.

PEER 2005/08 *Damage Accumulation in Lightly Confined Reinforced Concrete Bridge Columns.* R. Tyler Ranf, Jared M. Nelson, Zach Price, Marc O. Eberhard, and John F. Stanton. April 2006.

PEER 2005/07 *Experimental and Analytical Studies on the Seismic Response of Freestanding and Anchored Laboratory Equipment.* Dimitrios Konstantinidis and Nicos Makris. January 2005.

PEER 2005/06 *Global Collapse of Frame Structures under Seismic Excitations*. Luis F. Ibarra and Helmut Krawinkler. September 2005.

PEER 2005//05 *Performance Characterization of Bench- and Shelf-Mounted Equipment.* Samit Ray Chaudhuri and Tara C. Hutchinson. May 2006.

PEER 2005/04 *Numerical Modeling of the Nonlinear Cyclic Response of Shallow Foundations.* Chad Harden, Tara Hutchinson, Geoffrey R. Martin, and Bruce L. Kutter. August 2005.

PEER 2005/03 *A Taxonomy of Building Components for Performance-Based Earthquake Engineering.* Keith A. Porter. September 2005.

PEER 2005/02 *Fragility Basis for California Highway Overpass Bridge Seismic Decision Making*. Kevin R. Mackie and Božidar Stojadinović. June 2005.

PEER 2005/01 *Empirical Characterization of Site Conditions on Strong Ground Motion.* Jonathan P. Stewart, Yoojoong Choi, and Robert W. Graves. June 2005.

PEER 2004/09 *Electrical Substation Equipment Interaction: Experimental Rigid Conductor Studies.* Christopher Stearns and André Filiatrault. February 2005.

PEER 2004/08 *Seismic Qualification and Fragility Testing of Line Break 550-kV Disconnect Switches.* Shakhzod M. Takhirov, Gregory L. Fenves, and Eric Fujisaki. January 2005.

PEER 2004/07 *Ground Motions for Earthquake Simulator Qualification of Electrical Substation Equipment.* Shakhzod M. Takhirov, Gregory L. Fenves, Eric Fujisaki, and Don Clyde. January 2005.

PEER 2004/06 *Performance-Based Regulation and Regulatory Regimes.* Peter J. May and Chris Koski. September 2004.

PEER 2004/05 *Performance-Based Seismic Design Concepts and Implementation: Proceedings of an International Workshop.* Peter Fajfar and Helmut Krawinkler, editors. September 2004.

PEER 2004/04 *Seismic Performance of an Instrumented Tilt-up Wall Building.* James C. Anderson and Vitelmo V. Bertero. July 2004.

PEER 2004/03 *Evaluation and Application of Concrete Tilt-up Assessment Methodologies.* Timothy Graf and James O. Malley. October 2004.

PEER 2004/02 *Analytical Investigations of New Methods for Reducing Residual Displacements of Reinforced Concrete Bridge Columns.* Junichi Sakai and Stephen A. Mahin. August 2004.

PEER 2004/01 *Seismic Performance of Masonry Buildings and Design Implications.* Kerri Anne Taeko Tokoro, James C. Anderson, and Vitelmo V. Bertero. February 2004.

PEER 2003/18 *Performance Models for Flexural Damage in Reinforced Concrete Columns.* Michael Berry and Marc Eberhard. August 2003.

PEER 2003/17 *Predicting Earthquake Damage in Older Reinforced Concrete Beam-Column Joints.* Catherine Pagni and Laura Lowes. October 2004.

PEER 2003/16 *Seismic Demands for Performance-Based Design of Bridges.* Kevin Mackie and Božidar Stojadinović. August 2003.

PEER 2003/15 *Seismic Demands for Nondeteriorating Frame Structures and Their Dependence on Ground Motions.* Ricardo Antonio Medina and Helmut Krawinkler. May 2004.

PEER 2003/14 *Finite Element Reliability and Sensitivity Methods for Performance-Based Earthquake Engineering.* Terje Haukaas and Armen Der Kiureghian. April 2004.

PEER 2003/13 *Effects of Connection Hysteretic Degradation on the Seismic Behavior of Steel Moment-Resisting Frames.* Janise E. Rodgers and Stephen A. Mahin. March 2004.

PEER 2003/12 *Implementation Manual for the Seismic Protection of Laboratory Contents: Format and Case Studies.* William T. Holmes and Mary C. Comerio. October 2003.

PEER 2003/11 *Fifth U.S.-Japan Workshop on Performance-Based Earthquake Engineering Methodology for Reinforced Concrete Building Structures.* February 2004.

PEER 2003/10 *A Beam-Column Joint Model for Simulating the Earthquake Response of Reinforced Concrete Frames.* Laura N. Lowes, Nilanjan Mitra, and Arash Altoontash. February 2004.

PEER 2003/09 *Sequencing Repairs after an Earthquake: An Economic Approach.* Marco Casari and Simon J. Wilkie. April 2004.

PEER 2003/08 *A Technical Framework for Probability-Based Demand and Capacity Factor Design (DCFD) Seismic Formats*. Fatemeh Jalayer and C. Allin Cornell. November 2003.

PEER 2003/07 *Uncertainty Specification and Propagation for Loss Estimation Using FOSM Methods.* Jack W. Baker and C. Allin Cornell. September 2003.

PEER 2003/06 *Performance of Circular Reinforced Concrete Bridge Columns under Bidirectional Earthquake Loading*. Mahmoud M. Hachem, Stephen A. Mahin, and Jack P. Moehle. February 2003.

PEER 2003/05 *Response Assessment for Building-Specific Loss Estimation.* Eduardo Miranda and Shahram Taghavi. September 2003.

PEER 2003/04 *Experimental Assessment of Columns with Short Lap Splices Subjected to Cyclic Loads*. Murat Melek, John W. Wallace, and Joel Conte. April 2003.

PEER 2003/03 *Probabilistic Response Assessment for Building-Specific Loss Estimation.* Eduardo Miranda and Hesameddin Aslani. September 2003.

PEER 2003/02 *Software Framework for Collaborative Development of Nonlinear Dynamic Analysis Program.* Jun Peng and Kincho H. Law. September 2003.

PEER 2003/01 *Shake Table Tests and Analytical Studies on the Gravity Load Collapse of Reinforced Concrete Frames.* Kenneth John Elwood and Jack P. Moehle. November 2003.

PEER 2002/24 *Performance of Beam to Column Bridge Joints Subjected to a Large Velocity Pulse.* Natalie Gibson, André Filiatrault, and Scott A. Ashford. April 2002.

PEER 2002/23 *Effects of Large Velocity Pulses on Reinforced Concrete Bridge Columns.* Greg L. Orozco and Scott A. Ashford. April 2002.

PEER 2002/22 *Characterization of Large Velocity Pulses for Laboratory Testing.* Kenneth E. Cox and Scott A. Ashford. April 2002.

PEER 2002/21 *Fourth U.S.-Japan Workshop on Performance-Based Earthquake Engineering Methodology for Reinforced Concrete Building Structures*. December 2002.

PEER 2002/20 *Barriers to Adoption and Implementation of PBEE Innovations.* Peter J. May. August 2002.

PEER 2002/19 *Economic-Engineered Integrated Models for Earthquakes: Socioeconomic Impacts.* Peter Gordon, James E. Moore II, and Harry W. Richardson. July 2002.

PEER 2002/18 *Assessment of Reinforced Concrete Building Exterior Joints with Substandard Details.* Chris P. Pantelides, Jon Hansen, Justin Nadauld, and Lawrence D. Reaveley. May 2002.

PEER 2002/17 *Structural Characterization and Seismic Response Analysis of a Highway Overcrossing Equipped with Elastomeric Bearings and Fluid Dampers: A Case Study.* Nicos Makris and Jian Zhang. November 2002.

PEER 2002/16 *Estimation of Uncertainty in Geotechnical Properties for Performance-Based Earthquake Engineering.* Allen L. Jones, Steven L. Kramer, and Pedro Arduino. December 2002.

PEER 2002/15 *Seismic Behavior of Bridge Columns Subjected to Various Loading Patterns.* Asadollah Esmaeily-Gh. and Yan Xiao. December 2002.

PEER 2002/14 *Inelastic Seismic Response of Extended Pile Shaft Supported Bridge Structures.* T.C. Hutchinson, R.W. Boulanger, Y.H. Chai, and I.M. Idriss. December 2002.

PEER 2002/13 *Probabilistic Models and Fragility Estimates for Bridge Components and Systems.* Paolo Gardoni, Armen Der Kiureghian, and Khalid M. Mosalam. June 2002.

PEER 2002/12 *Effects of Fault Dip and Slip Rake on Near-Source Ground Motions: Why Chi-Chi Was a Relatively Mild M7.6 Earthquake.* Brad T. Aagaard, John F. Hall, and Thomas H. Heaton. December 2002.

PEER 2002/11 *Analytical and Experimental Study of Fiber-Reinforced Strip Isolators*. James M. Kelly and Shakhzod M. Takhirov. September 2002.

PEER 2002/10 *Centrifuge Modeling of Settlement and Lateral Spreading with Comparisons to Numerical Analyses***.** Sivapalan Gajan and Bruce L. Kutter. January 2003.

PEER 2002/09 *Documentation and Analysis of Field Case Histories of Seismic Compression during the 1994 Northridge, California, Earthquake.* Jonathan P. Stewart, Patrick M. Smith, Daniel H. Whang, and Jonathan D. Bray. October 2002.

PEER 2002/08 *Component Testing, Stability Analysis and Characterization of Buckling-Restrained Unbonded Braces™.* Cameron Black, Nicos Makris, and Ian Aiken. September 2002.

PEER 2002/07 *Seismic Performance of Pile-Wharf Connections.* Charles W. Roeder, Robert Graff, Jennifer Soderstrom, and Jun Han Yoo. December 2001.

PEER 2002/06 *The Use of Benefit-Cost Analysis for Evaluation of Performance-Based Earthquake Engineering Decisions*. Richard O. Zerbe and Anthony Falit-Baiamonte. September 2001.

PEER 2002/05 *Guidelines, Specifications, and Seismic Performance Characterization of Nonstructural Building Components and Equipment.* André Filiatrault, Constantin Christopoulos, and Christopher Stearns. September 2001.

PEER 2002/04 *Consortium of Organizations for Strong-Motion Observation Systems and the Pacific Earthquake Engineering Research Center Lifelines Program: Invited Workshop on Archiving and Web Dissemination of Geotechnical Data, 4–5 October 2001*. September 2002.

PEER 2002/03 *Investigation of Sensitivity of Building Loss Estimates to Major Uncertain Variables for the Van Nuys Testbed.* Keith A. Porter, James L. Beck, and Rustem V. Shaikhutdinov. August 2002.

PEER 2002/02 *The Third U.S.-Japan Workshop on Performance-Based Earthquake Engineering Methodology for Reinforced Concrete Building Structures*. July 2002.

PEER 2002/01 *Nonstructural Loss Estimation: The UC Berkeley Case Study.* Mary C. Comerio and John C. Stallmeyer. December 2001.

PEER 2001/16 *Statistics of SDF-System Estimate of Roof Displacement for Pushover Analysis of Buildings.* Anil K. Chopra, Rakesh K. Goel, and Chatpan Chintanapakdee. December 2001.

PEER 2001/15 *Damage to Bridges during the 2001 Nisqually Earthquake.* R. Tyler Ranf, Marc O. Eberhard, and Michael P. Berry. November 2001.

PEER 2001/14 *Rocking Response of Equipment Anchored to a Base Foundation.* Nicos Makris and Cameron J. Black. September 2001.

PEER 2001/13 *Modeling Soil Liquefaction Hazards for Performance-Based Earthquake Engineering.* Steven L. Kramer and Ahmed-W. Elgamal. February 2001.

PEER 2001/12 *Development of Geotechnical Capabilities in OpenSees.* Boris Jeremić. September 2001.

PEER 2001/11 *Analytical and Experimental Study of Fiber-Reinforced Elastomeric Isolators.* James M. Kelly and Shakhzod M. Takhirov. September 2001.

PEER 2001/10 *Amplification Factors for Spectral Acceleration in Active Regions.* Jonathan P. Stewart, Andrew H. Liu, Yoojoong Choi, and Mehmet B. Baturay. December 2001.

PEER 2001/09 *Ground Motion Evaluation Procedures for Performance-Based Design.* Jonathan P. Stewart, Shyh-Jeng Chiou, Jonathan D. Bray, Robert W. Graves, Paul G. Somerville, and Norman A. Abrahamson. September 2001.

PEER 2001/08 *Experimental and Computational Evaluation of Reinforced Concrete Bridge Beam-Column Connections for Seismic Performance.* Clay J. Naito, Jack P. Moehle, and Khalid M. Mosalam. November 2001.

PEER 2001/07 *The Rocking Spectrum and the Shortcomings of Design Guidelines.* Nicos Makris and Dimitrios Konstantinidis. August 2001.

PEER 2001/06 *Development of an Electrical Substation Equipment Performance Database for Evaluation of Equipment Fragilities.* Thalia Agnanos. April 1999.

PEER 2001/05 *Stiffness Analysis of Fiber-Reinforced Elastomeric Isolators.* Hsiang-Chuan Tsai and James M. Kelly. May 2001.

PEER 2001/04 *Organizational and Societal Considerations for Performance-Based Earthquake Engineering.* Peter J. May. April 2001.

PEER 2001/03 *A Modal Pushover Analysis Procedure to Estimate Seismic Demands for Buildings: Theory and Preliminary Evaluation.* Anil K. Chopra and Rakesh K. Goel. January 2001.

PEER 2001/02 *Seismic Response Analysis of Highway Overcrossings Including Soil-Structure Interaction.* Jian Zhang and Nicos Makris. March 2001.

PEER 2001/01 *Experimental Study of Large Seismic Steel Beam-to-Column Connections.* Egor P. Popov and Shakhzod M. Takhirov. November 2000.

PEER 2000/10 *The Second U.S.-Japan Workshop on Performance-Based Earthquake Engineering Methodology for Reinforced Concrete Building Structures.* March 2000.

PEER 2000/09 *Structural Engineering Reconnaissance of the August 17, 1999 Earthquake: Kocaeli (Izmit), Turkey.* Halil Sezen, Kenneth J. Elwood, Andrew S. Whittaker, Khalid Mosalam, John J. Wallace, and John F. Stanton. December 2000.

PEER 2000/08 *Behavior of Reinforced Concrete Bridge Columns Having Varying Aspect Ratios and Varying Lengths of Confinement.* Anthony J. Calderone, Dawn E. Lehman, and Jack P. Moehle. January 2001.

PEER 2000/07 *Cover-Plate and Flange-Plate Reinforced Steel Moment-Resisting Connections.* Taejin Kim, Andrew S. Whittaker, Amir S. Gilani, Vitelmo V. Bertero, and Shakhzod M. Takhirov. September 2000.

PEER 2000/06 *Seismic Evaluation and Analysis of 230-kV Disconnect Switches.* Amir S. J. Gilani, Andrew S. Whittaker, Gregory L. Fenves, Chun-Hao Chen, Henry Ho, and Eric Fujisaki. July 2000.

PEER 2000/05 *Performance-Based Evaluation of Exterior Reinforced Concrete Building Joints for Seismic Excitation.* Chandra Clyde, Chris P. Pantelides, and Lawrence D. Reaveley. July 2000.

PEER 2000/04 *An Evaluation of Seismic Energy Demand: An Attenuation Approach.* Chung-Che Chou and Chia-Ming Uang. July 1999.

PEER 2000/03 *Framing Earthquake Retrofitting Decisions: The Case of Hillside Homes in Los Angeles.* Detlof von Winterfeldt, Nels Roselund, and Alicia Kitsuse. March 2000.

PEER 2000/02 *U.S.-Japan Workshop on the Effects of Near-Field Earthquake Shaking.* Andrew Whittaker, ed. July 2000.

PEER 2000/01 *Further Studies on Seismic Interaction in Interconnected Electrical Substation Equipment.* Armen Der Kiureghian, Kee-Jeung Hong, and Jerome L. Sackman. November 1999.

PEER 1999/14 *Seismic Evaluation and Retrofit of 230-kV Porcelain Transformer Bushings.* Amir S. Gilani, Andrew S. Whittaker, Gregory L. Fenves, and Eric Fujisaki. December 1999.

PEER 1999/13 *Building Vulnerability Studies: Modeling and Evaluation of Tilt-up and Steel Reinforced Concrete Buildings.* John W. Wallace, Jonathan P. Stewart, and Andrew S. Whittaker, editors. December 1999.

PEER 1999/12 *Rehabilitation of Nonductile RC Frame Building Using Encasement Plates and Energy-Dissipating Devices.* Mehrdad Sasani, Vitelmo V. Bertero, James C. Anderson. December 1999.

PEER 1999/11 *Performance Evaluation Database for Concrete Bridge Components and Systems under Simulated Seismic Loads.* Yael D. Hose and Frieder Seible. November 1999.

PEER 1999/10 *U.S.-Japan Workshop on Performance-Based Earthquake Engineering Methodology for Reinforced Concrete Building Structures.* December 1999.

PEER 1999/09 *Performance Improvement of Long Period Building Structures Subjected to Severe Pulse-Type Ground Motions.* James C. Anderson, Vitelmo V. Bertero, and Raul Bertero. October 1999.

PEER 1999/08 *Envelopes for Seismic Response Vectors.* Charles Menun and Armen Der Kiureghian. July 1999.

PEER 1999/07 *Documentation of Strengths and Weaknesses of Current Computer Analysis Methods for Seismic Performance of Reinforced Concrete Members.* William F. Cofer. November 1999.

PEER 1999/06 *Rocking Response and Overturning of Anchored Equipment under Seismic Excitations.* Nicos Makris and Jian Zhang. November 1999.

PEER 1999/05 *Seismic Evaluation of 550 kV Porcelain Transformer Bushings.* Amir S. Gilani, Andrew S. Whittaker, Gregory L. Fenves, and Eric Fujisaki. October 1999.

PEER 1999/04 *Adoption and Enforcement of Earthquake Risk-Reduction Measures.* Peter J. May, Raymond J. Burby, T. Jens Feeley, and Robert Wood.

PEER 1999/03 *Task 3 Characterization of Site Response General Site Categories.* Adrian Rodriguez-Marek, Jonathan D. Bray, and Norman Abrahamson. February 1999.

PEER 1999/02 *Capacity-Demand-Diagram Methods for Estimating Seismic Deformation of Inelastic Structures: SDF Systems.* Anil K. Chopra and Rakesh Goel. April 1999.

PEER 1999/01 *Interaction in Interconnected Electrical Substation Equipment Subjected to Earthquake Ground Motions.* Armen Der Kiureghian, Jerome L. Sackman, and Kee-Jeung Hong. February 1999.

PEER 1998/08 *Behavior and Failure Analysis of a Multiple-Frame Highway Bridge in the 1994 Northridge Earthquake.* Gregory L. Fenves and Michael Ellery. December 1998.

PEER 1998/07 *Empirical Evaluation of Inertial Soil-Structure Interaction Effects.* Jonathan P. Stewart, Raymond B. Seed, and Gregory L. Fenves. November 1998.

PEER 1998/06 *Effect of Damping Mechanisms on the Response of Seismic Isolated Structures.* Nicos Makris and Shih-Po Chang. November 1998.

PEER 1998/05 *Rocking Response and Overturning of Equipment under Horizontal Pulse-Type Motions.* Nicos Makris and Yiannis Roussos. October 1998.

PEER 1998/04 *Pacific Earthquake Engineering Research Invitational Workshop Proceedings, May 14–15, 1998: Defining the Links between Planning, Policy Analysis, Economics and Earthquake Engineering.* Mary Comerio and Peter Gordon. September 1998.

PEER 1998/03 *Repair/Upgrade Procedures for Welded Beam to Column Connections.* James C. Anderson and Xiaojing Duan. May 1998.

PEER 1998/02 *Seismic Evaluation of 196 kV Porcelain Transformer Bushings.* Amir S. Gilani, Juan W. Chavez, Gregory L. Fenves, and Andrew S. Whittaker. May 1998.

PEER 1998/01 *Seismic Performance of Well-Confined Concrete Bridge Columns.* Dawn E. Lehman and Jack P. Moehle. December 2000.

ONLINE PEER REPORTS

The following PEER reports are available by Internet only at http://peer.berkeley.edu/publications/peer_reports_complete.html.

PEER 2012/103 *Performance-Based Seismic Demand Assessment of Concentrically Braced Steel Frame Buildings.* Chui-Hsin Chen and Stephen A. Mahin. December 2012.

PEER 2012/102 *Procedure to Restart an Interrupted Hybrid Simulation: Addendum to PEER Report 2010/103.* Vesna Terzic and Bozidar Stojadinovic. October 2012.

PEER 2012/101 *Mechanics of Fiber Reinforced Bearings.* James M. Kelly and Andrea Calabrese. February 2012.

PEER 2011/107 *Nonlinear Site Response and Seismic Compression at Vertical Array Strongly Shaken by 2007 Niigata-ken Chuetsu-oki Earthquake.* Eric Yee, Jonathan P. Stewart, and Kohji Tokimatsu. December 2011.

PEER 2011/106 *Self Compacting Hybrid Fiber Reinforced Concrete Composites for Bridge Columns.* Pardeep Kumar, Gabriel Jen, William Trono, Marios Panagiotou, and Claudia Ostertag. September 2011.

PEER 2011/105 *Stochastic Dynamic Analysis of Bridges Subjected to Spacially Varying Ground Motions.* Katerina Konakli and Armen Der Kiureghian. August 2011.

PEER 2011/104 *Design and Instrumentation of the 2010 E-Defense Four-Story Reinforced Concrete and Post-Tensioned Concrete Buildings.* Takuya Nagae, Kenichi Tahara, Taizo Matsumori, Hitoshi Shiohara, Toshimi Kabeyasawa, Susumu Kono, Minehiro Nishiyama (Japanese Research Team) and John Wallace, Wassim Ghannoum, Jack Moehle, Richard Sause, Wesley Keller, Zeynep Tuna (U.S. Research Team). June 2011.

PEER 2011/103 *In-Situ Monitoring of the Force Output of Fluid Dampers: Experimental Investigation.* Dimitrios Konstantinidis, James M. Kelly, and Nicos Makris. April 2011.

PEER 2011/102 *Ground-motion prediction equations 1964 - 2010.* John Douglas. April 2011.

PEER 2011/101 *Report of the Eighth Planning Meeting of NEES/E-Defense Collaborative Research on Earthquake Engineering.* Convened by the Hyogo Earthquake Engineering Research Center (NIED), NEES Consortium, Inc. February 2011.

PEER 2010/111 *Modeling and Acceptance Criteria for Seismic Design and Analysis of Tall Buildings.* Task 7 Report for the Tall Buildings Initiative - Published jointly by the Applied Technology Council. October 2010.

PEER 2010/110 *Seismic Performance Assessment and Probabilistic Repair Cost Analysis of Precast Concrete Cladding Systems for Multistory Buildlings.* Jeffrey P. Hunt and Božidar Stojadinovic. November 2010.

PEER 2010/109 *Report of the Seventh Joint Planning Meeting of NEES/E-Defense Collaboration on Earthquake Engineering. Held at the E-Defense, Miki, and Shin-Kobe, Japan, September 18–19, 2009.* August 2010.

PEER 2010/108 *Probabilistic Tsunami Hazard in California.* Hong Kie Thio, Paul Somerville, and Jascha Polet, preparers. October 2010.

PEER 2010/107 *Performance and Reliability of Exposed Column Base Plate Connections for Steel Moment-Resisting Frames.* Ady Aviram, Božidar Stojadinovic, and Armen Der Kiureghian. August 2010.

PEER 2010/106 *Verification of Probabilistic Seismic Hazard Analysis Computer Programs.* Patricia Thomas, Ivan Wong, and Norman Abrahamson. May 2010.

PEER 2010/105 *Structural Engineering Reconnaissance of the April 6, 2009, Abruzzo, Italy, Earthquake, and Lessons Learned.* M. Selim Günay and Khalid M. Mosalam. April 2010.

PEER 2010/104 *Simulating the Inelastic Seismic Behavior of Steel Braced Frames, Including the Effects of Low-Cycle Fatigue.* Yuli Huang and Stephen A. Mahin. April 2010.

PEER 2010/103 *Post-Earthquake Traffic Capacity of Modern Bridges in California.* Vesna Terzic and Božidar Stojadinović. March 2010.

PEER 2010/102 *Analysis of Cumulative Absolute Velocity (CAV) and JMA Instrumental Seismic Intensity (I_{JMA}) Using the PEER–NGA Strong Motion Database.* Kenneth W. Campbell and Yousef Bozorgnia. February 2010.

PEER 2010/101 *Rocking Response of Bridges on Shallow Foundations.* Jose A. Ugalde, Bruce L. Kutter, and Boris Jeremic. April 2010.

PEER 2009/109 *Simulation and Performance-Based Earthquake Engineering Assessment of Self-Centering Post-Tensioned Concrete Bridge Systems.* Won K. Lee and Sarah L. Billington. December 2009.

PEER 2009/108 *PEER Lifelines Geotechnical Virtual Data Center.* J. Carl Stepp, Daniel J. Ponti, Loren L. Turner, Jennifer N. Swift, Sean Devlin, Yang Zhu, Jean Benoit, and John Bobbitt. September 2009.

PEER 2009/107 *Experimental and Computational Evaluation of Current and Innovative In-Span Hinge Details in Reinforced Concrete Box-Girder Bridges: Part 2: Post-Test Analysis and Design Recommendations.* Matias A. Hube and Khalid M. Mosalam. December 2009.

PEER 2009/106 *Shear Strength Models of Exterior Beam-Column Joints without Transverse Reinforcement.* Sangjoon Park and Khalid M. Mosalam. November 2009.

PEER 2009/105 *Reduced Uncertainty of Ground Motion Prediction Equations through Bayesian Variance Analysis.* Robb Eric S. Moss. November 2009.

PEER 2009/104 *Advanced Implementation of Hybrid Simulation.* Andreas H. Schellenberg, Stephen A. Mahin, Gregory L. Fenves. November 2009.

PEER 2009/103 *Performance Evaluation of Innovative Steel Braced Frames.* T. Y. Yang, Jack P. Moehle, and Božidar Stojadinovic. August 2009.

PEER 2009/102 *Reinvestigation of Liquefaction and Nonliquefaction Case Histories from the 1976 Tangshan Earthquake.* Robb Eric Moss, Robert E. Kayen, Liyuan Tong, Songyu Liu, Guojun Cai, and Jiaer Wu. August 2009.

PEER 2009/101 *Report of the First Joint Planning Meeting for the Second Phase of NEES/E-Defense Collaborative Research on Earthquake Engineering.* Stephen A. Mahin et al. July 2009.

PEER 2008/104 *Experimental and Analytical Study of the Seismic Performance of Retaining Structures.* Linda Al Atik and Nicholas Sitar. January 2009.

PEER 2008/103 *Experimental and Computational Evaluation of Current and Innovative In-Span Hinge Details in Reinforced Concrete Box-Girder Bridges. Part 1: Experimental Findings and Pre-Test Analysis.* Matias A. Hube and Khalid M. Mosalam. January 2009.

PEER 2008/102 *Modeling of Unreinforced Masonry Infill Walls Considering In-Plane and Out-of-Plane Interaction.* Stephen Kadysiewski and Khalid M. Mosalam. January 2009.

PEER 2008/101 *Seismic Performance Objectives for Tall Buildings.* William T. Holmes, Charles Kircher, William Petak, and Nabih Youssef. August 2008.

PEER 2007/101 *Generalized Hybrid Simulation Framework for Structural Systems Subjected to Seismic Loading.* Tarek Elkhoraibi and Khalid M. Mosalam. July 2007.

PEER 2007/100 *Seismic Evaluation of Reinforced Concrete Buildings Including Effects of Masonry Infill Walls.* Alidad Hashemi and Khalid M. Mosalam. July 2007.

The Pacific Earthquake Engineering Research Center (PEER) is a multi-institutional research and education center with headquarters at the University of California, Berkeley. Investigators from over 20 universities, several consulting companies, and researchers at various state and federal government agencies contribute to research programs focused on performance-based earthquake engineering.

These research programs aim to identify and reduce the risks from major earthquakes to life safety and to the economy by including research in a wide variety of disciplines including structural and geotechnical engineering, geology/seismology, lifelines, transportation, architecture, economics, risk management, and public policy.

PEER is supported by federal, state, local, and regional agencies, together with industry partners.

PEER Core Institutions:
University of California, Berkeley (Lead Institution)
California Institute of Technology
Oregon State University
Stanford University
University of California, Davis
University of California, Irvine
University of California, Los Angeles
University of California, San Diego
University of Southern California
University of Washington

PEER reports can be ordered at http://peer.berkeley.edu/publications/peer_reports.html or by contacting

Pacific Earthquake Engineering Research Center
University of California, Berkeley
325 Davis Hall, mail code 1792
Berkeley, CA 94720-1792
Tel: 510-642-3437
Fax: 510-642-1655
Email: peer_editor@berkeley.edu

ISSN 1547-0587X